Dissertation zur Erlangung des Doktorgrades

der Fakultät für Chemie und Pharmazie

der Ludwig-Maximilians-Universität München

Integrin Subtype Specific Assembly of Focal Adhesion Proteins and Their Effect on Cell Contractility and Actin-based Signalling

Michaela-Rosemarie Hermann

aus

Aschaffenburg

2014

Erklärung

Diese Dissertation wurde im Sinne von § 7 der Promotionsordnung vom 28. November 2011 von Herrn Prof. Dr. Reinhard Fässler betreut.

Eidesstattliche Versicherung

Diese Dissertation wurde selbständig, ohne unerlaubte Hilfe erarbeitet.

München, 11.04.2014

……

Michaela-Rosemarie Hermann

Dissertation eingereicht am 11.04.2014

1. Gutachterin / 1. Gutachter: Prof. Dr. Reinhard Fässler

2. Gutachterin / 2. Gutachter: Prof. Dr. Christian Wahl-Schott

Mündliche Prüfung am 13.05.2014

Die vorliegende Arbeit wurde in der Zeit von Mai 2010 bis März 2014 in der Arbeitsgruppe von Herrn Prof. Dr. Fässler in der Abteilung für Molekulare Medizin am Max-Planck-Institut für Biochemie in Martinsried angefertigt.

Im Verlauf dieser Arbeit wurden u.a. folgende Veröffentlichungen publiziert oder zur Publikation vorbereitet:

Schiller HB*, **Hermann MR***, Polleux J, Vignaud T, Zanivan S, Friedel CC, Sun Z, Raducanu A, Gottschalk KE, Théry M, Mann M, Fässler R. **β1- and αV-class integrins cooperate to regulate myosin II during rigidity sensing of fibronectin-based microenvironments.** *Nat Cell Biol.* 2013 Jun;15(6):625-36.

Hermann MR, Rognoni E, Jakobson M, Widmaier M, Yeroslaviz A, Zent R, Posern G, Hofstädter F, Fässler R. **Integrins synergistically induce the MAL/SRF target gene ISG15 to ISGylate cytoskeletal and focal adhesion proteins necessary for cancer cell invasion.** *Manuscript in preparation.*

*: equal contribution

Meinen Eltern und Robert

Table of Content

Summary **7**

Abbreviations **9**

1 Introduction **12**

1.1 The Integrin Receptor Family *12*

1.1.1 Structure of Integrins 12

1.1.1.1 Extracellular domains and ligand binding 12

1.1.1.2 Transmembrane and cytoplasmic domains 14

1.1.2 Members of the integrin superfamily 17

1.1.3 Bi-directional signalling and Focal Adhesion proteins 20

1.1.4 Actin binding through integrins and the importance of mechanotransduction 22

1.1.5 Proteins and signalling processes mediating actin distribution and dynamics 25

1.1.5.1 Types of Actin-rich protrusions 25

1.1.5.2 Actin modifying proteins 25

1.1.6 Temporal short- and long-term effects by integrin mediated Actin dynamics 28

1.2 Fibronectin and its major integrin receptors *30*

1.2.1 Fibronectin – Assembly and features 30

1.2.2 The role of Fibronectin in mouse development 31

1.2.3 The major Fibronectin receptors 33

1.2.3.1 The β1-class of integrins 33

1.2.3.2 The αV-class of integrins 34

1.3 The concept of receptor cross-talk *35*

1.3.1 Integrin-integrin cross-talk 35

1.3.2 Integrins and growth factor receptor signalling cross-talk 36

1.3.3 Sensing matrix rigidity by integrins 37

1.4 SRF and the co-factor MAL *38*

1.4.1 SRF and MADS-box transcription factors 39

1.4.2 Ternary complex factors and SRF 40

1.4.3 Myocardins and the unique feature of MAL 42

1.5 ISG15 and ISGylation *45*

2 Aims of the thesis **47**

3 Short summaries of manuscripts 48

3.1 First manuscript 48

3.2 Second manuscript 48

4 References 50

5 Acknowledgements/Danksagungen 64

6 Curriculum vitae 65

7 Appendix 66

7.1 First publication (Co- first author) 66

7.2 Second publication (First author) 66

Summary

Mammalian cells usually co-express several integrins, which can recognize different ECM proteins, become activated and trigger their own intracellular signalling events. Those cues might also intersect and cross-talk with other signalling cascades initiated and/or modulated by other integrins or even by other receptors like growth factor receptors (GFRs). Almost all integrins bind to ECM proteins such as Collagen (Coll), Vitronectin (VN), and Fibronectin (FN). Hereby VN and FN are bound through the tri-peptide motif Arg-Gly-Asp (RGD), which mediates binding to β1- (α5β1, α8β1), all αV-class (αvβ1, αvβ3, αvβ5, αvβ6 and αvβ8) heterodimers and αIIbβ3, an integrin specific for platelets. *In vivo* and *in vitro* studies indicated that these Integrin classes exert both specific and redundant roles. However, how these distinct FN-binding heterodimers accomplish their individual functions and if they cooperate was unclear when I started my thesis. To make it possible to investigate and dissect integrin subtype-specific signalling events of FN-binding heterodimers, it is necessary to reduce the integrin complexity. For my studies, I therefore utilized pan-integrin-null kidney fibroblasts where either the αV- and/or β1- chain was/were re-expressed to gain reconstitution with either αV- (αVβ3, αVβ5) or β1-class (α5β1) integrins or both.

In my first paper I performed a functional analysis of β1- and αV-class integrins expressed in pan-integrin-null fibroblasts seeded on FN. A quantitative proteomics approach allowed for the first time a non-biased analysis of the molecular composition of FAs assembled by a single integrin class using biochemical isolation protocols in combination with quantitative mass spectrometry and biochemical assays, like immunoblotting, -staining, and -precipitation. **We could assign specific functions to distinct FN-binding integrins; α5β1 integrins are responsible for force generation, whereas αV-class integrins induce the generation of actin filaments, which enables cells to transduce force and to sense the substrate rigidity of FN-based microenvironments.**

In my second paper I investigated whether and if yes, how αV- and/or β1-class integrins can mediate changes in gene expression in order to regulate cell proliferation and differentiation. I could show that integrins compass these long-term effects by regulating cytoskeletal dynamics and thus releasing the interaction of the transcriptional co-activator Megakaryocyte Acute Leukemia protein (MAL; also known as MRTF-A or MKL1) with g-Actin to drive MAL/SRF-mediated gene expression. I found that αV- and β1-class integrins synergize to regulate expression of MAL/SRF target genes. Further-

more, the small ubiquitin-like modifier Interferon-specific gene 15 (ISG15) was identified as one of the MAL/SRF target genes. ISG15 binds covalently to specific lysine residues of numerous MAL/SRF target gene products including Vinculin, Talin and Eplin and thereby preventing their ubiquitination and degradation. **The study shows that αV-/β1-class integrins/MAL/SRF/ISG15 assign a novel auto-regulatory feed-forward loop that precisely adjusts adhesion- and actin-remodelling required for cell spreading, migration and invasion. Finally, we are providing a prognostic value of high αV-/β1-class integrin, ISG15 and nuclear MAL levels useful for breast cancer diagnosis.**

Abbreviations

aa	Amino acid
DAPI	4', 6-Diamidin-2-phenylindol-dihydrochloride
ABS	Actin binding site
ADF	Actin depolymerizing factor
Arp2/3 complex	Actin-related protein 2/3 complex
R	Arg, Arginine
D	Asp, Aspartic acid
A-T	Ataxia-telangiectasia
BSA	Bovine serum albumine
CH	Calponin homology
CP	Capping protein
JNK	C-Jun N-terminal kinase
Coll	Collagen
cDNA	Complementary DNA
DNA	Deoxyribonucleic acid
DMSO	Dimethylsulfoxide
PKR	DsRNA-dependent protein kinase
DMEM	Dulbecco's Modified Eagle Medium
Ets	E twenty-six domain transcription factors
E	Embryonic day
Ena/Vasp	Enabled/Vasodilator-stimulated phosphoprotein
ELISA	Enzyme-linked Immunosorbent Assay
EBS	Ets binding site
ECM	Extracellular matrix
ERK	Extracellular signal-regulated kinase
FCS	Fetal calf serum
FN	Fibronectin
f-Actin	Filamentous Actin
FA	Focal adhesion
FAK	Focal adhesion kinase
e.g.	For example
FERM	Four point one, Ezrin, Radexin, Moesin
g-Actin	Globular (monomeric) Actin
G	Gly, Glycin
GPCR	G-protein coupled receptor
GFR	Growth factor receptor
GAP	GTPase activating protein
GDI	Guanine nucleotide dissociation inhibitor
GEF	Guanine nucleotide exchange factor
GDP	Guanosine diphosphate
GTP	Guanosine triphosphate
H/E	Hematoxylin/Eosin

h	Hour(s)
IPP complex	ILK-PINCH-Parvin complex
Ig	Immunglobulin
IGF-1	Insulin-like growth factor 1
IGFR	Insulin-like growth factor receptor
Itg	Integrin
ICAP	Integrin cytoplasmic domain-associated protein 1
ILK	Integrin linked kinase
ICAM-1	Intercellular adhesion molecule-1
IFN	Interferon
ISG15	Interferon-induced 15 kDa protein
IL	Interleukin
kDa	Kilodalton
LAP	Latency-associated protein
LDV	Leucine-aspartic acidvaline
LIMK	LIM kinase
LIM	Lin11, Isl1, Mec3
mDia	Mammalian diaphanous
MECs	Mammary epithelial cells
MGDI	Mammary-derived growth inhibitor
Mn2+	Manganese-ion
MKK4	MAPK/ERK kinase 4
MEKK1	MAPK/ERK kinase kinase 1
MMP	Matrix metalloproteinase
MAL (or MRTF-A)	Megakaryocyte acute leukemia protein (or Myocardin related transcription factor A)
mRNA	messenger RNA
µg	Microgramm
µm	Micrometer
Min	Minutes
MAPK	Mitogen-activated protein kinase
MLCK	MLC kinase
MLCP	MLC phosphatase
M/mM	Molar/millimolar
MadCAM-1	Mucosal addressin cell adhesion molecule-1
MEF2	Myocyte enhancer factor-2
MYPT1	Myosin phosphatase-targeting subunit 1
MLC	Myosin regulatory light chain
NA	Nascent adhesion
Net	Neuroepithelial cell-transforming gene protein
PINCH	Particularly interesting Cys-His-rich protein
NPxY	Peptide motif asparagine (N), proline (P), any aa (x), tyrosine (Y)
GFFKR	Peptide motif glycine (G), phenylalanine (F), lysine (K), arginine (R)
PTB	Phosphotyrosinebinding
PM	Plasma membrane
PH	Pleckstrin homology
PCR	Polymerase chain reaction

Src	Proto-oncogene tyrosine-protein kinase Sarcoma
RhoA	Ras homolog gene family, member A
Rac1	Ras-related C3 botulinum toxin substrate 1
Ras	Rat sarcoma
ROCK	Rho-associated kinase
RNA	Ribonucleic acid
RSK2	Ribosomal protein S6 kinase 2
RNAi	RNA interference
SDS-PAGE	SDS polyacrylamid gel electrophoresis
S	Ser, Serine
SRE	Serum response element
SRF	Serum response factor
SHARPIN	Shank-associated RH domain-interacting protein
shRNA	Short hairpin RNA
SDS	Sodium dodecyl sulphate
SNX17	Sortin nexin 17
Sap-1	SRF accessory protein 1
SILAC	Stable isotope labelling by amino acids in culture
SCAI	Suppressor of cancer cell invasion
THD	Talin head domain
THATCH	Talin/HIP1R/Sla2p Actin-tethering C-terminal homology
TCF	Ternary complex factor
Tβ4	Thymosin β 4
TGF-β	Transforming growth factor β
TM	Transmembrane
RGD	Tripeptide motif Arg-Gly-Asp
VCAM1	Vascular cell adhesion molecule 1
DBP	Vitamin D-binding protein
VN	Vitronectin
WAVE	WASP-family verprolin-homologous protein
WASP	Wiskott-Aldrich syndrome protein
Y2H	Yeast two hybrid

1 Introduction

1.1 The Integrin Receptor Family

"*We propose the name integrin for this protein complex to denote its role as an integral membrane complex involved in the transmembrane association between the extracellular matrix and the cytoskeleton."* (Tamkun et al., 1986)

Integrins are key cell adhesion molecules that connect the extracellular matrix (ECM) with the Actin cytoskeleton (Humphries, 2000; Hynes, 2002). They establish a molecular platform where mechanical forces, cytoskeletal organization and biochemical signals intersect and modulate a plethora of cellular functions including cell migration, proliferation, differentiation and survival. Before integrins bind ECM they shift from a bent to an extended conformation and adopt high affinity for ligand (Hynes, 2002; Legate et al., 2009). ECM bound integrins aggregate and form different types of adhesion complexes, which differ in size, subcellular localization and function (Paszek et al., 2009). Nascent complexes are smaller than 0.5 µm and are usually short lived, while myosin II-mediated tensioning of nascent adhesions triggers their growth into large (1-10µm) multi-protein assemblies called focal adhesions (FAs). Around 150 proteins were identified in a data mining screen to be associated with FAs either constitutively or transiently (Zaidel-Bar et al., 2007). It has become increasingly apparent that FAs function as signalling hubs that sense the complex chemical and physical nature of the ECM (Geiger et al., 2009; Parsons et al., 2010). This exquisite property is required to orchestrate development and physiology of multicellular organisms.

1.1.1 Structure of Integrins

1.1.1.1 Extracellular domains and ligand binding

Integrins undergo one of the most complex and intense conformational changes among cell surface receptors. These rearrangements function to transmit bi-directional signals (see following paragraph) between the ligand-binding integrin headpiece and the Actin cytoskeleton.

Integrin heterodimers consist of one α and one β subunit. The subunits contain very large extracellular domains of up to 1104 amino acids (aa) for α- and 778 aa for β-subunits, a helical transmembrane (TM) domain of 25-29 aa and a very short C-terminal cytoplasmic segment of about 20-50 aa (Arnaout et al., 2005). The only exception is the β4 subunit which contains a long cytoplasmic segment of around 1000 aa. β4 subunit found in α6β4 is the only integrin that associates to intermediate filaments instead of the actin cytoskeleton and play a central role in the formation of hemidesmosomes.

In order to understand the activation states of integrins, researchers have elucidated the structural interactions of the integrin heterodimers and their different conformation states. The headpiece of the α subunit is composed of β-propeller and thigh domains (Figure 1; green) whereas the β subunit headpiece consists of βI, hybrid, and PSI (Plexin, Semaphorin, Integrin) domains (Figure 1; red). The α subunit calf-1 and calf-2 (β sandwich domains) (Figure 1; orange) and the β subunit I-EGF-2 to I-EGF-4 and β tail domains form the lower legs (Figure 1; grey) (Xiong et al., 2001; Zhu et al., 2008). X-ray crystal structures of the extracellular domain of the integrin αVβ3 identified a bent conformation of the legs (Xiong et al., 2001; Xiong et al., 2002). Based on these findings the prevailing view is that the bent conformation represents the physiological low-affinity state, whereas extended ectodomains exhibit high affinity for ligands. There are two models proposed for this change in affinity: (**a**) The "switchblade" model: In the low affinity conformation, the headpiece of the integrin folds over its legs at the genu and faces down towards the membrane. Separation of the cytoplasmic and TM segments causes a jackknife-like knee extension of the bent integrin, which leads to the dislocation of the epidermal growth factor (EGF)-like repeat in the β leg. As a consequence the hybrid domain is released, swings out and thus switching from a closed (low affinity) to an open (high affinity) conformation of the βI domain (Beglova et al., 2002; Kim et al., 2003; Takagi et al., 2002; Tan et al., 2000). (**b**) The "deadbolt" model for inside-out activation: Hereby the head is still bent in an activated integrin and the TM regions perform a piston-like movement that results in sliding of the extracellular legs of α and β subunits. As a result the interaction between headpiece and β legs is disrupted just beyond the membrane (Arnaout et al., 2005).

About half of the integrin α subunits (Coll-binding and the leukocyte specific α-subunits) contain a domain of about 200 amino acids known as an inserted (I) domain or von Willebrand factor-like A domain inserted into their β-propeller (αI domain). In integrins in which it is present, the αI domain is the major or exclusive ligand-binding site. It has strong similarity to the βI domain and can also change from a closed, low affinity to an open, high affinity state. The βI domain and αI domain con-

tain a central Mg^{2+} binding site (MIDAS – metal ion dependent adhesion site), important for regulating the switch between the affinity states. There are two flanking additional Ca^{2+} binding sites only present in the βI domain: (**a**) SyMBS (synergistic metal ion binding site) and (**b**) AdMIDAS (adjacent to MIDAS).

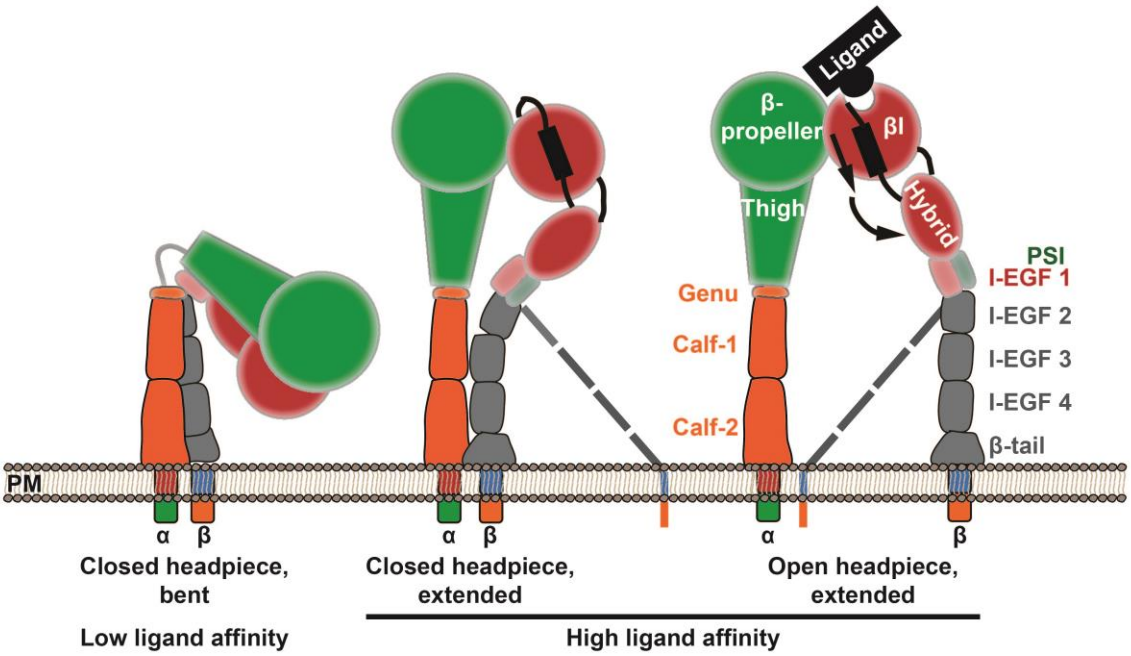

Figure 1. The three overall integrin conformational states.
The bent conformation has a closed headpiece and low affinity for ligand. Extension at the α- and β-knees releases an interface between the headpiece and lower legs and yields an extended-closed conformation. Swing-out of the hybrid domain at its interface with the βI domain is connected through the βI α7-helix (C-terminal of α7-helix of βI domain; black box) at the βI interface with the β-propeller domain that increase affinity for ligand (~1,000-fold) in the extended-open conformation. Two lower β leg conformations (one with a dashed line) are shown for the extended states because of their high flexibility. *(Modified after Luo et al., 2007; Springer and Dustin, 2012; Zhu et al., 2008; Zhu et al., 2013)*

1.1.1.2 Transmembrane and cytoplasmic domains

Integrins are TM receptors lacking enzymatic activity or Actin binding motifs. In order to fulfill their function, integrins have to recruit adaptor and signalling proteins to their cytoplasmic tails, which then trigger posttranslational modifications or interactions with additional proteins that mediate signalling. The membrane-proximal regions of both α- and β-subunits contain highly conserved aa sequences. The cytoplasmic tail of integrin β-subunits, exhibits strong sequence homology, whereas the α-subunit tails show greater variance in sequence apart from the conserved GFFKR motif (De Melker et al., 1997). It was shown with mutation studies that this motif is important for the association with the β-tail (called heterodimerization), because alterations in this motif activate integrins by destabilizing the association of α- and β-TM domain (Lu et al., 2001; O'Toole et al., 1994). However,

in β1 heterodimers tyrosine phosphorylation and the membrane-proximal salt bridge between α and β1 tails have no apparent function under homeostatic conditions *in vivo* (Czuchra et al., 2006). A large number of cytoskeletal and signalling proteins have been reported to bind to β cytoplasmic tails and while only comparably few have been identified to interact with specific α tails (Schiller et al., 2013; Takada et al., 2007). A recognition sequence for phosphotyrosine-binding (PTB) domains is found on most integrin β tails: a membrane proximal NPxY motif and a membrane distal NxxY motif. At these motifs, two integrin activating proteins are known to bind: Talin and Kindlin. Biochemical and crystallographic studies established that a complex is formed between the Talin F3 domain and the membrane proximal NPxY motif in β-integrin tails which is required for the Talin-mediated inside–out activation of integrins *in vitro* and *in vivo* (Calderwood et al., 2013). Kindlin binds the membrane distal NxxY motif in β-integrin tails, whereas the conserved, preceding Thr residues are also important for Kindlin binding. NPxY/NxxY protein sequences can be found in a large variety of cytoskeleton adaptors and signalling proteins, that are necessary to transmit signals from the ECM to the cytoskeleton or are critical for integrin activation (Hynes, 2002).

However, regulation of integrin-ligand interactions is a fine-tuned balance between integrin activation and inactivation. Hereby integrin-inactivating proteins are crucial for appropriate integrin functions *in vitro* and *in vivo* (Bouvard et al., 2013). Proteins mediating integrin inactivation can be classified into two groups: (**a**) Direct integrin binding proteins, which interfere with the recruitment of activators like Talin and Kindlin; and (**b**) proteins which inhibit integrins through alternative mechanisms including those that affect the phosphorylation states and the levels of cell surface integrin by regulating integrin trafficking.

Direct β-tail interactors leading to integrin inactivation (Figure 2): (**a**) NPxY motif binders (Talin competitors): Filamin, exists in an autoinhibited state until tension-induced binding to Actin causes conformational changes that expose several binding sites for integrins (Ehrlicher et al., 2011; Kiema et al., 2006; Pentikainen and Ylanne, 2009). Notably, the structurally defined Filamin binding site overlaps with that of the integrin-regulator Talin, and these proteins compete for binding to integrin tails, and thus influencing Talin-dependent integrin activation. Docking protein 1 (DOK1) contains a phosphotyrosine-binding (PTB) domain capable of binding integrins and inhibit their activity (Calderwood et al., 2003; Wegener et al., 2007). Tyr phosphorylation of the NPxY motif in β1, β3 and β7 integrins by Src kinases greatly increases DOK1 binding to the β-integrin cytoplasmic tail. As the affinity of Talin for integrins decreases upon Tyr phosphorylation, this phosphorylation event might provide a switch for integrin inactivation and a transition from talin-dependent to DOK1-dependent integrin signalling (Oxley et al., 2008). (**b**) Integrin cytoplasmic domain-associated protein 1 (ICAP1) is

a small protein containing also a PTB domain that interacts with the distal NxxY motif of β1 integrin by competing with Kindlin binding. ICAP1 does not bind β3 or β5 integrins (Calderwood et al., 2003; Chang et al., 1997).

Direct α-tail interactors leading to integrin inactivation: Shank-associated RH domain-interacting protein (SHARPIN) is thought to be a key regulator of integrin activity and thus far the only ubiquitously expressed integrin inhibitor that binds to integrin α tails. SHARPIN binds to the highly conserved GFFKR sequence of the α-subunit (Figure 2), suggesting that it inhibits most if not all integrins. By binding to the α tail, SHARPIN inhibits integrin activity through competing with Talin binding to the β integrin tail. This occurs likely by steric hindrance (Rantala et al., 2011). Further, the mammary-derived growth inhibitor (MDGI), was also shown to bind to the α subunit and inhibiting β1 integrin (Nevo et al., 2010).

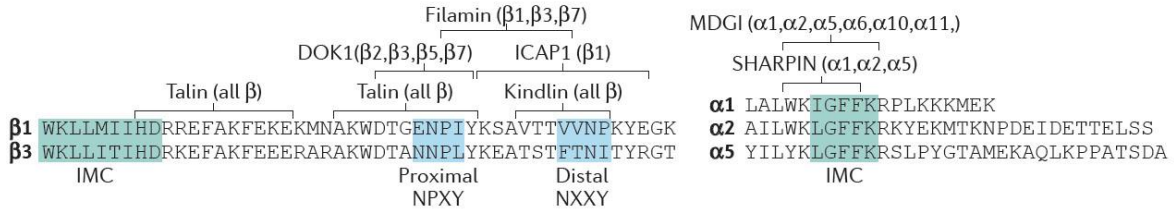

Figure 2. Integrin inactivation.
Binding sites of integrin inhibitory proteins as well as the integrin-activating proteins Talin and Kindlin in the α-integrin or β-integrin cytoplasmic tails. The integrin subunits that bind to each of the integrin-inhibiting or -activating proteins are indicated in brackets. The residues involved in the formation of the inner membrane clasp (IMC) between α and β subunits are shown in green, and the proximal NPxY and distal NxxY motifs are shown in blue. *(Taken from Bouvard et al., 2013)*

Proteins, which alter the phosphorylation status and therefore the functionality of integrins or integrin inactivators: The Tyr residues of NPxY/NxxY motifs and a Ser residue in the β-integrin cytoplasmic tail are phosphorylated in an Src-dependent manner (Sakai et al., 2001). As already mentioned above, DOK1 and ICAP1 contain PTB domains mediating their recruitment to sites which are tyrosine phosphorylated. Interestingly, oncogenic activation of Src can lead to cell rounding resulting of loss of cell adhesion. This promotes the recruitment of DOK1 to the integrin β tails and thus inhibits Talin and Kindlin binding (Bledzka et al., 2010; Oxley et al., 2008). Another example is the phosphorylation state of Thr758 of β2 integrins. Here, the integrin inhibitor Filamin can only bind to the non-phosphorylated β2-tail (Takala et al., 2008). In addition to integrin phosphorylation, phosphorylation of inhibitors regulates their binding to integrins and therefore integrin activation. Filamin is phosphorylated by ribosomal protein S6 kinase 2 (RSK2) in response to adhesion and epidermal growth factor (EGF) stimulation. RSK2 interacts with β1 and β7 integrins via the membrane proximal

NPxY motif. RSK2 becomes activated by phosphorylation through ERK and other kinases leading to Filamin phosphorylation and subsequent integrin inactivation (Gawecka et al., 2012).

Proteins, which affect levels of cell surface integrin by regulating integrin trafficking: Although both ligand-bound and ligand-free integrins can be endocytosed; recycling is faster for inactive integrins. Sortin Nexin 17 (SNX17), for example, is important for controlling the balance between recycling and lysosomal degradation of integrins. Upon endocytosis of integrins Kindlin dissociates from the β1 integrin tail, and Sortin Nexin 17 (SNX17) binds the NxxY motif in early endosomes to promote integrin recycling and prevent degradation (Bottcher et al., 2012).

1.1.2 Members of the integrin superfamily

Members of the integrin superfamily comprise 18 different α- and 8 different β-subunits in mammals. The various combinations of the α and β chains enable cells to form 24 integrin heterodimers, each of them capable of recognizing and adhering to a specific set of ECM proteins (Hynes, 2002), like (**a**) RGD (arginine-glycine-aspartic acid) tripepdide sequence containing ECM proteins, (**b**) Collagen (Coll), (**c**) Laminin (LN), and (**d**) LDV (leucine-aspartic acid-valine) tripeptide motif or structurally related motifs containing proteins.

(**a**) **Integrins bind to the RGD sequence found in ECM components such as FN, VN, Osteopontin, and Thrombospondin.** All αV containing heterodimers (αvβ1, αvβ3, αvβ5, αvβ6 and αvβ8) belong to this group. In addition, α5β1, α8β1 as well as αIIbβ3, an integrin specific for platelets bind to the RGD motif. Although a large number of diverse ligands share this subset of integrins, they exhibit variable affinity for the receptor, probably to the conformation of the RGD fitting into the binding pocket of the integrin headpiece.

(**b**) **Coll binding integrins** are the β1 heterodimers α1β1, α2β1, α10β1 and α11β1. All of these α-subunits contain a special αI domain, critical for ligand binding. Analogous to the β-subunits of αI-less heterodimers, β subunits change the conformation upon activation through Kindlin/Talin. These changes alter the structure of metal ion-dependent adhesion sites (MIDAS) in αI that bind Glu or Asp side chains in extrinsic or intrinsic ligands. Thus, the conformational change results intrinsic ligand binding (ligand analogon) by the β-subunit and a subsequent conformational change within the αI domain leading to integrin activation (Springer and Dustin, 2012). The different heterodimers vary in their preference to different Coll types.

(**c**) **LN binding heterodimers** are α3β1, α6β1, α7β1 together with α6β4 integrins. It has been demonstrated that different regions/motifs exist along LN which are recognized by distinct integrin dimers (Nishiuchi et al. 2006).

(**d**) **Integrins binding to the LDV sequence or structurally related motifs** are α4β7 and αEβ7 heterodimers as well as the β2 heterodimers αLβ2, αMβ2, αXβ2, αDβ2 specific for leucocytes. In addition to FN, this sequence motif is found in VCAM1 (vascular cell adhesion molecule 1), mucosal addressin cell adhesion molecule-1 (MAdCAM-1) and intercellular adhesion molecule 1 (ICAM1). VCAM-1, MAdCAM-1 and ICAM1 are surface proteins expressed by endothelial cells enabling leucocytes to bind to the endothelial layer and transmigrate into the tissue. The related integrins α9β1 and α4β1 can bind FN and VCAM1.

Many integrin heterodimers are essential for development (Bouvard et al., 2001), and under certain (patho-) physiological conditions when cells have to migrate and invade, they change their integrin expression and activation profile (Avraamides et al., 2008; Folkman, 2006; Martin, 1997). For example, the *de novo* expression of the three major FN-binding integrins α5β1 and αVβ3/αVβ5 is associated with, and in some cases crucial for both (tumor-) angiogenesis and skin wound healing. A change in integrin expression patterns and functions is also frequently observed during tumorigenesis (Mizejewski, 1999; Plantefaber and Hynes, 1989). Consequently, various anti-integrin agents, such as monoclonal antibodies and small-molecule inhibitors, are in clinical development for treating solid and hematologic tumors (Junttila and de Sauvage, 2013; Nemeth et al., 2007). It has also been shown that downstream signalling events of two different integrins (α5β1 and αVβ3), even when bound to the same ligand, are profoundly different (Danen et al., 2002; Danen et al., 2005). The molecular mechanisms enabling such selective signal transduction is unclear (Figure 3).

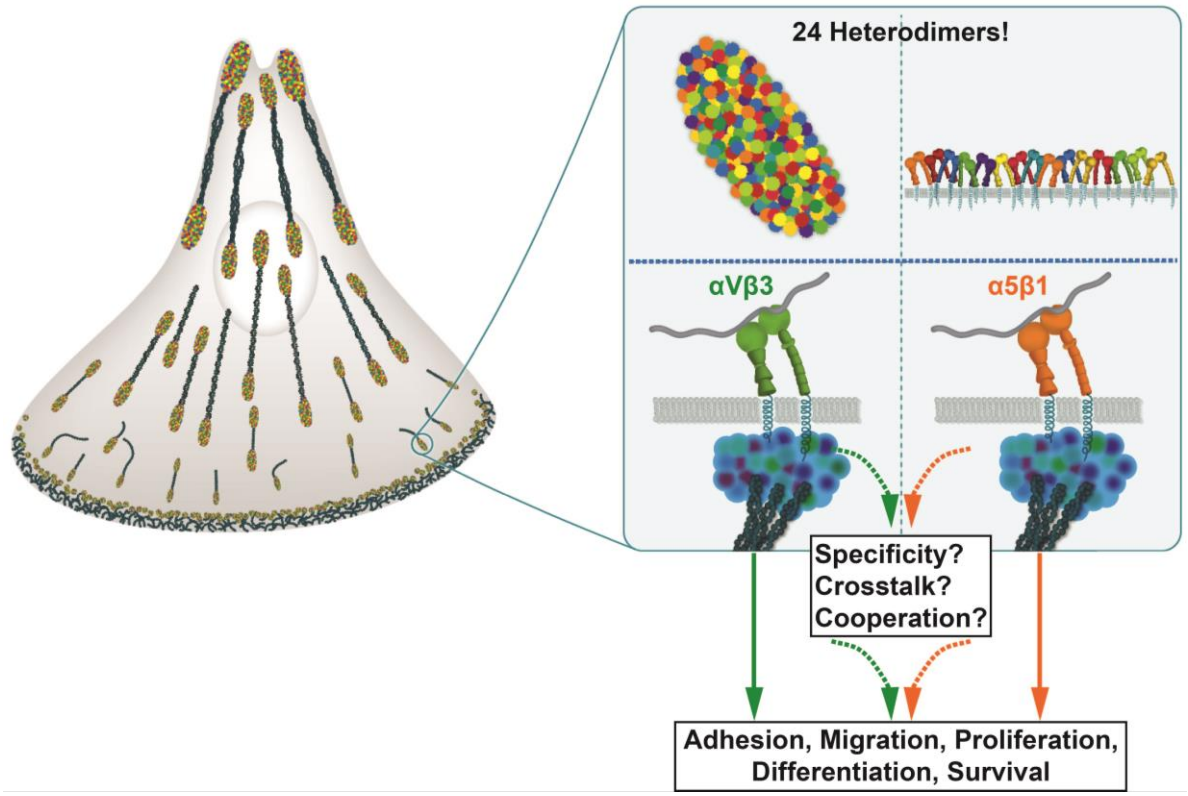

Figure 3. Integrin – Heterodimers, Specificity, Crosstalk and Cooperativity
Mammalian genomes contain 18 α subunit and 8 β subunit genes, and to date 24 different α/β combinations have been identified at the protein level. Heterodimer combinations in focal adhesions are depicted by different colors in a bird`s eye view within a whole cell on the right. Actin connections are presented as blue-lined structures. In the blow up picture the bird`s eye view and intersection of heterodimer combinations are presented in the upper panel. In the lower panel αVβ3 (green) and α5β1 (orange) integrins are shown. Biological processes such as cell migration depend on the integration of signals derived from different integrin heterodimers (e.g. α5β1 and αVβ3). Integrin heterodimer-specific signals could exert trans-dominant effects on or cooperate with other integrin signals. This allows a fine tuning of complex biological responses to the extracellular environment. The molecular details of this complex regulatory system are unknown. *(Modified from drawing by Monika Krause, MPIB, Public Relations)*

An important caveat in most experimental systems used in the past is that αVβ3/αVβ5 and α5β1 are co-expressed on most cells. For instance, during wound repair-induced angiogenesis, endothelial cells up-regulate the expression of αVβ3/αVβ5 and α5β1 and of FN (Brooks et al., 1994; Parsons-Wingerter et al., 2005; Silva et al., 2008). Therefore, it is crucial to reduce this complexity and express both integrins subsets separately in the same cellular background in order to study and comprehend their function.

1.1.3 Bi-directional signalling and Focal Adhesion proteins

As already mentioned above, integrin tails have no catalytic activity of their own, they must bind accessory molecules, which regulate the highly dynamic interactions with f-Actin and orchestrate the cross-talk with growth factor receptor signalling pathways to achieve a desired outcome (Legate et al., 2009). Intracellular changes arising from integrin-ligand binding consist of increased tyrosine phosphorylation of specific substrates, increased formation of lipid second messengers, and cyto-skeletal rearrangements that allow cells to adopt their characteristic shape and initiate migration via dynamic connections between integrins and f-Actin. The interaction between integrins and their various ECM ligands induces so called outside-in signals across the membrane, allowing the cell to sense the extracellular environment. Thus, integrins have the ability to signal in both directions (bi-directionally) across the plasma membrane. Nevertheless, the adhesion force of one integrin is too weak to conduct firm adhesion of the cell to the matrix. Lateral association of integrins to adhesion (termed as clustering) joins numerous weak links to the ECM in a synergistic manner to an accumulated strength of multiple affinities of individual non-covalent binding interactions (termed as avidity). It has been shown, that activation of integrins (Takagi et al., 2001) as well as their clustering (Bunch, 2010) is required for transmitting signals from the ECM into the cell, but how this integrin clustering is mechanistically executed, is not known yet. In one model, freely mobile receptors (integrins) and repellents (local glycocalyx (Ito, 1969)), bring the membrane into contact with a ligand-coated planar surface (ECM proteins) leading to the binding of receptors to the ligands in clusters. Once a stable integrin ligand bond is formed, the local glycocalyx is compressed. Thus adjacent integrins will need less glycocalyx compression to allow binding than distant ones and hence the binding occurs in clusters (Boettiger, 2012).

Integrin outside-in signalling results in downstream signalling events which can be subdivided into three temporal stages (**a, b, c**) (Figure 4):

(**a**) In the first stage up-regulation of lipid kinase activity is initiated leading to elevated levels of PtdIns-4,5-P2 and PtdIns-3,4,5-P3 as well as the induction of rapid phosphorylation and activation of specific protein substrates like important FAK and Src kinases.
(**b**) Phosphorylation of additional FA proteins like Paxillin and activation of signalling pathways like Ras/MAPK, Rho family GTPases and other Actin regulatory proteins is part of the second stage. All this leads to changes in the dynamics and distribution of the Actin cytoskeleton.

(**c**) The last stage represents the long-term consequences of integrin outside-in signalling, like proliferation, cell survival, alterations in cell morphology, as well as changes in the transcriptional program.

What are the integrin adaptor proteins? On the basis of a meta-study of the cell-adhesion literature around 180 proteins, including adapters, kinases, phosphatases and various other classes of proteins were compiled to be associated with FAs either constitutively or transiently (Zaidel-Bar and Geiger, 2010; Zaidel-Bar et al., 2007). In studies of adhesion protein isolations, 905 focal adhesion proteins were identified. Hereby 459 proteins changed in abundance with Myosin II inhibition, defining the myosin-II-responsive focal adhesion proteome (Kuo et al., 2011). In a parallel study by the use of chemical crosslinkers, 87 adhesion proteins (termed also as adhesome) were detected in kidney fibroblasts, where a subgroup of 64 proteins was found to be enriched on FN and along these set 40 proteins were myosin-II-responsive (Schiller et al., 2011).

The linker proteins connecting the cytoplasmic integrin domains to the cytoskeleton are multiple and their interaction is complex. The major signal transduction pathways and their key players are depicted in Figure 3. These proteins often act in concert with G protein-coupled or kinase receptors (Hynes, 2002; Shen et al., 2012). The major sub-membranous, integrin-associated links between integrins and these signal transduction pathways are shown within the “cloud” representing the adhesome structure and in the grey arrows, respectively (Figure 4). Since the main focus of the second manuscript is how cytoskeletal organization can alter the cells` transcriptome, involved proteins and signalling processes will be presented in more detail below.

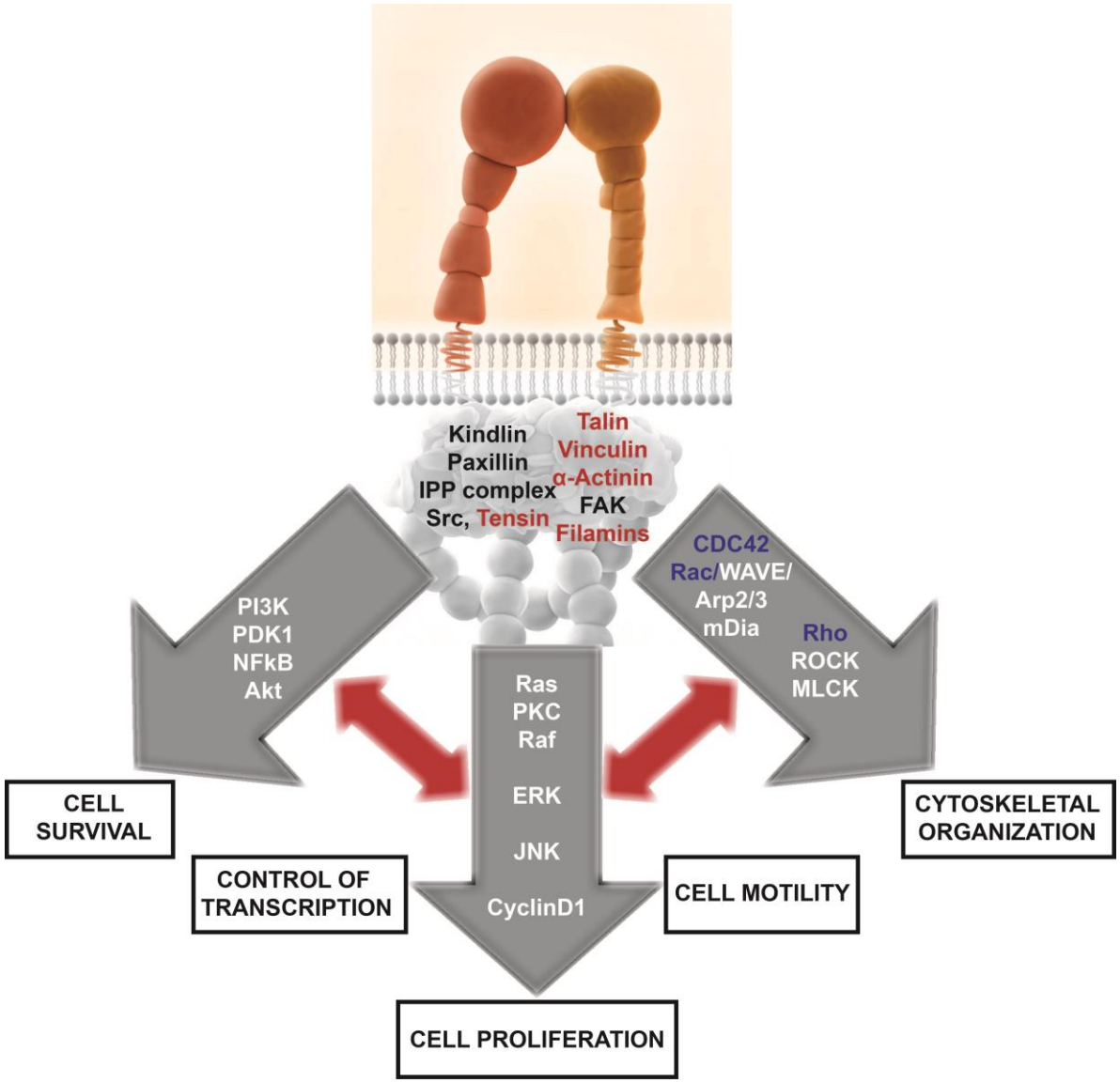

Figure 4. Outside-in signalling
Depicted are the major signal pathways and key players. They often act in concert with G protein-coupled or kinase receptors. The major integrin associated proteins are highlighted in the adhesome structure beneath the clustered integrins. Direct actin binding proteins are highlighted in red. *(Modified after Hynes, 2002)*

1.1.4 Actin binding through integrins and the importance of mechanotransduction

The major structural role of integrins is to mediate the connection of the extracellular matrix environment to the Actin cytoskeleton. This can be achieved by a variety of actin-binding proteins that bind integrins either directly or indirectly.

Direct actin-binding proteins include Talin (Critchley, 2000), Filamin (van der Flier and Sonnenberg, 2001), α-Actinin (Otey et al., 1993), Tensin (Lo, 2004) and Vinculin (Humphries et al., 2007). All of these proteins bind directly to the β tail, with the exception of Vinculin, which binds which interacts with integrins via Talin. Further contribution to this connection is achieved by integrin-bound pro-

teins that indirectly associate with the cytoskeleton or participate in its regulation such as Kindlin, IPP complex members, Paxillin, and FAK. A third group of proteins which regulate the interactions of the proteins above are a plethora of additional adaptor and signalling molecules (Figure 4).

During the formation of focal adhesions, the first linkage to the cytoskeleton after integrin-ligand-binding is the recruitment of Talin to the NPxY motif of integrin β tails. Thereby, a talin-dependent 2-pN slip bond is established, providing the initial force from the cytoskeleton to the ECM (Jiang et al., 2003). Since Talin is an important protein in the induction of integrin signalling and mechanical coupling, Figure 5 is presented to summarize modes how it can be activated.

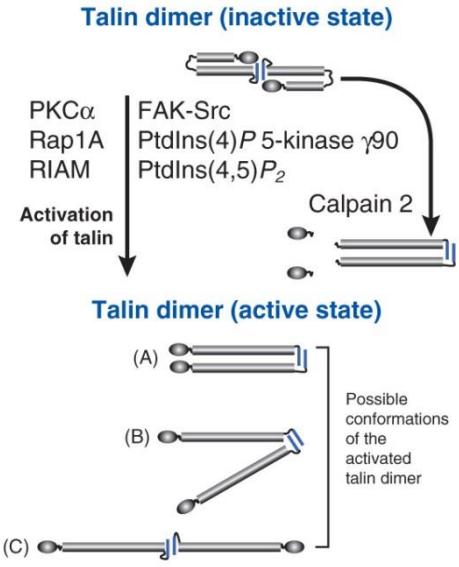

Figure 5. Talin activation

The majority of Talin exists in an inactive cytosolic pool and the Rap1-interacting adaptor molecule (RIAM) has been implicated in Talin activation. Further integrin signalling via FAK and Src promotes binding of PIPK1γ90 to the Talin F3 subdomain, the activation of PIPK1 γ 90 and translocation of the PIPK1γ90-talin complex to the plasma membrane. The Talin head binds acidic phospholipids, and PtdIns(4,5)P2 has been shown to activate the integrin-binding sites in Talin. Calpain 2 also increases the binding of Talin to integrins in vitro. *(Taken from Critchley and Gingras, 2008)*

Next, **Vinculin** is recruited to LxxAAxxVAxxVxxLIxxA motifs in the rod of Talin (Critchley and Gingras, 2008). These binding sites are usually masked (termed as cryptic binding site) and buried in the core of a series of helical bundles and probably mechanical stretch is required for exposing these sites. Along with this finding, expression of just Talin head in Talin knockout cells, activates integrins but fails to form detectable focal contacts because the Vinculin binding site is missing and thus the link to the actin cannot be properly established (Zhang et al., 2008). This suggests that Talin is required for the initial contacts, whereas Vinculin, by binding of Actin and Talin, is critical for maintaining and strengthening this connection. Interestingly, Talin owns a cryptic Actin binding site (ABS) in the C-terminal region of its rod domain. This Talin/HIP1R/Sla2p actin-tethering C-terminal homology (THATCH) is required for dimer formation (Gingras et al., 2008). Interestingly, Actin binds by an unknown mechanism only to a THATCH dimer, and thus binding of Talin to f-Actin is linked to its dimerization.

As force is generated, another Actin binding protein, α-Actinin, is recruited to focal adhesions (Laukaitis et al., 2001) via Vinculin, Talin and direct β-integrin interactions. Besides α-Actinin, α-Parvin uses an α-Actinin-like Actin binding domain to bind f-Actin which consists of two in tandem arranged Calponin homology (CH)-domains (Olski et al., 2001). Together with ILK and PINCH, it constitutes a protein hub termed as IPP (ILK/PINCH/Parvin) complex. The link to the integrin β-tails is hereby made by ILK which also binds to Paxillin, a direct integrin binder. The IPP complex exemplifies the elaborate interactions of FA proteins linking integrins to the Actin cytoskeleton.

Although sophisticated, there is order to these interactions. A topographical study (using high resolution microscopy) revealed that integrins and Actin are vertically separated by a 40-nm focal adhesion core region consisting of a membrane apposed integrin signalling layer (integrin cytoplasmic tails, FAK, Paxillin), an intermediate force transduction layer (Talin and Vinculin), and an uppermost actin-regulatory layer (Zyxin, VASP, α-Actinin) (Kanchanawong et al., 2010).

The connection of the ECM to the Actin cytoskeleton is one crucial task of integrins, it serves to convert mechanical stimuli into chemical activity, a process termed mechanotransduction. Already at the very beginning of integrin signalling, with the recruitment of Talin and opening of its cryptic binding sites for Vinculin and Actin binding (mentioned above), mechanical tension plays an essential role. Several other signalling proteins, like Src, P130Cas (130 KDa Crk-associated substrate) (Sawada et al., 2006) and Vinculin, exhibit also tension-dependent conformational changes that influence their kinase activity, availability of cryptic phosphorylation sites, or target the protein to a specific site (membrane, lysosome, etc.) within the cell (termed as intracellular compartimentalization) (Moore et al., 2010; Riveline et al., 2001; Sawada et al., 2006). A number of enzymes are known to change their kinetics due to mechanical stimulation. The focal adhesion kinase (FAK) for example is autoinhibited by its FERM domain, which maintains FAK in an underphosphorylated state. Autophosphorylation of FAK at Y397 is critical for many FAK-dependent functions, including phosphorylation of FAK on other residues. In addition, phosphorylation of Y397 creates a binding site for several SH2 domain-containing molecules, including phosphatidylinositol 3-kinase and Src. Importantly, these intramolecular interactions require mechanical activation of FAK in order to carry out its kinase function (Cooper et al., 2003). This is particularly relevant because loss of FAK inhibits the cells` ability to sense collagen stiffness (Li et al., 2002). Another example is the receptor-like tyrosine phosphatase α (RPTP-α) which interacts with αVβ3/αVβ5 integrins. Upon force application through FN-integrin binding an activation of downstream Src family kinases can occur (von Wichert et al., 2003) (Zheng et al., 2000).

Thus a variety of primary force-sensing mechanisms could be postulated, including opening of cryptic binding sites along cytoplasmic proteins, activation of ion channels, and formation of force-

stabilized receptor-ligand bonds (catch bonds) (Vogel and Sheetz, 2006), which would then activate downstream signalling pathways. However, the molecular mechanisms underlying the connection between mechanical elements and chemical signalling processes are still poorly understood.

1.1.5 Proteins and signalling processes mediating actin distribution and dynamics

The local accumulation of f-Actin in the form of a dense stress fiber template at the focal adhesion plaque was shown to facilitate not only the recruitment and stable association of FA proteins (Oakes et al., 2012) but also the well-controlled formation of cell protrusion/retraction during cell migration, cell morphology regulation, wound healing as well as cell contractility and matrix degradation.

1.1.5.1 Types of Actin-rich protrusions

To fulfil these listed functions, motile, invasive cells like cancer cells and fibroblasts express different types of actin-rich protrusions when plated on a two-dimensional surface:

(**a**) **Lamellipodia** (from Latin "*lamina"*, which means "*thin sheet"*, and "*pod"*, which stands for "*foot"*) form at the leading edge of cells, consisting of a dendritic Actin network in a thin membrane leaflet.

(**b**) **Filopodia** (or microspikes), are fine cytoplasmic projections which extend beyond the leading edge of lamellipodia in migrating cells. They are thought to be involved in sensation of chemical cues and directed cell movement.

(**c**) **Circular dorsal ruffles** are characterized as f-Actin-rich membrane projections on the apical cell surface and appear as highly dynamic "rings" which then mature and contract centrifugally before subsiding. They are thought to conduct a critical role in receptor internalization and cell migration.

1.1.5.2 Actin modifying proteins

To build the above mentioned Actin structures, various Actin binding proteins (ABPs) intersect, thereby regulating both the assembly and disassembly of globular (g)-Actin into filamentous (f)-Actin in a process called Actin (de-)polymerization.

As short dimeric or trimeric Actin intermediates are very unstable, this process is highly dependent on the presence of Actin nucleating proteins. One important nucleating factor is the Arp2/3 complex, which mimics a g-Actin dimer in order to stimulate the nucleation of g-Actin necessary for polymer growing. However, the isolated Arp2/3 complex has no endogenous actin nucleating activity and must be activated by the Wiskott-Aldrich Syndrome protein (WASP) family members (like Neu-

ronal (N)--WASP, WAVE, WASH) of activator proteins. Although full-length WASP is less effective, its activity can be greatly enhanced by Rho family GTPases (see below) and phosphatidylinositol (4,5) bisphosphate causing the WASP protein to expose a domain that binds and thus activates the Arp2/3 complex (Rohatgi et al., 1999). WASP binding leads to a conformational change in Arp2/3 which can then form a nucleation core for Actin filament elongation. Arp2/3 is recruited to nascent integrin adhesions through interactions with FAK as well as Vinculin to promote Actin polymerization directly at the site of adhesion (DeMali et al., 2003). Interestingly, Arp2/3 on the other hand si also required to form NAs. There exists apparently a positive forward loop between these molecular complexes.

To generate force and move membranes, the Arp2/3 complex must collaborate with other actin-associated proteins, including Capping protein (CP), ADF/Cofilin, Profilin, and Thymosin. CP, which is also known as β-Actinin, or CapZ in skeletal muscle, is an αβ heterodimer. CP caps the barbed ends of the Actin filament with high affinity, thereby preventing the addition or loss of Actin subunits (called Actin capping) (Wear and Cooper, 2004). ADF/Cofilin belong to a family of actin-binding proteins which bind g-Actin monomers and depolymerize Actin filaments by providing free barbed ends for further polymerization (termed as Actin severing) and increasing the off-rate for actin monomers from the minus end (Actin depolymerizing).

Actin assembly is further regulated by a selective interaction of Actin monomers with specific molecules that inhibit or promote their polymerization (termed Actin sequestering) by preventing their access to other monomers thus regulating Actin pool composition. Two important sequestering factors are Profilin and Thymosin β4 (Tβ4). Profilin binds to monomeric Actin by occupying an Actin-Actin contact site which leads to removal of Actin from the pool of polymerizable Actin monomers. However, Profilin also catalyzes the exchange of actin-bound ADP to ATP thereby converting poorly polymerizing ADP-Actin monomers into readily polymerizing ATP-actin monomers. Tβ4, originally isolated from the thymus, forms a 1:1 complex with g-Actin to buffer the polymerization process. This buffering is achieved by maintaining a large pool of Actin monomers through Tβ4 interaction and thus controlling the assembly and disassembly of Actin filaments that regulate the dynamics of the Actin cytoskeleton (Hertzog et al., 2004). Since one of my manuscripts are about MAL/SRF transcriptional regulation I will shortly introduce the influence of Profilin and Tβ4 on MAL-g-Actin interaction. The megakaryocyte acute leukemia protein (MAL) binds via its RPEL motif to g-Actin. Through this interaction, MAL translocation into the nucleus is inhibited. If it is unbound and translocates, MAL binds the transcription factor serum response factor (SRF) in order to initiate transcription of target genes. Interestingly, Posern et al. reported that Profilin bound g-Actin cannot interact with MAL anymore (Posern et al., 2002). Further, crystal structure analysis revealed unexpected similarity

between RPEL motif (found in MAL) and the Actin contacts of vitamin D-binding protein (DBP) (Mouilleron et al., 2008). DBPs is a large multi-domain actin-sequestering protein quite unrelated to the RPEL motif (Otterbein et al., 2002). The area of Actin covered by DBP within the complex approximately equals the sum of those covered by Profilin and most likely also by Tβ4 (Morita and Hayashi, 2013). *In vivo* and *in vitro* experiments have shown that administration of Tβ4 can promote migration of cells, formation of blood vessels, maturation and differentiation of stem cells, survival of various cell types and lowering of the production of pro-inflammatory cytokines. It is believed that these short- and long-term effects on cell behavior are due to the maintenance of a dynamic equilibrium between g- and f-Actin (Crockford et al., 2010). Thus it is possible that Tβ4-mediated release of MAL regulates cytoskeletal dynamics and adhesion through SRF/MAL mediated gene transcription.

On top of this, Actin crosslinking proteins (for example, α-Actinin and Filamin) can arrange f-Actin into distinct networks, such as Actin bundles. In the region directly behind the lamellopodium (this area termed as the lamellum), Actin is organized into parallel bundles to establish directed cell motility and cell stability. There, Actin assembly is mediated by the diaphanous-related formin (DRF) protein family of Actin polymerizing factors, including mDia or Ena/VASP, which associate with the fast-growing end (barbed end) of Actin filaments. Formins also prevent the binding of capping proteins to the barbed ends of Actin and thus inhibit further polymerization (Zigmond, 2004).

As already mentioned above, these processes are highly coordinated by an important group of small G proteins with 20–25 kDa in size: the Rho family of GTPases (Figure 6). The Rho family is a subfamily of the Ras (Rat sarcoma) protein family. Among them Cdc42, RhoA and Rac are the most important members. Rho family GTPases are active when GTP-bound and inactive when bound to GDP. Activation is catalyzed by guanine nucleotide exchange factors (GEFs) and inactivation is promoted by GTPase activating proteins (GAPs) that stimulate the intrinsic GTPase activity of the Rho proteins. Further regulation is conducted by Rho-GDP dissociation inhibitors (Rho-GDIs), which sequester inactive GDP-bound Rho-GTPases in the cytoplasm and thus removing them from their activation cycle by GEFs at the plasma membrane (PM). Rho-GDIs also mediate the cycling of Rho proteins between the cytosol and the membrane. Rho proteins contain a conserved CAAX sequence at the C terminus, which is modified by isoprenylation (through the addition of a geranyl geranyl moiety in the case of RhoA, Rac1 and Cdc42) of the cysteine residue (Seabra, 1998). The binding of Rho GTPases to effector proteins regulates Actin reorganization, in addition to other crucial biological events, such as gene expression and cell growth (Bishop and Hall, 2000). The influence of integrins on Rho GTPase signalling is exemplified by Rac binding sites, which can be found within cholesterol-rich membrane domains, are internalized when cells are deprived of adhesion. Endocytosis of these domains is me-

diated by caveolae and regulated Caveolin-1 phosphorylated at tyrosine-14. Further, Cdc42 also requires integrin-mediated adhesion for translocation to membranes. This mechanism can account for the control of multiple pathways by integrins, thus providing an important mechanism for anchorage dependence of growth (Del Pozo et al., 2002; Del Pozo and Schwartz, 2007).

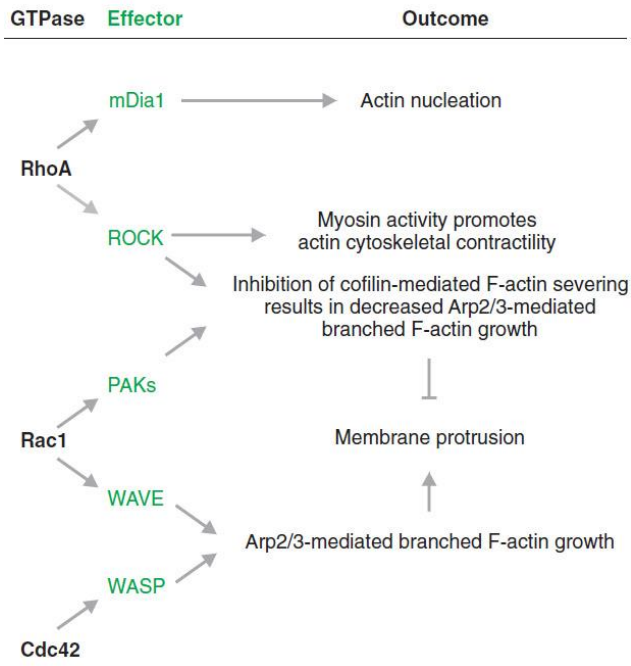

Figure 6. Overview of Rho-GTPases and the effector pathways that act downstream of integrins in order to regulate Actin
Through the recruitment and activation of different effector proteins (indicated in green), Rho-GTPases regulate the Actin cytoskeletal dynamics that are required for membrane protrusions and/or cytoskeletal contractility. *(Modified after Huveneers and Danen, 2009)*

While lamellipodia are built in a Rac and Arp2/3-complex-dependent fashion, filopodia rely on the activity of Cdc42, Ena/VASP family formins (Figure 6). The formation of stress fibers and the retraction of the cellular rear are mediated by RhoA (Hall, 2012; Ridley and Hall, 1992).

1.1.6 Temporal short- and long-term effects by integrin mediated Actin dynamics

The above described actin-based features of a cell account for and react to the properties of a certain microenvironment (e.g. elasticity and ECM composition) via mechanosensitive proteins that are subject to molecular forces thereby activating signalling pathways. This bi-directional interplay between the microenvironment and cellular mechanosensation is increasingly recognized as potent regulators of cell decisions that affect proliferation, migration, stem cell identity, apoptosis, and cell fate (Halder et al., 2012). Forces are constantly transmitted across cell-ECM and cell-cell adhesion sites leading to an adaptation to these external mechanical stimuli by adjusting the stiffness of the cells´ cytoskeleton (Janmey and Miller, 2011; Parsons et al., 2010; Vogel and Sheetz, 2006). Hereby integrins promote bundling of Actin filaments and activate Myosin II to generate intracellular tension. Reciprocally, the activity of Actin modifying proteins, the rate of Actin (de-)polymerization and spatial Actin organization influences integrin function and thus the adhesive state of a cell (Gardel et

al., 2010). **The effects of integrin mediated tensile forces can be temporally subdivided into short- and long-term effects of signalling:**

Short-term effects of integrin signalling consist of cytoskeletal rearrangements that allow cells to adopt their characteristic shape and initiate migration. ECM stiffness sensed by integrins promotes focal adhesion assembly and activation of the Rho family of GTPases. RhoA functions via Rho kinase (ROCK) to regulate myosin light chain phosphorylation through inhibitory phosphorylation of Myosin phosphatase which results in actin-myosin interaction and cell contractility. Actin modifying molecules, like (de-)polymerizing, capping and severing proteins, intersect and modulate these immediate adhesion induced signalling effects further.

Long-term effects of integrin signalling result from changes in gene expression, which regulate cell proliferation and differentiation. Integrin-dependent regulation of gene expression has primarily been thought to arise from cross-talk between the Rho-ROCK pathway and the epidermal growth-factor receptor (EGFR), which will lead to oncogene (Ras)-driven extracellular-signal-regulated kinase (ERK) activation and the subsequent activation of mitogen activating protein (MAP) kinase pathways (Jaalouk and Lammerding, 2009). A recent study, reported that β1-class integrins can change gene programs of mesenchymal stem cells involved in lineage commitment to bone, fat or cartilage by activating Rho GTPase signalling cascades, which result in the nuclear localization of the transcriptional co-activators Yes-associated protein (YAP) and transcriptional co-activator with PDZ-binding motif (TAZ) (Tang et al., 2013). Another study identified Actin modifying proteins as essential gatekeepers limiting YAP/TAZ activity in cells experiencing low mechanical load, including attenuation of proliferation by contact inhibition (Aragona et al., 2013). YAP (Yes-associated protein)/TAZ (transcriptional co-activator with PDZ-binding motif) are classically regulated by the Hippo cascade but also WNT and GPCR signalling were identified to modulate these co-activators of transcription (Azzolin et al., 2012; Pan, 2010; Yu et al., 2012).

In addition to the control of YAP/TAZ, Rho family GTPases can also control gene transcription by releasing the association of the transcriptional co-activator MAL (megakaryocyte acute leukemia protein; also known as MRTF-A and MKL1) from monomeric or globular (g-) Actin. Once g-Actin is assembled into Actin networks, free MAL translocates into the nucleus, where it associates with and activates the transcription factor serum response factor (SRF), which regulates mainly the expression of cytoskeletal proteins including Actin and FA proteins including Vinculin, Talin and integrins. Thus it is possible that integrin-mediated activation of Rho GTPases regulates cytoskeletal dynamics and adhesion through both effector proteins and the nuclear localisation and activation of MAL.

1.2 Fibronectin and its major integrin receptors

1.2.1 Fibronectin – Assembly and features

The extracellular matrix (ECM) constitutes the filling element in all tissues and organs and in addition, provides a physical scaffolding for cells and initiates crucial biochemical and biomechanical signals necessary for tissue morphogenesis, differentiation and homeostasis (Frantz et al., 2010). A major fraction of the ECM is composed of Collagens, Laminins and other glycoproteins such as FN, which serve as substrates for different adhesion molecules including integrins. Importantly, ECM components, especially FN are secreted by cells as non-functional building units, which assemble into functional supra-molecular structures in a highly regulated manner (Erickson and Carrell, 1983; Rocco et al., 1983).

In this hierarchical assembling process, FN fulfills several features: FN fibrills

(**a**) possess binding sites for multiple ECM components (Figure 7), which are used to assist in the assembly of several other ECM proteins (Dallas et al., 2006; Dallas et al., 2005; Sabatier et al., 2009), such as collagen types 1 and 3 (Kadler et al., 2008; Leiss et al., 2008); Therefore proper FN deposition and assembly might be essential to physiological and pathophysiological cell invasion by cross-linking the ECM and by providing a sufficiently dense scaffold for enabling cell migration.

(**b**) provide at the same time structural support for cell adhesion and integrins, thereby translating biomechanical into biochemical downstream signals (Mao and Schwarzbauer, 2005);

(**c**) control the availability of growth factors, for example by regulating their activation from latent complexes as shown for TGF-β (Fontana et al., 2005);

FN matrix assembly (termed as fibrillogenesis) is a multistep, integrin-dependent process. Among the FN-binding integrins, α5β1 is considered of major importance for the formation of an elaborate meshwork of FN fibrils (Fogerty et al., 1990; Leiss et al., 2008; McDonald et al., 1987). The α5β1 heterodimer binds FN, transduces a pulling force onto focal adhesions which leads to integrin separation, as α5β1 integrin is transported rearward along Actin stress fibers towards the cell centre. This leads to the growth of a adhesion structures called fibrillar adhesions (Ali and Hynes, 1978; Wu et al., 1995), where FN fibrils are aligned with α5β1 integrins, f-Actin filaments and multiple signalling molecules (Ohashi et al., 2002; Pankov et al., 2000; Zamir et al., 2000). This transduced mechanical stress seems to be a prerequisite for FN assembly, because treatments inducing higher contractile forces within the cell stimulate matrix assembly, whereas inhibition ofMyosin light chain kinase or RhoA GTPase reduces assembly (Zhang et al., 1994; Zhang et al., 1997; Zhong et al., 1998). Further-

more, it was shown that cells grown on rigid substrates stimulate Rho/ROCK and FN matrix assembly while cultures on soft substrates fail to do so (Carraher and Schwarzbauer, 2013).

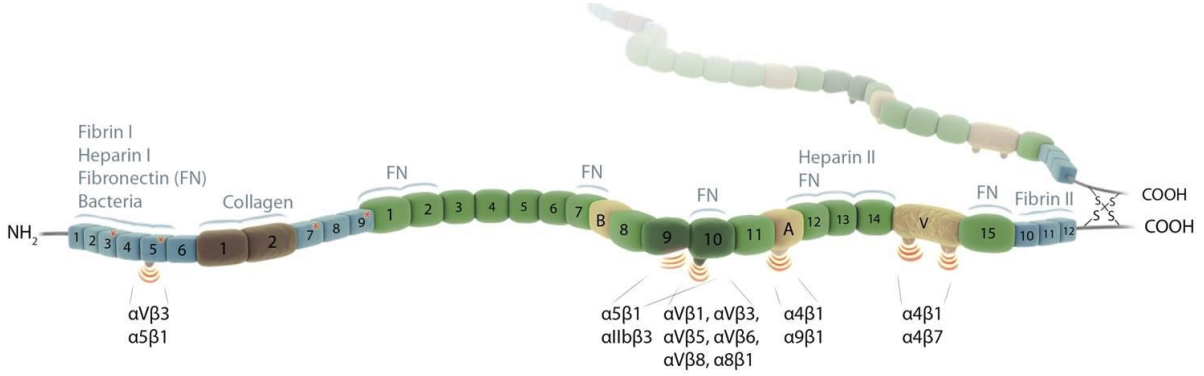

Figure 7. The modular structure of fibronectin
Numerous cell types synthesize and secrete FN as a disulfide-bonded dimer composed of 230–270 kDa subunits. These subunits comprise functional domains that mediate interactions with other ECM components, with cell surface receptors, GFs and with FN itself. FN consists of three different modules (type I, blue; type II, brown; type III, green). The dimer forms via two disulfide bonds at the C-terminus. Integrin binding sites are indicated. Binding domains for FN, Collagen, Fibrin, Heparin and bacteria are indicated. Note that the α5β1 as well as the αIIbβ3 integrins are believed to require the synergy region to bind to the RGD motif. *(Taken from Leiss et al., 2008)*

1.2.2 The role of Fibronectin in mouse development

Considering the multiple features and functions of FN, it is not surprising that its constitutive gene ablation in mice has dramatic consequences *in vivo*. As FN null embryos die because of defects in mesoderm and neo-vessel formation, I will first define what these structures are.

"It is not birth, marriage, or death, but gastrulation, which is truly the most important time in your life." Lewis Wolpert (1986)

Gastrulation is a phase in early embryonic development, during which the single-layered hollow sphere of cells (called blastomeres) surrounding an inner fluid-filled cavity (this fluid filed cavity is referred as blastocoel) forms (this whole structure is termed as blastocyst). The “single-layered” blastocyst is then reorganized into a "three-layered" structure known as the gastrula. These three germ layers are known as the ectoderm, mesoderm, and endoderm. The endoderm is the most internal germ layer, which gives rise to the lining of the gut and other internal organs. The ectoderm instead, lies most exterior and forms skin, brain, the nervous system, and other external tissues. The middle germ layer is called mesoderm. The mesoderm will differentiate into cells of the muscular, skeletal and the vascular systems. Thus, the primary function of gastrulation is the correct placement of precursor tissues for subsequent morphogenesis (Tam and Behringer, 1997).

During *de novo* vessel formation endothelial progenitor cells (so called angioblasts) differentiate to endothelial cells and form a primitive vascular plexus (this process is referred as vasculogenesis) (Figure 8). Angiogenesis leads to formation of new vessels from pre-existing capillaries in two different ways: Either through sprouting of capillaries or through splitting of a capillary into two. Growth factors including VEGF, TGF-β, FGF and PDGF, and importantly integrin interactions with a fibrillar FN matrix, in which the endothelial cells are embedded, are indispensable for proper new vessel formation.

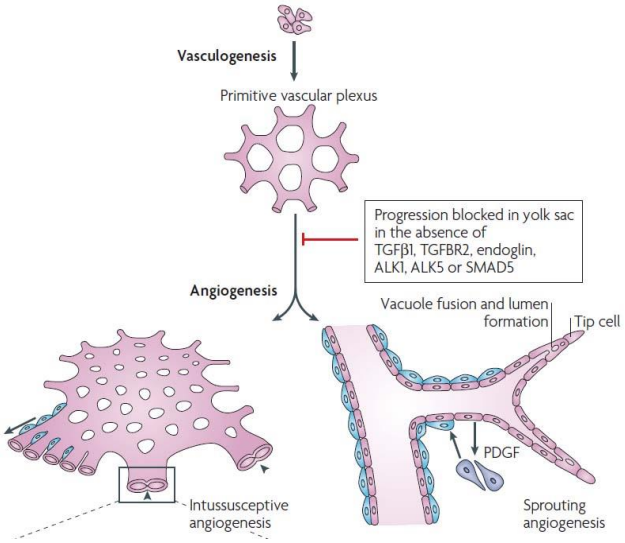

Figure 8. Neo-vasculogenesis
Vasculogenesis and two types of angiogenesis are shown: intussusceptive (means the process of blood vessel growth by splitting) and sprouting angiogenesis. *(Modified after ten Dijke and Arthur, 2007)*

The expression of FN in mice initiates at the blastocyst stage and remains later in gastrulation, FN expression is mainly localized to the ectodermal-mesodermal interface, where it may promote the migration of mesodermal cells (Smith et al., 1990). Targeted inactivation of the FN gene in mice leads to early embryonic lethality around embryonic day (E) 8.5 due to severe defects in the development of the mesoderm and mesoderm-derived tissues. Until E 7.5 in FN null embryos the three germlayers and the morphology of extraembryonic membranes seems to develop normally. Abnormalities are first visible by E 8.0 and are manifested by shortened anterior-posterior axis, a deficient head and vessel mesoderm, a disorganized notochord and a complete absence of somites. At E 8.5, the anterior-posterior axis is even more shortened and the head-folds have arrested development and appear distorted. In summary, the observed defects are proving the essential requirement of FN for normal development and in particular for the development of mesoderm-derived tissues. Interestingly, genetic interactions are important for FN function *in vivo*, as the genetic ablation on 129/Sv compared to C57/BL6 genetic background is more severe (George et al., 1997; George et al., 1993; Georges-Labouesse et al., 1996).

1.2.3 The major Fibronectin receptors

1.2.3.1 The β1-class of integrins

β1 heterodimers constitute the largest subfamily with 12 heterodimers (Figure 9). The critical roles of β1 integrins in development are reported by the phenotypic observations produced by a homozygous null mutation of the β1 subunit (Fassler and Meyer, 1995). This knockout results in very early embryonic lethality at day E 5.5 through defects in gastrulation. The dramatic phenotype of β1 null homozygotes does not appear to result from an absolute requirement for β1 integrins in cell survival or differentiation, since experiments with chimeric mice derived from a mixture of marked β1 null cells and wild type cells revealed that β1 null cells can contribute to all mature to all organs except liver and spleen (Fassler and Meyer, 1995), indicating critical roles of specific β1 heterodimers at early stages in development.

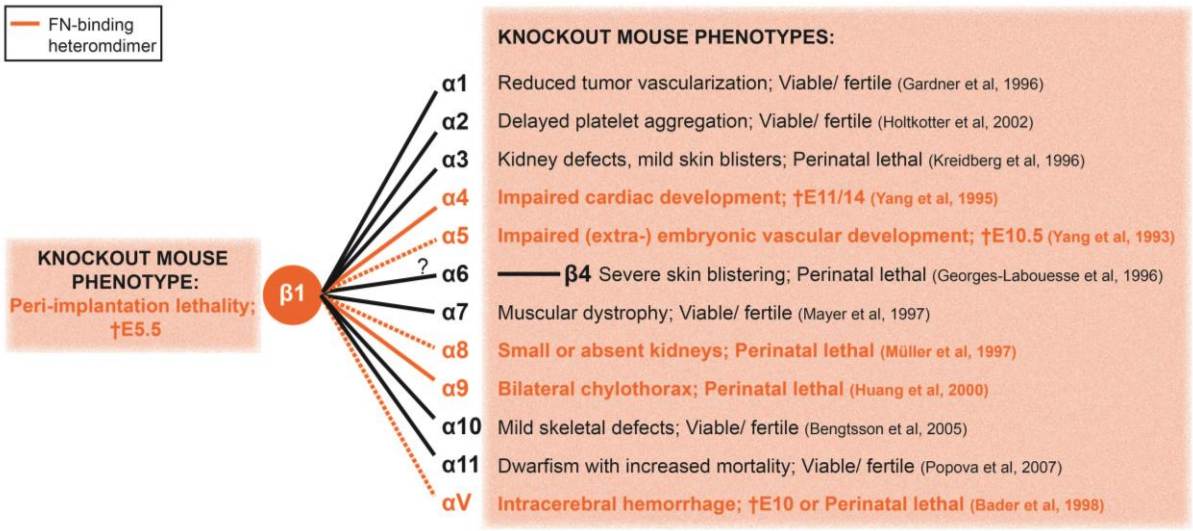

Figure 9. The β1-subfamily
The 12 β1-containing heterodimers constitute the largest integrin family. FN-binding heterodimers are marked in orange letters/lines. RGD binding dimers are marked with dashed lines. Their most important respective knockout phenotypes with references are described in the boxes.

Among the β1 heterodimers are five integrins capable of binding to FN (Figure 9). Of these, α5β1, α8β1 and αVβ1 recognize the RGD sequence in ECM proteins such as FN and VN. The α4β1 and α9β1 dimers bind to other sequences next to the RGD site in FN molecules (see also Figure 7).

1.2.3.2 The αV-class of integrins

αV-class integrins consist of five heterodimers, namely αVβ1, αVβ3, αVβ5, αVβ6 and αVβ8 (Figure 10) and one additional integrin, αIIbβ3, found on platelets. All of these members recognize the RGD motif in multiple ligands (Hynes, 2002). Crystal structures of αVβ3 and αIIbβ3 complexed with RGD ligands have revealed an identical atomic basis for this interaction (Xiong et al., 2002). Each αVβx heterodimer has a unique pattern of cell and tissue distribution. Based on *in vivo* observations and *in vitro* studies utilizing blocking antibodies and peptides, specific αV-class integrins have been suggested to play critical roles in diverse biologic processes including embryo implantation, angiogenesis, and wound healing. However, in contrast to mice lacking β1 integrins, mice lacking the αV subunit, and therefore lacking five of the six integrins in this family, survive until E 10 or perinatal due to abnormal blood vessel formation in the head region but also due to severe placenta defects at E 10 (Bader et al., 1998; Reynolds et al., 2002) (Figure 10). A subset of animals can even proceed through embryonic development and die after birth because of hemorrhages, indicating that, unlike α5, αV integrins are dispensable for vasculogenesis and partly also for angiogenesis (Bader et al., 1998).

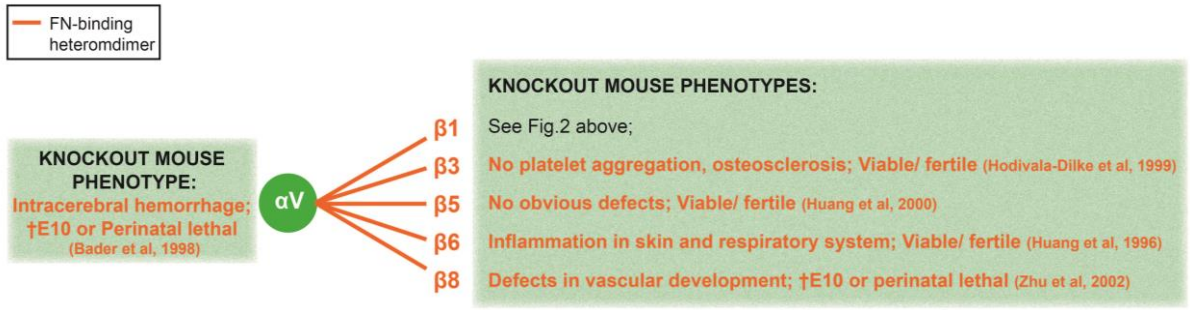

Figure 10. The αV-subfamily
The 5 αV-containing heterodimers recognize the RGD motif and can therefore bind to FN. Their respective knockout phenotypes with references are described in the boxes.

Although the α5β1 integrin is considered the major integrin responsible for FN assembly (Fogerty et al., 1990; McDonald et al., 1987), and its interaction with the RGD motif is required for this function, integrins of the αV subfamily can also compose FN into fibrils. This statement is corroborated by the phenotype observed in integrin α5-null mice. This deletion also leads to embryonic lethality and vascular defects, but these mice develop significantly further (until E 10.5) than the FN-null mice (Yang and Hynes, 1996; Yang et al., 1993). Only a double knockout of the αV and α5 integrin genes result in a loss of FN fibrillogenesis (Yang et al., 1999). Interestingly, although the RGD motif is central for the interaction of FN with α5β1 and αVβ3, the inactivation of this motif by a RGD to RGE

point mutation also allows FN fibrillogenesis *in vivo*. The knock-in mice carrying this mutation display a phenotype closely resembling that of the α5-null mice (Takahashi et al., 2007). This highlights the importance of this motif in FN signalling through α5β1, but also shows the ability of other integrin interaction sites on FN to take over the role of RGD in FN fibrillogenesis.

Altogether these studies imply overlapping and independent functions of α5β1 and αVβ3 in early mesodermal development (Yang et al., 1999).

1.3 The concept of receptor cross-talk

Cell surface receptors bind ligands expressed on other cells *(in trans)* in order to communicate with neighboring cells. However, an increasing number of cell surface receptors are found to also interact with ligands expressed on the same cell *(in cis)*. Integrins can interact with molecules on neighbouring cells or ECM and in addition, form *cis* associations with other receptors on the same cell to assemble multi-receptor complexes. These complexes recruit signalling molecules to sites of cell-cell or cell-matrix adhesions. This allows to cooperate with other cell-surface receptors and to influence a variety of signalling cascades. For example, integrins are able to utilize the platelet-derived growth factor (PDGF) receptor and its signalling pathway without any PDGF stimulus (Sundberg and Rubin, 1996). These complexes of integrins and partner receptors can be formed either in response to or independent of integrin activation but are able to modulate integrin signalling.

1.3.1 Integrin-integrin cross-talk

The downstream signalling events of two different integrin heterodimers binding to the same ligand can be profoundly different. For instance, α5β1 and αVβ3 were found to differentially modulate RhoA-GTP loading, organization of cell matrix adhesions, and FN fibrillogenesis (Danen et al., 2002). In addition, to the obvious selectivity of certain signals to a particular integrin heterodimer, it was also shown by using ligands specific for integrin αIIbβ3 induced effects on the functions of target integrins α5β1 and α2β1. This experiment exemplifies that the binding of integrin-specific ligands to a suppressive integrin (like αIIbβ3) can inhibit the function of other target integrins (like α5β1 and α2β1) (trans-dominant inhibition). Trans-dominant inhibition is a blockade of integrin signalling by the engagement of another integrin (Diaz-Gonzalez et al., 1996). Thus this finding introduces the concept of integrin cross-talk. Further it was shown that α5β1 signals can enhance αVβ3 dependent migration towards VN (Kim et al., 2000). In addition, exposure of cells to VN specifically inhibited β1-driven FN deposition (Hocking et al., 1999). Another example for FN-binding integrin cross-talk is

work on integrin recycling pathways. Hereby blocking αV-class integrins result in changes in α5β1 recycling leading to enhanced α5β1 driven signal transduction and cell invasion (Caswell et al., 2008; Caswell et al., 2007; White et al., 2007). Such a cross-talk of αVβ3 and α5β1 implies that in endothelial or cancer cells expressing both αVβ3 and α5β1, ligand binding to αVβ3 could alter FN-fibrillogenesis, migration toward FN or even long-term, integrin induced changes like differentiation and proliferation.

1.3.2 Integrins and growth factor receptor signalling cross-talk

The ECM not only provides physical support for cells and tissues, but also serves as an information-rich structure interpreted by cells for example through integrins and growth factor signalling members (Hynes, 2009). Hereby integrins, growth factors and ECM interact and extensively cross-talk with each other (Ivaska and Heino, 2010; Streuli and Akhtar, 2009). Integrins transmit information about the ECM components and mechanical properties, but also assemble and rearrange ECM proteins. In addition, growth factor signalling up-regulates expression of αVβ3, αVβ5, αVβ6, and several β1 integrins (Heino et al., 1989; Heino and Massague, 1989; Ignotz et al., 1989; Sheppard et al., 1992). Recently it was shown that inactivation of β1 integrin impairs growth factor from stimulating the motility of normal and malignant mammary epithelial cells (MECs) and results in robust compensatory expression of β3 integrin which restores growth factor induced phenotypes (Parvani et al., 2013). Many growth factors are stored within the ECM and can be released from ECM-binding. One prominent example is the transforming growth factor beta (TGF-β). TGF-β is secreted in a latent complex consisting of three proteins: (**a**) TGF-β; (**b**) latency-associated protein (LAP) an inhibitor, which is derived from the TGF-β propeptide; (**c**) one of the latent TGF-β binding proteins (LTBPs), an ECM-binding protein; LTBPs interact with Fibrillins and other ECM components and thus function to localize latent TGF-β in the ECM. LAP contains an integrin-binding site (RGD), thus several RGD-binding integrins (e.g. αVβ6 and αVβ8) are able to activate latent TGF-β through binding this site (Munger et al., 1999). TGF-β activation appears to be the critical step in conducting its effects, which include inhibition of proliferation of many cell types, regulation of the immune system (Li et al., 2006a), manipulation of ECM production, contribution to fibrosis (Sime et al., 1997), skin cancer (Rognoni et al., 2014) and breast cancer metastasis (Parvani et al., 2013). In addition, integrins contribute to growth factor receptor signalling pathways by directly acting on downstream components of the pathways via catalytic proteins recruited to integrin cytoplasmic tails (Munger and Sheppard, 2011). Interestingly, mutant mice defective in integrin-mediated activators and with Fibrillin (LTBPs and Fibrillins interact non-covalently, these proteins along with LTBPs are critical for proper placement of latent TGF-β in the ECM;) gene mutations, show the critical role of ECM and integrins in

regulating TGF-β signalling. This evidence is mirrored by strong overlaps among phenotypes of TGF-β-null and integrin-null mice (Figure 11). For example: **(a)** β6 null mice lack the αVβ6 integrin. αVβ6 is an epithelium-restricted integrin that is up-regulated after epithelial injury. These mice develop lymphocytic lung inflammation reminiscent of inflammations in TGF-β1 null mice (Huang et al., 1996). (**b**) Mice with a knockin mutation of TGF-β1 that alters the RGD binding site to a nonfunctional RGE sequence fully reproduce the phenotype of TGF-β null mice indicating that RGD-binding integrins are required for TGF-β1 activation during development and early life (Yang et al., 2007). (**c**) Integrin β6 null and Integrin β8 null mice have a high incidence of cleft palate, the main finding in TGF-β3 null mice (Aluwihare et al., 2009).

Mouse	Phenotype
Tgfb1$^{-/-}$	Variable (strain-dependent) embryonic lethality because of vasculogenesis failure; lethal multiorgan lymphocyte-mediated inflammation and lack of Langerhans cells in remainder.
Tgfb1$^{RGE/RGE}$	Identical to *Tgfb1*$^{-/-}$, reduced fibrosis in heterozygotes.
Tgfb2$^{-/-}$	Embryonic lethality with defects in multiple organ systems.
Tgfb3$^{-/-}$	Cleft palate caused by failure of fusion of palatal shelves; mild, variable delayed lung development.
Itgav$^{-/-}$	~80% embryonic lethality because of vasculogenesis failure; brain hemorrhage and cleft palate in remainder. Note that these mice lack αvβ1, αvβ3, αvβ5, αvβ6, and αvβ8 integrins.
Itgb6$^{-/-}$	Lymphocyte-predominant lung inflammation, reduced Langerhans cells, late-onset lung emphysema because of increased MMP-12, reduced fibrosis.
Itgb8$^{-/-}$	Variable embryonic lethality because of vasculogenesis failure, CNS hemorrhage, cleft palate (~10%); conditional KO in dendritic cells causes mild inflammation.
Itgb6$^{-/-}$ *Itgb8*$^{-/-}$	Individual phenotypes plus high incidence of cleft palate causing early postnatal death.
Itgb8$^{-/-}$ treated perinatally with anti-αvβ6	Lethal multiorgan lymphocyte-mediated inflammation, lack of Langerhans cells.

Figure 11. Comparison of phenotypes of mice with TGF-β gene mutations and mice lacking integrin activators of TGF-β. *(Taken from Munger and Sheppard, 2011)*

Besides TGF-β, also insulin-like growth factor (IGF-1) receptor (IGF1R) signalling reveals a significant degree of cross-talk with integrins that provides another good example of the intimate relationship between integrin and growth factor receptor-mediated signalling. Hereby an interaction between β1 integrin and IGF1R seems to be important for IGF1R activity (Legate et al., 2009).

1.3.3 Sensing matrix rigidity by integrins

Besides integrin-integrin and integrin-growth factor receptor cross-talk, there is also cross-talk between integrins and the ECM. By their linkage to the cytoskeleton, integrins form a scaffold for various signalling pathways and intersect into growth factor receptor signalling (described above), as they share several signalling intermediates with those receptors (Schwartz and Ginsberg, 2002).

Consequently, cells do not react to growth factor treatment in suspension or in very soft compliant matrices (Erler and Weaver, 2008). Mounting cytoskeletal tension by increasing matrix rigidity, a phenomenon which is frequently found at sites of tumorigenesis, was shown to promote malignant transformation by inducing FA formation (Paszek et al., 2005). Furthermore, cells tend to migrate in the direction of increasing matrix stiffness and ligand density which might explain the nature of tumors as stiff structures attractive for cells to proliferate (Discher et al., 2005). This implies that not only genotypic alterations lead to malignant transformation and invasion of cells, but also the 3-dimensional, biophysical context within the tumor microenvironment. Mechanotransduction mediated by integrins is central to this phenomenon. Interestingly, several studies suggested that the αVβ3/αVβ5 integrins are involved in sensing matrix stiffness by an unknown mechanism (Jiang et al., 2006; Roca-Cusachs et al., 2009).

Taking all this information into account, it will be important to understand the qualitative differences in signals derived from αV- and β1-class integrins, in order to gain progress in understanding cellular signalling cross-talk.

1.4 SRF and the co-factor MAL

An important signalling hub responding to changes in Actin dynamics as well as influencing important cellular processes including migration and differentiation (Arsenian et al., 1998; Descot et al., 2009; Medjkane et al., 2009; Schratt et al., 2002; Sun et al., 2006a) is a transcription machinery consisiting of the Serum response factor and the Myocardin-related transcription factor A (SRF/MRTF-A or SRF/MAL) (Geneste et al., 2002; Grosse et al., 2003; Mack et al., 2001; Miralles et al., 2003; Posern et al., 2002; Sotiropoulos et al., 1999). SRF controls independently of *de novo* protein synthesis the transcription of cellular “immediate-early”’ genes, whose expression is activated by mitogenic stimuli (e.g. serum addition). Immediate early genes encode signalling molecules, transcription factors and many cytoskeletal components.

There are two principal families of signal-regulated SRF cofactors, which fall into two classes according to their sensitivity to different signalling pathways (Figure 12): (**a**) Members of the ternary complex factor (TCF) family of Ets domain containing proteins, which are activated by mitogen activated protein (MAP) kinase phosphorylation. These proteins make sequence-specific DNA contacts with E twenty-six (Ets) motifs (see below) adjoining a consensus sequence (see below) of some immediate-early genes (like c-fos) leading to a ternary complex formation with SRF and DNA. (**b**) Members of

the Myocardin-related transcription factors (MRTFs) acting as signal-regulated SRF cofactors. The activity of MRTF-A (also termed MAL) and MRTF-B is regulated by Rho-family GTPases and monomeric Actin, whereas Myocardin, the founding member of this transcription factor family, acts independently of g-Actin and hence activates SRF constitutively (Posern and Treisman, 2006).

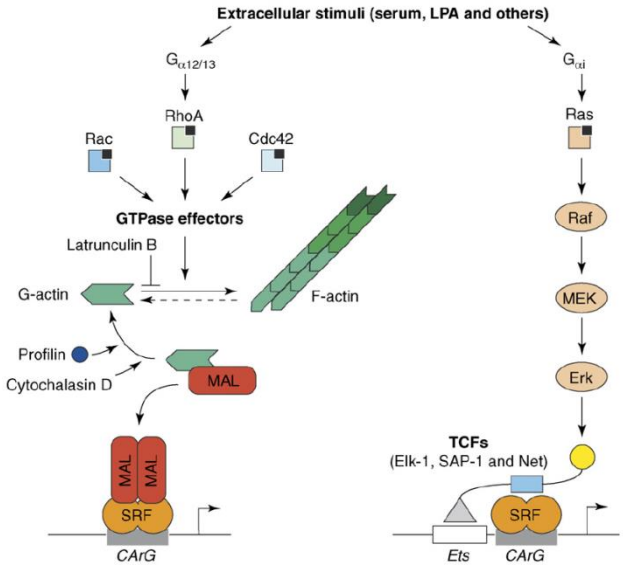

Figure 12. Model of two principal pathways regulating SRF activity
Activation of the MAP kinase pathway through Ras, Raf, MEK and ERK phosphorylates TCFs, which bind Ets DNA recognition sites and SRF (right). Signalling through Rho family GTPases (squares, with small black squares indicating GTP) and the actin treadmilling cycle leads to dissociation of MAL from g-Actin, which then binds and activates SRF (left). Overexpression of Profilin or Cytochalasin D treatment activates MAL. Treatment of cells with Latrunculin B, which prevents f-Actin assembly without dissociating the Actin–MAL complex, inhibits MAL activation. *(Taken from Posern and Treisman, 2006)*

1.4.1 SRF and MADS-box transcription factors

SRF belongs to the MADS (the name refers to four of the originally identified members: MCM1 (Transcription factor of morphogenesis), Agamous, Deficiens, SRF) family of transcription factors, which share homology in a 57-amino-acid MADS-box that mediates homo-dimerization and DNA binding to AT-rich DNA consensus sequences (Shore and Sharrocks, 1995b). Of interest, each member of the MADS family of TFs apparently possesses a distinct binding specificity. Moreover, several MADS-box proteins recruit other transcription factors into multi-component regulatory complexes. The only MADS-box proteins found in multicellular, mitochondrial eukaryotes (metazoans) are SRF and members of the MEF2 (Myocyte enhancer factor-2) (Black and Olson, 1998). The crystal structures of SRF and MEF2 revealed similar modes of DNA binding, which are reflected by similar sequences of their binding sites: (**a**) SRF binds to $CC(A/T)_6GG$ (known as a CArG-box); (**b**) MEF2 recognizes $CTA(A/T)_4TAG$; The conserved N-terminal region of the MADS-box forms an α-helical structure, which becomes oriented in an antiparallel manner within homodimers leading to the formation of a bipartite DNA-binding domain.

SRF, like other MADS-box transcription factors, interacts with a diverse array of transcriptional regulators to generate tissue-specific and signal-responsive patterns of gene expression (Messenguy and Dubois, 2003). The majority of SRF target genes are involved in cell growth, migration, cytoskeletal

organization and muscle development. Strikingly, the number of CArG-boxes as well as their degree of consensus sequence determine specificity of gene regulation: (**a**) The promoter of the prototypical SRF target gene, the oncogene *c-fos*, is controlled by a **single CArG-box**, referred to as a SRE (serum response element), which acts in concert with surrounding cis-regulatory elements (Norman et al., 1988). C-fos in involved in cell growth. (**b**) SRF-dependent genes involved in cell contractility and actin cytoskeletal dynmics are controlled by **duplicated CArG-boxes** (Chow and Schwartz, 1990; Miwa and Kedes, 1987). In addition, there is cell-type specific expression of CArG-box-dependent muscle genes. However, the mechanism underlying their specificity is still not understood. Additional modulatory proteins acting on/together with SRF are likely to drive transcriptomes. (**c**) The SRF target genes involved in cell growth can often be distinguished from those involved in myogenesis by the degree to which their CArG-boxes fit the perfect consensus. CArG-boxes in the promoters of several muscle genes deviate from the consensus sequence by one or more residues, resulting in a reduction in SRF-binding affinity (Chang et al., 2001), whereas the CArG-box upstream of c-fos perfectly fits the consensus. Thus, it appears that cell growth genes are permanent SRF targets, as they contain a perfect consensus CArG-box that binds SRF with high affinity. Myogenic SRF targets on the other hand, have only non-consensus CArG-boxes that require additional co-activation of SRF binding to activate their expression.

SRF expression in mouse embryos occurs in all germ layers at times before and after onset of mesoderm formation. At E 7.5, the SRF protein is detected in all three germ layers of wild-type embryos (Arsenian et al., 1998). Interestingly, subsequent to the onset of organogenesis at E 8.5 onwards, domains of localized, strong SRF protein expression are found in heart myocardium and the myotome (Arsenian et al., 1998). Given this broad expression pattern, it is not surprising that SRF deletion leads to embryonic lethality with a phenotype that is manifested at E 7.5. Knockout embryos are smaller in size, lack a primitive streak and, histologically, also mesodermal cells are missing (Arsenian et al., 1998). Towards E 8.5 knockout embryos consist of misfolded ectodermal and endodermal cell layers, lack a primitive streak or detectable mesoderm and fail to express developmental marker genes. After E 12.5 no SRF null embryos can be detected. Further, activation of the SRF-regulated “immediate early” genes and the α-Actin gene are severely impaired (Arsenian et al., 1998).

1.4.2 Ternary complex factors and SRF

The three ternary complex factors (TCFs) Elk-1, Net (neuroepithelial cell-transforming gene protein) and Sap-1 (SRF accessory protein 1) form a subfamily of the Ets domain transcription factors (Dalton and Treisman, 1992). Their characteristic property is the ability to form a ternary nucleoprotein

complex with SRF over the SRE of the *c-fos* promoter. The TCFs share four similar regions, A–D (Figure 13A), which were identified by sequence comparison between Elk-1 and Sap-1 (Dalton and Treisman, 1992).

The **A domain** corresponds to the Ets DNA binding domain. It has also been demonstrated to act as a transcriptional inhibitor in Elk-1 by recruiting co-repressors and DNA binding inhibitors (Yang et al., 2001; Yates et al., 1999).

The **B domain** interacts with the MADS box transcription factor family member SRF and allows ternary complex formation (Shore and Sharrocks, 1995a; Shore and Sharrocks, 1995b).

The **C domain** is an activation domain that is activated by phosphorylation by mitogen-activated protein (MAP) kinases. It contains multiple MAP kinase phosphorylation sites (Gille et al., 1995; Janknecht et al., 1993; Marais et al., 1993).

The **D domain** is a docking site for MAP kinases as well as a nuclear localization signal in Net (Buchwalter et al., 2004).

The **F domain** (FXFP motif) is an additional MAP kinase docking site with different binding properties (Jacobs et al., 1999).

Beside these domains, which are present in all three TCFs, there are other domains that are specific to one or two TCFs. The **J box in Net** is a JNK docking site, and phoshorylation of an adjacent export motif leads to nuclear export (Ducret et al., 2000). The presence of distinct docking sites in the TCFs generates a modular system, which allows complex integration of the signals from different MAP kinase pathways. The **R motif in Elk-1** is a repressor domain that dampens the activity of the C-terminal activation domain (Yang et al., 2002). Net contains two inhibitory domains, the net inhibitory domain and the C-terminal binding protein (CtBP) inhibition domain (Figure 13A). Of interest is that this domain organization is modified in alternative forms of the TCFs. When it comes to TCF/SRE binding, the Ets DNA binding domain binds specifically to Ets binding sites (EBSs) (Figure 13B). Hereby the TCFs form complexes with SRF dimers on SREs, as shown for example for the *c-fos* promoter (Treisman et al., 1992). Further regulation of TCF DNA binding can be achieved by intramolecular interactions of the Ets DNA binding domain (A in Figure 13A) with the B box (SRF interaction domain), the C box (transactivation domain) and the NID (inhibitor of transcription and DNA binding inhibitor) which inhibit DNA binding (Figure 13A and B). As already indicated by the domain features of the TCFs, phosphorylation by MAP kinases stimulates their transcriptional activity. This activation is particularly striking for Net, which is converted from a strong repressor to an activator. Activation

by phosphorylation does not directly inactivate repression but rather masks it, suggesting that other mechanisms may regulate the activity of the repression domains (Criqui-Filipe et al., 1999).

There are at least four MAP kinase pathways, of which the best known are the ERK (ERK1 and ERK2; extracellular signal regulated kinase), JNK (JNK1, JNK2 and JNK3; c-Jun N-terminal kinase) and p38 cascades (Robinson and Cobb, 1997). The ERK cascade responds to growth factors and mitogens, whereas the JNK and p38 cascades are triggered by cytokines and stress.

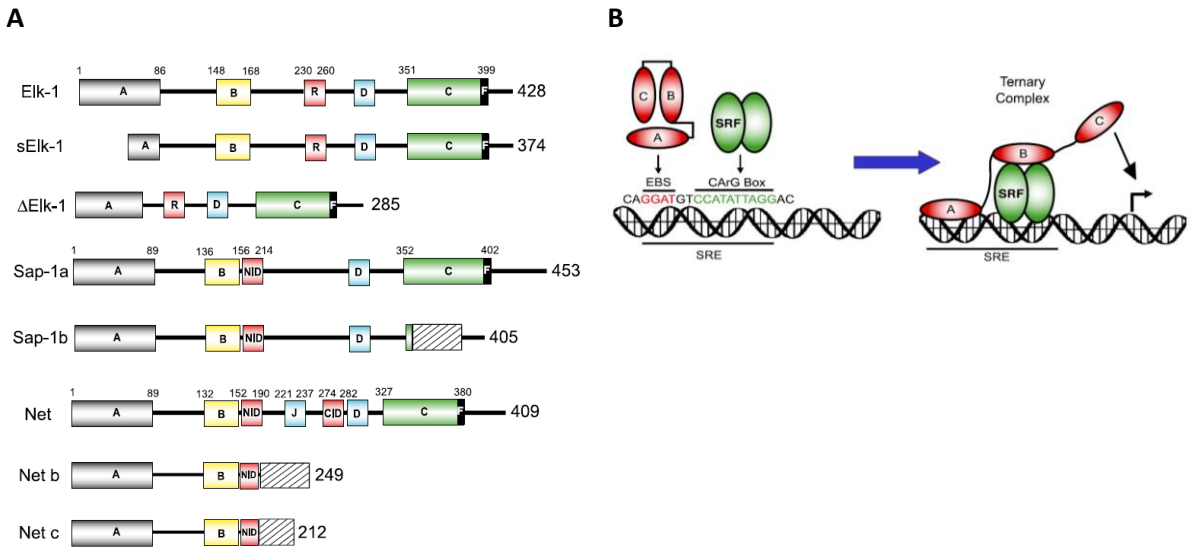

Figure 13. Structure of TCF subfamily members.
(A) The three TCFs (Elk-1, Sap-1a and Net) and their isoforms (sElk-1, DElk-1, Sap-1b, Net b and Net c) are represented. They share several conserved domains. The A box (grey) is the Ets DNA-binding domain whose location at the N-termini is one of the characteristics of the TCF subfamily. The B box (yellow) is the SRF interaction domain. The C box (green) is responsible for transcriptional activation and contains MAP kinase phosphorylation sites. The D box (blue) and F box (black) are docking sites for MAP kinases. Net also contains a specific docking site for JNK kinase (J box; blue). The NID, CID and R boxes (red) are repression domains. Hatched boxes in represent altered amino-acid sequences.
(B) Schematic representation of ternary complex formation. The SRF dimer interacts with the CArG box.
The A domain of the TCF binds to an EBS. The B domain of the TCF contains the interface for the protein-protein interaction with SRF. The represented EBS and CArG sequences correspond to the c-fos promoter SRE.
(Taken from Buchwalter et al., 2004)

1.4.3 Myocardins and the unique feature of MAL

The association of transcriptional co-activators with sequence-specific DNA-binding proteins provides versatility and specificity to gene regulation. Members of the Myocardin family of co-activators activate transcription of genes involved in cell proliferation, migration, and myogenesis by associating with SRF. The partnership of Myocardin family members and SRF controls genes encoding components of the Actin cytoskeleton and confers responsiveness to extracellular growth signals and changes in the Actin distribution and dynamics, thereby creating a transcriptional-cytoskeletal regulation circuit (Pipes et al., 2006). Each of the Myocardin family members possesses a conserved N-

terminal region containing three actin-binding RPEL motifs (RPEL1 to RPEL3; the “RPEL domain”, Figure 13).

MAL (or MRTF-A) is cytoplasmic, accumulating in the nucleus upon activation of RhoGTPase signalling, which alters interactions between g-Actin and the RPEL domain (Cen et al., 2003; Miralles et al., 2003). Of interest, Myocardin, the founding member, but also MRTF-B, are nuclear proteins and do not shuttle between cytoplasm and nucleus. The unique shuttling feature of MAL is based on the RPEL domain, which binds Actin more avidly than that of other Myocardins. RPEL1 and RPEL2 of other Myocardins bind Actin weakly compared with those of MAL, while RPEL3 is of comparably low affinity in the two proteins. Thus, differential Actin occupancy of multiple RPEL motifs regulates nucleo-cytoplasmic transport and activity of MAL.

A depletion of g-Actin levels results in diminished g-Actin-MAL interaction. As a consequence the nuclear export of MAL is inhibited because this requires binding to Actin and the exportin Crm1 (Vartiainen et al., 2007). In contrast, when the g-Actin concentration in unstimulated cells is artificially increased, the nuclear import of MAL is inhibited, because g-Actin binding displaces importin α-importin β dimers from a bipartite nuclear localization signal (NLS) in the RPEL domain (Nakamura et al., 2010; Pawlowski et al., 2010). In unstimulated cells, inactivation of the exportin Crm1 by its specific inhibitory drug Leptomycin B leads to nuclear accumulation of MAL and this required the putative NLS within MAL. This shows that MAL continuously shuttles through the nucleus (Miralles et al., 2003; Vartiainen et al., 2007). The assembly of g-Actin into filamentous structures during Actin polymerization results in a release of MAL from g-Actin binding. As a consequence MAL is accessible for transcription factor activation. As already described above, MAL interacts with g-Actin via its RPEL motif. Through this interaction MAL is retained in the cytoplasm thus preventing translocation into the nucleus, binding to SRF, and initiation of transcription. Profilin and Tβ4 compete with MAL for g-Actin binding by binding the same Actin contacts leading to enhanced SRF/MAL activity and subsequent target gene expression. Thus, alternations in Actin dynamics are both necessary and sufficient for the activation of SRF by extracellular signals or in the absence of any stimuli (Mack et al., 2001; Sotiropoulos et al., 1999).

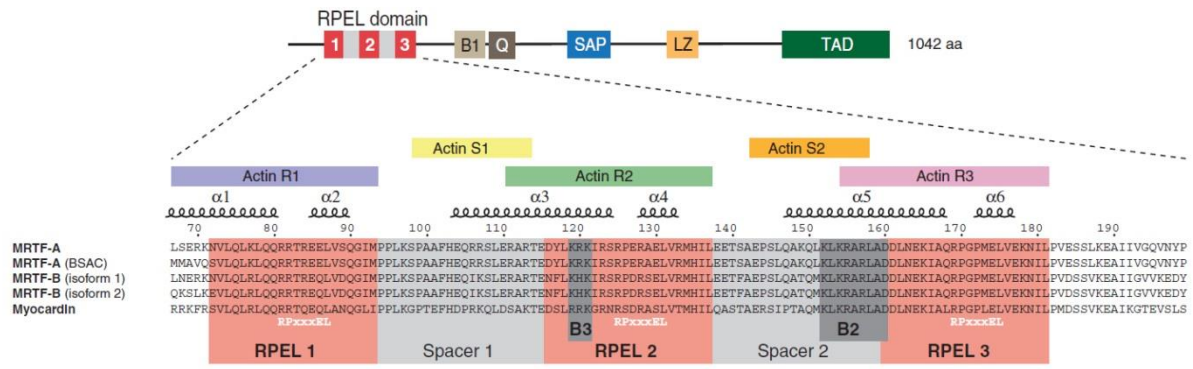

Figure 13. Domain organization and actin-binding motifs of Myocardins
Upper panel: Domain organization of MAL and Myocardin: B1, basic region 1; Q, Q(Gln)-rich region; SAP (after SAF-A/B, Acinus and PIAS) motif is a putative DNA/RNA binding domain found in diverse nuclear and cytoplasmic proteins; LZ, leucine zipper motif; TAD, transcription activation domain;
Lower panel: Schematic of MRTF-A domain organization and alignment of the MRTF-A sequences with the corresponding MRTF-B and Myocardin sequences from *Mus musculus.* RPEL motifs are highlighted in red, spacer sequences in gray, and the two basic elements of the bipartite nuclear import signal, B3 and B2, in dark gray. Colored bars indicate the major contacts with RPEL-actins R1, R2, and R3 (pale blue, pale green, and magenta) and spacer-actins S1 and S2 (pale yellow and orange). The secondary structure of six helices (α1 to α6) is indicated by twisted lines. *(Modified after Mouilleron et al., 2011)*

MAL binding to SRF regulates the expression of signalling molecules, other transcription factors, cytoskeletal and contractile genes but also FA proteins (Balza and Misra, 2006; Cen et al., 2003; Cooper et al., 2007; Descot et al., 2009; Leitner et al., 2011; Miralles et al., 2003; Philippar et al., 2004; Posern and Treisman, 2006; Schratt et al., 2002; Selvaraj and Prywes, 2004; Sun et al., 2006a; Zhang et al., 2005). Sequence analysis of the mouse and human β1 integrin gene revealed a CArG box proximal to the translation start (Brandt et al., 2009a; Sun et al., 2006a) and β1 integrin was shown to be indeed a SRF/MAL target gene. A recent study showed that suppressor of cancer cell invasion (SCAI) inhibits the transcriptional activator complex by forming a ternary complex with MAL/SRF, resulting in reduced expression of β1-integrins and loss of invasive potential (Brandt et al., 2009a). Other SRF/MAL target proteins are Actin cytoskeleton regulators affecting cell migration, differentiation and survival, and therefore implying a strong link of this transcriptional machinery towards cancer development and progression (Crowley et al., 2009; Leitner et al., 2010; Liang et al., 2011; Medjkane et al., 2009; Verdoni et al., 2010).

MAL mutant mice show defective differentiation and function of mammary myoepithelial cells, which are required for maintenance of lactation (Li et al., 2006b; Sun et al., 2006b). Despite the importance of Srf in multiple transcriptional pathways and widespread MAL expression (Wang et al., 2002), the degree of abnormalities associated with MAL depletion appears surprisingly restricted.
Of note, analysis of homozygous but also heterozygous MAL knockout intercrosses reveal that only a small population of the progeny was born. This partial fetal wastage is probably due to MAL's role in

development of muscle lineages from mesodermal tissues (Sun et al., 2006b). Analysis of the MRTF-B knockout phenotype, which showed a specific failure in neural crest-derived vascular smooth muscle cells, indicated that at least in some situations MAL apparently cannot functionally substitute for MRTF-B (Li et al., 2005; Oh et al., 2005). This suggests that MAL and MRTF-B have distinct but also redundant functions and/or targets in specific cells. Thus it is possible that the knockout of either MAL or MRTF-B reduces total MRTF activity in the affected cells below a functional threshold.

1.5 ISG15 and ISGylation

The interferon-stimulated gene 15 (ISG15) protein is the first reported ubiquitin-like protein. Its expression and conjugation to target proteins is induced by type I interferons (IFNs), genotoxic stress, and pathogen infections, suggesting that ISG15 plays an important role in innate immune responses (Der et al., 1998; Haas et al., 1987; Yuan and Krug, 2001). It can be conjugated to protein substrates in a process similar to ubiquitin modification, termed ISGylation. The E1 enzyme responsible for ISG15 activation is the ubiquitin-activating enzyme E1-like (UBE1L, also UBA1 can activate ISG15 but also ubiquitin) which is specific for ISG15. Ubiquitin-conjugating enzyme in humans (UbcH) 6 and UbcH8 (UBE2L6 in mouse) are E2 enzymes for ISG15 but also serve as conjugation enzymes for Ubiquitin, demonstrating an overlap between the ISG15- and ubiquitin-modification machinery (Takeuchi et al., 2005; Zhao et al., 2004). Reported E3 ligases for the ISGylation process are the HECT E3 ligases HERC5 and HERC6, Estrogene-responsive finger protein (EFP) and Human homolog of drosophila ariadne (HHARI) (Dastur et al., 2006; Ketscher et al., 2012; Kim et al., 2004; Okumura et al., 2007; Oudshoorn et al., 2012; Wong et al., 2006; Zou and Zhang, 2006). HERC5 is thought to be the major E3 ligase in the human and Herc6 the major ISG15 E3 ligase in the murine system. Appropriately, all of the enzymes identified in the ISGylation pathway are induced in a coordinated manner by type I IFNs. Importantly, ISG15 modification can be reversed by the ISG15 specific isopeptidase UBP43 but also by proteases like USP2, USP5, USP13 and USP14 (Catic et al., 2007; Malakhov et al., 2002). Besides MAL, also ISG15 was reported to play an important role in tumorigenesis. It is still enigmatic how ISG15 regulates tumorigenesis and furthermore, also the consequences of ISGylation within the context of the whole organism are not known. Cell culture based experiments have provided evidence for four different modes of action: (**a**) **ISGylation of proteins alter target protein functions.** For example ISGylation of Filamin B led to the release of Rac1, MAPK/ERK kinase kinase 1 (MEKK1) and MAPK/ERK kinase 4 (MKK4) from the scaffold protein and thus to the prevention of JNK-mediated apoptosis. (Jeon et al., 2009). (**b**) **Competition with ubiquitin modification and therefore proteasomal degradation.** For instance, recent studies revealed that the constitutively elevated ISG15 pathway impairs ubiquitin (Ub)-targeted proteasomal protein degradation in Ataxia-

telangiectasia (A-T, is a cerebellar neurodegenerative disorder) cells (Desai et al., 2013). Further, E2 Ub ligase Ubc13 forms a unique ubiquitin-conjugating enzyme (Ubc) complex with ubiquitin enzyme variant Mms2 and generates atypical Lys63-linked ubiquitin conjugates, as one of the targets of ISG15 modification. Ubc13 gets ISGylated leading to disruption of its ability to form thioester bond with ubiquitin. (Zou et al., 2005). (**c**) **Functions mediated by unconjugated ISG15.** For example, free ISG15 is specifically bound to E3 Ub ligase Nedd4 and blocked its interaction with Ub E2 molecules, thus preventing further Ub transfer from E2 to E3. Therefore, Nedd4 is negatively regulated by ISG15. (Malakhova and Zhang, 2008). On top of this, free ISG15 inhibits budding of Ebola virus by interaction with Nedd4 ubiquitin ligase and inhibits ubiquitination of VP40 virus-like particles of Ebola virus (Okumura et al., 2008). (**d**) **ISGylation alters protein translation capacity.** The mRNA 5' cap structure-binding protein 4EHP acts as a translation suppressor and is modified by ISG15. ISGylated 4EHP increases cap structure-binding activity. Recently it was shown that ISG15-modified dsRNA-dependent protein kinase (PKR) is more active compared to non-ISG15-conjugated form, and phosphorylates eukaryotic translation initiation factor 2 subunit alpha (eIF2α) to down-regulate protein translation. (Okumura et al., 2013; Okumura et al., 2007).

Biochemically ISG15, similar to MAL, was shown to alter cytoskeletal architecture thereby promoting motility in human breast cancer cells (Desai et al., 2012). In addition ISG15, similar to MAL, inhibits proteasome-mediated turnover of proteins implicated in tumor cell motility, invasion and metastasis (Desai et al., 2006). An increasing number of studies identified an up-regulation of either ISG15 and its conjugates (Andersen et al., 2006; Bektas et al., 2008; Brandt et al., 2009b; Desai et al., 2006; Kiessling et al., 2009) or signalling (Brandt et al., 2009b; Leitner et al., 2010; Ma et al., 2001; Medjkane et al., 2009) in several cancer entities. An important issue to investigate is whether the coordinated up-regulation of several interferon-stimulated genes (ISGs), besides ISG15, in tumors is cell autonomous or is the outcome of signals from tumor microenvironment, such as IFNs produced by infiltrating immune cells or even the stress response to chemotherapy. Microarray studies identified 50 to 1000 ISGs, with 200 to 500 genes typical of many cell types depending on cell type, IFN dose and time of treatment (de Veer et al., 2001; Lanford et al., 2006; Sarasin-Filipowicz et al., 2008). Interestingly, microarray data show that levels of several ISGs loose correlation with ISG15 expression when cells were taken into culture (Hoeflich et al., 2009; Neve et al., 2006; Sgorbissa and Brancolini, 2012; Wagner et al., 2007). These findings indicate that the tumor microenvironment also regulates ISG protein expression. An explanation why ISG15 still is expressed *ex vivo* in the absence of microenvironment induced IFN production is unknown.

2 Aims of the thesis

An important caveat to most experimental systems used in the past is that αVβ3/β5 and α5β1 are co-expressed on cells. For instance, endothelial cells during angiogenesis or keratinocytes during wound repair up-regulate the expression of αVβ3/β5 and α5β1 and of FN (Brooks et al., 1994; Parsons-Wingerter et al., 2005; Silva et al., 2008). Therefore, it is crucial to reduce this complexity and express both integrins separately in the same cellular background in order to study and comprehend their function. To do so my studies used pan-integrin knockout cells ($\alpha V^{-/-}$, $\beta 1^{-/-}$, $\beta 2^{-/-}$, and $\beta 7^{-/-}$; pKO) that were derived from genetically modified mice and engineered *in vitro* to express αVβ3/β5 or α5β1 integrin, or both, αVβ3/β5 and α5β1 integrins.

In my PhD project I analyzed integrin heterodimer-specific signalling events regulated by proteins that are recruited to integrin adhesions selectively via either αVβ3/β5 or α5β1. The recent technological progress in quantitative proteomics allowed for the first time a non-biased analysis of the molecular composition of focal adhesions using biochemical isolation protocols followed by quantitative mass spectrometry. Thus, the integrin adhesion-associated molecular complexes but also the (phospho-) proteome of pan-integrin-null fibroblasts reconstituted with αV and/or β1 integrin were analyzed by quantitative mass spectrometry. These studies led to the identification of integrin-specific FA components but also to signalling processes which are differentially regulated possibly in an integrin subtype-specific manner.

Aim 1

Studying the **molecular basis of the differential protein recruitment** to αVβ3/β5- and α5β1-containing focal adhesions (e.g. protein-protein interaction networks and their post-translational modifications).

Aim 2

Investigating the impact of the selected proteins of interest on **functional parameters** that were defined based on the difference between αVβ3/β5 and α5β1 expressing cells, like cell contractility.

Aim 3

Identifying the **molecular mechanisms leading to differential protein expression and/or modification** of differential expressed proteins in αVβ3/β5 and α5β1 expressing cells (e.g. regulation of transcription, translation).

3 Short summaries of manuscripts

3.1 First manuscript

Title: β1- and αV-class integrins cooperate to regulate myosin II during rigidity sensing of fibronectin-based microenvironments.

How different integrins that bind to the same type of extracellular matrix protein mediate specific functions is unclear. In this project the functional properties of β1- and αV-class integrins expressed in pan-integrin-null fibroblasts seeded on Fibronectin were analyzed. Reconstitution with β1-class integrins promotes myosin-II-independent formation of small peripheral adhesions and cell protrusions, whereas expression of αV-class integrins induces the formation of large focal adhesions. Co-expression of both integrin classes leads to full Myosin activation and traction-force development on stiff fibronectin-coated substrates, with αV-class integrins accumulating in adhesion areas exposed to high traction forces. Quantitative proteomics linked αv-class integrins to a GEF-H1-RhoA pathway coupled to the formin mDia1 but not myosin II, and α5β1 integrins to a RhoA-Rock-myosin II pathway. This study assigns specific functions to distinct fibronectin-binding integrins, demonstrating that α5β1integrins accomplish force generation, whereas αV-class integrins mediate the structural adaptations to forces, which cooperatively enable cells to sense the rigidity of fibronectin-based microenvironments.

3.2 Second manuscript

Title: Integrins synergistically induce the MAL/SRF target gene ISG15 to ISGylate cytoskeletal and focal adhesion proteins necessary for cancer cell invasion

This study reports that αV- and/or β1-class integrin expressing fibroblasts contain different g-Actin pools correlating with low nuclear MAL levels and MAL/SRF activities in αV, intermediate in β1 and extremely high in αV,β1 double expressing cells. The interferon-stimulated gene 15 (ISG15) was identified as one of the most abundant SRF/MAL gene targets without any interferon stimulus. Mass spectrometry of ISG15 interacting proteins revealed ISGylation of novel proteins such as Talin and Eplin. Mechanistically, multi-layered ISGylation of integrins, adhesion proteins, Actin and its modifiers prevent mainly ubiquitination leading to increased protein stability. High integrin and ISG15 levels correlate with increased human breast cancer cell invasion and poor patient survival. Our findings identify a novel mode how fibronectin-binding integrins synergistically control cell invasion by regulating transcription and subsequent ISGylation. Thus, we propose that integrin adhesions,

MAL/SRF and ISG15 constitute an a new autoregulatory feed-forward loop that precisely adjusts actin- and adhesion-based functions required for cell spreading, migration and invasion.

4 References

Ali, I. U., and Hynes, R. O. (1978). Role of disulfide bonds in the attachment and function of large, external, transformation-sensitive glycoprotein at the cell surface. Biochim Biophys Acta *510*, 140-150.
Aluwihare, P., Mu, Z., Zhao, Z., Yu, D., Weinreb, P. H., Horan, G. S., Violette, S. M., and Munger, J. S. (2009). Mice that lack activity of alphavbeta6- and alphavbeta8-integrins reproduce the abnormalities of Tgfb1- and Tgfb3-null mice. Journal of cell science *122*, 227-232.
Andersen, J. B., Aaboe, M., Borden, E. C., Goloubeva, O. G., Hassel, B. A., and Orntoft, T. F. (2006). Stage-associated overexpression of the ubiquitin-like protein, ISG15, in bladder cancer. British journal of cancer *94*, 1465-1471.
Aragona, M., Panciera, T., Manfrin, A., Giulitti, S., Michielin, F., Elvassore, N., Dupont, S., and Piccolo, S. (2013). A mechanical checkpoint controls multicellular growth through YAP/TAZ regulation by actin-processing factors. Cell *154*, 1047-1059.
Arnaout, M. A., Mahalingam, B., and Xiong, J. P. (2005). Integrin structure, allostery, and bidirectional signalling. Annual review of cell and developmental biology *21*, 381-410.
Arsenian, S., Weinhold, B., Oelgeschlager, M., Ruther, U., and Nordheim, A. (1998). Serum response factor is essential for mesoderm formation during mouse embryogenesis. The EMBO journal *17*, 6289-6299.
Avraamides, C. J., Garmy-Susini, B., and Varner, J. A. (2008). Integrins in angiogenesis and lymphangiogenesis. Nature reviews Cancer *8*, 604-617.
Azzolin, L., Zanconato, F., Bresolin, S., Forcato, M., Basso, G., Bicciato, S., Cordenonsi, M., and Piccolo, S. (2012). Role of TAZ as mediator of Wnt signalling. Cell *151*, 1443-1456.
Bader, B. L., Rayburn, H., Crowley, D., and Hynes, R. O. (1998). Extensive vasculogenesis, angiogenesis, and organogenesis precede lethality in mice lacking all alpha v integrins. Cell *95*, 507-519.
Balza, R. O., Jr., and Misra, R. P. (2006). Role of the serum response factor in regulating contractile apparatus gene expression and sarcomeric integrity in cardiomyocytes. The Journal of biological chemistry *281*, 6498-6510.
Beglova, N., Blacklow, S. C., Takagi, J., and Springer, T. A. (2002). Cysteine-rich module structure reveals a fulcrum for integrin rearrangement upon activation. Nature structural biology *9*, 282-287.
Bektas, N., Noetzel, E., Veeck, J., Press, M. F., Kristiansen, G., Naami, A., Hartmann, A., Dimmler, A., Beckmann, M. W., Knuchel, R.*, et al.* (2008). The ubiquitin-like molecule interferon-stimulated gene 15 (ISG15) is a potential prognostic marker in human breast cancer. Breast cancer research : BCR *10*, R58.
Bishop, A. L., and Hall, A. (2000). Rho GTPases and their effector proteins. The Biochemical journal *348 Pt 2*, 241-255.
Black, B. L., and Olson, E. N. (1998). Transcriptional control of muscle development by myocyte enhancer factor-2 (MEF2) proteins. Annual review of cell and developmental biology *14*, 167-196.
Bledzka, K., Bialkowska, K., Nie, H., Qin, J., Byzova, T., Wu, C., Plow, E. F., and Ma, Y. Q. (2010). Tyrosine phosphorylation of integrin beta3 regulates kindlin-2 binding and integrin activation. The Journal of biological chemistry *285*, 30370-30374.
Boettiger, D. (2012). Mechanical control of integrin-mediated adhesion and signalling. Current opinion in cell biology *24*, 592-599.
Bottcher, R. T., Stremmel, C., Meves, A., Meyer, H., Widmaier, M., Tseng, H. Y., and Fassler, R. (2012). Sorting nexin 17 prevents lysosomal degradation of beta1 integrins by binding to the beta1-integrin tail. Nat Cell Biol *14*, 584-592.

Bouvard, D., Brakebusch, C., Gustafsson, E., Aszodi, A., Bengtsson, T., Berna, A., and Fassler, R. (2001). Functional consequences of integrin gene mutations in mice. Circulation Research *89*, 211-223.
Bouvard, D., Pouwels, J., De Franceschi, N., and Ivaska, J. (2013). Integrin inactivators: balancing cellular functions in vitro and in vivo. Nat Rev Mol Cell Biol *14*, 430-442.
Brandt, D. T., Baarlink, C., Kitzing, T. M., Kremmer, E., Ivaska, J., Nollau, P., and Grosse, R. (2009a). SCAI acts as a suppressor of cancer cell invasion through the transcriptional control of beta1-integrin. Nat Cell Biol *11*, 557-568.
Brandt, D. T., Xu, J., Steinbeisser, H., and Grosse, R. (2009b). Regulation of myocardin-related transcriptional coactivators through cofactor interactions in differentiation and cancer. Cell cycle *8*, 2523-2527.
Brooks, P. C., Clark, R. A., and Cheresh, D. A. (1994). Requirement of vascular integrin alpha v beta 3 for angiogenesis. Science *264*, 569-571.
Buchwalter, G., Gross, C., and Wasylyk, B. (2004). Ets ternary complex transcription factors. Gene *324*, 1-14.
Bunch, T. A. (2010). Integrin alphaIIbbeta3 activation in Chinese hamster ovary cells and platelets increases clustering rather than affinity. The Journal of biological chemistry *285*, 1841-1849.
Calderwood, D. A., Campbell, I. D., and Critchley, D. R. (2013). Talins and kindlins: partners in integrin-mediated adhesion. Nat Rev Mol Cell Biol *14*, 503-517.
Calderwood, D. A., Fujioka, Y., de Pereda, J. M., Garcia-Alvarez, B., Nakamoto, T., Margolis, B., McGlade, C. J., Liddington, R. C., and Ginsberg, M. H. (2003). Integrin beta cytoplasmic domain interactions with phosphotyrosine-binding domains: a structural prototype for diversity in integrin signalling. Proceedings of the National Academy of Sciences of the United States of America *100*, 2272-2277.
Carraher, C. L., and Schwarzbauer, J. E. (2013). Regulation of matrix assembly through rigidity-dependent fibronectin conformational changes. The Journal of biological chemistry *288*, 14805-14814.
Caswell, P. T., Chan, M., Lindsay, A. J., McCaffrey, M. W., Boettiger, D., and Norman, J. C. (2008). Rab-coupling protein coordinates recycling of alpha5beta1 integrin and EGFR1 to promote cell migration in 3D microenvironments. The Journal of cell biology *183*, 143-155.
Caswell, P. T., Spence, H. J., Parsons, M., White, D. P., Clark, K., Cheng, K. W., Mills, G. B., Humphries, M. J., Messent, A. J., Anderson, K. I.*, et al.* (2007). Rab25 associates with alpha5beta1 integrin to promote invasive migration in 3D microenvironments. Dev Cell *13*, 496-510.
Catic, A., Fiebiger, E., Korbel, G. A., Blom, D., Galardy, P. J., and Ploegh, H. L. (2007). Screen for ISG15-crossreactive deubiquitinases. PloS one *2*, e679.
Cen, B., Selvaraj, A., Burgess, R. C., Hitzler, J. K., Ma, Z., Morris, S. W., and Prywes, R. (2003). Megakaryoblastic leukemia 1, a potent transcriptional coactivator for serum response factor (SRF), is required for serum induction of SRF target genes. Mol Cell Biol *23*, 6597-6608.
Chang, D. D., Wong, C., Smith, H., and Liu, J. (1997). ICAP-1, a novel beta1 integrin cytoplasmic domain-associated protein, binds to a conserved and functionally important NPXY sequence motif of beta1 integrin. The Journal of cell biology *138*, 1149-1157.
Chang, P. S., Li, L., McAnally, J., and Olson, E. N. (2001). Muscle specificity encoded by specific serum response factor-binding sites. The Journal of biological chemistry *276*, 17206-17212.
Chow, K. L., and Schwartz, R. J. (1990). A combination of closely associated positive and negative cis-acting promoter elements regulates transcription of the skeletal alpha-actin gene. Mol Cell Biol *10*, 528-538.
Cooper, L. A., Shen, T. L., and Guan, J. L. (2003). Regulation of focal adhesion kinase by its amino-terminal domain through an autoinhibitory interaction. Mol Cell Biol *23*, 8030-8041.
Cooper, S. J., Trinklein, N. D., Nguyen, L., and Myers, R. M. (2007). Serum response factor binding sites differ in three human cell types. Genome research *17*, 136-144.

Criqui-Filipe, P., Ducret, C., Maira, S. M., and Wasylyk, B. (1999). Net, a negative Ras-switchable TCF, contains a second inhibition domain, the CID, that mediates repression through interactions with CtBP and de-acetylation. The EMBO journal *18*, 3392-3403.
Critchley, D. R. (2000). Focal adhesions - the cytoskeletal connection. Current opinion in cell biology *12*, 133-139.
Critchley, D. R., and Gingras, A. R. (2008). Talin at a glance. Journal of cell science *121*, 1345-1347.
Crockford, D., Turjman, N., Allan, C., and Angel, J. (2010). Thymosin beta4: structure, function, and biological properties supporting current and future clinical applications. Annals of the New York Academy of Sciences *1194*, 179-189.
Crowley, J. L., Smith, T. C., Fang, Z., Takizawa, N., and Luna, E. J. (2009). Supervillin reorganizes the actin cytoskeleton and increases invadopodial efficiency. Molecular biology of the cell *20*, 948-962.
Czuchra, A., Meyer, H., Legate, K. R., Brakebusch, C., and Fassler, R. (2006). Genetic analysis of beta1 integrin "activation motifs" in mice. The Journal of cell biology *174*, 889-899.
Dallas, S. L., Chen, Q., and Sivakumar, P. (2006). Dynamics of assembly and reorganization of extracellular matrix proteins. Current topics in developmental biology *75*, 1-24.
Dallas, S. L., Sivakumar, P., Jones, C. J., Chen, Q., Peters, D. M., Mosher, D. F., Humphries, M. J., and Kielty, C. M. (2005). Fibronectin regulates latent transforming growth factor-beta (TGF beta) by controlling matrix assembly of latent TGF beta-binding protein-1. The Journal of biological chemistry *280*, 18871-18880.
Dalton, S., and Treisman, R. (1992). Characterization of SAP-1, a protein recruited by serum response factor to the c-fos serum response element. Cell *68*, 597-612.
Danen, E. H., Sonneveld, P., Brakebusch, C., Fassler, R., and Sonnenberg, A. (2002). The fibronectin-binding integrins alpha5beta1 and alphavbeta3 differentially modulate RhoA-GTP loading, organization of cell matrix adhesions, and fibronectin fibrillogenesis. Journal of Cell Biology *159*, 1071-1086.
Danen, E. H., van Rheenen, J., Franken, W., Huveneers, S., Sonneveld, P., Jalink, K., and Sonnenberg, A. (2005). Integrins control motile strategy through a Rho-cofilin pathway. Journal of Cell Biology *169*, 515-526.
Dastur, A., Beaudenon, S., Kelley, M., Krug, R. M., and Huibregtse, J. M. (2006). Herc5, an interferon-induced HECT E3 enzyme, is required for conjugation of ISG15 in human cells. The Journal of biological chemistry *281*, 4334-4338.
De Melker, A. A., Kramer, D., Kuikman, I., and Sonnenberg, A. (1997). The two phenylalanines in the GFFKR motif of the integrin alpha6A subunit are essential for heterodimerization. The Biochemical journal *328 (Pt 2)*, 529-537.
de Veer, M. J., Holko, M., Frevel, M., Walker, E., Der, S., Paranjape, J. M., Silverman, R. H., and Williams, B. R. (2001). Functional classification of interferon-stimulated genes identified using microarrays. Journal of leukocyte biology *69*, 912-920.
Del Pozo, M. A., Kiosses, W. B., Alderson, N. B., Meller, N., Hahn, K. M., and Schwartz, M. A. (2002). Integrins regulate GTP-Rac localized effector interactions through dissociation of Rho-GDI. Nat Cell Biol *4*, 232-239.
Del Pozo, M. A., and Schwartz, M. A. (2007). Rac, membrane heterogeneity, caveolin and regulation of growth by integrins. Trends in cell biology *17*, 246-250.
Der, S. D., Zhou, A., Williams, B. R., and Silverman, R. H. (1998). Identification of genes differentially regulated by interferon alpha, beta, or gamma using oligonucleotide arrays. Proceedings of the National Academy of Sciences of the United States of America *95*, 15623-15628.
Desai, S. D., Haas, A. L., Wood, L. M., Tsai, Y. C., Pestka, S., Rubin, E. H., Saleem, A., Nur, E. K. A., and Liu, L. F. (2006). Elevated expression of ISG15 in tumor cells interferes with the ubiquitin/26S proteasome pathway. Cancer research *66*, 921-928.
Desai, S. D., Reed, R. E., Babu, S., and Lorio, E. A. (2013). ISG15 deregulates autophagy in genotoxin-treated ataxia telangiectasia cells. The Journal of biological chemistry *288*, 2388-2402.

Desai, S. D., Reed, R. E., Burks, J., Wood, L. M., Pullikuth, A. K., Haas, A. L., Liu, L. F., Breslin, J. W., Meiners, S., and Sankar, S. (2012). ISG15 disrupts cytoskeletal architecture and promotes motility in human breast cancer cells. Experimental biology and medicine *237*, 38-49.
Descot, A., Hoffmann, R., Shaposhnikov, D., Reschke, M., Ullrich, A., and Posern, G. (2009). Negative regulation of the EGFR-MAPK cascade by actin-MAL-mediated Mig6/Errfi-1 induction. Molecular cell *35*, 291-304.
Diaz-Gonzalez, F., Forsyth, J., Steiner, B., and Ginsberg, M. H. (1996). Trans-dominant inhibition of integrin function. Molecular biology of the cell *7*, 1939-1951.
Discher, D. E., Janmey, P., and Wang, Y. L. (2005). Tissue cells feel and respond to the stiffness of their substrate. Science *310*, 1139-1143.
Ducret, C., Maira, S. M., Lutz, Y., and Wasylyk, B. (2000). The ternary complex factor Net contains two distinct elements that mediate different responses to MAP kinase signalling cascades. Oncogene *19*, 5063-5072.
Ehrlicher, A. J., Nakamura, F., Hartwig, J. H., Weitz, D. A., and Stossel, T. P. (2011). Mechanical strain in actin networks regulates FilGAP and integrin binding to filamin A. Nature *478*, 260-263.
Erickson, H. P., and Carrell, N. A. (1983). Fibronectin in extended and compact conformations. Electron microscopy and sedimentation analysis. The Journal of biological chemistry *258*, 14539-14544.
Erler, J. T., and Weaver, V. M. (2008). Three-dimensional context regulation of metastasis. Clinical and Experimental Metastasis.
Fassler, R., and Meyer, M. (1995). Consequences of lack of beta 1 integrin gene expression in mice. Genes Dev *9*, 1896-1908.
Fogerty, F. J., Akiyama, S. K., Yamada, K. M., and Mosher, D. F. (1990). Inhibition of binding of fibronectin to matrix assembly sites by anti-integrin (alpha 5 beta 1) antibodies. The Journal of cell biology *111*, 699-708.
Folkman, J. (2006). Angiogenesis. Annu Rev Med *57*, 1-18.
Fontana, L., Chen, Y., Prijatelj, P., Sakai, T., Fassler, R., Sakai, L. Y., and Rifkin, D. B. (2005). Fibronectin is required for integrin alphavbeta6-mediated activation of latent TGF-beta complexes containing LTBP-1. FASEB journal : official publication of the Federation of American Societies for Experimental Biology *19*, 1798-1808.
Frantz, C., Stewart, K. M., and Weaver, V. M. (2010). The extracellular matrix at a glance. Journal of cell science *123*, 4195-4200.
Garcia Arguinzonis, M. I., Galler, A. B., Walter, U., Reinhard, M., and Simm, A. (2002). Increased spreading, Rac/p21-activated kinase (PAK) activity, and compromised cell motility in cells deficient in vasodilator-stimulated phosphoprotein (VASP). The Journal of biological chemistry *277*, 45604-45610.
Gardel, M. L., Schneider, I. C., Aratyn-Schaus, Y., and Waterman, C. M. (2010). Mechanical integration of actin and adhesion dynamics in cell migration. Annual review of cell and developmental biology *26*, 315-333.
Gawecka, J. E., Young-Robbins, S. S., Sulzmaier, F. J., Caliva, M. J., Heikkila, M. M., Matter, M. L., and Ramos, J. W. (2012). RSK2 protein suppresses integrin activation and fibronectin matrix assembly and promotes cell migration. The Journal of biological chemistry *287*, 43424-43437.
Geiger, B., Spatz, J. P., and Bershadsky, A. D. (2009). Environmental sensing through focal adhesions. Nat Rev Mol Cell Biol *10*, 21-33.
Geneste, O., Copeland, J. W., and Treisman, R. (2002). LIM kinase and Diaphanous cooperate to regulate serum response factor and actin dynamics. The Journal of cell biology *157*, 831-838.
George, E. L., Baldwin, H. S., and Hynes, R. O. (1997). Fibronectins are essential for heart and blood vessel morphogenesis but are dispensable for initial specification of precursor cells. Blood *90*, 3073-3081.

George, E. L., Georges-Labouesse, E. N., Patel-King, R. S., Rayburn, H., and Hynes, R. O. (1993). Defects in mesoderm, neural tube and vascular development in mouse embryos lacking fibronectin. Development *119*, 1079-1091.
Georges-Labouesse, E. N., George, E. L., Rayburn, H., and Hynes, R. O. (1996). Mesodermal development in mouse embryos mutant for fibronectin. Developmental dynamics : an official publication of the American Association of Anatomists *207*, 145-156.
Gille, H., Kortenjann, M., Thomae, O., Moomaw, C., Slaughter, C., Cobb, M. H., and Shaw, P. E. (1995). ERK phosphorylation potentiates Elk-1-mediated ternary complex formation and transactivation. The EMBO journal *14*, 951-962.
Gingras, A. R., Bate, N., Goult, B. T., Hazelwood, L., Canestrelli, I., Grossmann, J. G., Liu, H., Putz, N. S., Roberts, G. C., Volkmann, N.*, et al.* (2008). The structure of the C-terminal actin-binding domain of talin. The EMBO journal *27*, 458-469.
Grosse, R., Copeland, J. W., Newsome, T. P., Way, M., and Treisman, R. (2003). A role for VASP in RhoA-Diaphanous signalling to actin dynamics and SRF activity. The EMBO journal *22*, 3050-3061.
Haas, A. L., Ahrens, P., Bright, P. M., and Ankel, H. (1987). Interferon induces a 15-kilodalton protein exhibiting marked homology to ubiquitin. The Journal of biological chemistry *262*, 11315-11323.
Haas, B., Mayer, P., Jennissen, K., Scholz, D., Diaz, M. B., Bloch, W., Herzig, S., Fassler, R., and Pfeifer, A. (2009). Protein kinase g controls brown fat cell differentiation and mitochondrial biogenesis. Sci Signal *2*, ra78.
Halbrugge, M., and Walter, U. (1989). Purification of a vasodilator-regulated phosphoprotein from human platelets. Eur J Biochem *185*, 41-50.
Halbrugge, M., and Walter, U. (1990). Analysis, purification and properties of a 50,000-dalton membrane-associated phosphoprotein from human platelets. J Chromatogr *521*, 335-343.
Halder, G., Dupont, S., and Piccolo, S. (2012). Transduction of mechanical and cytoskeletal cues by YAP and TAZ. Nat Rev Mol Cell Biol *13*, 591-600.
Hall, A. (2012). Rho family GTPases. Biochem Soc Trans *40*, 1378-1382.
Heino, J., Ignotz, R. A., Hemler, M. E., Crouse, C., and Massague, J. (1989). Regulation of cell adhesion receptors by transforming growth factor-beta. Concomitant regulation of integrins that share a common beta 1 subunit. The Journal of biological chemistry *264*, 380-388.
Heino, J., and Massague, J. (1989). Transforming growth factor-beta switches the pattern of integrins expressed in MG-63 human osteosarcoma cells and causes a selective loss of cell adhesion to laminin. The Journal of biological chemistry *264*, 21806-21811.
Hertzog, M., van Heijenoort, C., Didry, D., Gaudier, M., Coutant, J., Gigant, B., Didelot, G., Preat, T., Knossow, M., Guittet, E., and Carlier, M. F. (2004). The beta-thymosin/WH2 domain; structural basis for the switch from inhibition to promotion of actin assembly. Cell *117*, 611-623.
Hocking, D. C., Sottile, J., Reho, T., Fassler, R., and McKeown-Longo, P. J. (1999). Inhibition of fibronectin matrix assembly by the heparin-binding domain of vitronectin. Journal of Biological Chemistry *274*, 27257-27264.
Hoeflich, K. P., O'Brien, C., Boyd, Z., Cavet, G., Guerrero, S., Jung, K., Januario, T., Savage, H., Punnoose, E., Truong, T.*, et al.* (2009). In vivo antitumor activity of MEK and phosphatidylinositol 3-kinase inhibitors in basal-like breast cancer models. Clinical cancer research : an official journal of the American Association for Cancer Research *15*, 4649-4664.
Huang, X. Z., Wu, J. F., Cass, D., Erle, D. J., Corry, D., Young, S. G., Farese, R. V., Jr., and Sheppard, D. (1996). Inactivation of the integrin beta 6 subunit gene reveals a role of epithelial integrins in regulating inflammation in the lung and skin. The Journal of cell biology *133*, 921-928.
Humphries, J. D., Wang, P., Streuli, C., Geiger, B., Humphries, M. J., and Ballestrem, C. (2007). Vinculin controls focal adhesion formation by direct interactions with talin and actin. The Journal of cell biology *179*, 1043-1057.

Humphries, M. J. (2000). Integrin structure. Biochem Soc Trans *28*, 311-339.
Huveneers, S., and Danen, E. H. (2009). Adhesion signalling - crosstalk between integrins, Src and Rho. Journal of cell science *122*, 1059-1069.
Hynes, R. O. (2002). Integrins: bidirectional, allosteric signalling machines. Cell *110*, 673-687.
Hynes, R. O. (2009). The extracellular matrix: not just pretty fibrils. Science *326*, 1216-1219.
Ignotz, R. A., Heino, J., and Massague, J. (1989). Regulation of cell adhesion receptors by transforming growth factor-beta. Regulation of vitronectin receptor and LFA-1. The Journal of biological chemistry *264*, 389-392.
Ito, S. (1969). Structure and function of the glycocalyx. Federation proceedings *28*, 12-25.
Ivaska, J., and Heino, J. (2010). Interplay between cell adhesion and growth factor receptors: from the plasma membrane to the endosomes. Cell and tissue research *339*, 111-120.
Jaalouk, D. E., and Lammerding, J. (2009). Mechanotransduction gone awry. Nat Rev Mol Cell Biol *10*, 63-73.
Jacobs, D., Glossip, D., Xing, H., Muslin, A. J., and Kornfeld, K. (1999). Multiple docking sites on substrate proteins form a modular system that mediates recognition by ERK MAP kinase. Genes Dev *13*, 163-175.
Janknecht, R., Ernst, W. H., Pingoud, V., and Nordheim, A. (1993). Activation of ternary complex factor Elk-1 by MAP kinases. The EMBO journal *12*, 5097-5104.
Janmey, P. A., and Miller, R. T. (2011). Mechanisms of mechanical signalling in development and disease. Journal of cell science *124*, 9-18.
Jeon, Y. J., Choi, J. S., Lee, J. Y., Yu, K. R., Kim, S. M., Ka, S. H., Oh, K. H., Kim, K. I., Zhang, D. E., Bang, O. S., and Chung, C. H. (2009). ISG15 modification of filamin B negatively regulates the type I interferon-induced JNK signalling pathway. EMBO Rep *10*, 374-380.
Jiang, G., Giannone, G., Critchley, D. R., Fukumoto, E., and Sheetz, M. P. (2003). Two-piconewton slip bond between fibronectin and the cytoskeleton depends on talin. Nature *424*, 334-337.
Jiang, G., Huang, A. H., Cai, Y., Tanase, M., and Sheetz, M. P. (2006). Rigidity sensing at the leading edge through alphavbeta3 integrins and RPTPalpha. Biophys J *90*, 1804-1809.
Junttila, M. R., and de Sauvage, F. J. (2013). Influence of tumour micro-environment heterogeneity on therapeutic response. Nature *501*, 346-354.
Kadler, K. E., Hill, A., and Canty-Laird, E. G. (2008). Collagen fibrillogenesis: fibronectin, integrins, and minor collagens as organizers and nucleators. Current opinion in cell biology *20*, 495-501.
Kanchanawong, P., Shtengel, G., Pasapera, A. M., Ramko, E. B., Davidson, M. W., Hess, H. F., and Waterman, C. M. (2010). Nanoscale architecture of integrin-based cell adhesions. Nature *468*, 580-584.
Ketscher, L., Basters, A., Prinz, M., and Knobeloch, K. P. (2012). mHERC6 is the essential ISG15 E3 ligase in the murine system. Biochemical and biophysical research communications *417*, 135-140.
Kiema, T., Lad, Y., Jiang, P., Oxley, C. L., Baldassarre, M., Wegener, K. L., Campbell, I. D., Ylanne, J., and Calderwood, D. A. (2006). The molecular basis of filamin binding to integrins and competition with talin. Molecular cell *21*, 337-347.
Kiessling, A., Hogrefe, C., Erb, S., Bobach, C., Fuessel, S., Wessjohann, L., and Seliger, B. (2009). Expression, regulation and function of the ISGylation system in prostate cancer. Oncogene *28*, 2606-2620.
Kim, K. I., Giannakopoulos, N. V., Virgin, H. W., and Zhang, D. E. (2004). Interferon-inducible ubiquitin E2, Ubc8, is a conjugating enzyme for protein ISGylation. Mol Cell Biol *24*, 9592-9600.
Kim, M., Carman, C. V., and Springer, T. A. (2003). Bidirectional transmembrane signalling by cytoplasmic domain separation in integrins. Science *301*, 1720-1725.

Kim, S., Harris, M., and Varner, J. A. (2000). Regulation of integrin alpha vbeta 3-mediated endothelial cell migration and angiogenesis by integrin alpha5beta1 and protein kinase A. Journal of Biological Chemistry *275*, 33920-33928.
Kuo, J. C., Han, X., Hsiao, C. T., Yates Iii, J. R., and Waterman, C. M. (2011). Analysis of the myosin-II-responsive focal adhesion proteome reveals a role for beta-Pix in negative regulation of focal adhesion maturation. Nat Cell Biol.
Lanford, R. E., Guerra, B., Lee, H., Chavez, D., Brasky, K. M., and Bigger, C. B. (2006). Genomic response to interferon-alpha in chimpanzees: implications of rapid downregulation for hepatitis C kinetics. Hepatology *43*, 961-972.
Laukaitis, C. M., Webb, D. J., Donais, K., and Horwitz, A. F. (2001). Differential dynamics of alpha 5 integrin, paxillin, and alpha-actinin during formation and disassembly of adhesions in migrating cells. The Journal of cell biology *153*, 1427-1440.
Legate, K. R., Wickstrom, S. A., and Fassler, R. (2009). Genetic and cell biological analysis of integrin outside-in signalling. Genes Dev *23*, 397-418.
Leiss, M., Beckmann, K., Giros, A., Costell, M., and Fassler, R. (2008). The role of integrin binding sites in fibronectin matrix assembly in vivo. Current opinion in cell biology.
Leitner, L., Shaposhnikov, D., Descot, A., Hoffmann, R., and Posern, G. (2010). Epithelial Protein Lost in Neoplasm alpha (Eplin-alpha) is transcriptionally regulated by G-actin and MAL/MRTF coactivators. Molecular cancer *9*, 60.
Leitner, L., Shaposhnikov, D., Mengel, A., Descot, A., Julien, S., Hoffmann, R., and Posern, G. (2011). MAL/MRTF-A controls migration of non-invasive cells by upregulation of cytoskeleton-associated proteins. Journal of cell science *124*, 4318-4331.
Li, J., Zhu, X., Chen, M., Cheng, L., Zhou, D., Lu, M. M., Du, K., Epstein, J. A., and Parmacek, M. S. (2005). Myocardin-related transcription factor B is required in cardiac neural crest for smooth muscle differentiation and cardiovascular development. Proceedings of the National Academy of Sciences of the United States of America *102*, 8916-8921.
Li, L., Okura, M., and Imamoto, A. (2002). Focal adhesions require catalytic activity of Src family kinases to mediate integrin-matrix adhesion. Mol Cell Biol *22*, 1203-1217.
Li, M. O., Wan, Y. Y., Sanjabi, S., Robertson, A. K., and Flavell, R. A. (2006a). Transforming growth factor-beta regulation of immune responses. Annual review of immunology *24*, 99-146.
Li, S., Chang, S., Qi, X., Richardson, J. A., and Olson, E. N. (2006b). Requirement of a myocardin-related transcription factor for development of mammary myoepithelial cells. Mol Cell Biol *26*, 5797-5808.
Liang, G., Ahlqvist, K., Pannem, R., Posern, G., and Massoumi, R. (2011). Serum response factor controls CYLD expression via MAPK signalling pathway. PloS one *6*, e19613.
Lo, S. H. (2004). Tensin. The international journal of biochemistry & cell biology *36*, 31-34.
Lu, C., Takagi, J., and Springer, T. A. (2001). Association of the membrane proximal regions of the alpha and beta subunit cytoplasmic domains constrains an integrin in the inactive state. The Journal of biological chemistry *276*, 14642-14648.
Luo, B. H., Carman, C. V., and Springer, T. A. (2007). Structural basis of integrin regulation and signalling. Annual review of immunology *25*, 619-647.
Ma, Z., Morris, S. W., Valentine, V., Li, M., Herbrick, J. A., Cui, X., Bouman, D., Li, Y., Mehta, P. K., Nizetic, D.*, et al.* (2001). Fusion of two novel genes, RBM15 and MKL1, in the t(1;22)(p13;q13) of acute megakaryoblastic leukemia. Nature genetics *28*, 220-221.
Mack, C. P., Somlyo, A. V., Hautmann, M., Somlyo, A. P., and Owens, G. K. (2001). Smooth muscle differentiation marker gene expression is regulated by RhoA-mediated actin polymerization. The Journal of biological chemistry *276*, 341-347.
Malakhov, M. P., Malakhova, O. A., Kim, K. I., Ritchie, K. J., and Zhang, D. E. (2002). UBP43 (USP18) specifically removes ISG15 from conjugated proteins. The Journal of biological chemistry *277*, 9976-9981.
Malakhova, O. A., and Zhang, D. E. (2008). ISG15 inhibits Nedd4 ubiquitin E3 activity and enhances the innate antiviral response. The Journal of biological chemistry *283*, 8783-8787.

Mao, Y., and Schwarzbauer, J. E. (2005). Fibronectin fibrillogenesis, a cell-mediated matrix assembly process. Matrix biology : journal of the International Society for Matrix Biology *24*, 389-399.
Marais, R., Wynne, J., and Treisman, R. (1993). The SRF accessory protein Elk-1 contains a growth factor-regulated transcriptional activation domain. Cell *73*, 381-393.
Martin, P. (1997). Wound healing--aiming for perfect skin regeneration. Science *276*, 75-81.
McDonald, J. A., Quade, B. J., Broekelmann, T. J., LaChance, R., Forsman, K., Hasegawa, E., and Akiyama, S. (1987). Fibronectin's cell-adhesive domain and an amino-terminal matrix assembly domain participate in its assembly into fibroblast pericellular matrix. The Journal of biological chemistry *262*, 2957-2967.
Medjkane, S., Perez-Sanchez, C., Gaggioli, C., Sahai, E., and Treisman, R. (2009). Myocardin-related transcription factors and SRF are required for cytoskeletal dynamics and experimental metastasis. Nat Cell Biol *11*, 257-268.
Messenguy, F., and Dubois, E. (2003). Role of MADS box proteins and their cofactors in combinatorial control of gene expression and cell development. Gene *316*, 1-21.
Miralles, F., Posern, G., Zaromytidou, A. I., and Treisman, R. (2003). Actin dynamics control SRF activity by regulation of its coactivator MAL. Cell *113*, 329-342.
Miwa, T., and Kedes, L. (1987). Duplicated CArG box domains have positive and mutually dependent regulatory roles in expression of the human alpha-cardiac actin gene. Mol Cell Biol *7*, 2803-2813.
Mizejewski, G. J. (1999). Role of integrins in cancer: survey of expression patterns. Proceedings of the Society for Experimental Biology and Medicine *222*, 124-138.
Moore, S. W., Roca-Cusachs, P., and Sheetz, M. P. (2010). Stretchy proteins on stretchy substrates: the important elements of integrin-mediated rigidity sensing. Dev Cell *19*, 194-206.
Morita, T., and Hayashi, K. (2013). G-actin sequestering protein thymosin-beta4 regulates the activity of myocardin-related transcription factor. Biochemical and biophysical research communications *437*, 331-335.
Mouilleron, S., Guettler, S., Langer, C. A., Treisman, R., and McDonald, N. Q. (2008). Molecular basis for G-actin binding to RPEL motifs from the serum response factor coactivator MAL. The EMBO journal *27*, 3198-3208.
Mouilleron, S., Langer, C. A., Guettler, S., McDonald, N. Q., and Treisman, R. (2011). Structure of a pentavalent G-actin*MRTF-A complex reveals how G-actin controls nucleocytoplasmic shuttling of a transcriptional coactivator. Sci Signal *4*, ra40.
Munger, J. S., Huang, X., Kawakatsu, H., Griffiths, M. J., Dalton, S. L., Wu, J., Pittet, J. F., Kaminski, N., Garat, C., Matthay, M. A.*, et al.* (1999). The integrin alpha v beta 6 binds and activates latent TGF beta 1: a mechanism for regulating pulmonary inflammation and fibrosis. Cell *96*, 319-328.
Munger, J. S., and Sheppard, D. (2011). Cross talk among TGF-beta signalling pathways, integrins, and the extracellular matrix. Cold Spring Harbor perspectives in biology *3*, a005017.
Nakamura, S., Hayashi, K., Iwasaki, K., Fujioka, T., Egusa, H., Yatani, H., and Sobue, K. (2010). Nuclear import mechanism for myocardin family members and their correlation with vascular smooth muscle cell phenotype. The Journal of biological chemistry *285*, 37314-37323.
Nemeth, J. A., Nakada, M. T., Trikha, M., Lang, Z., Gordon, M. S., Jayson, G. C., Corringham, R., Prabhakar, U., Davis, H. M., and Beckman, R. A. (2007). Alpha-v integrins as therapeutic targets in oncology. Cancer Invest *25*, 632-646.
Neve, R. M., Chin, K., Fridlyand, J., Yeh, J., Baehner, F. L., Fevr, T., Clark, L., Bayani, N., Coppe, J. P., Tong, F.*, et al.* (2006). A collection of breast cancer cell lines for the study of functionally distinct cancer subtypes. Cancer cell *10*, 515-527.
Nevo, J., Mai, A., Tuomi, S., Pellinen, T., Pentikainen, O. T., Heikkila, P., Lundin, J., Joensuu, H., Bono, P., and Ivaska, J. (2010). Mammary-derived growth inhibitor (MDGI) interacts with integrin alpha-subunits and suppresses integrin activity and invasion. Oncogene *29*, 6452-6463.

Norman, C., Runswick, M., Pollock, R., and Treisman, R. (1988). Isolation and properties of cDNA clones encoding SRF, a transcription factor that binds to the c-fos serum response element. Cell *55*, 989-1003.
O'Toole, T. E., Katagiri, Y., Faull, R. J., Peter, K., Tamura, R., Quaranta, V., Loftus, J. C., Shattil, S. J., and Ginsberg, M. H. (1994). Integrin cytoplasmic domains mediate inside-out signal transduction. The Journal of cell biology *124*, 1047-1059.
Oakes, P. W., Beckham, Y., Stricker, J., and Gardel, M. L. (2012). Tension is required but not sufficient for focal adhesion maturation without a stress fiber template. The Journal of cell biology *196*, 363-374.
Oh, J., Richardson, J. A., and Olson, E. N. (2005). Requirement of myocardin-related transcription factor-B for remodeling of branchial arch arteries and smooth muscle differentiation. Proceedings of the National Academy of Sciences of the United States of America *102*, 15122-15127.
Ohashi, T., Kiehart, D. P., and Erickson, H. P. (2002). Dual labeling of the fibronectin matrix and actin cytoskeleton with green fluorescent protein variants. Journal of cell science *115*, 1221-1229.
Okumura, A., Pitha, P. M., and Harty, R. N. (2008). ISG15 inhibits Ebola VP40 VLP budding in an L-domain-dependent manner by blocking Nedd4 ligase activity. Proceedings of the National Academy of Sciences of the United States of America *105*, 3974-3979.
Okumura, F., Okumura, A. J., Uematsu, K., Hatakeyama, S., Zhang, D. E., and Kamura, T. (2013). Activation of double-stranded RNA-activated protein kinase (PKR) by interferon-stimulated gene 15 (ISG15) modification down-regulates protein translation. The Journal of biological chemistry *288*, 2839-2847.
Okumura, F., Zou, W., and Zhang, D. E. (2007). ISG15 modification of the eIF4E cognate 4EHP enhances cap structure-binding activity of 4EHP. Genes Dev *21*, 255-260.
Olski, T. M., Noegel, A. A., and Korenbaum, E. (2001). Parvin, a 42 kDa focal adhesion protein, related to the alpha-actinin superfamily. Journal of cell science *114*, 525-538.
Otey, C. A., Vasquez, G. B., Burridge, K., and Erickson, B. W. (1993). Mapping of the alpha-actinin binding site within the beta 1 integrin cytoplasmic domain. The Journal of biological chemistry *268*, 21193-21197.
Otterbein, L. R., Cosio, C., Graceffa, P., and Dominguez, R. (2002). Crystal structures of the vitamin D-binding protein and its complex with actin: structural basis of the actin-scavenger system. Proceedings of the National Academy of Sciences of the United States of America *99*, 8003-8008.
Oudshoorn, D., van Boheemen, S., Sanchez-Aparicio, M. T., Rajsbaum, R., Garcia-Sastre, A., and Versteeg, G. A. (2012). HERC6 is the main E3 ligase for global ISG15 conjugation in mouse cells. PloS one *7*, e29870.
Oxley, C. L., Anthis, N. J., Lowe, E. D., Vakonakis, I., Campbell, I. D., and Wegener, K. L. (2008). An integrin phosphorylation switch: the effect of beta3 integrin tail phosphorylation on Dok1 and talin binding. The Journal of biological chemistry *283*, 5420-5426.
Pan, D. (2010). The hippo signalling pathway in development and cancer. Dev Cell *19*, 491-505.
Pankov, R., Cukierman, E., Katz, B. Z., Matsumoto, K., Lin, D. C., Lin, S., Hahn, C., and Yamada, K. M. (2000). Integrin dynamics and matrix assembly: tensin-dependent translocation of alpha(5)beta(1) integrins promotes early fibronectin fibrillogenesis. The Journal of cell biology *148*, 1075-1090.
Parsons-Wingerter, P., Kasman, I. M., Norberg, S., Magnussen, A., Zanivan, S., Rissone, A., Baluk, P., Favre, C. J., Jeffry, U., Murray, R., and McDonald, D. M. (2005). Uniform overexpression and rapid accessibility of alpha5beta1 integrin on blood vessels in tumors. Am J Pathol *167*, 193-211.
Parsons, J. T., Horwitz, A. R., and Schwartz, M. A. (2010). Cell adhesion: integrating cytoskeletal dynamics and cellular tension. Nat Rev Mol Cell Biol *11*, 633-643.
Parvani, J. G., Galliher-Beckley, A. J., Schiemann, B. J., and Schiemann, W. P. (2013). Targeted inactivation of beta1 integrin induces beta3 integrin switching, which drives breast cancer metastasis by TGF-beta. Molecular biology of the cell *24*, 3449-3459.

Paszek, M. J., Boettiger, D., Weaver, V. M., and Hammer, D. A. (2009). Integrin clustering is driven by mechanical resistance from the glycocalyx and the substrate. PLoS Comput Biol *5*, e1000604.
Paszek, M. J., Zahir, N., Johnson, K. R., Lakins, J. N., Rozenberg, G. I., Gefen, A., Reinhart-King, C. A., Margulies, S. S., Dembo, M., Boettiger, D.*, et al.* (2005). Tensional homeostasis and the malignant phenotype. Cancer cell *8*, 241-254.
Pawlowski, R., Rajakyla, E. K., Vartiainen, M. K., and Treisman, R. (2010). An actin-regulated importin alpha/beta-dependent extended bipartite NLS directs nuclear import of MRTF-A. The EMBO journal *29*, 3448-3458.
Pentikainen, U., and Ylanne, J. (2009). The regulation mechanism for the auto-inhibition of binding of human filamin A to integrin. Journal of molecular biology *393*, 644-657.
Philippar, U., Schratt, G., Dieterich, C., Muller, J. M., Galgoczy, P., Engel, F. B., Keating, M. T., Gertler, F., Schule, R., Vingron, M., and Nordheim, A. (2004). The SRF target gene Fhl2 antagonizes RhoA/MAL-dependent activation of SRF. Molecular cell *16*, 867-880.
Pipes, G. C., Creemers, E. E., and Olson, E. N. (2006). The myocardin family of transcriptional coactivators: versatile regulators of cell growth, migration, and myogenesis. Genes Dev *20*, 1545-1556.
Plantefaber, L. C., and Hynes, R. O. (1989). Changes in integrin receptors on oncogenically transformed cells. Cell *56*, 281-290.
Posern, G., Sotiropoulos, A., and Treisman, R. (2002). Mutant actins demonstrate a role for unpolymerized actin in control of transcription by serum response factor. Molecular biology of the cell *13*, 4167-4178.
Posern, G., and Treisman, R. (2006). Actin' together: serum response factor, its cofactors and the link to signal transduction. Trends in cell biology *16*, 588-596.
Rantala, J. K., Pouwels, J., Pellinen, T., Veltel, S., Laasola, P., Mattila, E., Potter, C. S., Duffy, T., Sundberg, J. P., Kallioniemi, O.*, et al.* (2011). SHARPIN is an endogenous inhibitor of beta1-integrin activation. Nat Cell Biol *13*, 1315-1324.
Reynolds, L. E., Wyder, L., Lively, J. C., Taverna, D., Robinson, S. D., Huang, X., Sheppard, D., Hynes, R. O., and Hodivala-Dilke, K. M. (2002). Enhanced pathological angiogenesis in mice lacking beta3 integrin or beta3 and beta5 integrins. Nature medicine *8*, 27-34.
Ridley, A. J., and Hall, A. (1992). The small GTP-binding protein rho regulates the assembly of focal adhesions and actin stress fibers in response to growth factors. Cell *70*, 389-399.
Riveline, D., Zamir, E., Balaban, N. Q., Schwarz, U. S., Ishizaki, T., Narumiya, S., Kam, Z., Geiger, B., and Bershadsky, A. D. (2001). Focal contacts as mechanosensors: externally applied local mechanical force induces growth of focal contacts by an mDia1-dependent and ROCK-independent mechanism. The Journal of cell biology *153*, 1175-1186.
Robinson, M. J., and Cobb, M. H. (1997). Mitogen-activated protein kinase pathways. Current opinion in cell biology *9*, 180-186.
Roca-Cusachs, P., Gauthier, N. C., Del Rio, A., and Sheetz, M. P. (2009). Clustering of alpha(5)beta(1) integrins determines adhesion strength whereas alpha(v)beta(3) and talin enable mechanotransduction. Proceedings of the National Academy of Sciences of the United States of America *106*, 16245-16250.
Rocco, M., Carson, M., Hantgan, R., McDonagh, J., and Hermans, J. (1983). Dependence of the shape of the plasma fibronectin molecule on solvent composition. Ionic strength and glycerol content. The Journal of biological chemistry *258*, 14545-14549.
Rohatgi, R., Ma, L., Miki, H., Lopez, M., Kirchhausen, T., Takenawa, T., and Kirschner, M. W. (1999). The interaction between N-WASP and the Arp2/3 complex links Cdc42-dependent signals to actin assembly. Cell *97*, 221-231.
Sabatier, L., Chen, D., Fagotto-Kaufmann, C., Hubmacher, D., McKee, M. D., Annis, D. S., Mosher, D. F., and Reinhardt, D. P. (2009). Fibrillin assembly requires fibronectin. Molecular biology of the cell *20*, 846-858.
Sakai, T., Jove, R., Fassler, R., and Mosher, D. F. (2001). Role of the cytoplasmic tyrosines of beta 1A integrins in transformation by v-src. Proceedings of the National Academy of Sciences of the United States of America *98*, 3808-3813.

Sarasin-Filipowicz, M., Oakeley, E. J., Duong, F. H., Christen, V., Terracciano, L., Filipowicz, W., and Heim, M. H. (2008). Interferon signalling and treatment outcome in chronic hepatitis C. Proceedings of the National Academy of Sciences of the United States of America *105*, 7034-7039.
Sawada, Y., Tamada, M., Dubin-Thaler, B. J., Cherniavskaya, O., Sakai, R., Tanaka, S., and Sheetz, M. P. (2006). Force sensing by mechanical extension of the Src family kinase substrate p130Cas. Cell *127*, 1015-1026.
Schiller, H. B., Friedel, C. C., Boulegue, C., and Fassler, R. (2011). Quantitative proteomics of the integrin adhesome show a myosin II-dependent recruitment of LIM domain proteins. EMBO Rep *12*, 259-266.
Schiller, H. B., Hermann, M. R., Polleux, J., Vignaud, T., Zanivan, S., Friedel, C. C., Sun, Z., Raducanu, A., Gottschalk, K. E., Thery, M.*, et al.* (2013). beta1- and alphav-class integrins cooperate to regulate myosin II during rigidity sensing of fibronectin-based microenvironments. Nat Cell Biol *15*, 625-636.
Schratt, G., Philippar, U., Berger, J., Schwarz, H., Heidenreich, O., and Nordheim, A. (2002). Serum response factor is crucial for actin cytoskeletal organization and focal adhesion assembly in embryonic stem cells. The Journal of cell biology *156*, 737-750.
Schwartz, M. A., and Ginsberg, M. H. (2002). Networks and crosstalk: integrin signalling spreads. Nat Cell Biol *4*, E65-68.
Seabra, M. C. (1998). Membrane association and targeting of prenylated Ras-like GTPases. Cellular signalling *10*, 167-172.
Selvaraj, A., and Prywes, R. (2004). Expression profiling of serum inducible genes identifies a subset of SRF target genes that are MKL dependent. BMC molecular biology *5*, 13.
Sgorbissa, A., and Brancolini, C. (2012). IFNs, ISGylation and cancer: Cui prodest? Cytokine & growth factor reviews *23*, 307-314.
Shen, B., Delaney, M. K., and Du, X. (2012). Inside-out, outside-in, and inside-outside-in: G protein signalling in integrin-mediated cell adhesion, spreading, and retraction. Current opinion in cell biology *24*, 600-606.
Sheppard, D., Cohen, D. S., Wang, A., and Busk, M. (1992). Transforming growth factor beta differentially regulates expression of integrin subunits in guinea pig airway epithelial cells. The Journal of biological chemistry *267*, 17409-17414.
Shore, P., and Sharrocks, A. D. (1995a). The ETS-domain transcription factors Elk-1 and SAP-1 exhibit differential DNA binding specificities. Nucleic acids research *23*, 4698-4706.
Shore, P., and Sharrocks, A. D. (1995b). The MADS-box family of transcription factors. Eur J Biochem *229*, 1-13.
Silva, R., D'Amico, G., Hodivala-Dilke, K. M., and Reynolds, L. E. (2008). Integrins: the keys to unlocking angiogenesis. Arterioscler Thromb Vasc Biol *28*, 1703-1713.
Sime, P. J., Xing, Z., Graham, F. L., Csaky, K. G., and Gauldie, J. (1997). Adenovector-mediated gene transfer of active transforming growth factor-beta1 induces prolonged severe fibrosis in rat lung. The Journal of clinical investigation *100*, 768-776.
Smith, J. C., Symes, K., Hynes, R. O., and DeSimone, D. (1990). Mesoderm induction and the control of gastrulation in Xenopus laevis: the roles of fibronectin and integrins. Development *108*, 229-238.
Sotiropoulos, A., Gineitis, D., Copeland, J., and Treisman, R. (1999). Signal-regulated activation of serum response factor is mediated by changes in actin dynamics. Cell *98*, 159-169.
Springer, T. A., and Dustin, M. L. (2012). Integrin inside-out signalling and the immunological synapse. Current opinion in cell biology *24*, 107-115.
Streuli, C. H., and Akhtar, N. (2009). Signal co-operation between integrins and other receptor systems. The Biochemical journal *418*, 491-506.
Sun, Q., Chen, G., Streb, J. W., Long, X., Yang, Y., Stoeckert, C. J., Jr., and Miano, J. M. (2006a). Defining the mammalian CArGome. Genome research *16*, 197-207.
Sun, Y., Boyd, K., Xu, W., Ma, J., Jackson, C. W., Fu, A., Shillingford, J. M., Robinson, G. W., Hennighausen, L., Hitzler, J. K.*, et al.* (2006b). Acute myeloid leukemia-associated Mkl1 (Mrtf-a) is a key regulator of mammary gland function. Mol Cell Biol *26*, 5809-5826.

Sundberg, C., and Rubin, K. (1996). Stimulation of beta1 integrins on fibroblasts induces PDGF independent tyrosine phosphorylation of PDGF beta-receptors. The Journal of cell biology *132*, 741-752.
Takada, Y., Ye, X., and Simon, S. (2007). The integrins. Genome biology *8*, 215.
Takagi, J., Erickson, H. P., and Springer, T. A. (2001). C-terminal opening mimics 'inside-out' activation of integrin alpha5beta1. Nature structural biology *8*, 412-416.
Takagi, J., Petre, B. M., Walz, T., and Springer, T. A. (2002). Global conformational rearrangements in integrin extracellular domains in outside-in and inside-out signalling. Cell *110*, 599-511.
Takahashi, S., Leiss, M., Moser, M., Ohashi, T., Kitao, T., Heckmann, D., Pfeifer, A., Kessler, H., Takagi, J., Erickson, H. P., and Fassler, R. (2007). The RGD motif in fibronectin is essential for development but dispensable for fibril assembly. The Journal of cell biology *178*, 167-178.
Takala, H., Nurminen, E., Nurmi, S. M., Aatonen, M., Strandin, T., Takatalo, M., Kiema, T., Gahmberg, C. G., Ylanne, J., and Fagerholm, S. C. (2008). Beta2 integrin phosphorylation on Thr758 acts as a molecular switch to regulate 14-3-3 and filamin binding. Blood *112*, 1853-1862.
Takeuchi, T., Iwahara, S., Saeki, Y., Sasajima, H., and Yokosawa, H. (2005). Link between the ubiquitin conjugation system and the ISG15 conjugation system: ISG15 conjugation to the UbcH6 ubiquitin E2 enzyme. Journal of biochemistry *138*, 711-719.
Tam, P. P., and Behringer, R. R. (1997). Mouse gastrulation: the formation of a mammalian body plan. Mechanisms of development *68*, 3-25.
Tan, S. M., Hyland, R. H., Al-Shamkhani, A., Douglass, W. A., Shaw, J. M., and Law, S. K. (2000). Effect of integrin beta 2 subunit truncations on LFA-1 (CD11a/CD18) and Mac-1 (CD11b/CD18) assembly, surface expression, and function. Journal of immunology *165*, 2574-2581.
Tang, Y., Rowe, R. G., Botvinick, E. L., Kurup, A., Putnam, A. J., Seiki, M., Weaver, V. M., Keller, E. T., Goldstein, S., Dai, J.*, et al.* (2013). MT1-MMP-dependent control of skeletal stem cell commitment via a beta1-integrin/YAP/TAZ signalling axis. Dev Cell *25*, 402-416.
ten Dijke, P., and Arthur, H. M. (2007). Extracellular control of TGFbeta signalling in vascular development and disease. Nat Rev Mol Cell Biol *8*, 857-869.
Treisman, R., Marais, R., and Wynne, J. (1992). Spatial flexibility in ternary complexes between SRF and its accessory proteins. The EMBO journal *11*, 4631-4640.
van der Flier, A., and Sonnenberg, A. (2001). Structural and functional aspects of filamins. Biochim Biophys Acta *1538*, 99-117.
Vartiainen, M. K., Guettler, S., Larijani, B., and Treisman, R. (2007). Nuclear actin regulates dynamic subcellular localization and activity of the SRF cofactor MAL. Science *316*, 1749-1752.
Verdoni, A. M., Schuster, K. J., Cole, B. S., Ikeda, A., Kao, W. W., and Ikeda, S. (2010). A pathogenic relationship between a regulator of the actin cytoskeleton and serum response factor. Genetics *186*, 147-157.
Vogel, V., and Sheetz, M. (2006). Local force and geometry sensing regulate cell functions. Nat Rev Mol Cell Biol *7*, 265-275.
von Wichert, G., Jiang, G., Kostic, A., De Vos, K., Sap, J., and Sheetz, M. P. (2003). RPTP-alpha acts as a transducer of mechanical force on alphav/beta3-integrin-cytoskeleton linkages. The Journal of cell biology *161*, 143-153.
Wagner, K. W., Punnoose, E. A., Januario, T., Lawrence, D. A., Pitti, R. M., Lancaster, K., Lee, D., von Goetz, M., Yee, S. F., Totpal, K.*, et al.* (2007). Death-receptor O-glycosylation controls tumor-cell sensitivity to the proapoptotic ligand Apo2L/TRAIL. Nature medicine *13*, 1070-1077.
Waldmann, R., Nieberding, M., and Walter, U. (1987). Vasodilator-stimulated protein phosphorylation in platelets is mediated by cAMP- and cGMP-dependent protein kinases. Eur J Biochem *167*, 441-448.
Wang, D. Z., Li, S., Hockemeyer, D., Sutherland, L., Wang, Z., Schratt, G., Richardson, J. A., Nordheim, A., and Olson, E. N. (2002). Potentiation of serum response factor activity by

a family of myocardin-related transcription factors. Proceedings of the National Academy of Sciences of the United States of America *99*, 14855-14860.
Wear, M. A., and Cooper, J. A. (2004). Capping protein: new insights into mechanism and regulation. Trends in biochemical sciences *29*, 418-428.
Wegener, K. L., Partridge, A. W., Han, J., Pickford, A. R., Liddington, R. C., Ginsberg, M. H., and Campbell, I. D. (2007). Structural basis of integrin activation by talin. Cell *128*, 171-182.
White, D. P., Caswell, P. T., and Norman, J. C. (2007). alpha v beta3 and alpha5beta1 integrin recycling pathways dictate downstream Rho kinase signalling to regulate persistent cell migration. The Journal of cell biology *177*, 515-525.
Wong, J. J., Pung, Y. F., Sze, N. S., and Chin, K. C. (2006). HERC5 is an IFN-induced HECT-type E3 protein ligase that mediates type I IFN-induced ISGylation of protein targets. Proceedings of the National Academy of Sciences of the United States of America *103*, 10735-10740.
Wu, C., Keivens, V. M., O'Toole, T. E., McDonald, J. A., and Ginsberg, M. H. (1995). Integrin activation and cytoskeletal interaction are essential for the assembly of a fibronectin matrix. Cell *83*, 715-724.
Xiong, J. P., Stehle, T., Diefenbach, B., Zhang, R., Dunker, R., Scott, D. L., Joachimiak, A., Goodman, S. L., and Arnaout, M. A. (2001). Crystal structure of the extracellular segment of integrin alpha Vbeta3. Science *294*, 339-345.
Xiong, J. P., Stehle, T., Zhang, R., Joachimiak, A., Frech, M., Goodman, S. L., and Arnaout, M. A. (2002). Crystal structure of the extracellular segment of integrin alpha Vbeta3 in complex with an Arg-Gly-Asp ligand. Science *296*, 151-155.
Yang, J. T., Bader, B. L., Kreidberg, J. A., Ullman-Cullere, M., Trevithick, J. E., and Hynes, R. O. (1999). Overlapping and independent functions of fibronectin receptor integrins in early mesodermal development. Dev Biol *215*, 264-277.
Yang, J. T., and Hynes, R. O. (1996). Fibronectin receptor functions in embryonic cells deficient in alpha 5 beta 1 integrin can be replaced by alpha V integrins. Molecular biology of the cell *7*, 1737-1748.
Yang, J. T., Rayburn, H., and Hynes, R. O. (1993). Embryonic mesodermal defects in alpha 5 integrin-deficient mice. Development *119*, 1093-1105.
Yang, S. H., Bumpass, D. C., Perkins, N. D., and Sharrocks, A. D. (2002). The ETS domain transcription factor Elk-1 contains a novel class of repression domain. Mol Cell Biol *22*, 5036-5046.
Yang, S. H., Vickers, E., Brehm, A., Kouzarides, T., and Sharrocks, A. D. (2001). Temporal recruitment of the mSin3A-histone deacetylase corepressor complex to the ETS domain transcription factor Elk-1. Mol Cell Biol *21*, 2802-2814.
Yang, Z., Mu, Z., Dabovic, B., Jurukovski, V., Yu, D., Sung, J., Xiong, X., and Munger, J. S. (2007). Absence of integrin-mediated TGFbeta1 activation in vivo recapitulates the phenotype of TGFbeta1-null mice. The Journal of cell biology *176*, 787-793.
Yates, P. R., Atherton, G. T., Deed, R. W., Norton, J. D., and Sharrocks, A. D. (1999). Id helix-loop-helix proteins inhibit nucleoprotein complex formation by the TCF ETS-domain transcription factors. The EMBO journal *18*, 968-976.
Yu, F. X., Zhao, B., Panupinthu, N., Jewell, J. L., Lian, I., Wang, L. H., Zhao, J., Yuan, H., Tumaneng, K., Li, H.*, et al.* (2012). Regulation of the Hippo-YAP pathway by G-protein-coupled receptor signalling. Cell *150*, 780-791.
Yuan, W., and Krug, R. M. (2001). Influenza B virus NS1 protein inhibits conjugation of the interferon (IFN)-induced ubiquitin-like ISG15 protein. The EMBO journal *20*, 362-371.
Zaidel-Bar, R., and Geiger, B. (2010). The switchable integrin adhesome. Journal of cell science *123*, 1385-1388.
Zaidel-Bar, R., Itzkovitz, S., Ma'ayan, A., Iyengar, R., and Geiger, B. (2007). Functional atlas of the integrin adhesome. Nat Cell Biol *9*, 858-867.
Zamir, E., Katz, M., Posen, Y., Erez, N., Yamada, K. M., Katz, B. Z., Lin, S., Lin, D. C., Bershadsky, A., Kam, Z., and Geiger, B. (2000). Dynamics and segregation of cell-matrix adhesions in cultured fibroblasts. Nat Cell Biol *2*, 191-196.

Zhang, Q., Checovich, W. J., Peters, D. M., Albrecht, R. M., and Mosher, D. F. (1994). Modulation of cell surface fibronectin assembly sites by lysophosphatidic acid. The Journal of cell biology *127*, 1447-1459.
Zhang, Q., Magnusson, M. K., and Mosher, D. F. (1997). Lysophosphatidic acid and microtubule-destabilizing agents stimulate fibronectin matrix assembly through Rho-dependent actin stress fiber formation and cell contraction. Molecular biology of the cell *8*, 1415-1425.
Zhang, S. X., Garcia-Gras, E., Wycuff, D. R., Marriot, S. J., Kadeer, N., Yu, W., Olson, E. N., Garry, D. J., Parmacek, M. S., and Schwartz, R. J. (2005). Identification of direct serum-response factor gene targets during Me2SO-induced P19 cardiac cell differentiation. The Journal of biological chemistry *280*, 19115-19126.
Zhang, X., Jiang, G., Cai, Y., Monkley, S. J., Critchley, D. R., and Sheetz, M. P. (2008). Talin depletion reveals independence of initial cell spreading from integrin activation and traction. Nat Cell Biol *10*, 1062-1068.
Zhao, C., Beaudenon, S. L., Kelley, M. L., Waddell, M. B., Yuan, W., Schulman, B. A., Huibregtse, J. M., and Krug, R. M. (2004). The UbcH8 ubiquitin E2 enzyme is also the E2 enzyme for ISG15, an IFN-alpha/beta-induced ubiquitin-like protein. Proceedings of the National Academy of Sciences of the United States of America *101*, 7578-7582.
Zheng, X. M., Resnick, R. J., and Shalloway, D. (2000). A phosphotyrosine displacement mechanism for activation of Src by PTPalpha. The EMBO journal *19*, 964-978.
Zhong, C., Chrzanowska-Wodnicka, M., Brown, J., Shaub, A., Belkin, A. M., and Burridge, K. (1998). Rho-mediated contractility exposes a cryptic site in fibronectin and induces fibronectin matrix assembly. The Journal of cell biology *141*, 539-551.
Zhu, J., Luo, B. H., Xiao, T., Zhang, C., Nishida, N., and Springer, T. A. (2008). Structure of a complete integrin ectodomain in a physiologic resting state and activation and deactivation by applied forces. Molecular cell *32*, 849-861.
Zhu, J., Zhu, J., and Springer, T. A. (2013). Complete integrin headpiece opening in eight steps. The Journal of cell biology *201*, 1053-1068.
Zigmond, S. H. (2004). Beginning and ending an actin filament: control at the barbed end. Current topics in developmental biology *63*, 145-188.
Zou, W., Papov, V., Malakhova, O., Kim, K. I., Dao, C., Li, J., and Zhang, D. E. (2005). ISG15 modification of ubiquitin E2 Ubc13 disrupts its ability to form thioester bond with ubiquitin. Biochemical and biophysical research communications *336*, 61-68.
Zou, W., and Zhang, D. E. (2006). The interferon-inducible ubiquitin-protein isopeptide ligase (E3) EFP also functions as an ISG15 E3 ligase. The Journal of biological chemistry *281*, 3989-3994.

5 Acknowledgements/Danksagungen

Diese Arbeit wäre nicht möglich gewesen ohne die Hilfe und Unterstützung von vielen Menschen aus meinem wissenschaftlichen und privaten Umfeld. An dieser Stelle möchte ich die Wichtigsten nennen:

Zuerst möchte ich Herrn Prof. Reinhard Fässler danken, der mir es ermöglicht hat in großartiger wissenschaftlicher Umgebung zu arbeiten und erfolgreich zu sein. Er hat mir beigebracht wie Forschung „funktioniert", wie man die Dinge bis ins kleinste Detail objektiv betrachtet und verarbeitet. Während der letzten vier Jahre hat er mich fortwährend unterstützt und war immer zur Stelle wenn ich Hilfe oder seinen Rat brauchte. Ich habe in dieser Zeit viel von ihm gelernt.

Prof. Dr. Christian Wahl-Schott gilt besonderer Dank. Er hat sich für meine Arbeit als Zweitgutachter/-prüfer zur Verfügung gestellt.

Außerdem möchte ich den weiteren Mitgliedern des Prüfungskomitees **Prof. Dr. Martin Biel, PD Dr. Stefan Zahler, Prof. Dr. Karl-Peter Hopfner und Prof. Dr. Angelika Vollmar** für die Zeit zur Evaluation meiner Arbeit herzlich danken.

Dr. Kevin Flynn möchte ich für das Korrekturlesen dieser Arbeit herzlich danken.

Für das tolle Arbeitsklima, die Kollegialität und daraus entstandene Freundschaft möchte ich **Emanuel Rognoni, Moritz Widmaier, Dr. Ina Rohwedder, Tom (alias Hui-Yuan) Tseng, Dr. Madis Jakobson, Dr. Julien Polleux, Hildegard Reiter (Mischa)** und nicht zu vergessen meiner lieben **Uschi Kuhn** danken. Es war eine tolle Zeit mit euch! Danke fürs Aufmuntern, Mitdenken, Mitexperimentieren und fürs Mittanzen.

Bei **Dr. Armin Lambacher, Klaus Weber, Ines Lach-Kusevic und Lidia Wimmer** danke ich für die administrative oder technische Unterstützung.

Für die unterhaltsamen Besuche und guten Zusprüche möchte ich **meiner ganzen Familie** danken.

Außerdem gilt ganz besonderer Dank **meinen Eltern.** „Danke, dass ihr mir dieses Studium mit Promotion ermöglicht habt, dass ihr immer an mich geglaubt habt und dass es ok war uns deswegen nur noch selten zu sehen!"

Besonders unterstützt hat mich **Robert.** Er war in allen Lebenslagen für mich da und das werde ich nie vergessen.

6 Curriculum vitae

Michaela-Rosemarie Hermann
Schöttlstrasse 10 - 81369 München
Tel.: +49(0)176-22884391
ela.h@gmx.de

15th May 1984
Aschaffenburg, Germany

- **Intense laboratory experience in Biomedical Research**
- **PhD at MPIB in Molecular Medicine** (Defense on 13th May 2014)
- **Studied Molecular Biomedicine at Rheinische Friedrich-Wilhelms-University, Bonn**
- **Studied Biology at Technical University Darmstadt**
- **International team experience**
- **Excellent network and communication skills**

EDUCATION

2010 to present
Max-Planck-Institute of Biochemistry
Molecular Medicine Department
Group of Prof. Dr. Reinhard Fässler
Am Klopferspitz 18
D-82152 Martinsried

Boehringer Ingelheim Fond fellow
Member of Faculty of 1000 (since 2012)

PhD thesis: „Integrin Subtype Specific Assembly of Focal Adhesion Proteins and Their Effect on Cell Contractility and Actin-based Signalling"
Publications:
1. **Hermann MR et al.,** *Manuscript in preparation*
2. **Hermann MR et al.,** *Manuscript in preparation*
3. **Hermann MR** and Schiller et al., *Nature Cell Biology*, 2013
4. Jennissen K, **Hermann MR** et al., *Science Signaling*, 2012

03/2009 to 03/2010
Rheinische Friedrich-Wilhelms-University Bonn
Institute of Pharmacology and Toxicology
Group of Prof. Dr. Alexander Pfeifer (Head of the Dept.)
University Clinic Bonn, Biomedical Center
Sigmund-Freud-Str. 25
D-53105 Bonn

Student of excellence program with 30 students per year in collaboration with Dr. Hanno Wild, Bayer Health Care, Assistant Professor and Tutor: **Molecular Biomedicine**
Diploma thesis:
„Role of VASP in mesenchymal stem cell and murine embryonic fibroblast differentiation"
Final grade: 1.0 (Highest possible grade: 1.0, Pass grade: 4.0)

10/2006 to 03/2010
Diploma studies disciplines, subdivided in clusters:
A: Genetics, Pathology, Neuropathology, and Developmental Biology
B: Chemical Biology, Biochemistry, Bioinformatics, and Pharmacology
C: Biology of Infections, Microbiology, Immunology, and Immunobiology
D: Pharmakology/Toxikology, Pathophysiology/ -biochemistry, Basics of Clinical Medicine, and Pharmakotherapy
Final grade: 1.8 (Highest possible grade: 1.0, Pass grade: 4.0)

Further Specialization and Internships:

Bayer Schering Pharma
Screening and Lead Discovery
Dr. Benjamin Bader
Müllerstrasse 178 - 13342 Berlin
Mission: „Establishment of a Co-activator Recruitment Assay on a TR-FRET based system in 384 well format and screening of about 6400 substances."

The University of York
Department of Biology
Dr. Christopher J H Elliott
P.O. Box 373, York YO1 5YW, UK
Mission: "Investigation of the neurotransmitter proctolin and its effects in *Drosophila Melanogaster* reproduction."

10/2004 to 10/2006
Technical University Darmstadt
Diploma student of Biology
Pre-diploma grade: 2.0 (Highest possible grade: 1.0, Pass grade: 4.0)

LABORATORY SKILLS

A very broad biochemical and -medical spectrum:
Cell Culture: Isolation, Immortalization, Viral Reconstitution and Transfection of Cell Lines, RNAi;
Mouse Work: Design and Cloning of Knockout Animal, Breeding, Analysis of Phenotype, Isolation of various Cell types;
Methods: Immunostaining, -blotting, Confocal Microscopy, Life Imaging of Cells and Tissues, FACS analysis, Luciferase Assay, Mass Spectrometry Analysis, In Situ Hybridization, Real-Time PCR, ELISA, 3D Invasion Assays and all standard daily lab work;

PRESENTATIONS/POSTERS

List of the most important:
1. Hermann MR et al., **Gordon Research Conference** (GRC) "Fibronectin, Integrins & Related Molecules" in Ventura Beach Marriott, from February 10th to 15th 2013.
2. Hermann MR et al., **5th Mechanobiology Conference at the National University of Singapore**, from November 9th to 11th 2011
3. Hermann MR et al., SFB863 Meeting in Hohenkammern, 2011

REFERENCE

Prof. Dr. Reinhard Fässler, Director
MPI of Biochemistry
Am Klopferspitz 18 - 82152 Martinsried
Phone: +49 89 8578 - 2424

7 Appendix

7.1 First publication (Co- first author)

7.2 Second publication (First author)

Publication 1

β1- and αv-class integrins cooperate to regulate myosin II during rigidity sensing of fibronectin-based microenvironments.

published as

Schiller HB, Hermann MR, Polleux J, Vignaud T, Zanivan S, Friedel CC, Sun Z, Raducanu A, Gottschalk KE, Théry M, Mann M, Fässler R: **β1- and αv-class integrins cooperate to regulate myosin II during rigidity sensing of fibronectin-based microenvironments.** Nat Cell Biol. 2013 Jun;15(6):625-36. doi: 10.1038/ncb2747. Epub 2013 May 26

Supplementary Information:

Videos

1. **Video 1:** Time-lapse movie of pKO-αv cells plated on FN. (2,362 KB, Download) Cells were plated on FN-coated (5 μg ml−1; blocked with 1% BSA) tissue culture dishes in the presence of 10% serum and video tracked over 20 h with a frame rate of 1 picture every 4 min. Pictures were acquired with a phase contrast microscope at ×20 magnification.

2. **Video 2:** Time-lapse movie of pKO-αv/β1 cells plated on FN. (2,014 KB, Download) Cells were plated on FN-coated (5 μg ml−1; blocked with 1% BSA) tissue culture dishes in the presence of 10% serum and video tracked over 20 h with a frame rate of 1 picture every 4 min. Pictures were acquired with a phase contrast microscope at ×20 magnification.

3. **Video 3:** Time-lapse movie of pKO-β1 cells plated on FN. (2,710 KB, Download) Cells were plated on FN-coated (5 μg ml−1; blocked with 1% BSA) tissue culture dishes in the presence of 10% serum and video tracked over 20 h with a frame rate of 1 picture every 4 min. Pictures were acquired with a phase contrast microscope at ×20 magnification.

PDF files

1. Supplementary Information (3,019 KB)

Excel files

1. Supplementary Table 1 (1,714 KB)
2. Supplementary Table 2 (980 KB)
3. Supplementary Table 3 (1,278 KB)
4. Supplementary Table 4 (181 KB)
5. Supplementary Table 5 (12 KB)
6. Supplementary Table 6 (13 KB)

nature cell biology

β_1- and α_v-class integrins cooperate to regulate myosin II during rigidity sensing of fibronectin-based microenvironments

Herbert B. Schiller[1,6], Michaela-Rosemarie Hermann[1,6], Julien Polleux[1], Timothée Vignaud[2], Sara Zanivan[3], Caroline C. Friedel[4], Zhiqi Sun[1], Aurelia Raducanu[1], Kay-E. Gottschalk[5], Manuel Théry[2], Matthias Mann[3] and Reinhard Fässler[1,7]

How different integrins that bind to the same type of extracellular matrix protein mediate specific functions is unclear. We report the functional analysis of β_1- and α_v-class integrins expressed in pan-integrin-null fibroblasts seeded on fibronectin. Reconstitution with β_1-class integrins promotes myosin-II-independent formation of small peripheral adhesions and cell protrusions, whereas expression of α_v-class integrins induces the formation of large focal adhesions. Co-expression of both integrin classes leads to full myosin activation and traction-force development on stiff fibronectin-coated substrates, with α_v-class integrins accumulating in adhesion areas exposed to high traction forces. Quantitative proteomics linked α_v-class integrins to a GEF-H1–RhoA pathway coupled to the formin mDia1 but not myosin II, and $\alpha_5\beta_1$ integrins to a RhoA–Rock–myosin II pathway. Our study assigns specific functions to distinct fibronectin-binding integrins, demonstrating that $\alpha_5\beta_1$ integrins accomplish force generation, whereas α_v-class integrins mediate the structural adaptations to forces, which cooperatively enable cells to sense the rigidity of fibronectin-based microenvironments.

Integrins are α/β heterodimers that mediate cell adhesion to the extracellular matrix (ECM) and to receptors on other cells[1], thereby regulating numerous biological processes that are essential for development, postnatal homeostasis and pathology[1–4]. The mammalian genome encodes 18 α and 8 β integrin genes, which form 24 heterodimers. Mammalian cells usually co-express several integrins, which recognize ECM components by binding specific amino-acid stretches such as the Arg-Gly-Asp (RGD) motif[1,5]. RGD motifs are found in many matrix proteins including fibronectin, in which RGD mediates binding to $\alpha_5\beta_1$ and all α_v-class integrins[6]. *In vivo* and *in vitro* studies indicated that $\alpha_5\beta_1$ and α_v-class integrins (for example, $\alpha_v\beta_3$) exert both specific and redundant functions[7–15]; however, how these distinct integrins accomplish their individual functions and whether these cooperate remains unclear. The signalling properties and functions of integrins are executed by specialized adhesive structures with distinct morphology, subcellular localization, lifespan and molecular composition. Nascent adhesions are short-lived adhesive structures in membrane protrusions[16] that promote the activity of Rho–GTPases such as Rac1. Some nascent adhesions develop into large focal adhesions that initiate multiple signalling pathways, which activate effectors including myosin II. Myosin II exerts contractile forces resulting in adhesion reinforcement and recruitment of more proteins to focal adhesions, which induces a further increase in myosin II activity[17]. This feedback signalling to myosin II critically depends on biophysical parameters such as ECM stiffness. The identity of mechanosensor(s) in focal adhesions, whether it is an integrin, a focal adhesion protein or a combination of both, is unknown[18]. Quantitative mass spectrometry (MS) was previously used to determine the protein composition of adhesion structures (adhesomes) of cells seeded on fibronectin, and the dynamic changes on myosin-II-induced adhesion maturation[19,20]. As cells recruit different integrin classes to fibronectin-induced adhesions, these studies did not assign specific proteins and signalling outputs to particular integrins.

Here we developed a cell system to investigate the protein composition and signalling properties of adhesion sites anchored selectively through $\alpha_5\beta_1$ and/or α_v-class integrins. We found marked integrin-class-specific differences in the morphology of focal adhesions, in their requirement for mechanical tension, in the protein composition of their adhesomes and their signalling capacity. Furthermore, we

[1]Department of Molecular Medicine, Max Planck Institute of Biochemistry, 82152 Martinsried, Germany. [2]Laboratoire de Physiologie Cellulaire et Végétale, Institut de Recherche en Technologies et Sciences pour le Vivant, CNRS/UJF/INRA/CEA, 17 Rue des Martyrs, 38054 Grenoble, France. [3]Department of Proteomics and Signal Transduction, Max Planck Institute of Biochemistry, 82152 Martinsried, Germany. [4]Institute for Informatics, Ludwig-Maximilians-Universität München, 80333 Munich, Germany. [5]Institute of Experimental Physics, University of Ulm, 89069 Ulm, Germany. [6]These authors contributed equally to this work.
[7]Correspondence should be addressed to R.F. (e-mail: faessler@biochem.mpg.de)

Received 2 November 2012; accepted 4 April 2013; published online 26 May 2013; DOI: 10.1038/ncb2747

© 2013 Macmillan Publishers Limited. All rights reserved.

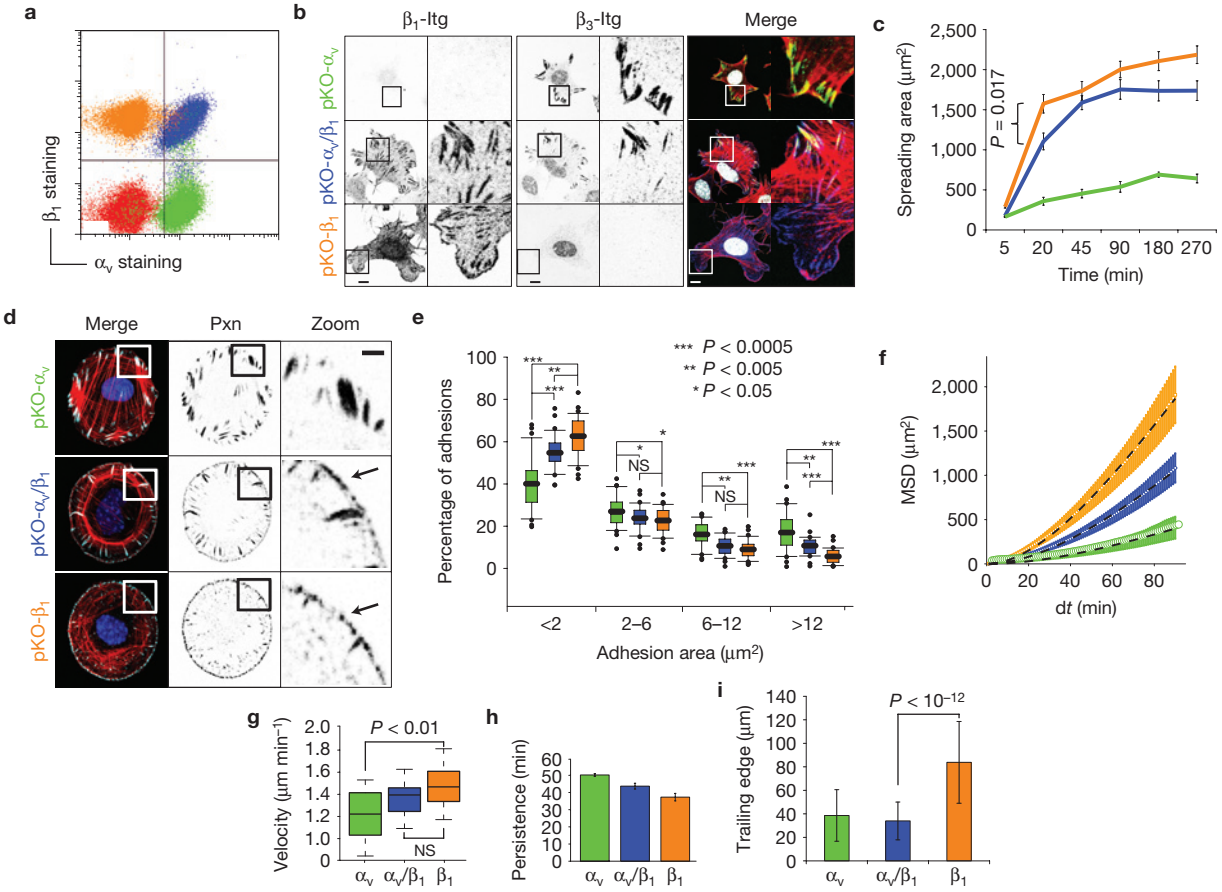

Figure 1 Different morphologies and adhesive functions of pKO-α_v, pKO-β_1 and pKO-α_v/β_1 cells. (**a**) Flow cytometry analysis of β_1 and α_v cell surface levels. (**b**) Immunostaining of indicated cell types plated for 90 min on fibronectin for β_1 and β_3. The merged images show an overlay of integrin (β_1, blue; β_3, green), F-actin (red) and nuclear (DAPI, blue) staining. Scale bars, 10 μm. (**c**) Spreading areas of cells seeded on fibronectin. Error bars represent s.e.m. ($n = 20$ cells per time point; 1 representative of 2 independent experiments is shown). The P value is derived from a t-test. (**d**) Cells were plated on circular fibronectin-coated micropatterns and immunostained for paxillin (Pxn). The merged images show an overlay of paxillin (white), F-actin (red) and nuclear (DAPI, blue) staining. Arrows indicate nascent adhesions (<2 μm²) in the cell periphery. Scale bar, 10 μm. (**e**) Boxplots show the distribution of adhesion size classes. Significance was calculated using a t-test ($n = 30$ cells; 1 representative of 2 independent experiments is shown; boxplot whisker ends are at 1.5 interquartile range and outliers are shown as dots). (**f-h**) Migration velocity (**g**) and mean persistence time (**h**) was determined with the MSD values of cell nuclei (**f**) by filming migrating cells over a period of 90 min with a 1 min time lapse (pKO-α_v $n = 12$, pKO-β_1 $n = 14$, pKO-α_v/β_1 $n = 12$; data aggregated over 5 independent experiments). The P value for velocities (**g**) was calculated using an unpaired Wilcoxon test and the persistence time bar graph (**g**) shows the fit error as implemented in the MatLab software. NS, not significant. (**i**) Trailing edge lengths of migrating cells are shown with mean lengths from the cell rear to the middle of the nucleus. Error bars represent s.d. and the P values were calculated using a t-test (pKO-α_v $n = 51$, pKO-β_1 $n = 66$, pKO-α_v/β_1 $n = 40$; 1 representative of 2 independent experiments is shown). pKO-α_v, green; pKO-α_v/β_1, blue; pKO-β_1, orange.

identified a functional synergy between $\alpha_5\beta_1$ and α_v-class integrin signalling hubs leading to feedback amplification of myosin II activity required for focal-adhesion-mediated rigidity sensing.

RESULTS

Differential functions of $\alpha_5\beta_1$ and α_v-class integrins in adhesion formation and cell migration

To obtain cells expressing β_1- and/or α_v-class integrins we intercrossed mice carrying conditional null mutations for the α_v and β_1 integrin genes and constitutive null mutations for the β_2 and β_7 integrin genes ($\beta_1^{f/f}$, $\alpha_v^{f/f}$, $\beta_2^{-/-}$, $\beta_7^{-/-}$ mice)[21], isolated kidney fibroblasts and immortalized them with the SV40 large T antigen (parental fibroblasts). Deletion of floxed α_v and β_1 integrin genes by adenoviral *Cre* transduction removed all integrins from the parental fibroblast clones (pan-knockouts, pKO; Supplementary Fig. S1a–c). Next we transduced parental fibroblasts with α_v or β_1 or both complementary DNAs and simultaneously transduced *Cre* to delete the floxed integrin alleles. This produced cells expressing α_v (pKO-α_v), β_1 (pKO-β_1) or α_v and β_1 (pKO-α_v/β_1) integrins, respectively (Fig. 1a). The pKO-α_v, pKO-β_1 and pKO-α_v/β_1 cells were sorted for comparable integrin surface levels to the parental cell clones (Supplementary Fig. S1d,e). Using western blotting, flow cytometry and MS we identified the following fibronectin-binding integrins; $\alpha_5\beta_1$ in pKO-β_1 cells, $\alpha_v\beta_3$ and $\alpha_v\beta_5$ in pKO-α_v cells, and $\alpha_5\beta_1$, $\alpha_v\beta_3$ and $\alpha_v\beta_5$ in pKO-α_v/β_1 cells (Supplementary Fig. S1f,g). Calibration of our flow cytometry analysis estimated the presence of 170,000 $\alpha_5\beta_1$ and 300,000 α_v-class integrins on the surface of each cell, resulting in approximately equimolar surface levels for β_1, β_3 and β_5 integrins.

All three cell lines specifically adhered to fibronectin, whereas adhesion on vitronectin was similar for pKO-α_v and pKO-α_v/β_1 cells

© 2013 Macmillan Publishers Limited. All rights reserved.

and absent for pKO-β_1 cells (Supplementary Fig. S1h). To compare the size distribution of focal adhesions we seeded cells for 90 min on fibronectin and immunostained for paxillin, integrin β_1 and β_3 (Fig. 1b and Supplementary Fig. S2a,b). The percentage of small nascent adhesions ($<2\,\mu m^2$) was significantly elevated in pKO-β_1 and pKO-α_v/β_1 cells, whereas large focal adhesions of 6–12 μm^2 dominated in pKO-α_v cells (Supplementary Fig. S2a,b). The cell spreading area on fibronectin was significantly lower in pKO-α_v relative to pKO-β_1 and pKO-α_v/β_1 cells and reduced in pKO-α_v/β_1 relative to pKO-β_1 (Fig. 1c and Supplementary Fig. S1i). As cell shape and spreading area can affect cell contractility, focal adhesion size and distribution[22], we seeded cells on circular fibronectin-coated micropatterns surrounded by non-adhesive polyethylene glycol (PEG), and confirmed the different adhesion size distribution in the three cell lines (Fig. 1d,e). pKO-α_v/β_1 cells contained both small nascent adhesions and large focal adhesions (Fig. 1d). pKO-β_1 and pKO-α_v/β_1 cells showed increased protrusive activity when compared with pKO-α_v cells (Supplementary Fig. S2a,c), which correlated with increased migration speed. The mean square displacement (MSD) of cells migrating on fibronectin showed that pKO-β_1 cells migrated significantly faster than pKO-α_v cells, and that pKO-α_v/β_1 cells exhibited an intermediate migration speed (Fig. 1f,g). As previously shown[13,23,24], expression of α_v-class integrins increased migration persistence (Fig. 1h). pKO-β_1 cells exhibited a significant defect in trailing edge detachment (Fig. 1i and Supplementary Fig. S2c and Videos S1–S3). These results identify a role for $\alpha_5\beta_1$ in protrusive activities and nascent adhesion formation, whereas co-expression of α_v-class integrins also promotes the production of large, stable focal adhesions and trailing edge detachment in migrating cells.

Differential functions of $\alpha_5\beta_1$ and α_v-class integrins synergize to regulate cell contractility

Adhesion maturation and trailing edge retraction in migrating fibroblasts requires coordinated control of myosin-II-mediated cell contractility[25]. We measured myosin II activity using fibronectin-coated X- or crossbow-shaped micropatterns, which report subtle changes in myosin II activity and traction forces along non-adhesive edges[26–28]. Parental fibroblasts cultured on X-shaped fibronectin-coated micropatterns showed a dose-dependent decrease of phosphoT18/S19-myosin light chain (pMLC), paxillin fluorescence intensities and cell area following treatment with the myosin II inhibitor blebbistatin (Supplementary Fig. S2d–g). Crossbow patterns polarize cells into a low contractile front and a highly contractile rear[28]. Immunofluorescence analysis revealed that pMLC and paxillin intensities were the highest in pKO-α_v/β_1, lower in pKO-β_1 and the lowest in pKO-α_v cells (Fig. 2a). Myosin II activity was low in the cell front (Fig. 2b) and high in the cell rear (Fig. 2c) and the cooperative effect of the two integrin classes on pMLC and paxillin intensities in pKO-α_v/β_1 was most prominent in the cell rear (Fig. 2a–c). Treatment with the α_v-class-specific small-molecule inhibitor cilengitide reduced contractility of pKO-α_v/β_1 cells to intermediate levels (Fig. 2b,c), confirming that the adhesive function of α_v-class integrins is required for the synergy with $\alpha_5\beta_1$. We corroborated these results with fibronectin-coated X-shapes, revealing phenotypes that resembled the rear of crossbow shapes (Supplementary Fig. S2h–j).

The ability to form large focal adhesions and stress fibres indicative of high contractile forces together with low pMLC levels in pKO-α_v cells was surprising. Traction-force microscopy experiments on polyacrylamide gels of 35 kPa stiffness revealed good correlation of traction forces and pMLC levels, confirming that traction forces on fibronectin-coated crossbow micropatterns are the lowest in pKO-α_v, the highest in pKO-α_v/β_1 and intermediate in pKO-β_1 cells (Fig. 2d). Along the cell front, traction forces were significantly higher in pKO-β_1 cells when compared with pKO-α_v cells and the highest in pKO-α_v/β_1 (Fig. 2e). Similar differences were observed by calculating the total contractile energy of individual cells (Fig. 2f).

α_v-class integrins accumulate in areas of high traction force and mediate rigidity sensing

$\alpha_v\beta_3$ integrins are known to become immobilized in large and static focal adhesions, whereas $\alpha_5\beta_1$ integrins are mobile, separate from the $\alpha_v\beta_3$ integrins and translocate rearward to fibrillar adhesions[10,29]. To investigate whether $\alpha_5\beta_1$ and α_v-class integrins segregate owing to differential dependence on myosin-II-mediated tension at focal adhesions we seeded pKO-α_v/β_1 and parental floxed cells on fibronectin-coated crossbow shapes and immunostained β_1 and β_3 integrins. Indeed, β_3 heavily accumulated in areas that were shown to be exposed to the highest traction forces, whereas β_1 levels remained very low at these sites (Fig. 3a,b). The β_3 integrins in contractile focal adhesions at the cell rear were lost following blebbistatin treatment, whereas small β_1-containing focal adhesions in the cell periphery were still forming (Fig. 3a). To confirm these findings we plated pKO-α_v/β_1 cells on 1-μm-thin fibronectin-coated lines separated by 3-μm-wide non-adhesive PEG lines. This set-up allows distinguishing ligand-bound from unbound integrins, which is impossible on uniformly coated fibronectin surfaces. Whereas the β_1 integrin staining co-localized with fibronectin lines almost throughout the entire cell length, small β_3 clusters overlaid with lines in the cell periphery associated with F-actin bundles. Blebbistatin treatment or inhibition of Rock with Y-27632 disassembled the β_3 integrin clusters on fibronectin lines, whereas β_1 remained unchanged (Fig. 3c). The differential dependence of $\alpha_5\beta_1$ and α_v-class integrins on myosin-II-mediated tension at focal adhesions suggested that tension-dependent stabilization of α_v-class integrins contributes to rigidity sensing. In line with this hypothesis, traction-force measurements of pKO-β_1 and pKO-α_v/β_1 cells plated on micropatterned polyacrylamide gels of 3 different rigidities (1.4, 10 and 35 kPa) revealed that only pKO-α_v/β_1, but not pKO-β_1, cells were able to increase contractile energies concomitantly with the substrate rigidity. Most notably, the traction forces and contractile energies generated by pKO-β_1 and pKO-α_v/β_1 cells were similar on soft, 1.4 kPa substrates, whereas they differed significantly on stiffer substrates (Fig. 3d,e). We therefore conclude that stabilization of $\alpha_v\beta_3$–fibronectin bonds through actomyosin-mediated tension is required to adjust cell contractility to defined substrate stiffnesses.

Adhesome composition and stoichiometry is controlled by the integrin class and myosin II activity

Cells sense their environment through integrins and numerous plaque proteins in focal adhesions[17,30]. The composition and stoichiometry of the adhesome in fibronectin-bound fibroblasts is controlled by myosin II (refs 19,20). We therefore reasoned that specific binding activities of the integrin cytoplasmic tails and also the differential myosin II activities in pKO-α_v, pKO-β_1 and pKO-α_v/β_1

© 2013 Macmillan Publishers Limited. All rights reserved.

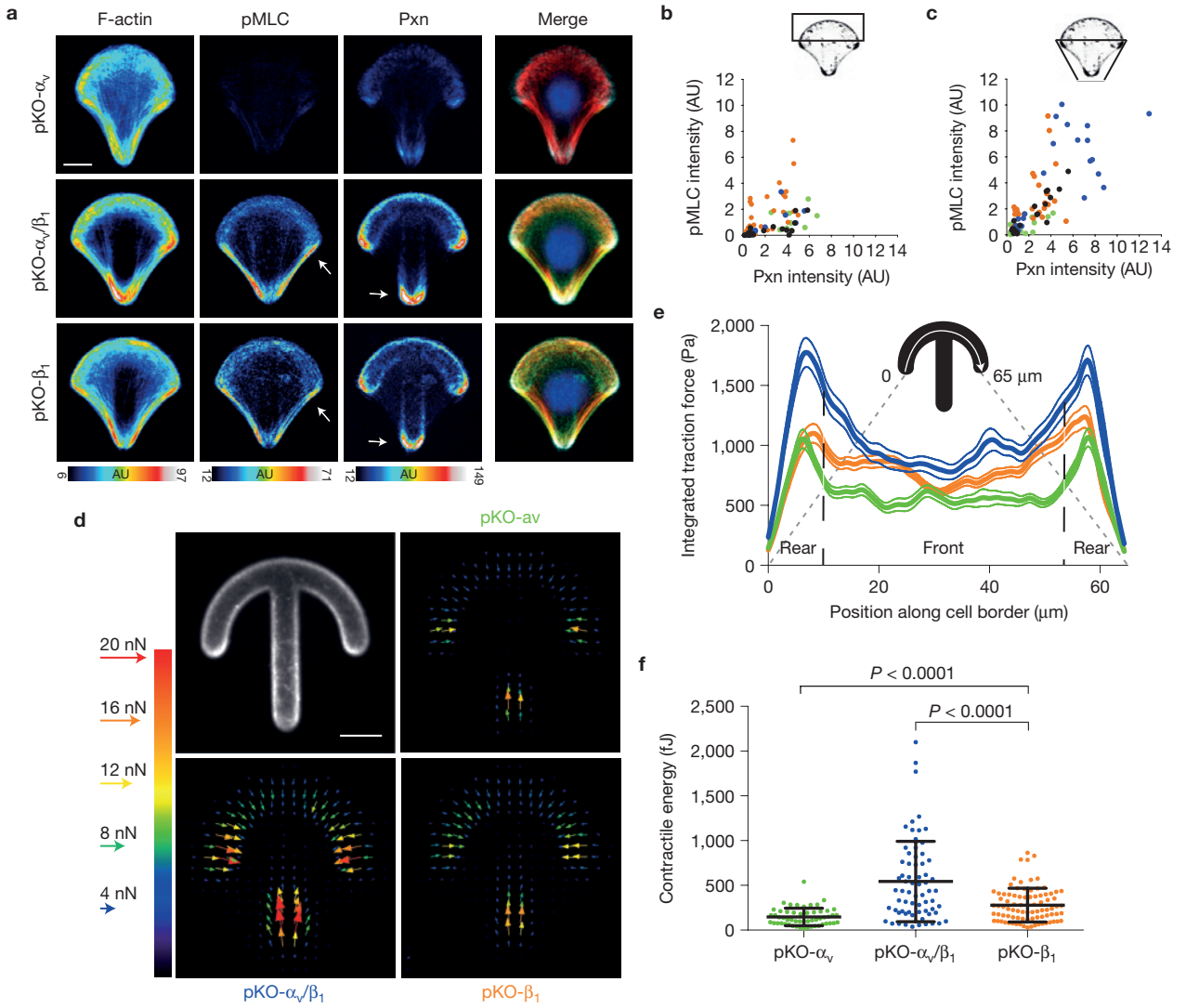

Figure 2 α_v-class integrins cooperate with $\alpha_5\beta_1$ for myosin II reinforcement on stiff fibronectin-coated substrates. (**a**) Averaged confocal images of immunostainings (Merge: F-actin, red; pMLC, green; paxillin, blue; DAPI, blue) of the indicated cell lines plated for 3 h on fibronectin-coated micropatterns (pKO-α_v $n = 55$, pKO-β_1 $n = 36$, pKO-α_v/β_1 $n = 71$; data aggregated over 3 independent experiments). Areas with strong pMLC and paxillin fluorescent signals are marked with arrows. Scale bar, 10 µm. (**b**,**c**) Intensities of pMLC and paxillin (Pxn) fluorescence in the front (**b**) and rear (**c**) regions of individual cells (pKO-α_v $n = 25$, pKO-β_1 $n = 32$, pKO-α_v/β_1 $n = 26$; 1 representative of 3 independent experiments is shown). Optionally, cells were treated with the α_v-class integrin inhibitor cilengitide (1 µM). (**d**) Average traction-force fields of indicated cell types (pKO-α_v $n = 54$, pKO-β_1 $n = 86$, pKO-α_v/β_1 $n = 68$; data aggregated over 3 independent experiments). Arrows indicate force orientation; colour and length represent local force magnitude in nanonewtons. Scale bar, 10 µm. (**e**) Average integrated traction forces along the cell border (pKO-α_v $n = 54$, pKO-β_1 $n = 86$, pKO-α_v/β_1 $n = 58$; data aggregated over 3 independent experiments; thin lines represent s.e.m.). (**f**) Contractile energy of individual cells (pKO-α_v $n = 54$, pKO-β_1 $n = 86$, pKO-α_v/β_1 $n = 68$; data aggregated over 3 independent experiments). Each data point corresponds to the total contractile energy of an individual cell measured by traction-force microscopy. All statistical comparisons were *t*-tests (error bars represent s.e.m.). pKO-α_v (green); pKO-α_v/β_1 (blue); pKO-β_1 (orange); pKOα_v/β_1 + 1 µM cilengitide (black).

cells may contribute to their specific adhesome composition. To test this hypothesis we determined the integrin-class-specific protein composition of focal adhesions. The three cell lines were plated for 45 or 90 min on fibronectin or poly-L-lysine (PLL; permits integrin-independent adhesion) followed by chemical crosslinking and purification of focal adhesions, sample elution and quantitative MS as described previously[19] (Supplementary Fig. S4a and Table S1). Isolated adhesome proteins were quantified using the label-free quantification algorithm of the MaxQuant software[31]. We calculated median MS intensities of 3–4 replicates and performed hierarchical clustering to compare the three cell lines at different time points with and without blebbistatin. This approach allowed identifying protein groups with high correlation of their intensity changes across different substrates, time points and cell lines. We identified a cluster containing 168 proteins significantly enriched for known (previously annotated) focal adhesion proteins. In addition to the 168 proteins, we also considered all previously annotated focal adhesion proteins[32] assigned to other clusters in our analysis. This led to 245 proteins used for further analysis (Supplementary Fig. S4b). Analysis of variance (ANOVA) tests revealed that MS intensities of 62% (152/245) of them were significantly changed

© 2013 Macmillan Publishers Limited. All rights reserved.

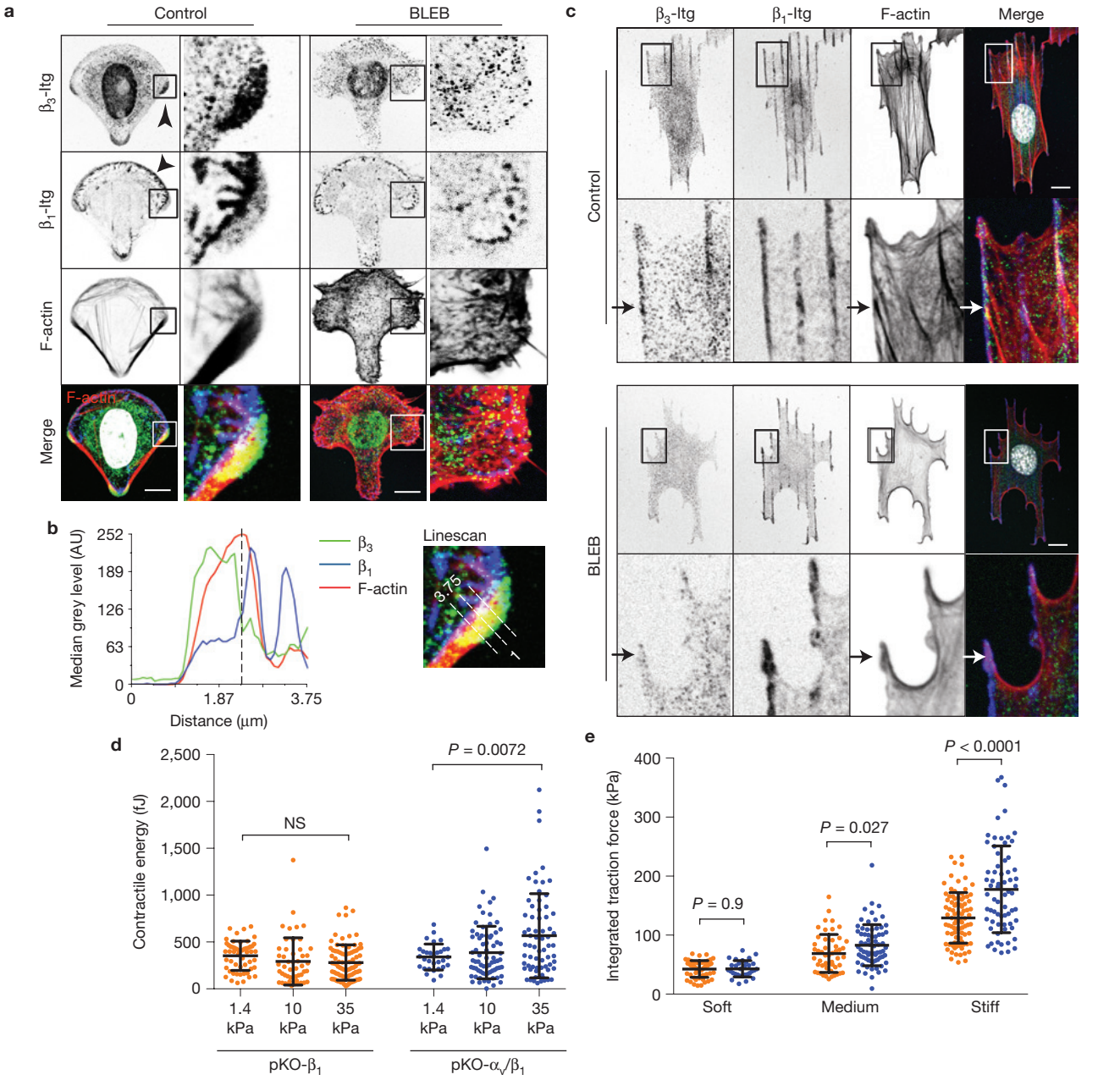

Figure 3 α_v-class integrins accumulate in adhesion areas exposed to high traction force and cooperate with $\alpha_5\beta_1$ for rigidity sensing on fibronectin. (**a**) pKO-α_v/β_1 cells were plated on fibronectin-coated crossbow shapes for 3 h with and without blebbistatin (BLEB) and immunostained for β_1 (blue), β_3 (green) integrins and F-actin (red). Scale bars, 10 μm. DAPI, white (left panel, merge). (**b**) Fluorescence intensity profile of the indicated stainings along the depicted linescan (3.75 μm). (**c**) pKO-α_v/β_1 cells were plated on 1 μm thin fibronectin-coated lines for 90 min with and without blebbistatin and stained for β_1 (blue), β_3 (green) integrin and F-actin (red). Scale bars, 10 μm. DAPI, white (merge). (**d**) Each data point represents the total contractile energy of individual cells measured by traction-force microscopy on gels of indicated rigidities (pKO-β_1: soft $n = 54$, medium $n = 50$, stiff $n = 86$; pKO-α_v/β_1: soft $n = 31$, medium $n = 71$, stiff $n = 68$; data aggregated over 3 independent experiments; all pairwise statistical comparisons from *t*-tests are shown in Supplementary Table S5; NS, not significant). (**e**) Each data point represents the total integrated traction force in kilo Pascal (kPa) of individual cells measured by traction-force microscopy on gels of indicated rigidities (pKO-β_1: soft $n = 54$, medium $n = 50$, stiff $n = 86$; pKO-α_v/β_1: soft $n = 31$, medium $n = 71$, stiff $n = 68$; data aggregated over 3 independent experiments; *P* values of pairwise comparisons were calculated with a *t*-test). pKO-α_v/β_1 (blue); pKO-β_1 (orange).

in at least one of the three cell lines or one of the two time points (Supplementary Table S1).

In line with our previous report[19], blebbistatin induced different intensity reductions in floxed fibroblasts for different classes of adhesome proteins. Following blebbistatin treatment pKO-α_v/β_1 and pKO-β_1 cells were still able to recruit integrin-proximal proteins such as Talin-1, Kindlin-2 and ILK, whereas LIM-domain-containing proteins were reduced to background levels defined by MS intensities from cells seeded on PLL (Fig. 4a). Strikingly, blebbistatin reduced almost all focal adhesion proteins to background levels in pKO-α_v cells, indicating that

© 2013 Macmillan Publishers Limited. All rights reserved.

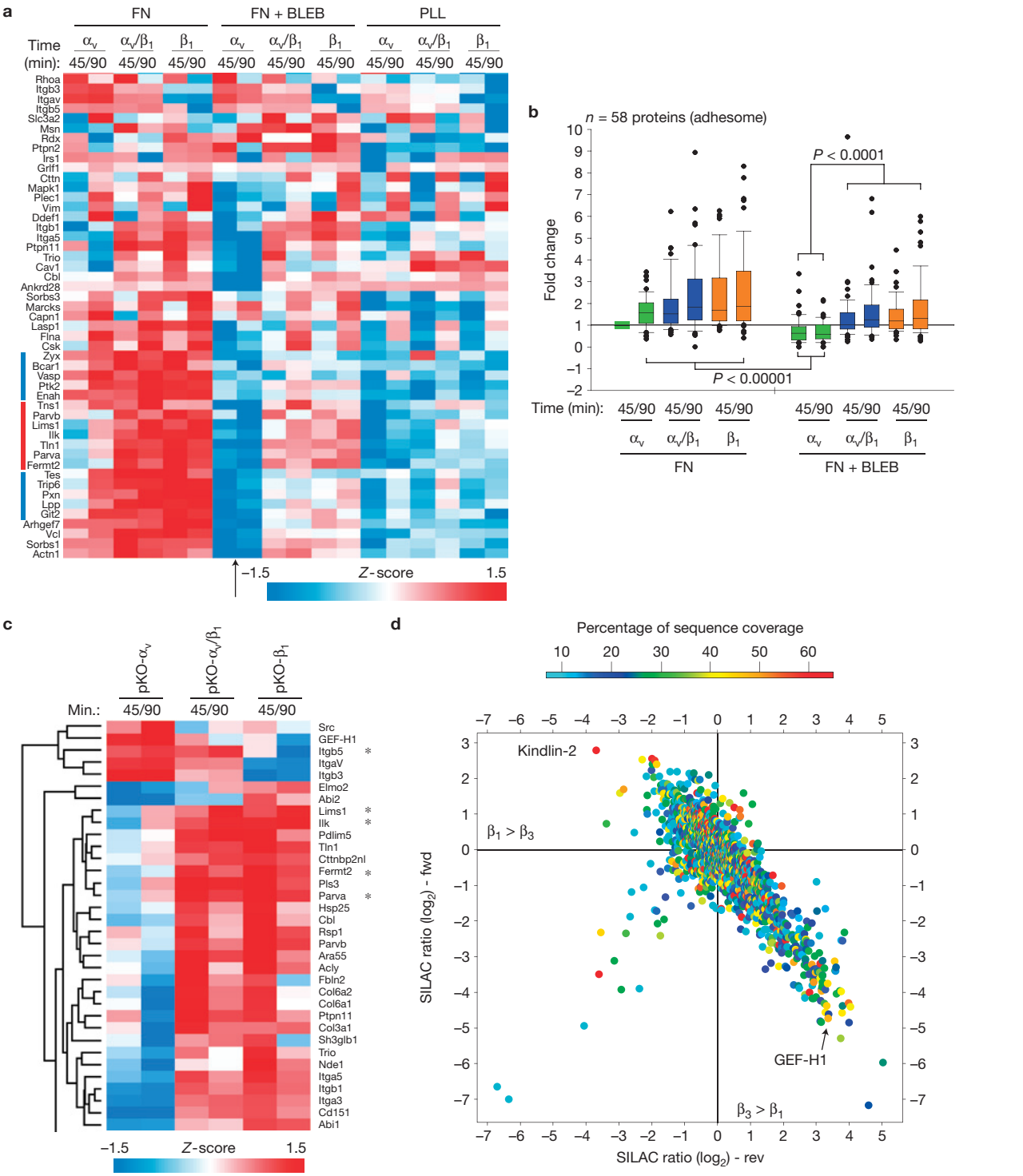

Figure 4 Composition and stoichiometry of the adhesome is determined by the individual integrin and myosin II activity. (**a**) Focal-adhesion-enriched fractions analysed by MS before and after blebbistatin (BLEB) treatment. The *Z*-scores of median MS intensities ($n = 3$–4) are colour coded to show relative protein abundance. A blebbistatin-insensitive cluster is marked with a red bar and blebbistatin-sensitive clusters are marked with blue bars. The arrow highlights the pronounced effect of blebbistatin on pKO-α_v cells. FN, fibronectin. (**b**) Boxplots showing MS intensity differences of 58 known focal adhesion proteins of the indicated cells relative to pKO-α_v cells cultured for 45 min without blebbistatin. A *t*-test revealed significant MS intensity changes after blebbistatin treatment. Boxplot whisker ends are at 1.5 interquartile range and outliers are shown as dots. (**c**) Focal adhesion proteins with similar *Z*-score profiles (colour coded) as $\alpha_5\beta_1$ or α_v-class integrins (selection based on Supplementary Fig. S6) were subjected to hierarchical cluster analysis. Focal-adhesion-enriched fractions were collected 45 and 90 min after plating on fibronectin. (**d**) SILAC ratio plot from label-inverted replicates comparing β_1 with β_3 tail pulldowns. Specific interactors have high SILAC ratios in the forward experiment (fwd) and low SILAC ratios in the label swapped reverse experiment (rev). The colour code shows the percentage of sequence coverage of the proteins identified by MS analysis ($n = 4$; 2 independent experiments). pKO-α_v (green); pKO-α_v/β_1 (blue); pKO-β_1 (orange).

© 2013 Macmillan Publishers Limited. All rights reserved.

the protein recruitment to focal adhesions in blebbistatin-treated pKO-α_v/β_1 cells was mediated by $\alpha_5\beta_1$ (Fig. 4a). A paired Student's *t*-test for 58 known focal adhesion proteins confirmed a significant reduction of crosslinked focal adhesion proteins in pKO-α_v cells by blebbistatin (Fig. 4b). Furthermore, comparing the 45 and 90 min time points revealed that protein recruitment to focal adhesions was delayed in pKO-α_v cells (Fig. 4a,b). Importantly, blebbistatin did not change the MS intensities of α_v-class integrins, excluding inefficient integrin crosslinking as the cause for the diminished recruitment of focal adhesion proteins, and indicating that short-lived/weak α_v-class integrin–fibronectin interactions occur in the absence of cell contractility and can be crosslinked. These findings together with those depicted in Fig. 3 indicate that $\alpha_5\beta_1$ can cluster and induce adhesome assemblies in the absence of myosin-II-mediated tension, whereas the ability of α_v-class integrins to cluster and recruit adhesome proteins depends on myosin II activation and/or the stress fibre architecture at focal adhesions.

ILK and GEF-H1 are required for myosin II reinforcement on stiff substrates

Consulting published protein–protein interactions within the adhesome[30], we established a putative core interactome of fibronectin-bound $\alpha_5\beta_1$ or α_v-class integrins (Supplementary Fig. S5). Hierarchical cluster analysis of MS intensities of the 125 core proteins of the integrin interactome from all conditions tested (Supplementary Fig. S6) revealed 29 proteins correlating with MS intensities of $\alpha_5\beta_1$ at both time points and 2 proteins correlating with MS intensities of α_v-class integrins (Fig. 4c). In addition to this integrin interactome, we analysed the MS intensities of all actin-binding proteins in the focal-adhesion-enriched fraction and found that WAVE and Arp2/3 complexes, which drive lamellipodia formation, correlated with $\alpha_5\beta_1$, whereas the RhoA effector mDia1 (Diap1), which drives stress-fibre formation, correlated with α_v-class integrins (Supplementary Fig. S7). We performed stable isotope labelling with amino acids in cell culture (SILAC)-based peptide pulldown assays with β_1 and β_3 integrin tail peptides and scrambled control peptides followed by MS (ref. 33) to identify which of the 29 $\alpha_5\beta_1$-enriched and 2 αv-class integrin-enriched adhesome proteins were enriched through differential associations with integrin cytoplasmic tails. Comparison of integrin-tail interactors with scrambled peptide interactors identified common and specific β_1 tail- and β_3 tail-binding proteins (Supplementary Fig. S8). Talin-1 showed equal binding to β_1 and β_3 tails and was therefore used to control the experiments. In line with the adhesome analysis (Fig. 4c) we observed very high β_1-tail-specific enrichment for Kindlin-2 and a lower enrichment for the ILK/PINCH/Parvin (IPP) complex, and a high β_3-tail-specific enrichment of the RhoA guanine nucleotide exchange factor GEF-H1 (Fig. 4d). Thus, the recruitment of Kindlin-2, the IPP complex and GEF-H1 to focal adhesions is controlled by the integrin tail sequence rather than the different focal adhesion architecture in pKO-β_1 and pKO-α_v cells. Ratiometric analysis of fluorescence intensities in focal adhesions confirmed higher Kindlin-2 and ILK levels in pKO-β_1 cells and pKO-α_v/β_1 cells (Fig. 5a–d). To analyse GEF-H1 levels in focal adhesions we first chemically crosslinked and unroofed the cells to remove the large cytoplasmic and microtubule-associated GEF-H1 pool, and then performed immunostainings, which revealed that crosslinked GEF-H1 levels were significantly higher in pKO-α_v and pKO-α_v/β_1 cells than in pKO-β_1 cells (Fig. 5e–g).

To investigate whether the IPP complex and GEF-H1 contribute to myosin II regulation by $\alpha_5\beta_1$ and α_v-class integrins we seeded $ILK^{fl/fl}$ (control) and $ILK^{-/-}$ fibroblasts[34] on fibronectin-coated X-shapes and stained for pMLC. $ILK^{-/-}$ fibroblasts had similarly low pMLC signals as pKO-α_v cells (Fig. 5h,i). Furthermore, inhibition of $\alpha_5\beta_1$ with blocking antibodies or α_v-class integrins with cilengitide in $ILK^{fl/fl}$ cells significantly reduced pMLC levels (Fig. 5h,i), confirming that both fibronectin-binding integrin classes are required to activate myosin II. To examine whether GEF-H1 regulates integrin-mediated activation of myosin II on fibronectin-coated X-shapes we depleted GEF-H1 messenger RNA using short interfering RNA (siRNA; Fig. 5j) and found significantly reduced pMLC levels in GEF-H1-silenced pKO-α_v/β_1 cells, slightly reduced levels in pKO-β_1 cells and unaffected levels in pKO-α_v cells (Fig. 5k,l) indicating that GEF-H1 reinforces myosin II activity in a $\alpha_5\beta_1$-dependent manner.

The IPP complex and GEF-H1 have been implicated in cell contractility regulation by tuning RhoA GTPases[35–37]. Therefore, we investigated whether the activity of RhoA and Rac1 are affected in our cell lines. Seeding the three cell lines for 45 min on fibronectin induced a significantly higher RhoA activity in pKO-α_v cells when compared with pKO-β_1 and pKO-α_v/β_1 cells (Fig. 5m). Rac1 activity was the lowest in pKO-α_v cells, higher in pKO-β_1 and the highest in pKO-α_v/β_1 cells (Fig. 5n). As the high GEF-H1 and RhoA levels in focal adhesions of pKO-α_v cells are not able to promote high pMLC, we conclude that only $\alpha_5\beta_1$ can elicit signals for mediating RhoA-driven myosin II activation.

Integrin-specific signalling pathways cooperate for feedback regulation of myosin II

The coupling of active RhoA to its effector Rock requires unknown signalling events that depend on cell adhesion, cell shape and cytoskeletal tension[22]. To uncover integrin-specific regulators of myosin II upstream and downstream of active RhoA we performed SILAC-based quantitative phosphoproteomics of adhesion signalling on fibronectin. We quantified a total of 3,180 proteins (Supplementary Table S2) and 7,529 phosphorylation sites (Supplementary Table S3) in the three cell lines seeded for 45 min on fibronectin. ANOVA tests of triplicate experiments identified 150 proteins and 1,010 phosphorylation events as significantly regulated in at least one of the three cell lines (Fig. 6a and Supplementary Fig. S9, Tables S2 and S3). Hierarchical cluster analysis of the SILAC ratios of the 1,010 phosphorylation events revealed clusters dominated by $\alpha_5\beta_1$ and clusters dominated by α_v-class integrins. We also observed clusters regulated oppositely by $\alpha_5\beta_1$ and α_v-class integrins, indicating antagonistic regulation, and clusters regulated by both integrin classes, indicating synergistic regulation. Using ratio thresholds for the different pairwise comparisons allowed assignment of 646 of the 1,010 determined phospho-sites into either the antagonistic, dominant or synergistic category (Fig. 6b and Supplementary Table S4).

We searched for phospho-sites that influence myosin II activity in an integrin-dependent manner and found that pKO-β_1 and pKO-$\alpha_v\beta_1$ cells showed increased phosphorylation of the RhoA/Rock targets S693-myosin phosphatase-1 (Mypt1; Fig. 6c–e) and S3-cofilin (Fig. 6c–e). MLC phosphorylation can also be induced by Mlck, whose activity is controlled by Ca^{2+} or Erk2 in focal adhesions[38,39]. We observed synergistic downregulation of S364-Mlck and synergistic

© 2013 Macmillan Publishers Limited. All rights reserved.

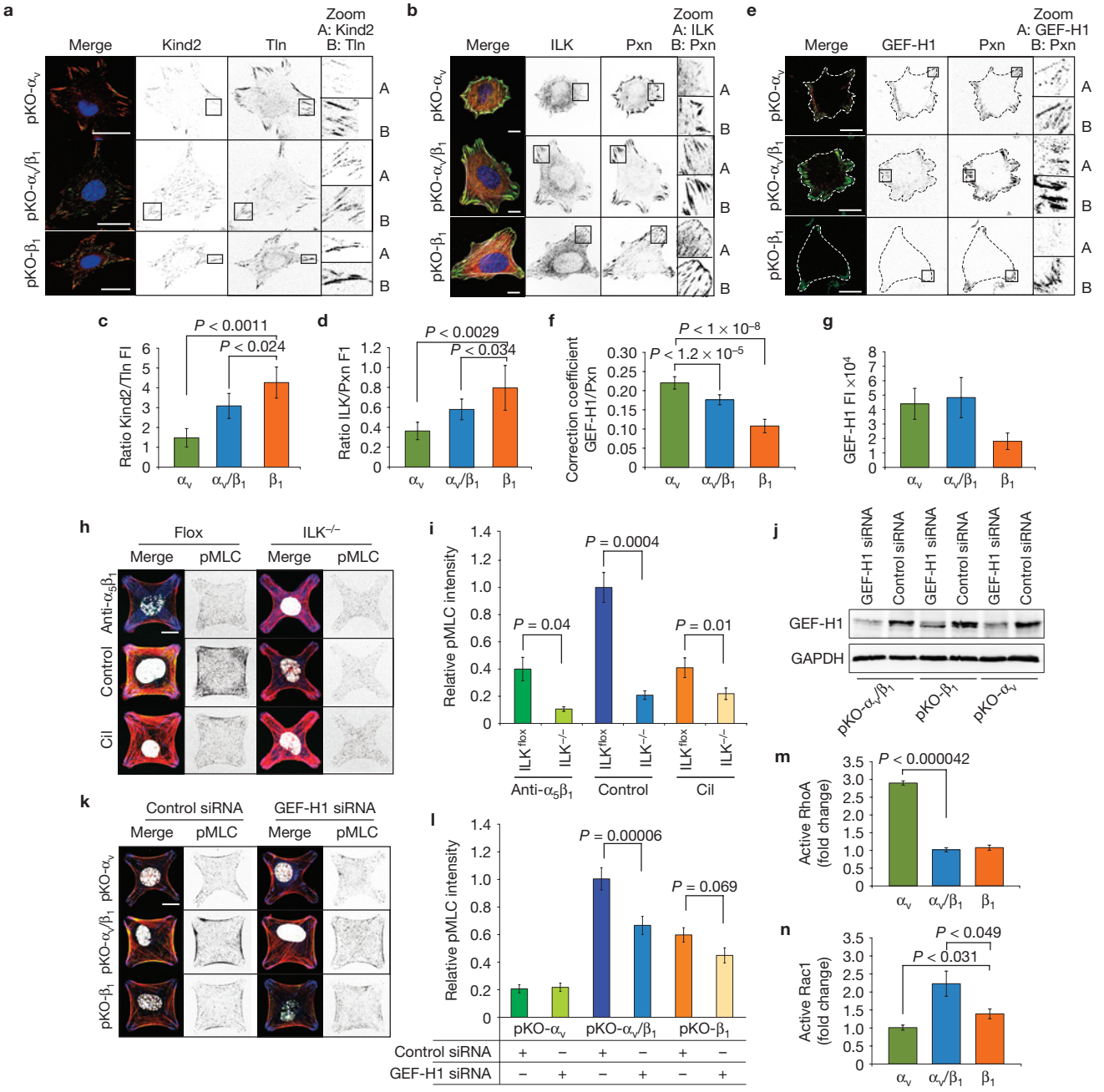

Figure 5 α_v- and β_1-mediated activation of myosin II requires ILK and GEF-H1. (**a**–**f**) Cells were plated on fibronectin-coated glass coverslips for 90 min and immunostained for: Talin-1 (Tln; red) and Kindlin-2 (Kind2; green) (**a**); ILK (red), paxillin (Pxn; green) and F-actin (white) (**b**); or GEF-H1 (red) and paxillin (green) (**e**); scale bars, 10 μm. DAPI, blue (**a**,**b**). Ratios of thresholded fluorescence intensities (FI) were calculated for Kindlin-2 and Talin-1 (pKO-α_v $n = 12$, pKO-β_1 $n = 22$, pKO-α_v/β_1 $n = 22$; results are aggregated over 3 independent experiments) (**c**), and ILK and paxillin (pKO-α_v $n = 33$, pKO-β_1 $n = 40$, pKO-α_v/β_1 $n = 40$; aggregated over 3 independent experiments) (**d**). The correlation coefficient for GEF-H1 and paxillin staining (pKO-α_v $n = 11$, pKO-β_1 $n = 10$, pKO-α_v/β_1 $n = 15$; aggregated over 3 independent experiments) was determined (**f**). (**g**) Total fluorescence intensity of focal-adhesion-retained GEF-H1 after crosslinking and unroofing of cells (pKO-α_v $n = 11$, pKO-β_1 $n = 10$, pKO-α_v/β_1 $n = 15$; aggregated over 3 independent experiments). (**h**) *ILK*$^{-/-}$ and ILK-floxed fibroblasts plated for 3 h on fibronectin-coated X-shapes stained for pMLC, F-actin and paxillin were treated with cilengitide (Cil) to block α_v-class integrins and with monoclonal antibody 2575 to block $\alpha_5\beta_1$. Scale bar, 10 μm. (**i**) Quantification of the relative fluorescence intensities for pMLC to untreated ILK-floxed cells (ILK-flox $n = 26$; ILK-null $n = 17$; ILK-flox +Cil $n = 24$; ILK-null +Cil $n = 12$; ILK-flox +anti-$\alpha_5\beta_1$ $n = 16$, ILK-null anti-$\alpha_5\beta_1$ $n = 10$; data aggregated over 2 independent experiments). (**j**) siRNA-mediated depletion of GEF-H1 confirmed by western blotting. (**k**) Cells were plated on fibronectin-coated X-shapes and stained for pMLC, F-actin and paxillin. Scale bar, 10 μm. (**l**) Quantification of the relative fluorescence intensities for pMLC in siRNA-treated cells (pKO-α_v +control siRNA $n = 24$, pKO-β_1 +control siRNA $n = 48$, pKO-α_v/β_1 +control siRNA $n = 56$, pKO-α_v + GefH1 siRNA $n = 22$, pKO-β_1 + GefH1 siRNA $n = 34$, pKO-α_v/β_1 + GefH1 siRNA $n = 59$; data aggregated over 2 independent experiments). (**m**) Relative RhoA–GTP loading in cells plated for 45 min on fibronectin ($n = 9$; 1 representative of 3 independent experiments is shown). (**n**) Relative Rac1–GTP loading in cells plated for 45 min on fibronectin ($n = 9$; 1 representative out of 3 independent experiments is shown). Error bars represent s.e.m. and *P* values were calculated using a *t*-test. pKO-α_v (green); pKO-α_v/β_1 (blue); pKO-β_1 (orange).

© 2013 Macmillan Publishers Limited. All rights reserved.

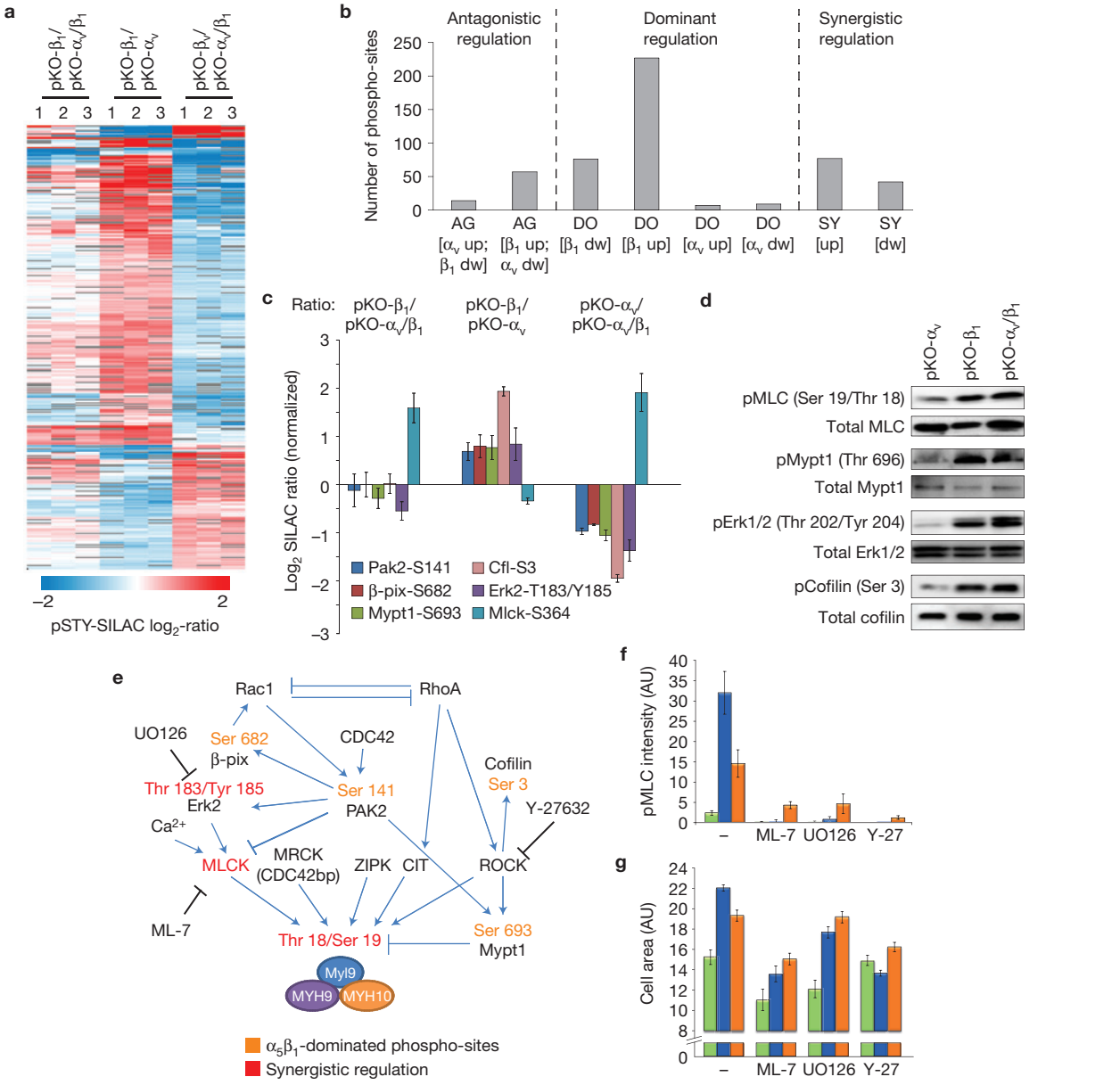

Figure 6 Integrin-specific phosphorylation landscapes on adhesion to fibronectin. (**a**) Hierarchical cluster analysis of SILAC ratios of 1,010 significantly regulated (ANOVA test and Benjamini/Hochberg false discovery rate) phosphorylation events in the indicated cells plated for 45 min on fibronectin from 3 independent replicates. The colour code depicts the normalized $\log_2$ SILAC ratio between cell lines. (**b**) The bar graph shows the number of phosphorylation events grouped into different modes of regulation based on the indicated SILAC ratio threshold criteria. AG, antagonistic; DO, dominant; SY, synergistic. (**c**) SILAC ratios for selected phosphorylation events. The bar graph depicts the median of 3 independent experiments with error bars showing the s.d. (**d**) A selection of differentially regulated phosphorylation events confirmed by western blotting using phospho-site-specific antibodies. (**e**) Signalling network with differentially regulated phosphorylation events shown to be functionally relevant in cell protrusion or contraction. Sites dominated by $\alpha_5\beta_1$ or synergistically upregulated in pKO-α_v/β_1 cells are shown. (**f**,**g**) Mean pMLC fluorescence intensity (**f**) and mean cell area (**g**) on fibronectin-coated X-shapes before and after treatment with ML-7 (25 μM) to inhibit Mlck, UO126 (50 μM) to inhibit ERK and Y-27632 (10 μM) to inhibit Rock. (pKO-α_v: untreated $n = 12$, +ML-7 $n = 10$, +U0126 $n = 15$, +Y-27 $n = 16$; pKO-β_1: untreated $n = 16$, +ML-7 $n = 17$, +U0126 $n = 19$, +Y-27 $n = 21$; pKO-α_v/β_1: untreated $n = 11$, +ML-7 $n = 18$, +U0126 $n = 19$, +Y-27 $n = 30$; 1 representative of 3 independent experiments is shown; all pairwise statistical comparisons using *t*-tests are shown in Supplementary Table S5; error bars represent s.e.m.). pKO-α_v, green; pKO-α_v/β_1, blue; pKO-β_1, orange.

upregulation of pT183/pY185-Erk2 activities in pKO-α_v/β_1 cells (Fig. 6c–e). Western blotting using phospho-site-specific antibodies corroborated these results (Fig. 6d). We uncovered three pathways (Erk2, Rock, Mlck) that were differentially regulated by the two integrin classes following adhesion to fibronectin, and reasoned that inhibition of either one or any combination of these pathways would abrogate synergistic myosin II reinforcement. Indeed, the cooperative activation of myosin II in pKO-α_v/β_1 cells was blocked by inhibiting Erk (UO126), Rock (Y-27632) or Mlck (ML-7; Fig. 6f,g). To confirm the relevance of this finding, we overexpressed constitutively active (ca-) kinase

© 2013 Macmillan Publishers Limited. All rights reserved.

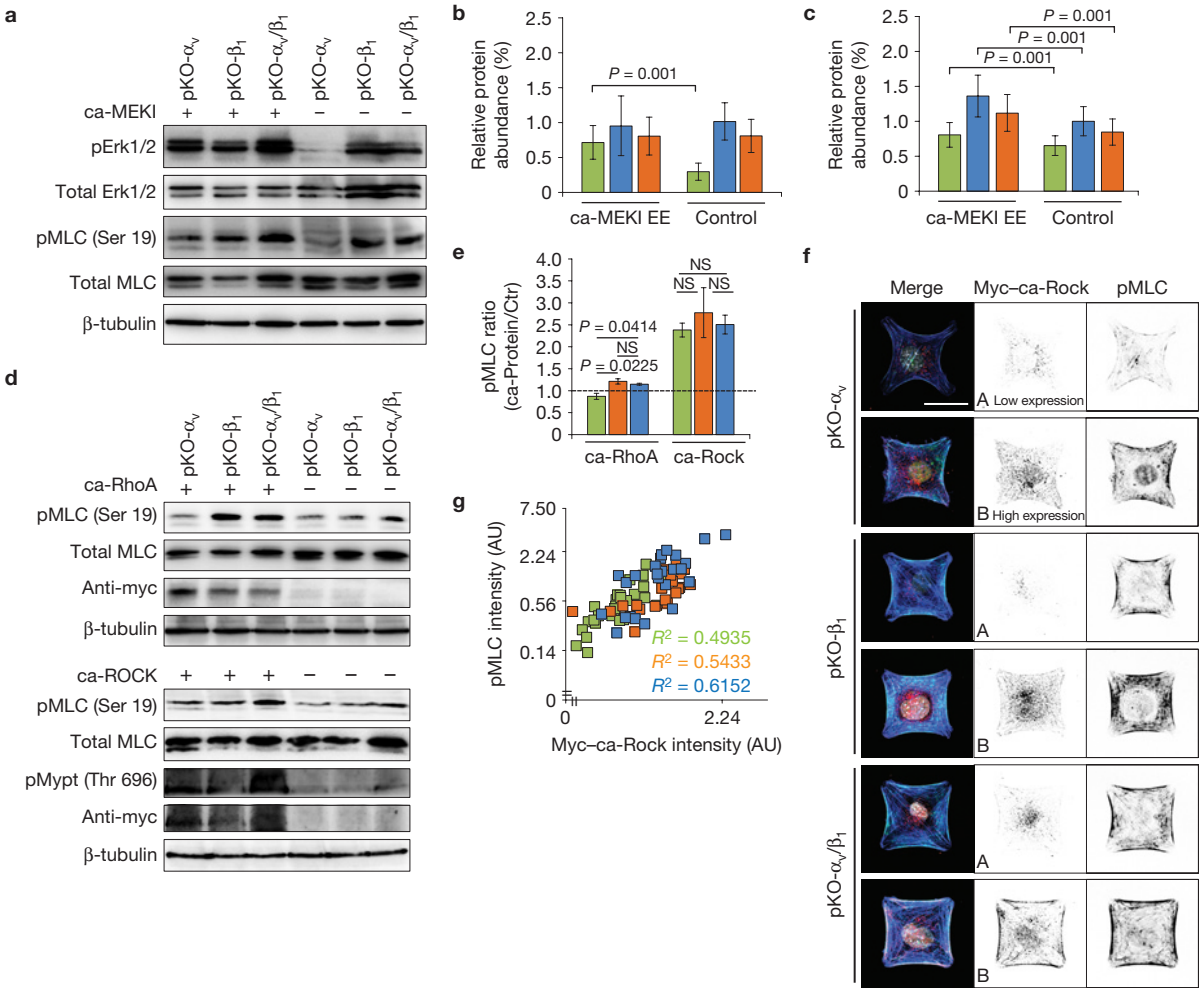

Figure 7 Activation of Rock is $\alpha_5\beta_1$-dependent. (**a**–**c**) Total cell lysates of cells plated for 90 min on fibronectin in the indicated conditions and analysed by western blotting with phospho-specific antibodies. The levels of pErk2 (**b**) and pMLC (**c**) were quantified using densitometry ($n = 3$). (**d**) A representative western blot analysis of cells transfected with myc-tagged ca-RhoA or myc-tagged ca-ROCK constructs and probed with the indicated antibodies. (**e**) Densitometric quantification of western blots ($n = 3$). The bar graphs show ratios of pMLC signals from cells expressing ca-RhoA or ca-Rock over the empty vector control. NS, not significant. (**f**) Confocal image of indicated cells transfected with a myc-tagged ca-ROCK construct, seeded on fibronectin-coated crossbow shapes and immunostained with Myc (red), pMLC (green), F-actin (blue) and DAPI (white). Scale bar, 25 μm. (**g**) Pearson correlation coefficient of fluorescence intensities of pMLC and Myc staining for the three cell lines (pKO-α_v $n = 30$; pKO-β_1 $n = 25$; pKO-α_v/β_1 $n = 25$; 1 representative of 3 independent experiments is shown). All error bars represent s.d. and P values were calculated using a t-test. pKO-α_v (green); pKO-α_v/β_1 (blue); pKO-β_1 (orange). Uncropped images of blots are shown in Supplementary Fig. S10.

constructs and measured their effects on pMLC. Overexpression of ca-MEK1 rescued the low pErk2 levels and significantly increased pMLC in pKO-α_v cells (Fig. 7a–c). The high RhoA and low Rock and pMLC activities in pKO-α_v cells (Figs 5 and 6) suggest that α_v-class integrins are unable to couple active RhoA to Rock, which was tested by overexpressing ca-RhoA or ca-Rock in the three cell lines. Whereas ca-RhoA significantly increased pMLC in pKO-β_1 and pKO-α_v/β_1, pMLC levels remained unchanged in pKO-α_v cells. In sharp contrast, ca-Rock increased pMLC twofold in all three cell lines (Fig. 7d,e), indicating that endogenous Rock in pKO-α_v cells remained inactive even in the presence of high RhoA–GTP. This finding was further confirmed with pMLC staining of cells seeded on fibronectin-coated X shapes (Fig. 7f,g). In conclusion, the Mek1/Erk2 and the RhoA/Rock/pMLC pathways are preferentially induced by $\alpha_5\beta_1$, whereas the high RhoA activity induced in pKO-α_v cells is not coupled to Rock/pMLC.

DISCUSSION

We reconstituted pan-integrin-deficient fibroblasts with β_1- and/or α_v-class integrins and correlated integrin-class-specific cellular phenotypes with integrin-class-specific adhesome composition and signalling events. Fibroblasts exploring fibronectin-based microenvironments engage $\alpha_5\beta_1$ and α_v-class integrins to orchestrate membrane protrusions, cell contractility and cell migration. Our cell line analyses revealed a series of signalling events accomplished by $\alpha_5\beta_1$ integrins, which activate Rac1, induce membrane protrusions, assemble nascent adhesions and generate RhoA/Rock-mediated myosin II activity. In conjunction with these events, mechanosensitive α_v-class integrins accumulate in areas subjected to high tension and reinforce adhesive sites to induce further activation of myosin II and development of large focal adhesions and actomyosin bundles (Fig. 8). Our study uncovers a sequence of tightly integrated biophysical and biochemical events induced by $\alpha_5\beta_1$ and

© 2013 Macmillan Publishers Limited. All rights reserved.

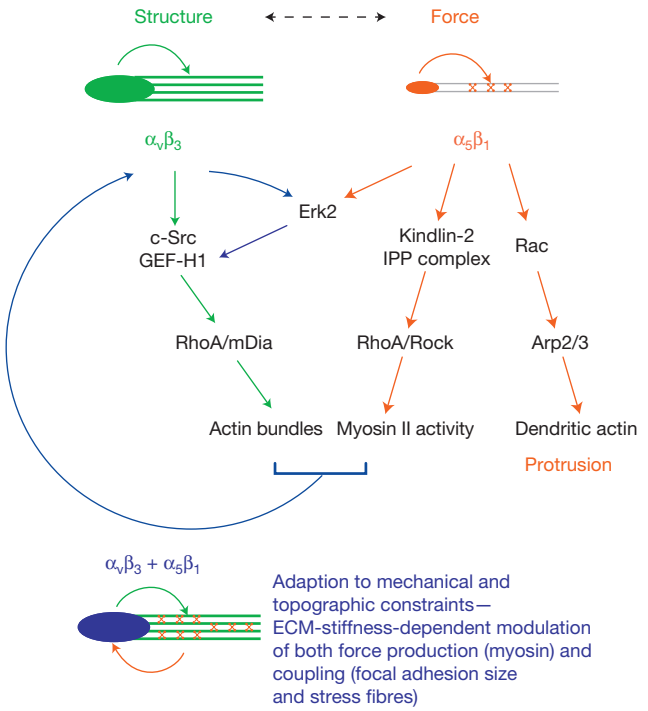

Figure 8 Model of $\alpha_5\beta_1$ and α_v-class integrin cooperation during rigidity sensing. $\alpha_5\beta_1$ integrins adhere to fibronectin, and assemble Kindlin-2- and ILK-rich small peripheral adhesions in a myosin-II-independent manner. The protein assembly in $\alpha_5\beta_1$-containing adhesions activates Rac1, Wave and Arp2/3-driven actin polymerization to induce membrane protrusions, and RhoA/Rock-mediated myosin II activation to induce tension. This tension increases the adhesion lifetime of α_v-class integrins bound to ligand on stiff substrates, which reinforces and stabilizes focal adhesions. α_v-class integrins recruit GEF-H1 to focal adhesions, which reinforces RhoA/myosin II in a $\alpha_5\beta_1$-dependent manner, and increases RhoA activity to promote mDia-mediated stress fibre formation. The combination of α_v-class integrin-mediated structure (focal-adhesion anchoring and stress-fibre formation) with the $\alpha_5\beta_1$-mediated force generation (myosin II activity) constitutes a synergistic system, which is important for adapting cellular contractility and architecture to the rigidity of fibronectin-based microenvironments.

α_v-class integrins that adjust fibroblast contractility to the rigidity of fibronectin-coated substrates. The cooperation of $\alpha_5\beta_1$ and α_v-class integrins to sense the rigidity of fibronectin-based microenvironments predicts that cell migration towards a rigidity gradient, called durotaxis, may also depend on the cooperation of both integrins. These findings have potential ramifications for certain pathologies, such as fibrosis and tumour metastasis where rigidity sensing of fibronectin matrices is crucial in disease progression[40].

To better understand how distinct integrin classes individually and cooperatively probe the biophysical properties of a fibronectin-based microenvironment, we established a cell model system and used proteomics methods to characterize their focal adhesion composition, phospho-signalling and proteome changes. Our comprehensive proteomic data set of adhesion signalling revealed that integrin-class-specific adhesomes and phospho-proteomes are enriched with integrin-specific adapter proteins and signalling intermediates. Several well-known integrin outside-in signalling pathways, including the Rac1/Wave/Arp2,3 and RhoA/Rock pathways, were dominated by $\alpha_5\beta_1$ integrins. Interestingly, the pKO-β_1 cells developed very few stress fibres, indicating that $\alpha_5\beta_1$-induced RhoA activity was preferably used for production of myosin-II-mediated force but not formin-mediated stress-fibre formation. In contrast, the pKO-α_v cells exhibited high RhoA activity, which in turn induced the formation of thick stress fibres, most likely through the activation of mDia, but did not activate Rock/pMLC/myosin II. The coupling of active RhoA to different downstream effectors by distinct integrin classes was unanticipated. The underlying mechanism(s) are unclear, but probably involve specific mark(s) either attached to active RhoA or to the effectors enabling differential interactions with GTP-bound RhoA.

Although forces play an important role in the assembly of focal adhesions, pKO-α_v cells induced the largest focal adhesions among the three cell lines and also exhibited the lowest myosin II activities and traction forces. Focal adhesion size is not the sole predictor of traction forces and the final focal adhesion size can also be determined by an mDia-dependent mechanism[41,42]. Therefore, we propose that the large size of focal adhesions in pKO-α_v cells depends on RhoA/mDia-induced stress fibres rather than on myosin II. However, although the final focal adhesion size in pKO-α_v cells was myosin-II-independent, their formation and/or stability were strictly myosin-II-dependent, evidenced by the pronounced destabilization of α_v-class integrin adhesions with blebbistatin. A role for α_v-class integrins for focal adhesion stabilization has also been obtained from single-protein tracking experiments of β_1 and β_3 integrins, which showed that β_3 integrins are immobilized in large focal adhesions, whereas β_1 integrins are more mobile[29]. The necessity of $\alpha_v\beta_3$ for cell stiffening following force application has also been postulated[43]. Similarly, the recruitment of GEF-H1 to focal adhesions and Erk2 activity was reported as necessary for cell stiffening following force application[35]. Our results link these observations and suggest that force-mediated stabilization of α_v–fibronectin bonds will reinforce focal adhesions, increase local concentrations of GEF-H1 and activate RhoA following $\alpha_5\beta_1$-induced Erk2 activation. Therefore, α_v-class integrins could be capable of forming stronger extracellular catch bonds with fibronectin than $\alpha_5\beta_1$ integrins do[44], resulting in longer bond lifetimes of α_v-class integrins with fibronectin when force is applied. However, as the influence of force on the on and off rates of $\alpha_5\beta_1$ and α_v-class integrins with fibronectin have not been systematically studied, this hypothesis awaits future testing. □

METHODS

Methods and any associated references are available in the online version of the paper.

Note: Supplementary Information is available in the online version of the paper

ACKNOWLEDGEMENTS

We thank J. Cox for software tool development, U. Kuhn and C. Boulegue (MPIB) and A. F. Christ (CNRS/UJF/INRA/CEA) for excellent technical support, and A. Meves, T. Geiger and D. Boettiger for discussions. H.B.S. was a fellow of the European Molecular Biology Organisation (EMBO) and M-R.H. a fellow of the Boehringer Ingelheim fonds. The work was financially supported by the ERC, DFG and the Max Planck Society.

AUTHOR CONTRIBUTIONS

R.F. initiated the project; R.F. and H.B.S. designed the experiments and wrote the paper; H.B.S., M-R.H., T.V., S.Z., J.P., Z.S. and A.R. performed experiments; H.B.S., M-R.H., T.V., S.Z., K-E.G., C.C.F. and R.F. analysed data; J.P., M.T., K-E.G. and M.M. provided important reagents and/or analytical tools; all authors read and approved the manuscript.

© 2013 Macmillan Publishers Limited. All rights reserved.

COMPETING FINANCIAL INTERESTS
The authors declare no competing financial interests.

Published online at www.nature.com/doifinder/10.1038/ncb2747
Reprints and permissions information is available online at www.nature.com/reprints

1. Hynes, R. O. Integrins: bidirectional, allosteric signaling machines. *Cell* **110,** 673–687 (2002).
2. Desgrosellier, J. S. & Cheresh, D. A. Integrins in cancer: biological implications and therapeutic opportunities. *Nat. Rev. Cancer* **10,** 9–22 (2010).
3. Avraamides, C. J., Garmy-Susini, B. & Varner, J. A. Integrins in angiogenesis and lymphangiogenesis. *Nat. Rev. Cancer* **8,** 604–617 (2008).
4. Liu, H. *et al.* MYC suppresses cancer metastasis by direct transcriptional silencing of α(v) and β(3) integrin subunits. *Nat. Cell Biol.* **14,** 567–574 (2012).
5. Humphries, J. D., Byron, A. & Humphries, M. J. Integrin ligands at a glance. *J. Cell Sci.* **119,** 3901–3903 (2006).
6. Leiss, M., Beckmann, K., Giros, A., Costell, M. & Fassler, R. The role of integrin binding sites in fibronectin matrix assembly *in vivo*. *Curr. Opin. Cell Biol.* **20,** 502–507 (2008).
7. Yang, J. T., Rayburn, H. & Hynes, R. O. Embryonic mesodermal defects in α_5 integrin-deficient mice. *Development* **119,** 1093–1105 (1993).
8. Bader, B. L., Rayburn, H., Crowley, D. & Hynes, R. O. Extensive vasculogenesis, angiogenesis, and organogenesis precede lethality in mice lacking all α_v integrins. *Cell* **95,** 507–519 (1998).
9. Yang, J. T. *et al.* Overlapping and independent functions of fibronectin receptor integrins in early mesodermal development. *Dev. Biol.* **215,** 264–277 (1999).
10. Zamir, E. *et al.* Dynamics and segregation of cell–matrix adhesions in cultured fibroblasts. *Nat. Cell Biol.* **2,** 191–196 (2000).
11. Ballestrem, C., Hinz, B., Imhof, B. A. & Wehrle-Haller, B. Marching at the front and dragging behind: differential $\alpha_v\beta_3$-integrin turnover regulates focal adhesion behavior. *J. Cell Biol.* **155,** 1319–1332 (2001).
12. Danen, E. H., Sonneveld, P., Brakebusch, C., Fassler, R. & Sonnenberg, A. The fibronectin-binding integrins $\alpha_5\beta_1$ and $\alpha_v\beta_3$ differentially modulate RhoA–GTP loading, organization of cell matrix adhesions, and fibronectin fibrillogenesis. *J. Cell Biol.* **159,** 1071–1086 (2002).
13. White, D. P., Caswell, P. T. & Norman, J. C. $\alpha_v\beta_3$ and $\alpha_5\beta_1$ integrin recycling pathways dictate downstream Rho kinase signaling to regulate persistent cell migration. *J. Cell Biol.* **177,** 515–525 (2007).
14. Morgan, M. R., Byron, A., Humphries, M. J. & Bass, M. D. Giving off mixed signals-distinct functions of α(5)β(1) and α(v)β(3) integrins in regulating cell behaviour. *IUBMB Life* **61,** 731–738 (2009).
15. Van der Flier, A. *et al.* Endothelial α_5 and α_v integrins cooperate in remodeling of the vasculature during development. *Development* **137,** 2439–2449 (2010).
16. Choi, C. K. *et al.* Actin and α-actinin orchestrate the assembly and maturation of nascent adhesions in a myosin II motor-independent manner. *Nat. Cell Biol.* **10,** 1039–1050 (2008).
17. Geiger, B., Spatz, J. P. & Bershadsky, A. D. Environmental sensing through focal adhesions. *Nat. Rev. Mol. Cell Biol.* **10,** 21–33 (2009).
18. Bershadsky, A., Kozlov, M. & Geiger, B. Adhesion-mediated mechanosensitivity: a time to experiment, and a time to theorize. *Curr. Opin. Cell Biol.* **18,** 472–481 (2006).
19. Schiller, H. B., Friedel, C. C., Boulegue, C. & Fassler, R. Quantitative proteomics of the integrin adhesome show a myosin II-dependent recruitment of LIM domain proteins. *EMBO Rep.* **12,** 259–266 (2011).
20. Kuo, J. C., Han, X., Hsiao, C. T., Yates Iii, J. R. & Waterman, C. M. Analysis of the myosin II-responsive focal adhesion proteome reveals a role for β-Pix in negative regulation of focal adhesion maturation. *Nat. Cell Biol.* **13,** 383–393 (2011).
21. Lammermann, T. *et al.* Rapid leukocyte migration by integrin-independent flowing and squeezing. *Nature* **453,** 51–55 (2008).
22. Bhadriraju, K. *et al.* Activation of ROCK by RhoA is regulated by cell adhesion, shape, and cytoskeletal tension. *Exp. Cell Res.* **313,** 3616–3623 (2007).
23. Danen, E. H. *et al.* Integrins control motile strategy through a Rho-cofilin pathway. *J. Cell Biol.* **169,** 515–526 (2005).
24. Worth, D. C. *et al.* $\alpha_v\beta_3$ integrin spatially regulates VASP and RIAM to control adhesion dynamics and migration. *J. Cell Biol.* **189,** 369–383 (2010).
25. Huttenlocher, A. & Horwitz, A. R. Integrins in cell migration. *Cold Spr. Harbor Perspec. Biol.* **3,** a005074 (2011).
26. Thery, M. *et al.* Anisotropy of cell adhesive microenvironment governs cell internal organization and orientation of polarity. *Proc. Natl Acad. Sci. USA* **103,** 19771–19776 (2006).
27. Thery, M. Micropatterning as a tool to decipher cell morphogenesis and functions. *J. Cell Sci.* **123,** 4201–4213 (2010).
28. Tseng, Q. *et al.* A new micropatterning method of soft substrates reveals that different tumorigenic signals can promote or reduce cell contraction levels. *Lab on a Chip* **11,** 2231–2240 (2011).
29. Rossier, O. *et al.* Integrins β_1 and β_3 exhibit distinct dynamic nanoscale organizations inside focal adhesions. *Nat. Cell Biol.* **14,** 1057–1067 (2012).
30. Zaidel-Bar, R., Itzkovitz, S., Ma'ayan, A., Iyengar, R. & Geiger, B. Functional atlas of the integrin adhesome. *Nat. Cell Biol.* **9,** 858–867 (2007).
31. Cox, J. & Mann, M. MaxQuant enables high peptide identification rates, individualized p.p.b.-range mass accuracies and proteome-wide protein quantification. *Nat. Biotech.* **26,** 1367–1372 (2008).
32. Zaidel-Bar, R. & Geiger, B. The switchable integrin adhesome. *J. Cell Sci.* **123,** 1385–1388 (2010).
33. Meves, A. *et al.* {β}1 integrin cytoplasmic tyrosines promote skin tumorigenesis independent of their phosphorylation. *Proc. Natl Acad. Sci. USA* **108,** 15213–15218 (2011).
34. Sakai, T. *et al.* Integrin-linked kinase (ILK) is required for polarizing the epiblast, cell adhesion, and controlling actin accumulation. *Genes Dev.* **17,** 926–940 (2003).
35. Guilluy, C. *et al.* The Rho GEFs LARG and GEF-H1 regulate the mechanical response to force on integrins. *Nat. Cell Biol.* **13,** 722–727 (2011).
36. Montanez, E., Wickstrom, S. A., Altstatter, J., Chu, H. & Fassler, R. α-parvin controls vascular mural cell recruitment to vessel wall by regulating RhoA/ROCK signalling. *EMBO J.* **28,** 3132–3144 (2009).
37. Montanez, E. *et al.* Kindlin-2 controls bidirectional signaling of integrins. *Genes Dev.* **22,** 1325–1330 (2008).
38. Holzapfel, G., Wehland, J. & Weber, K. Calcium control of actin-myosin based contraction in triton models of mouse 3T3 fibroblasts is mediated by the myosin light chain kinase (MLCK)-calmodulin complex. *Exp. Cell Res.* **148,** 117–126 (1983).
39. Fincham, V. J., James, M., Frame, M. C. & Winder, S. J. Active ERK/MAP kinase is targeted to newly forming cell–matrix adhesions by integrin engagement and v-Src. *EMBO J.* **19,** 2911–2923 (2000).
40. Butcher, D. T., Alliston, T. & Weaver, V. M. A tense situation: forcing tumour progression. *Nat. Rev. Cancer* **9,** 108–122 (2009).
41. Oakes, P. W., Beckham, Y., Stricker, J. & Gardel, M. L. Tension is required but not sufficient for focal adhesion maturation without a stress fibre template. *J. Cell Biol.* **196,** 363–374 (2012).
42. Stricker, J., Aratyn-Schaus, Y., Oakes, P. W. & Gardel, M. L. Spatiotemporal constraints on the force-dependent growth of focal adhesions. *Biophys. J.* **100,** 2883–2893 (2011).
43. Roca-Cusachs, P., Gauthier, N. C., Del Rio, A. & Sheetz, M. P. Clustering of α(5)β(1) integrins determines adhesion strength whereas α(*v*)β(3) and talin enable mechanotransduction. *Proc. Natl Acad. Sci. USA* **106,** 16245–16250 (2009).
44. Kong, F., Garcia, A. J., Mould, A. P., Humphries, M. J. & Zhu, C. Demonstration of catch bonds between an integrin and its ligand. *J. Cell Biol.* **185,** 1275–1284 (2009).

© 2013 Macmillan Publishers Limited. All rights reserved.

METHODS

Antibodies. Information about antibodies is provided in Supplementary Table S6.

Isolation, immortalization, viral reconstitution and transfection of cell lines. Mouse pKO fibroblasts and reconstituted pKO-α_v, pKO-β_1 and pKOα_v/β_1 cell lines were generated from fibroblasts (floxed parental) derived from the kidney of 21-day-old male mice carrying floxed α_v and β_1 alleles ($\alpha_v^{flox/flox}$, $\beta_1^{flox/flox}$), and constitutive β_2 and β_7 null alleles ($\beta_2^{-/-}$, $\beta_7^{-/-}$; ref. 21). Individual kidney fibroblast clones were immortalized by retroviral delivery of the SV40 large T. The immortalized floxed fibroblast clones were then retrovirally transduced with mouse α_v and/or β_1 integrin cDNAs and the endogenous floxed β_1 and α_v integrin loci were simultaneously deleted by adenoviral transduction of the *Cre* recombinase. Reconstituted cell lines were FACS sorted to obtain cell populations with comparable integrin surface levels to the parental cell clones. Transduction of ca-RhoA (myc–RhoA pcDNA3.1) and ca-ROCK (myc–ROCKD4 pcDNA3.1) was carried out with Lipofectamine 2000 (Invitrogen through Life Technologies) according to the manufacturer's instructions. The transfection control was an empty pcDNA3.1 vector.

Adhesion and cell migration analysis. Adhesion assays were carried out as previously described[45]. Briefly, cells were plated for 20 min in 96-well plates coated with varying concentrations of ECM ligands. After washing the plates the number of adhered cells that remained on the plate was quantified using attenuance at 595 nm.

To analyse random migration, cell culture dishes were coated with fibronectin (5 μg ml^{-1} in PBS; 2 h at room temperature) and blocked with 1% BSA in PBS. After seeding, video time-lapse microscopy was performed using phase contrast at ×20 magnification. A total of 12 migrating pKO-α_v, 12 migrating pKO-α_v/β_1 and 14 migrating pKO-β_1 cells from 5 independent movies were analysed. One pixel in each cell nucleus was marked manually and served as the cell's coordinate. Each tracked cell j with a track length N_j was recorded by its $x_{j,i}$ and yj,i position for every frame i. A tracking point was made every $D_t = 1$ min. The time difference between the tracking coordinates $x_{j,i}$ and $x_{j,i+n}$ is $t = nD_t$, where n is the frame number. The mean squared displacement (msd) of the cell j at time $t = nD_t$ was calculated by

$$msd_j(t) = \frac{1}{N_j - n}\sum_{i=1}^{N_j-n}\left[\left(x_{j,i+n} - x_{j,i}\right)^2 + \left(y_{j,i+n} - y_{j,i}\right)^2\right]$$

All msd values were calculated for all cells and averaged. The used propagated uncertainty for the $msd(t)$ is the standard deviation of the mean. For an increasing n the number of given tracks contributes to $msd(t)$ decreases as well as the propagated uncertainty caused by the tracking uncertainty increases. Therefore, the $msd(t)$ has been cut at $n = 90$. To determine the persistence time P and the diffusion constant D, Fürths formula

$$msd(t) = 4D\left(t - P\left(1 - \exp\left(-\frac{t}{P}\right)\right)\right)$$

has been fitted through the data. The mean velocity of a cell j has been computed as the average of the distance travelled each time step divided by the time step.

Micropatterning and immunostainings. Micropatterns were generated on PEG-coated glass coverslips with deep-ultraviolet lithography[46]. Glass coverslips were incubated in a 1 mM solution of a linear PEG, CH_3–$(O$–CH_2–$CH_2)_{43}$–NH–CO–NH–CH_2–CH_2–CH_2–$Si(OEt)_3$ in dry toluene for 20 h at 80 °C under a nitrogen atmosphere. The substrates were removed, rinsed intensively with ethyl acetate, methanol and water, and dried with nitrogen. A pegylated glass coverslip and a chromium-coated quartz photomask (ML&C, Jena) were immobilized with vacuum onto a mask holder, which was immediately exposed to deep ultraviolet light using a low-pressure mercury lamp (NIQ 60/35 XL longlife lamp, quartz tube, 60 W from Heraeus Noblelight) at 5 cm distance for 7 min. The patterned substrates were subsequently incubated overnight with 100 μl of fibronectin (20 μg ml^{-1} in PBS) at 4 °C and washed once with PBS.

For immunofluorescence microscopy, cells were seeded on micropatterns in DMEM (GIBCO by Life Technologies) containing 0.5 % FBS at 37 °C, 5% CO_2. After 90 or 180 min the medium was soaked off, and cells were fixed with 3% PFA in PBS for 5 min at room temperature, washed with PBS, blocked with 1% BSA in PBS for 1 h at room temperature and then incubated with antibodies. The fluorescent images were collected with a laser scanning confocal microscope (Leica SP5).

Acrylamide micropatterning. Micropatterns were first produced on glass coverslips as previously described[46]. Briefly, 20 mm square glass coverslips were oxidized through oxygen plasma (FEMTO, Diener Electronics) for 10 s at 30 W before incubating with 0.1 mg ml^{-1} poly-L-lysine (PLL)–PEG (PLL20K-G35-PEG2K, JenKem) in 10 mM HEPES, pH 7.4, for 30 min. After drying, coverslips were exposed to 165 nm ultraviolet (UVO cleaner, Jelight) through a photomask (Toppan) for 5 min. Then, coverslips were incubated with 20 mg ml^{-1} of fibronectin (Sigma) and 2 mg ml^{-1} of rhodamine-labelled fibronectin (Cytoskeleton) in 100 mM sodium bicarbonate solution for 30 min. Acrylamide solution containing acrylamide and bisacrylamide (Sigma) was degassed for 20 min under house vacuum and mixed with passivated fluorescent beads (Invitrogen) by sonication before addition of APS and TEMED. A 25 μl drop of this solution was put directly on the micropatterned glass coverslip. A silanized coverslip was placed over the drop and left polymerizing for 30 min (fluorescent beads passivation and glass silanization were performed as previously described[4]). The sandwich was then put in 100 mM sodium bicarbonate solution and the gel was gently removed from the patterned glass coverslip while staying attached to the other coverslip owing to the silanization treatment. This process transferred the protein micropatterns onto the gel as previously described[47]. Three different solutions of 3%/0.225%, 5%/0.225%, 8%/0.264% acrylamide/bisacrylamide were used. The corresponding Young's modulus of the gels was 1.4, 9.6 and 34.8 kPa respectively as measured using AFM. Coverslips were mounted in magnetic chambers (Cytoo) and washed with sterile PBS before plating cells.

AFM measurements of the Young's modulus of acrylamide gels. We measured gel stiffness through nanoindentation using an atomic force microscope (Bruker Nanoscope) mounted with silica-bead-tipped cantilevers (r(bead) = 2.5 μm, nominal spring constant 0.06 N m^{-1}, Novascan Technologies). Initially, we determined the sensitivity of the photodiode to cantilever deflection by measuring the slope of a force distance curve when pressing the cantilever onto a glass coverslip, and the force constant of the cantilever using the thermal noise method included in the Bruker Nanoscope software. For each acrylamide/bisacrylamide ratio used in the traction-force microscopy measurements we acquired 27 force curves in 3 by 3 grids (2 μm spacing between points) at three different locations on the gels. Before and during indentation experiments gels were kept in PBS. To obtain stiffness values from force curves we used the NanoScope Analysis software. Specifically, we corrected for baseline tilt, and used the linear fitting option for the Hertz model with a Poisson ration of 0.48 on the indentation curve.

Traction-force microscopy and image analysis. Confocal acquisition was performed on an Eclipse TI-E Nikon inverted microscope equipped with a CSUX1-A1 Yokogawa confocal head and an Evolve EMCCD camera (Ropert Scientific, Princeton Instrument). A CFI Plan APO VC oil ×60/1.4 objective (Nikon) was used. The system was driven by the Metamorph software (Universal Imaging).

Traction-force microscopy was performed as previously described[28]. Displacement fields describing the deformation of the polyacrylamide substrate are determined from the analysis of fluorescent bead images before and after removal of the adhering cell with trypsin treatment. Images of fluorescent beads were first aligned to correct experimental drift using the Align slices in stack ImageJ plugin. The displacement field was subsequently calculated by a custom-written particle image velocimetry (PIV) program implemented as an ImageJ (http://rsb.info.nih.gov/ij) plugin. The PIV was performed through an iterative scheme. In all iterations the displacement was calculated by the normalized correlation coefficient algorithm, so that an individual interrogation window was compared with a larger searching window. The next iteration takes into account the displacement field measured previously, so that a false correlation peak due to insufficient image features is avoided. The normalized cross-correlation also allowed us to define an arbitrary threshold to filter out low correlation values due to insufficient beads present in the window. The resulting final grid size for the displacement field was 2.67 × 2.67 μm. The erroneous displacement vectors due to insufficient beads present in the window were filtered out by their low correlation value and replaced by the median value from the neighbouring vectors. With the displacement field obtained from the PIV analysis, the traction-force field was reconstructed by the Fourier transform traction cytometry (FTTC) method with regularized scheme on the same grid (2.67 × 2.67 μm) without further interpolation or remapping. The regularization parameter was set at 1 × 10–11 for all traction-force reconstructions. The Fourier transform traction cytometry code was also written in Java as an ImageJ plugin, so that the whole traction-force microscopy procedure from PIV to force calculation could be performed with ImageJ. The entire package of traction-force microscopy software is available at https://sites.google.com/site/qingzongtseng/tfm. Contractile

© 2013 Macmillan Publishers Limited. All rights reserved.

DOI: 10.1038/ncb2747

energy was then computed as the integral under the cell of the scalar product of force and displacement vectors using a custom-written code in MatLab. Force profiles along the cell front were generated by integration of the traction maps over the width of the circular part of the pattern. Average pictures were generated after alignment using the Align slices in stack ImageJ plugin. Focal adhesion intensity profiles were generated by integration of the paxillin intensity along the border of the circular part of the micropattern.

Rho–GTPase assays. Cells were serum-starved overnight, detached with trypsin–EDTA and kept in suspension in serum-free medium for 1 h. Cells were then plated on fibronectin-coated dishes (blocked with 1% BSA) in serum-free medium for 45 min. Cell lysis and active Rho–GTPase pulldown was performed using the active Rac1 Pull-Down and Detection Kit or the active Rho Pull-Down and Detection Kit (Cat#16118, 16116, Pierce) according to the manufacturer's instruction. The active GTPase signal was normalized to total protein level of the GTPase. Western blots were quantified with Totallab.

RNA interference. Cells were transiently transfected with a final concentration of 300 nM siRNA (stealth RNAi; Invitrogen) using Lipofectamine 2000 (Invitrogen) according to the manufacturer's protocol, using the targeting sequence sense-5′-CCCGGAACUUUGUCAUCCAUCGUUU-3′ for GEF-H1. As a control we used the scrambled sequence sense-5′-CCCUCAAUGUUCUACCUACGGGUUU-3′.

MS. For proteome and phosphoproteome analysis fibroblasts were cultured in lysine/arginine-free DMEM with 10% FBS (10 KDa dialysed, PAA) and SILAC labelled with light (L-arginine (R0) and L-lysine (K0))], medium (L-arginine-U-$^{13}C_6$ (R6) and L-lysine-$^{2}H_4$(K4)) or heavy (L-arginine-U-$^{13}C_6$ $-^{15}N_4$ (R10) and L-lysine-U-$^{13}C_6$ $-^{15}N_2$ (K8)) amino acids (Cambridge Isotope Laboratories). For phosphoproteome analysis, cells were serum-starved for 6 h and then plated in serum-free medium on fibronectin-coated and BSA-blocked culture dishes for 45 min. Cells were lysed in lysis buffer (100 mM Tris–HCl, at pH 7.5, containing 4% SDS and 100 mM dithiothreitol), boiled 5 min at 95 °C, and sonicated. Lysate was clarified by a 10 min centrifugation at 16,000*g*. Cleared light/medium/heavy proteins were mixed at a 1:1:1 ratio and digested with trypsin using the FASP protocol[48]. For proteome analysis, 40 µg of peptides was separated with strong anion exchange chromatography[49]. For phosphoproteome analysis, 3 mg of peptides was fractionated with strong cation exchange chromatography and enriched for phosphorylated peptides with titanium dioxide (TiO_2) as described previously[50]. Peptides were then analysed on a LTQ-Orbitrap Velos equipped with a nanoelectrospray source (Thermo Fisher Scientific). The full-scan MS spectra were acquired in the Orbitrap with a resolution of 30,000 at m/z 400. The ten most intense ions were fragmented by higher-energy collisional dissociation and the spectra of the fragmented ions were acquired in the Orbitrap analyser with a resolution of 7,500. Peptides were identified and quantified using the MaxQuant software[31] and searched with the Andromeda search engine against the mouse IPI database 3.68 (ref. 51). Phosphorylations were assigned as previously described[50].

The adhesome analysis was performed as previously described[19]. In brief, cells were serum-starved for 4 h and plated for either 45 or 90 min in serum-free medium on fibronectin-coated, BSA-blocked, culture dishes. Optionally, cells were treated with 50 µM blebbistatin for 30 or 75 min. Enrichment for focal-adhesion-associated proteins was achieved by shortly fixing the ventral cell cortex using chemical crosslinkers, followed by removal of non-crosslinked proteins and big organelles by stringent cell lysis and hydrodynamic sheer flow washing. Quantitative mass spectrometric analysis was performed on an LTQ Orbitrap mass spectrometer (Thermo Electron) and analysed using the label-free quantification algorithm[52], which is embedded in the MaxQuant software[31], as previously described[19].

For in-gel digestion, gel bands were cut into 1 mm^3 cubes and washed two times with 50 mM ammonium bicarbonate in 50% ethanol. For protein reduction, gel pieces were incubated with 10 mM dithiothreitol in 50 mM ammonium bicarbonate for 1 h at 56 °C. Alkylation of cysteines was performed with 10 mM iodoacetamide in 50 mM ammonium bicarbonate for 45 min at 25 °C in the dark. Gel pieces were washed two times with 50 mM ammonium bicarbonate in 50% ethanol, dehydrated with 100% ethanol, and dried in a vacuum concentrator. The gel pieces were rehydrated with 12.5 ng µl^{-1} trypsin (sequencing grade, Promega) in 50 mM ammonium bicarbonate and digested overnight at 37 °C. Supernatants were transferred to fresh tubes, and the remaining peptides were extracted by incubating gel pieces two times with 30% acetonitrile in 3% TFA followed by dehydration with 100% acetonitrile. The extracts were combined and desalted using RP-C18 StageTip columns, and the eluted peptides used for mass spectrometric analysis.

For nanoLC–MS/MS, peptide mixtures were separated by on-line nanoLC and analysed by electrospray tandem MS. The experiments were performed on an Agilent 1200 nanoflow system connected to an LTQ Orbitrap mass spectrometer (Thermo Electron) equipped with a nanoelectrospray ion source (Proxeon Biosystems). Binding and chromatographic separation of the peptides took place in a 15-cm fused-silica emitter (75-µm inner diameter from Proxeon Biosystems) in-house packed with reversed-phase ReproSil-Pur C18-AQ 3 µm resin (Dr. Maisch). Peptide mixtures were injected onto the column with a flow of 500 nl min^{-1} and subsequently eluted with a flow of 2500 nl min^{-1} from 2% to 40% acetonitrile in 0.5% acetic acid, in a 100 min gradient. The precursor ion spectra were acquired in the Orbitrap analyser (m/z 300–1,800, $R = 60{,}000$, and ion accumulation to a target value of 1,000,000), and the ten most intense ions were fragmented and recorded in the ion trap. The lock mass option enabled accurate mass measurement in both MS and Orbitrap MS/MS mode as described previously[53]. Target ions already selected for MS/MS were dynamically excluded for 60 s.

For peptide identification and peptide quantification, the data analysis was performed with the MaxQuant software as described previously[31,54], supported by Andromeda as the database search engine for peptide identifications. Peaks in MS scans were determined as three-dimensional hills in the mass-retention time plane. MS/MS peak lists were filtered to contain at most six peaks per 100 Da interval and searched by Andromeda (in-house-developed software) against the Mouse International Protein Index database. The initial mass tolerance in MS mode was set to 7 ppm and MS/MS mass tolerance was 0.5 Da. Cysteine carbamidomethylation was searched as a fixed modification, whereas N-acetyl protein, oxidized methionine, *N*-carbamidomethylated DSP protein and carbamidomethylated DSP lysine were searched as variable modifications. Finally, the label-free quantification algorithm implemented in the MaxQuant software was used as described earlier[52].

SILAC-based peptide pulldowns were carried out with the cytoplasmic tails of β_1 integrin (5′-HDRREFAKFEKEKMNAKWDTGENPIYKSAVTTVVNPKYEGK-3′) and the tails of β_3 integrin (5′-HDRKEFAKFEEERARAKWDTANNPLYKEATS-TFTNITYRGT-3′). The tail peptides were *de novo* synthesized with a desthiobiotin on the amino terminus, coupled to magnetic streptavidin beads (MyOne Streptavidin C1—Invitrogen) and pulldowns from SILAC-labelled cell lysates were performed as described previously[33]. After a mild wash the bound proteins were eluted from the magnet using 16 mM biotin (Sigma-Aldrich). After protein precipitation and in-solution digestion, LC-MS/MS and data analysis was performed as described above. The peptide pulldown experiments were done as reverse SILAC labelling experiments in duplicate (4 biological replicates). We generally considered outliers with high SILAC ratios and high sequence coverage/intensity as more significant than proteins that had only a high SILAC ratio.

Bioinformatics and statistics. ANOVA analysis of the cellular proteome and phosphoproteome was performed using the Perseus bioinformatics toolbox of MaxQuant (J. Cox *et al.*; manuscript in preparation). Multiple testing corrections were performed using the inbuilt permutation method and significant hits were identified at a significance level of 0.01 and 0.05, respectively. ANOVA analysis of the 245 core adhesome proteins was performed using the statistical programming language R (http://www.R-project.org) with the adaptive Benjamini and Hochberg step-up false discovery rate-controlling procedure for multiple testing and a significance level of 0.05. Hierarchical clustering was performed using an average linkage approach and Euclidean distances. Enrichment analysis of clusters for Gene Ontology (GO) terms, KEGG pathways and PFAM and INTERPRO protein domains was performed with the DAVID webserver[55] using the multiple testing correction method by Benjamini and Hochberg and a significance level of 0.05. Protein–protein interactions (PPIs) were compiled from different sources including: PPI databases (DIP (ref. 56; version of December 2009), IntAct (ref. 57) and MINT (ref. 58) (both downloaded on 19 May 2010), BIOGRID (ref. 59; version 3.0.64) and HPRD (ref. 60; Release 9)); the adhesome network database[32]; and the KEGG pathway database[61]. For the adhesome network database, we distinguished between undirected PPIs and directed activating and inhibiting interactions as annotated in the adhesome database and in KEGG. Human and mouse interactions were combined using the orthologue tables of the Mouse Genome Database (MGI) to increase coverage. The high-confidence network of PPIs from public databases contained only interactions reported in at least two separate publications. Networks were visualized using the Cytoscape software. Bar graphs throughout the study were generated in Microsoft Office and depict, unless otherwise indicated, the means and standard errors of the means. Box plots and dot plots were generated using the SigmaPlot software or the MatLab software.

© 2013 Macmillan Publishers Limited. All rights reserved.

Data deposition. Raw data for the phosphoproteome and proteome analyses of the three cell lines are deposited in the Tranche database (https://proteomecommons.org/tranche/) with the following accession numbers: Schiller_Integrins_Phosphoproteome, on33gw4tEXu5YErn5zrp; Schiller_Integrins_Proteome, EvAbqut9c7fC9OQTyawI.

45. Schiller, H. B., Szekeres, A., Binder, B. R., Stockinger, H. & Leksa, V. Mannose 6-phosphate/insulin-like growth factor 2 receptor limits cell invasion by controlling $\alpha_v\beta_3$ integrin expression and proteolytic processing of urokinase-type plasminogen activator receptor. *Mol. Biol. Cell* **20,** 745–756 (2009).
46. Azioune, A., Carpi, N., Tseng, Q., Thery, M. & Piel, M. Protein micropatterns: a direct printing protocol using deep UVs. *Meth. Cell Biol.* **97,** 133–146 (2010).
47. Rape, A. D., Guo, W. H. & Wang, Y. L. The regulation of traction force in relation to cell shape and focal adhesions. *Biomaterials* **32,** 2043–2051 (2011).
48. Wisniewski, J. R., Zougman, A., Nagaraj, N. & Mann, M. Universal sample preparation method for proteome analysis. *Nat. Methods* **6,** 359–362 (2009).
49. Wisniewski, J. R., Zougman, A. & Mann, M. Combination of FASP and StageTip-based fractionation allows in-depth analysis of the hippocampal membrane proteome. *J. Proteome Res.* **8,** 5674–5678 (2009).
50. Olsen, J. V. *et al*. Global, *in vivo*, and site-specific phosphorylation dynamics in signaling networks. *Cell* **127,** 635–648 (2006).
51. Cox, J. *et al*. Andromeda: a peptide search engine integrated into the MaxQuant environment. *J. Proteome Res.* **10,** 1794–1805 (2011).
52. Luber, C. A. *et al*. Quantitative proteomics reveals subset-specific viral recognition in dendritic cells. *Immunity* **32,** 279–289 (2010).
53. Olsen, J. V. *et al*. Parts per million mass accuracy on an Orbitrap mass spectrometer via lock mass injection into a C-trap. *Mol. Cell Proteomics* **4,** 2010–2021 (2005).
54. Cox, J. *et al*. A practical guide to the MaxQuant computational platform for SILAC-based quantitative proteomics. *Nat. Protocols* **4,** 698–705 (2009).
55. Huang da, W., Sherman, B. T. & Lempicki, R. A. Systematic and integrative analysis of large gene lists using DAVID bioinformatics resources. *Nat. Protocols* **4,** 44–57 (2009).
56. Xenarios, I. *et al*. DIP, the database of interacting proteins: a research tool for studying cellular networks of protein interactions. *Nucleic Acids Res.* **30,** 303–305 (2002).
57. Aranda, B. *et al*. The IntAct molecular interaction database in 2010. *Nucleic Acids Res.* **38,** D525–D531 (2010).
58. Ceol, A. *et al*. MINT, the molecular interaction database: 2009 update. *Nucleic Acids Res.* **38,** D532–D539 (2010).
59. Breitkreutz, B. J. *et al*. The BioGRID Interaction Database: 2008 update. *Nucleic Acids Res.* **36,** D637–D640 (2008).
60. Prasad, T. S., Kandasamy, K. & Pandey, A. Human protein reference database and human proteinpedia as discovery tools for systems biology. *Methods Mol. Biol.* **577,** 67–79 (2009).
61. Kanehisa, M., Goto, S., Sato, Y., Furumichi, M. & Tanabe, M. KEGG for integration and interpretation of large-scale molecular data sets. *Nucleic Acids Res.* **40,** D109–D114 (2012).

© 2013 Macmillan Publishers Limited. All rights reserved.

DOI: 10.1038/ncb2747

nature cell biology

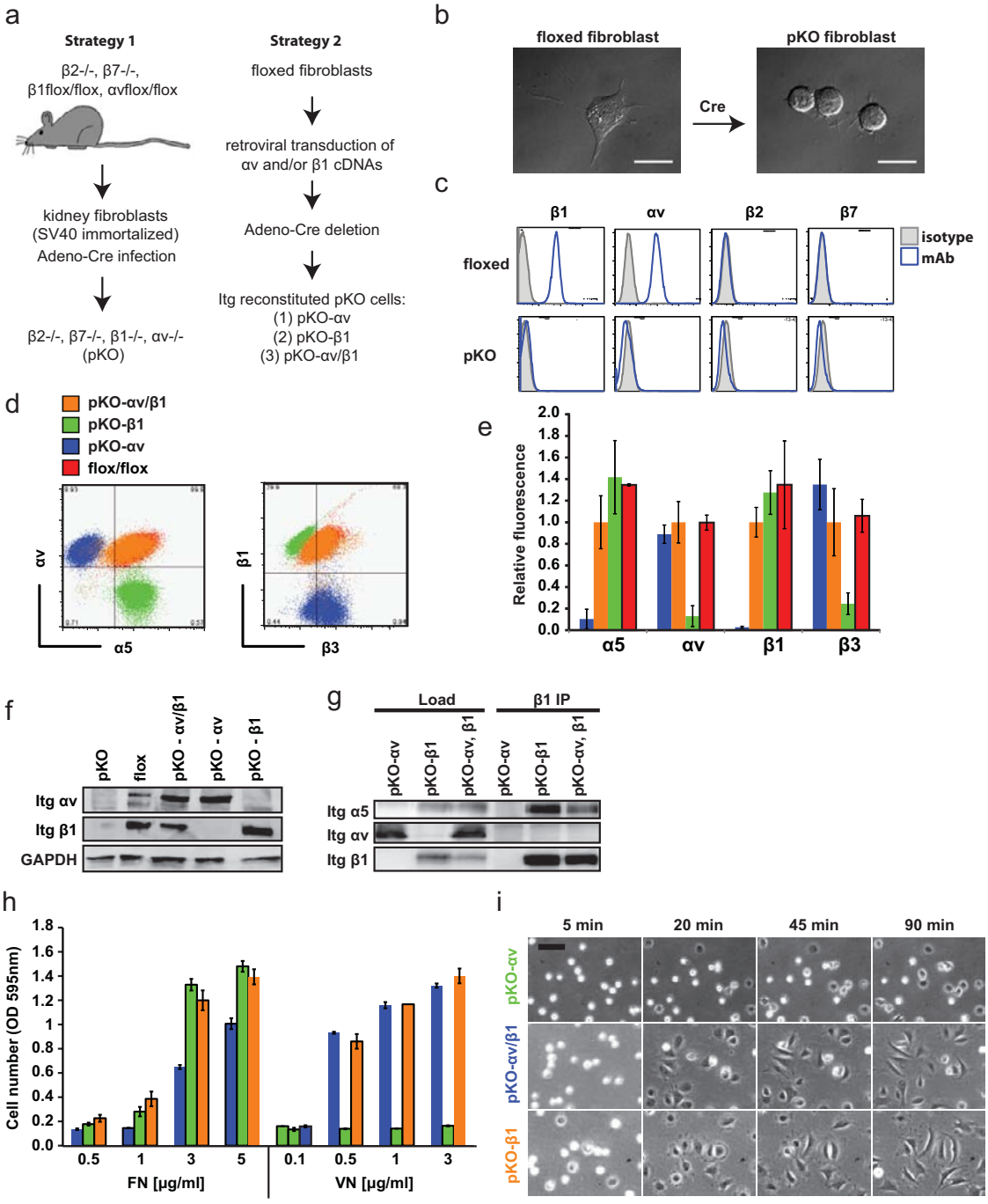

Figure S1 Generation of pKO-αv, pKO-β1 and pKO-αv/β1 cell lines. (**a**) Workflow of the generation of pKO kidney fibroblasts (strategy 1) and integrin reconstituted pKO fibroblasts (strategy 2). (**b**) Phase contrast image of the floxed and pKO cells plated on FN. Scale bar 20 μm. (**c**) Integrin profile of floxed and pKO cells analysed by flow cytometry. (**d**) Cell surface levels of indicated integrins analysed by flow cytometry. (**e**) Relative fluorescence intensities of indicated integrins from three independent stainings analysed by flow cytometry. The means (n=3) and standard deviations are shown. (**f**) Western blots for αv and β1 integrins. GAPDH was used as loading control. (**g**) Cell lysates and immunoprecipitates of β1 integrin were immunoblotted for αv, α5 and β1 integrins. Note that αv does not associate with β1 in pKO-αv/β1 cells. (**h**) Adhesion assay on fibronectin (FN) or vitronectin (VN). Numbers of adherent cells 20 minutes after seeding are shown as relative values of OD=595nm. The bar graph shows the mean and s.e.m. (n=3; one representative out of 2 independent experiments is shown). (i) Cells plated on FN and time-lapse imaged using a phase contrast microscope at 20x magnification. Scale bar 100 μm. pKO-β1 (green); pKO-αv (blue); pKO-αv/β1 (orange); parental β1/αv floxed cell (red).

© 2013 Macmillan Publishers Limited. All rights reserved.

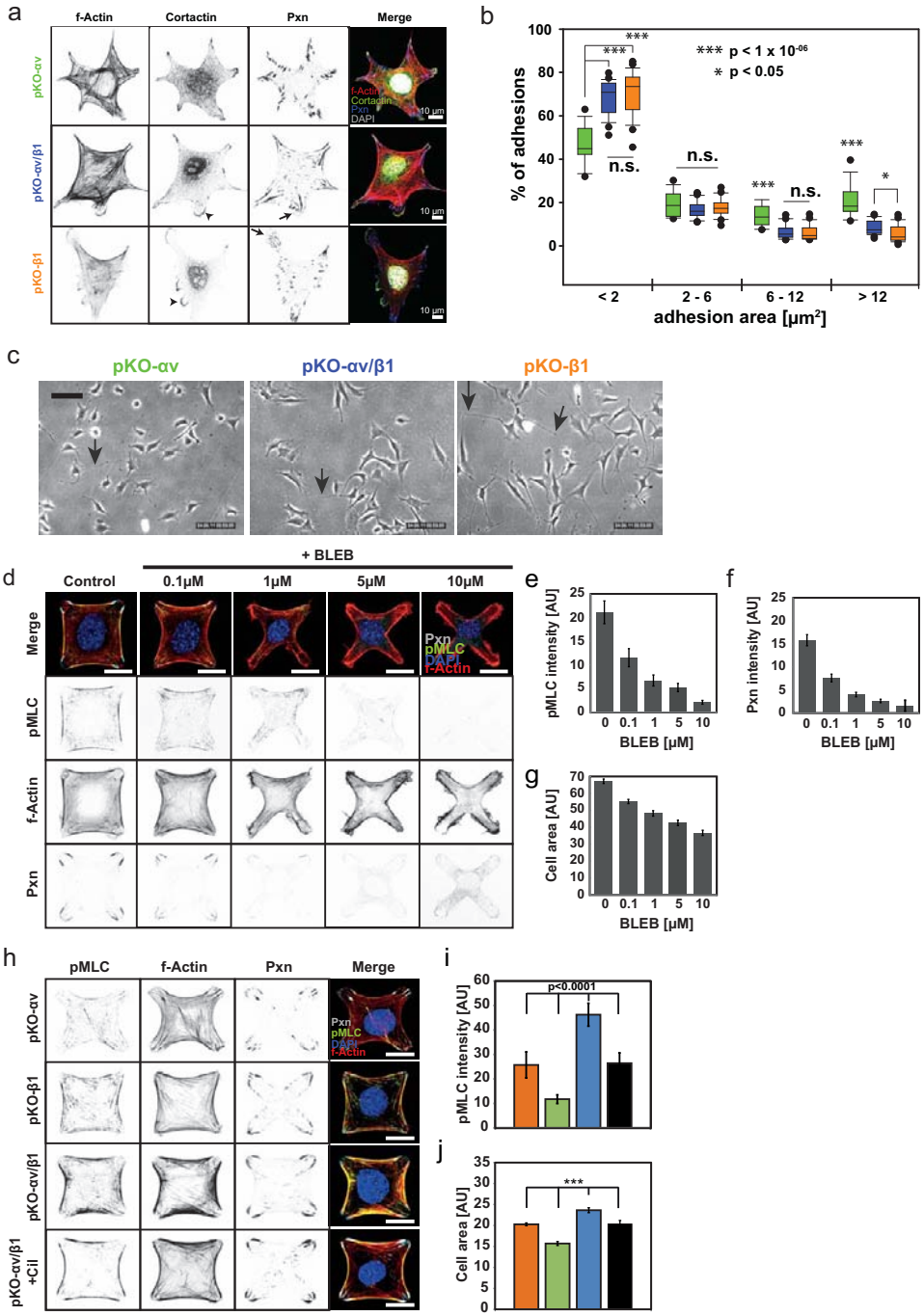

Figure S2 α5β1 and αv-class integrins induce different spreading areas, membrane protrusions and adhesion sites on FN. (**a**) Cells were plated on FN for 90 minutes and immunostained with the indicated antibodies. Arrowheads indicate cortactin-positive lamellipodia and arrows mark the small NAs in lamellipodia. Scale bar 10µm. (**b**) Size distribution of adhesive sites of cells stained with Paxillin calculated with the Metamorph software. Boxplots show the percentage of adhesions in the depicted size classes (pKO-αv n=15; pKO-αv/β1 n= 29; pKO-β1 n=23; one representative out of 2 independent experiments is shown). Boxplot whisker ends are at 1.5 interquartile range and outliers are shown as dots. Significance was calculated using a *t* test (*=p<0.05; ***=p<10 E-06). (**c**) Still pictures taken from supplementary movies S1-S3 showing trailing edge detachment defects indicated by the arrows. Scale bar 100 µm. (**d**) Floxed cells cultured 3 hours on FN-coated X-shapes treated for 1 hour with indicated concentrations of blebbistatin (BLEB), and then stained for Paxillin, pMLC and f-actin. Scale bar 10 µm. (**e**) Fluorescence intensities of pT18/S19-MLC, **(f)** Paxillin (Pxn) and **(g)** cell areas after blebbistatin treatment (n=20 cells; error bars represent s.e.m.). (**h**) Cells plated on FN-coated X-shapes and stained for pMLC, Paxillin and f-actin. Scale bar 10 µm. (**i**) Fluorescence intensities of pS18/T19-MLC and (**j**) cell areas (pKO-αV n=46, pKO-β1 n=46, pKO-αV/β1 n=21, pKO-αV/β1 +Cil n=10; one representative out of 3 independent experiments is shown; error bars represent s.e.m.). Cilengitide (Cil) was used to block αv-class integrins. Significance was calculated using a ttest. pKO-αv (green); pKOαv/β1 (blue); pKO-β1 (orange); pKOαv/β1 + 1 µM cilengitide (black).

© 2013 Macmillan Publishers Limited. All rights reserved.

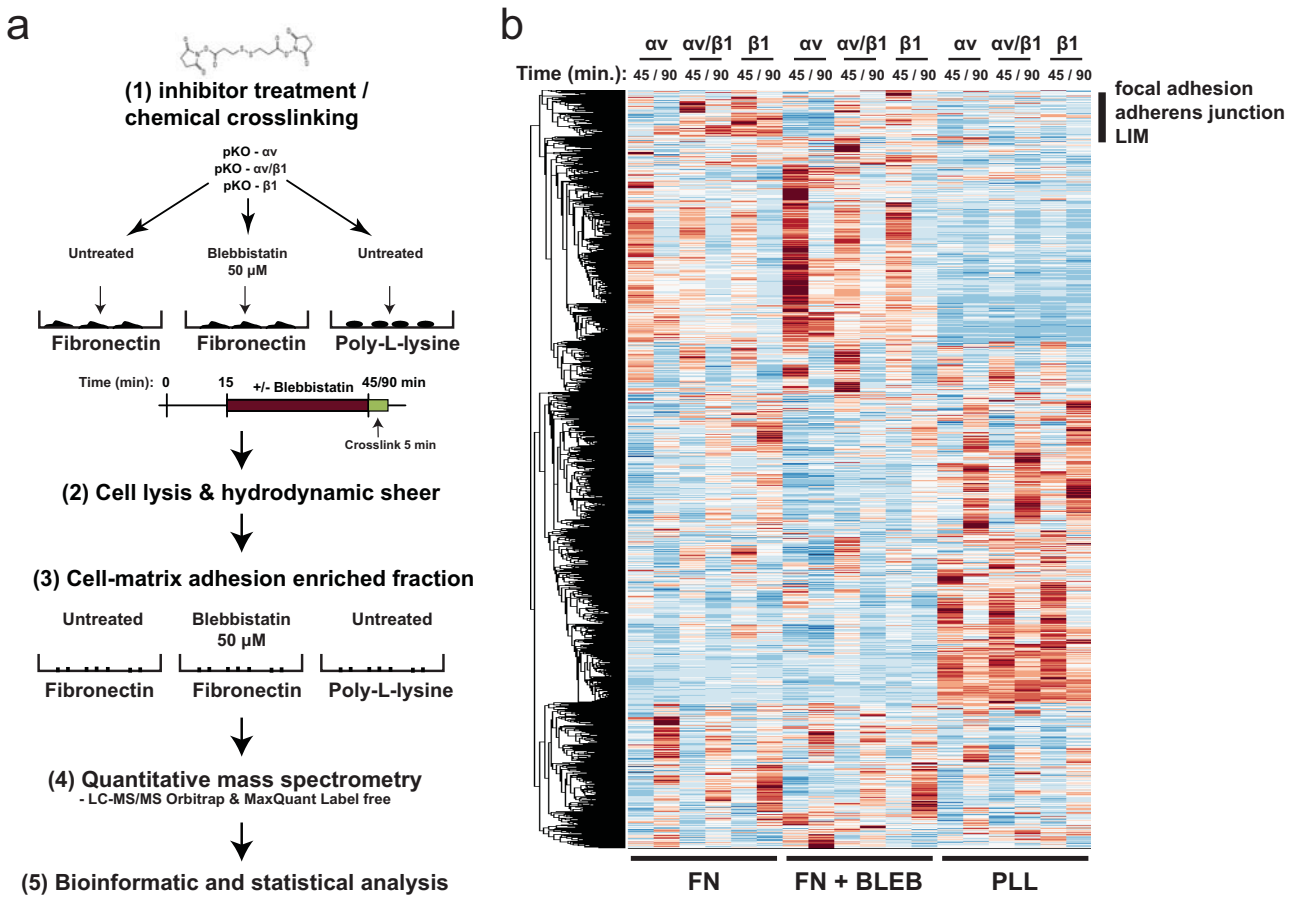

Figure S3 Adhesome analysis of pKO-αv, pKO-β1 and pKOαv/β1 cells. (**a**) Workflow for isolation of FA enriched fractions and analysis of adhesome components. (**b**) Adhesomes derived from cells plated on indicated substrates for 45 or 90 minutes were examined by non-supervised hierarchical cluster analysis of Z-scores of median MS intensities (n=3-4). The labels on the right indicate significantly enriched gene ontology (GO) terms.

© 2013 Macmillan Publishers Limited. All rights reserved.

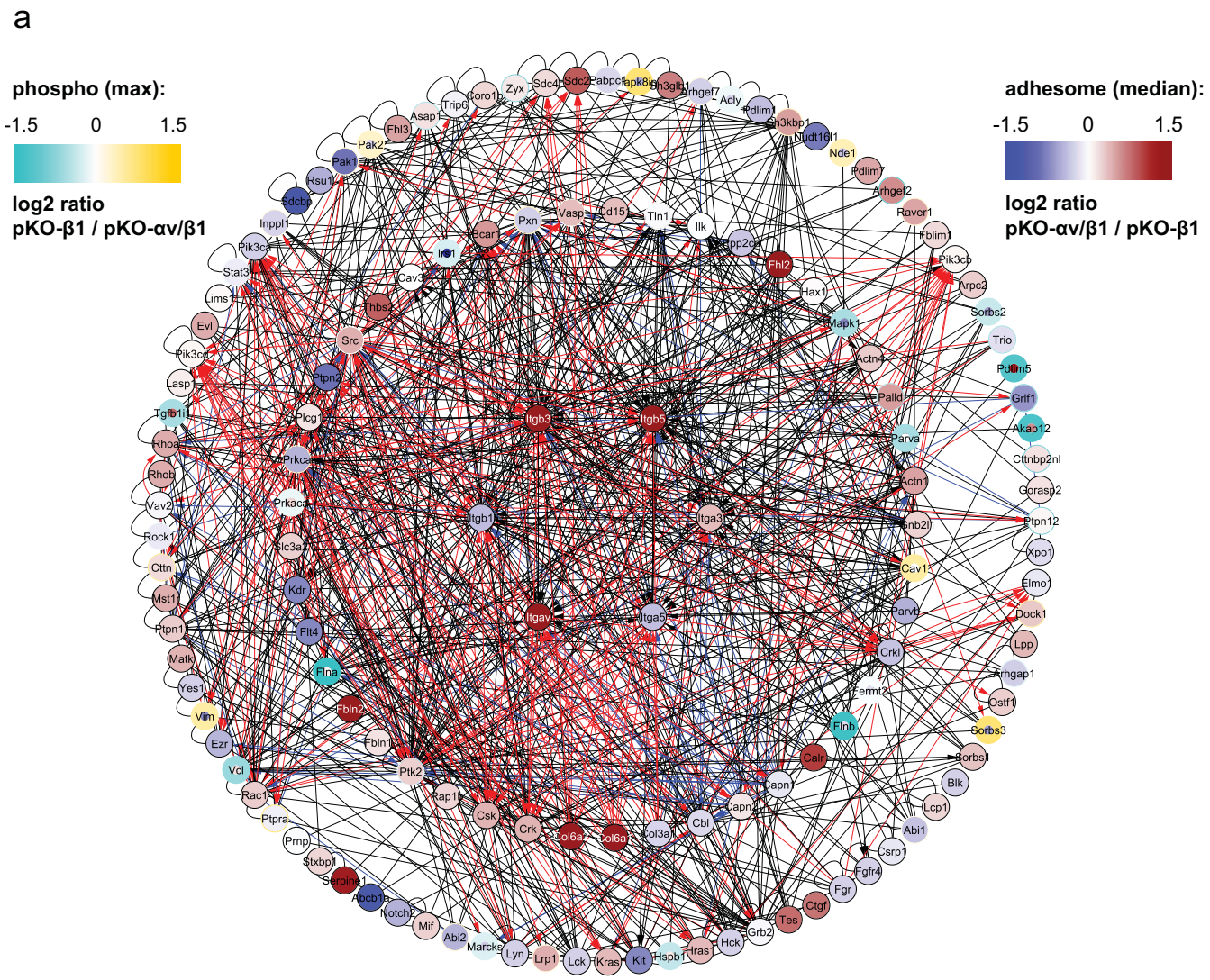

Figure S4 α5β1- and αv-class-specific PPIs and phosphosites. (**a**) The PPI network derived from FA-enriched samples. Integrin subunits are in the centre and their direct and indirect interactors are in the inner and outer circles, respectively. Black lines between nodes indicate high confidence PPI, red arrows indicate activating interactions and blue lines indicate inhibiting interactions. The nodes were labelled with gene symbols and colour-coded according to the MS intensity ratio of pKO-αv/β1 versus pKO-β1. Node edges were colour-coded according to the SILAC ratio of the maximally regulated phosphosite on each significantly regulated protein. (**b**) The PPI-network was derived as in (a). The nodes and node edges were colour-coded according to the MS intensity ratio of pKO-αv versus pKO-αv/β1. (**c**) The PPI-network was derived as described in (a). The nodes and node edges were colour-coded according to the MS intensity ratio of pKO-αv versus pKO-β1.

© 2013 Macmillan Publishers Limited. All rights reserved.

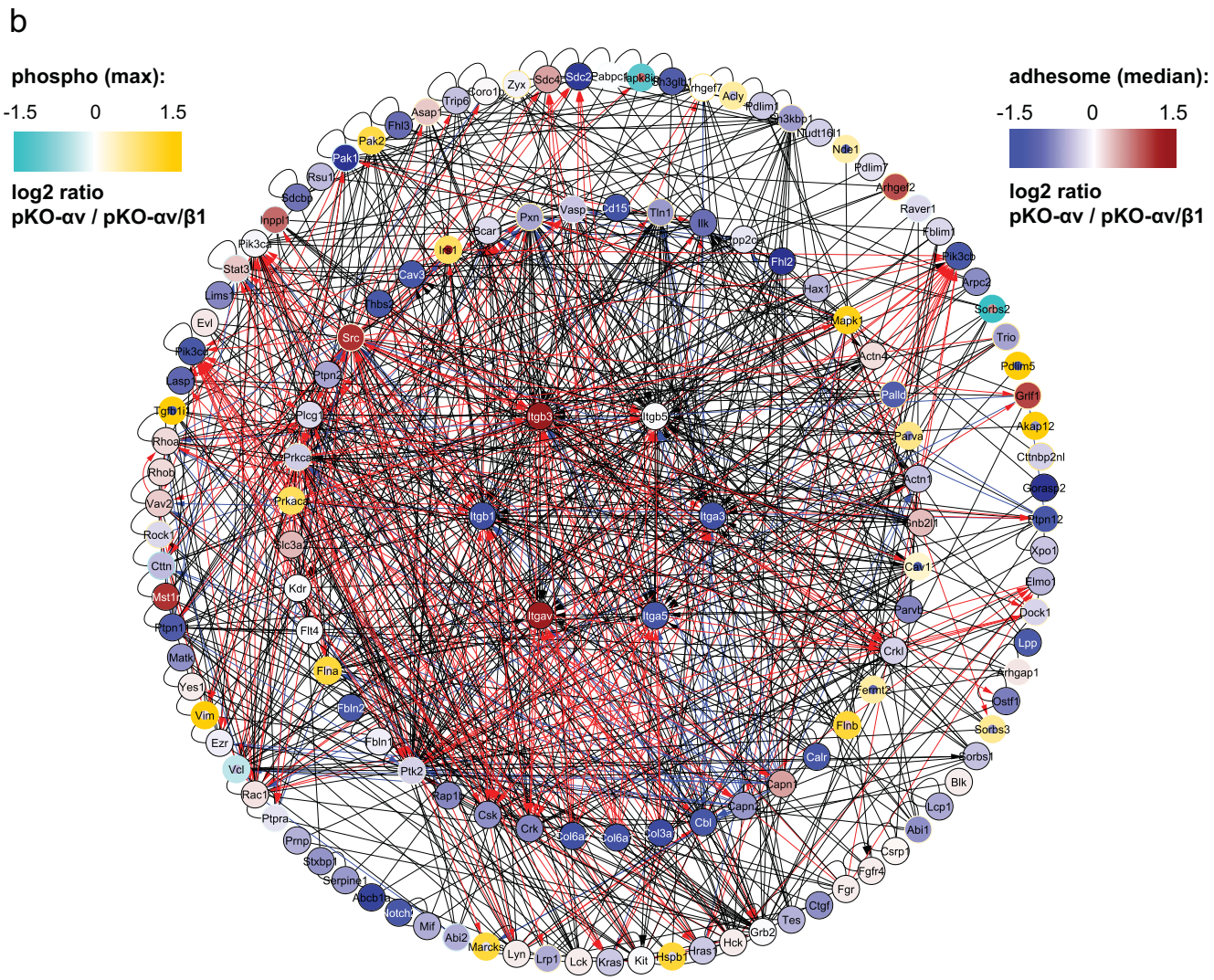

Figure S4 continued

© 2013 Macmillan Publishers Limited. All rights reserved.

C

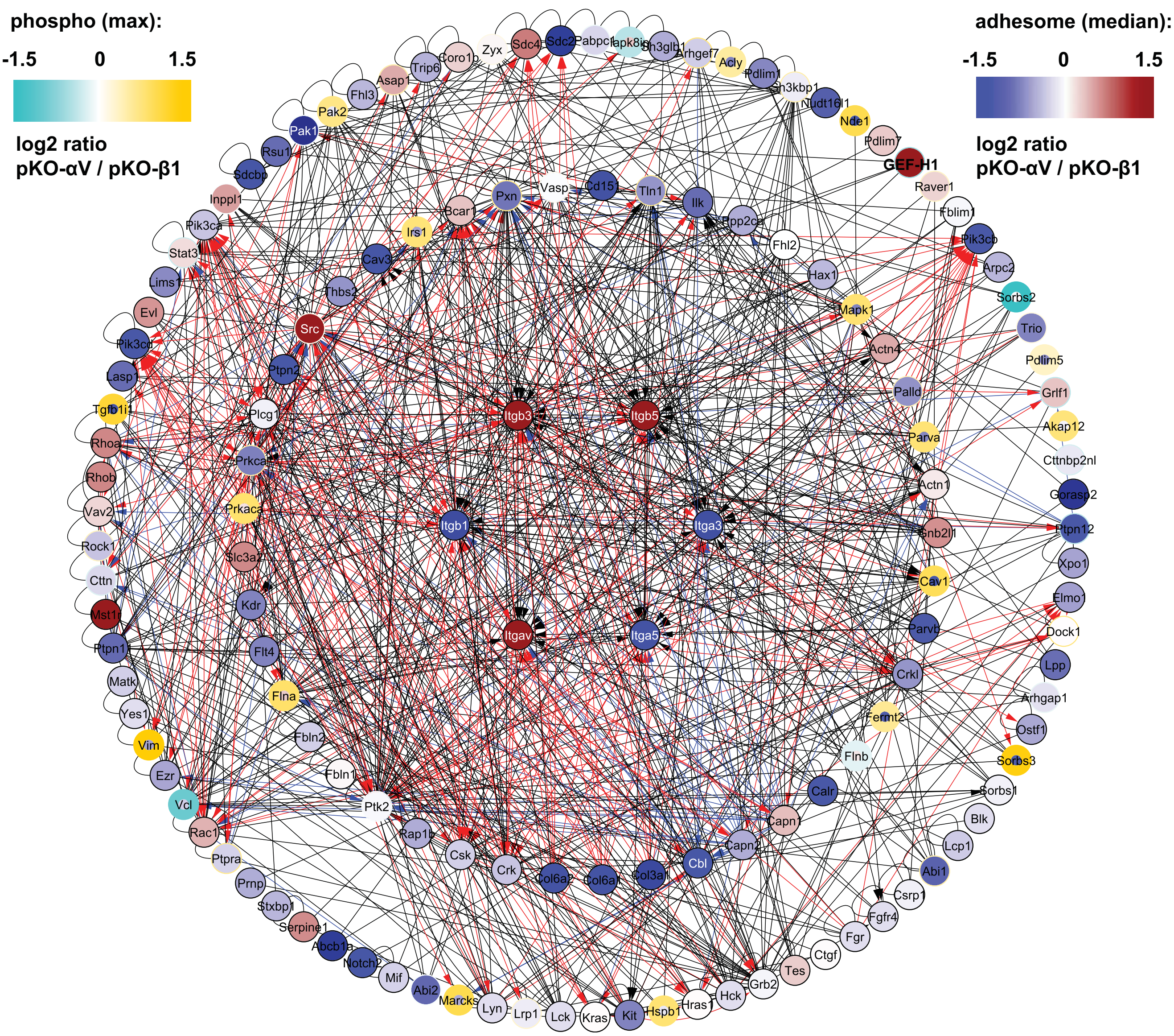

Figure S4 continued

© 2013 Macmillan Publishers Limited. All rights reserved.

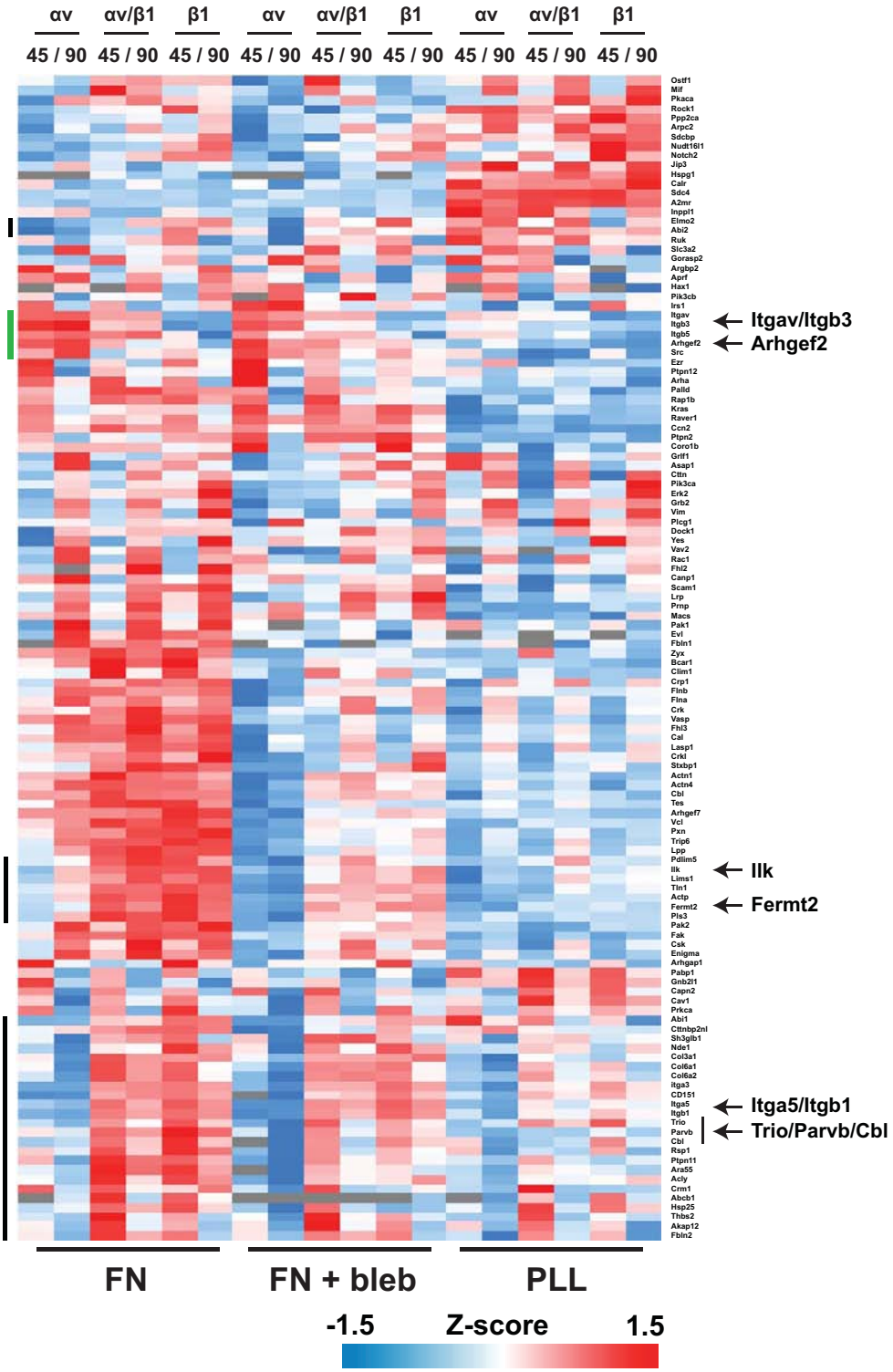

Figure S5 Integrin-specific differences in the "core integrin interactome". The Z-scores of median MS intensities (n=3-4) of the 125 core integrin-interactome proteins (Fig. S4) were subjected to hierarchical clustering. The black bars on the left indicate α5β1-dependent FA proteins, while the green bar indicates the αv-class integrin-dependent FA proteins selected for the clustering in Fig. 4c.

© 2013 Macmillan Publishers Limited. All rights reserved.

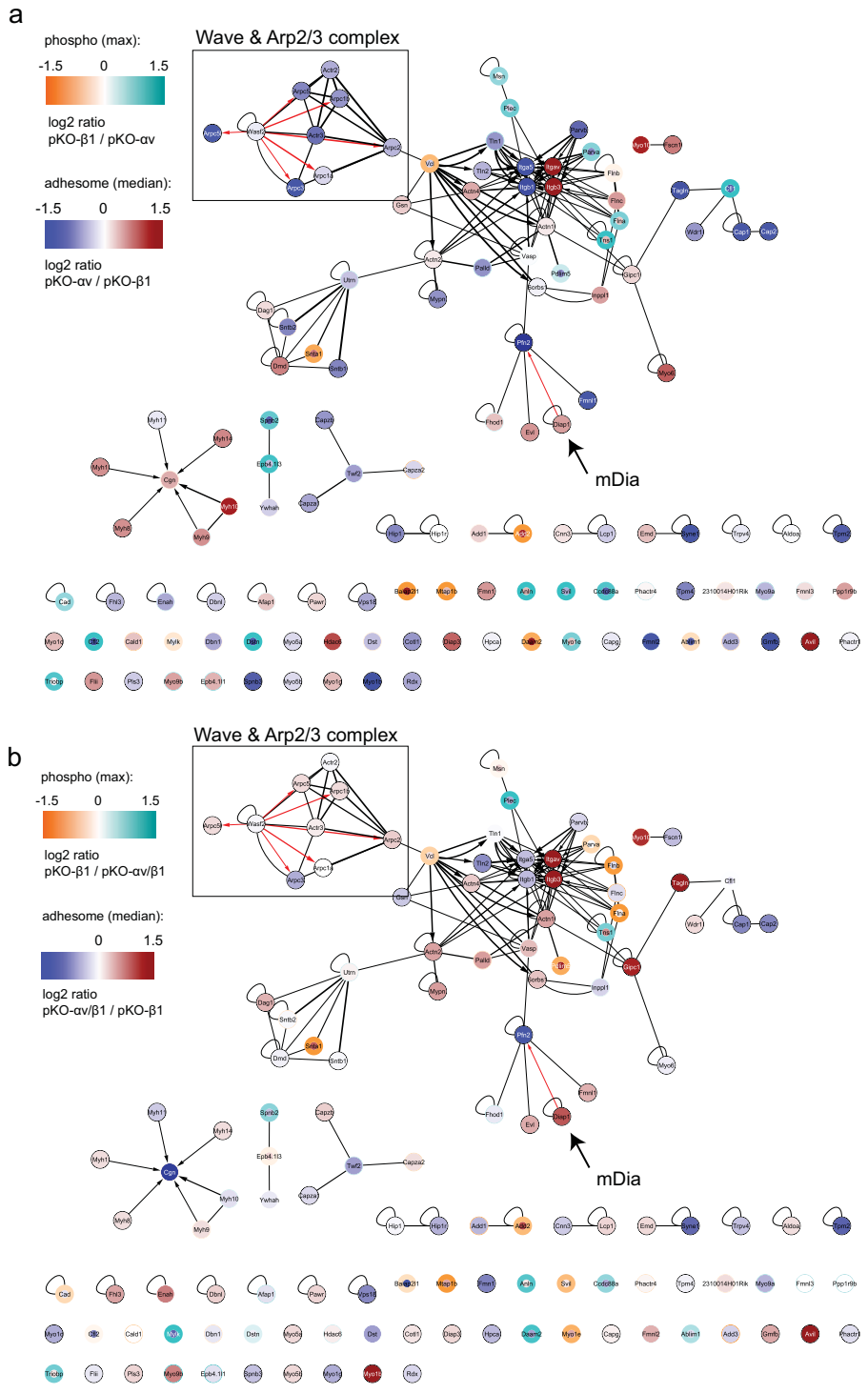

Figure S6 Network analysis of actin binding proteins enriched in the adhesome preparations. (**a**) Actin binding proteins were extracted from the adhesome dataset using gene ontology annotations. Black lines between nodes indicate high confidence PPI, red arrows indicate activating and blue lines indicate inhibiting interactions. The nodes were labelled with gene symbols and colour coded according to the log2 MS intensity ratio of pKO-αv over the pKO-β1 sample. Node edges were colour-coded according to the log2 SILAC ratio of the maximally regulated phosphosite on each significantly regulated protein. The box marks components of the WAVE and Arp2/3 complex, while the arrowhead marks the formin mDia. (**b**) The graph was generated as in (a), except that the nodes were colour-coded according to the log2 MS intensity ratio of pKO-αv/β1 over the pKO-β1 sample.

© 2013 Macmillan Publishers Limited. All rights reserved.

a

β1-tail:	Desthiobiotin - HDRREFAKFEKEKMNAKWDTGENPIYKSAVTTVVNPKYEGK - OH
β1-tail scr:	Desthiobiotin - ANYETKTNPKFKRAWKDNTKYEVVMSHAGFDIEVPREGKEK - OH
β3-tail:	Desthiobiotin - HDRKEFAKFEEERARAKWDTANNPLYKEATSTFTNITYRGT - OH
β3-tail scr:	Desthiobiotin - AETFLSRHYNKGFDKATKRPAEDRYWNTARENETAKTTIFE - OH

b

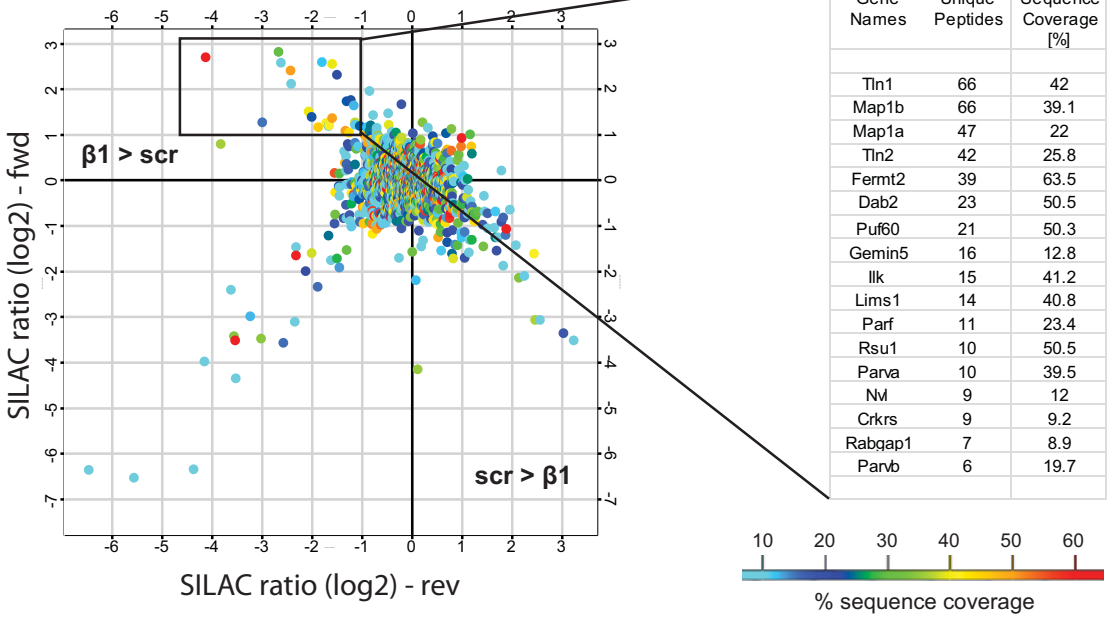

Gene Names	Unique Peptides	Unique Sequence Coverage [%]
Tln1	66	42
Map1b	66	39.1
Map1a	47	22
Tln2	42	25.8
Fermt2	39	63.5
Dab2	23	50.5
Puf60	21	50.3
Gemin5	16	12.8
Ilk	15	41.2
Lims1	14	40.8
Parf	11	23.4
Rsu1	10	50.5
Parva	10	39.5
Nvl	9	12
Crkrs	9	9.2
Rabgap1	7	8.9
Parvb	6	19.7

c

Gene Names	Unique Peptides	Unique Sequence Coverage [%]
Dync1h1	169	43.8
Iqgap1	91	67.2
Tln1	57	35.3
Iqgap2	50	41.1
Vim	49	85.6
Frap1	49	27.5
Usp9x	49	23
Lmo7	48	36.1
Ccdc88a	48	30.3
Fn1	46	29.9
Nes	44	33.4
Arhgef2	38	48.7
Svil	36	20.9
Cep170	35	31.4
Synj1	33	23.6
Hnrnpm	31	48.8
Rictor	31	24.4
Phldb1	31	26.7
KIAA1967	29	44.3

Gene Names	Unique Peptides	Unique Sequence Coverage [%]
Flnc	29	15.9
Irs1	29	34.4
Esf1	28	31.4
Fermt2	28	51
Spata5	27	44.2
Gigyf2	25	25.3
Lmna	25	39.8
Setd2	25	15
Cep55	25	45.2
Dab2	24	53.7
Rgnef	24	19.2
Mcm5	24	43.6
Pik3c2a	23	16
Ctnnd1	23	35.3
Jak1	23	28.6
Hadha	22	37
Dsp	22	9.1
Arhgef17	21	14.4
Rngtt	20	37.2
Dock7	20	11.5

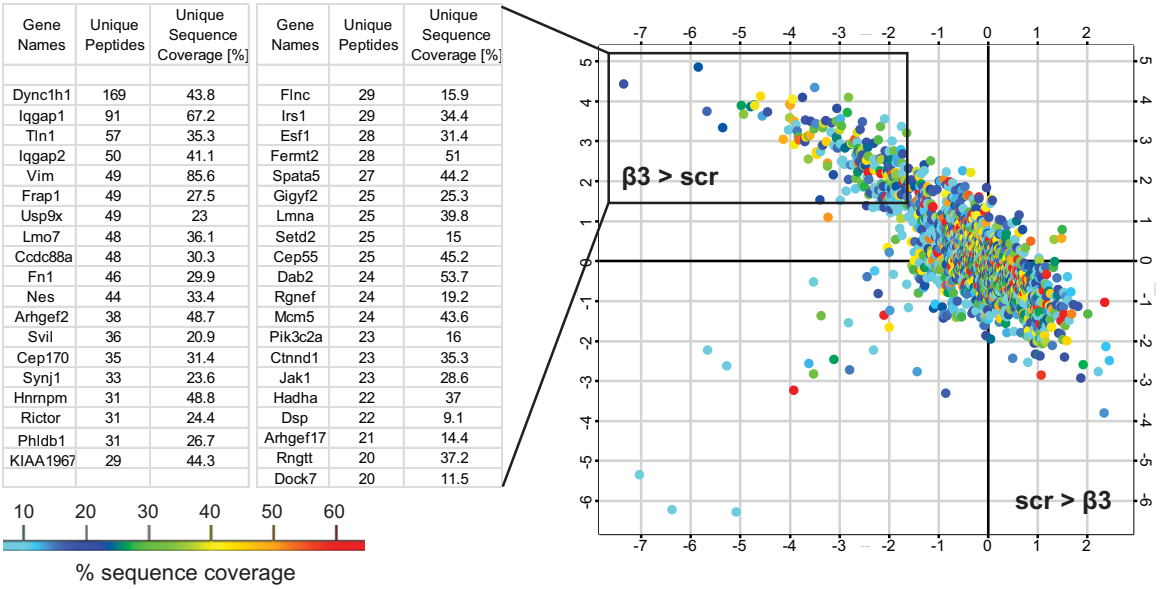

Figure S7 Integrin tail peptide pulldowns. (**a**) Sequence of synthetic desthiobiotinylated peptides used for the pull down experiments. (**b**) SILAC ratio plot from label inverted replicates (specific interactors have high SILAC ratio in the forward experiment and low SILAC ratios in the label swapped reverse experiment) comparing the β1-tail peptide with a scrambled control. The table shows the most intense β1-specific interactors with high sequence coverage that were reproducibly enriched versus the scrambled control peptide (scr) (n=4; 2 independent experiments). (**c**) SILAC ratios of proteins from inverted replicates comparing the β3-tail peptide with a scrambled control. The table shows the most intense β3-specific interactors with high sequence coverage that were reproducibly enriched versus the scrambled control peptide (scr) (n=4; 2 independent experiments).

© 2013 Macmillan Publishers Limited. All rights reserved.

a

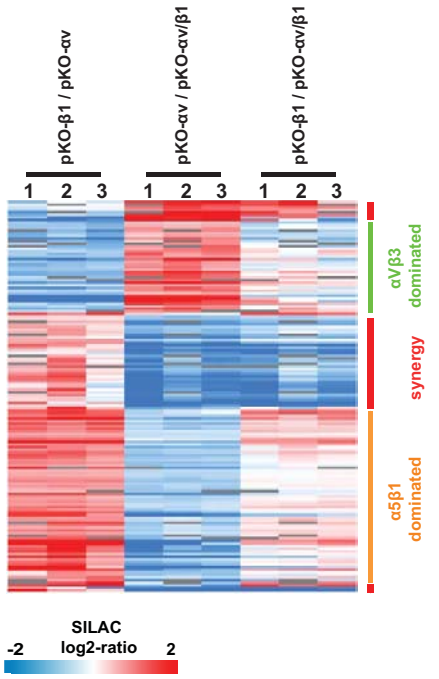

b

Synergy up/down	αvβ3 dominated	α5β1 dominated	α5β1 dominated
Actn1 *	AA881470	Acbd3	Lox
Adir	Abcc4	Acss2	Lxn
Apol9a	Add2	Ahnak2	Man2a1
Ass	Aif1l	Anx1	Mdh2
Bal	Aim1	Anx8	Me2
BC006779	Baiap2l1	Cap	Metap2
Bst2	Bckdha	Capn2	Mme
Clim1	Cadm1	Cav *	Mrc2
Cmpk2	Ctsl	Cdkn2a	Mre11
Ddx58	Daglb	Ckap4	Msra
Dtx3l	Dbt	Clp	Napg
Eif2ak2	Dcoh	Cnn2	Nudt9
G1p2	Dhx33	Col1a1	P4ha1
Galm	Eml2	Col1a2	P4ha2
Garg39	Enpep	Col3a1	Pea15
Garg49	Epb4.1l5	Col6a1	Pk3
Gbp2	Fam129a	Col6a2	Plod2
Gbp3	Fan1	Crabp1	Plod3
Gbp6	Fbxo2	Ctsb	Por
Gstm1	Gsta	D7Ertd671e	Ptmb4
Gstm2	Hist3h2bb	Dpysl3	Rad50
H2-D1	Hk2	Dsn	Rca1
Ifi1	Hmg2a	Ergic53	Rexo2
Ifi205b	Itgav	Fabp5	Rgc32
Ifi35	Jip3	Fam114a1	Sept5
Ifit1	Kiaa0193	Glud	Sparc
Ifitm3	Kiaa1102	H2-K	Svil *
Inf2	Nipsnap1	Igtp	Trp32
Kiaa2005	Polr1d	Ikbip	Tubb6
Mylk *	Ptplad1	Itga3	Ufc1
Nfkb2	Rpl5	Itgb1	Vcl *
Oasl2	Sp2	Kiaa1830	Wdr1
Parp12	Steap	Lamb-1	
Pdlim5	Tjp2	Lbr	
Pml	Wipi2	Lmp7	
Rnf213		Loh11cr2a	
RP23-399J8.4-002			
Sm22			
Stat1			
Tpm1			
Zfp185			

c

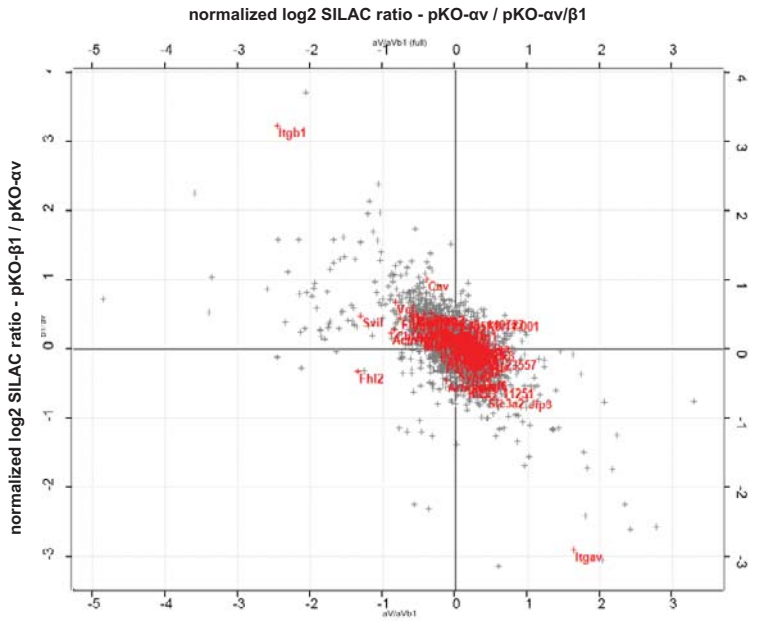

Figure S8 Cellular proteome of pKO-αv, pKO-β1 and pKO-αv/β1 cells. (**a**) SILAC labelled cells cultured on FN for several passages were analysed by MS. SILAC ratios of 150 significantly regulated proteins (ANOVA, Benjamini/Hochberg FDR) were subjected to non-supervised hierarchical cluster analysis and colour coded. The bars depict differentially regulated clusters of proteins. (**b**) Gene names of the 3 differentially regulated groups (a) are shown. Known FA proteins are marked with an asterisk. (**c**) Scatter plot showing SILAC ratios. Previously annotated FA proteins are labelled in red.

© 2013 Macmillan Publishers Limited. All rights reserved.

Figure 5c

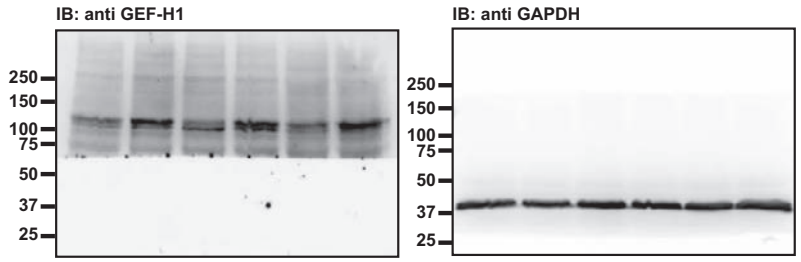

Figure 6d

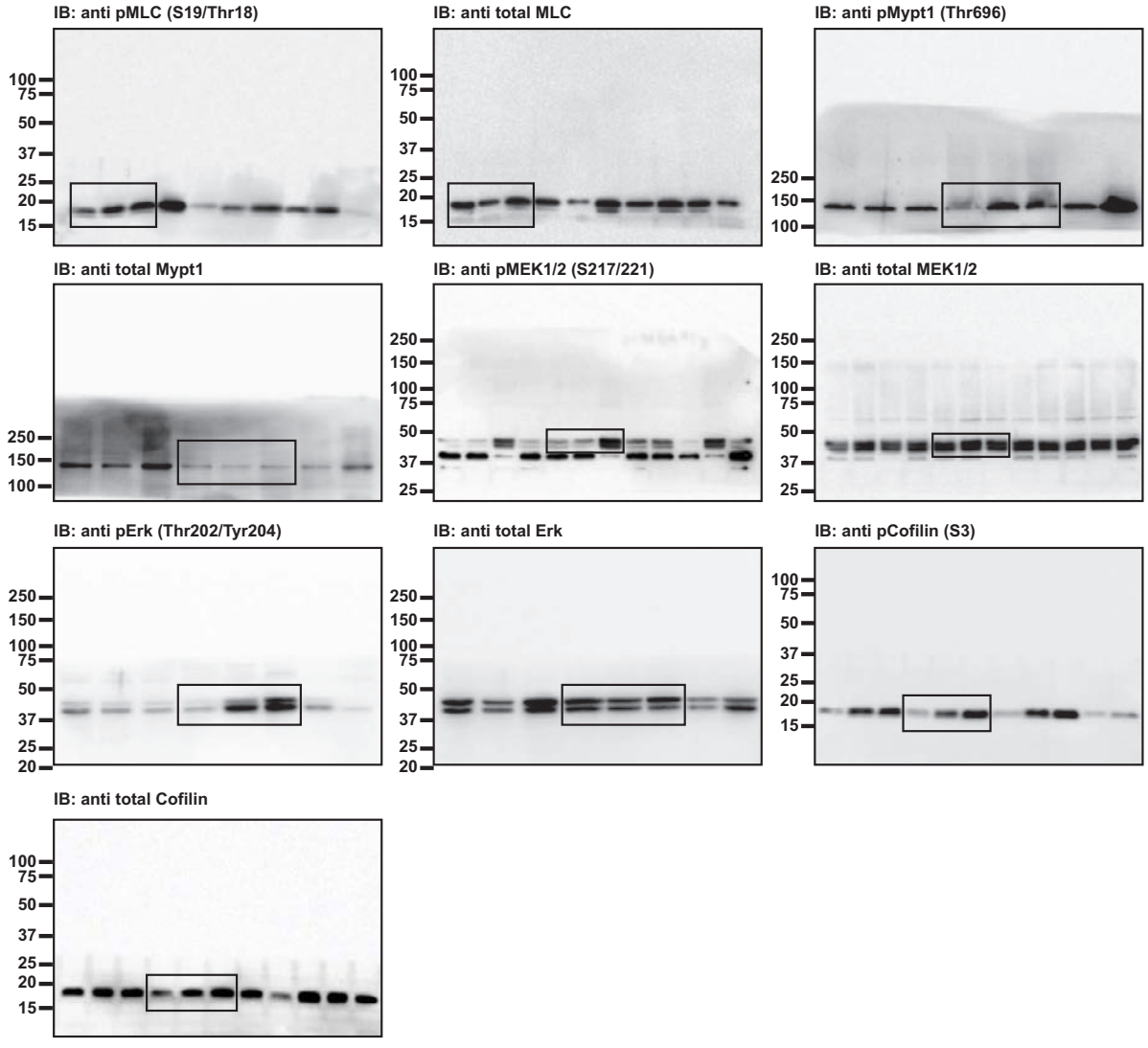

Figure S9 Uncropped western blots.

© 2013 Macmillan Publishers Limited. All rights reserved.

Figure 7c

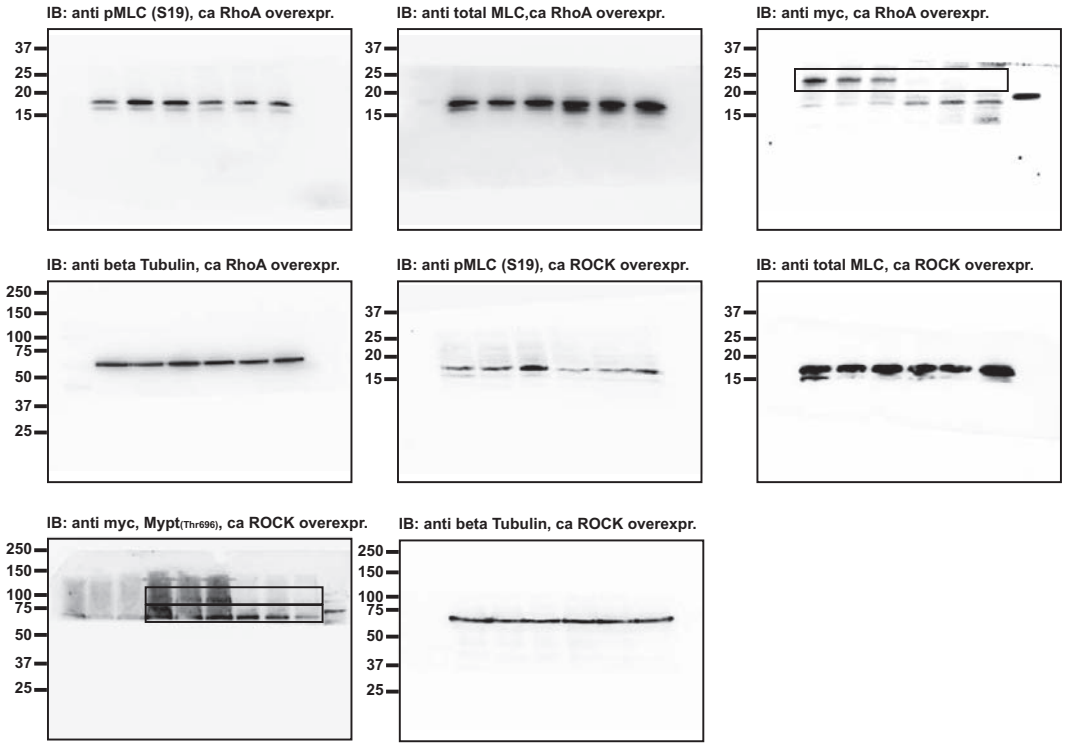

Figure S1f

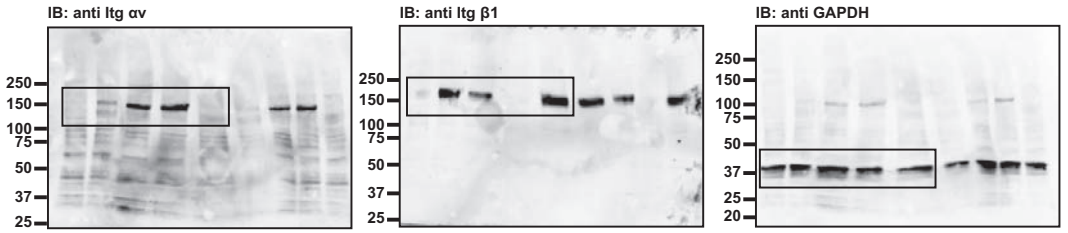

Figure S1g

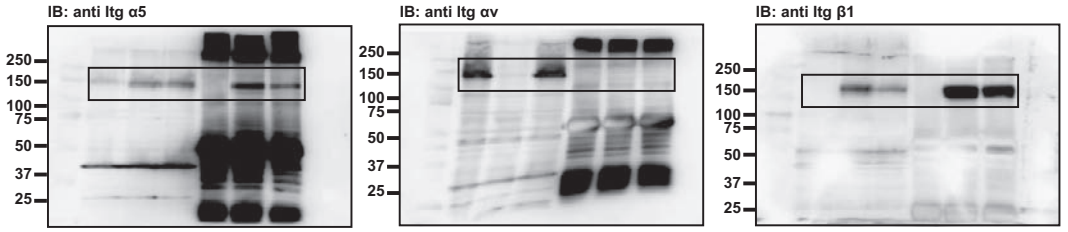

Figure S9 continued

© 2013 Macmillan Publishers Limited. All rights reserved.

Supplementary video legends

Video S1 Time-lapse movie of pKO-αv cells plated on FN. Cells were plated on FN coated (5 μg/ml; blocked with 1% BSA) tissue culture dishes in presence of 10% serum and video tracked over 20 hours with a frame rate of 1 picture every 4 minutes. Pictures were acquired with a phase contrast microscope at magnification 20x.

Video S2 Time-lapse movie of pKO-αv/β1 cells plated on FN. Cells were plated on FN coated (5 μg/ml; blocked with 1% BSA) tissue culture dishes in presence of 10% serum and video tracked over 20 hours with a frame rate of 1 picture every 4 minutes. Pictures were acquired with a phase contrast microscope at magnification 20x.

Video S3 Time-lapse movie of pKO-β1 cells plated on FN. Cells were plated on FN coated (5 μg/ml; blocked with 1% BSA) tissue culture dishes in presence of 10% serum and video tracked over 20 hours with a frame rate of 1 picture every 4 minutes. Pictures were acquired with a phase contrast microscope at magnification 20x.

© 2013 Macmillan Publishers Limited. All rights reserved.

Publication 2 (in preparation)

Integrins synergistically induce the MAL/SRF target gene ISG15 to ISGylate cytoskeletal and focal adhesion proteins necessary for cancer cell invasion.

will be published as

Michaela-Rosemarie Hermann, Emanuel Rognoni, Madis Jakobson, Moritz Widmaier, Assa Yeroslaviz, Roy Zent, Guido Posern, Ferdinand Hofstädter and Reinhard Fässler: **Integrins synergistically induce the MAL/SRF target gene ISG15 to ISGylate cytoskeletal and focal adhesion proteins necessary for cancer cell invasion.** Manuscript in preparation;

Supplementary Information:

PDF files

Fig. S1. Different total Actin levels and distribution observed in pKO-αV, pKO-β1 and pKO-αV, β1 cells.

Fig. S2. αV-class integrins cooperate with α5β1 to induce SRF/MAL activity.

Fig. S3. Type I interferon response independent but SRF/MAL dependent ISG15 transcription in pKO-αV, pKO-β1 and pKO-αV, β1 cells.

Fig. S5. αV- and β1-class integrin induced ISGylation of SRF/MAL targets results in bad breast cancer patient prognosis.

Excel files

Table S1. ISG15 pull-down mass spectrometry analysis

Table S2. List of primer sequences

Table S3. List of antibodies

Integrins synergistically induce the MAL/SRF target gene ISG15 to ISGylate cytoskeletal and focal adhesion proteins necessary for cancer cell invasion

Michaela-Rosemarie Hermann[1], Emanuel Rognoni[1], Madis Jakobson[1], Moritz Widmaier[1], Assa Yeroslaviz[2], Roy Zent[3], Guido Posern[4], Ferdinand Hofstädter[5] and Reinhard Fässler[1]

[1]Department of Molecular Medicine and [2]Bioinformatics Group, Max Planck Institute of Biochemistry, 82152 Martinsried, Germany; [3]Division of Nephrology, Department of Medicine, Vanderbilt Medical Center, Nashville, TN, 37232, USA; [4]Institute of Physiological Chemistry, 06114 Halle, Germany; [5]Institute of Pathology, 93053 Regensburg, Germany

Keywords: Integrin, Focal Adhesion, Adhesome, SRF, MAL, ISG15

Corresponding author: Reinhard Fässler (faessler@biochem.mpg.de)

Integrin-mediated activation of small GTPases polymerizes g-Actin into different Actin structures. Here we report that the g-Actin pools correlated with low nuclear MAL levels and MAL/SRF activities in αV single, intermediate in β1 single and high in αV, β1 double expressing cells. Integrin-mediated activation of MAL/SRF induced expression of the ubiquitin-like modifier interferon-stimulated gene 15 (ISG15) resulting in the ISGylation of integrins, Actin, Focal Adhesion and Actin binding proteins. The increased stability and/or activity of these proteins enhanced kidney fibroblast but also human breast cancer cell invasion and correlated with poor patient survival. Our findings show that integrin adhesions, MAL/SRF and ISG15 constitute a new autoregulatory feed-forward loop that precisely adjusts actin- and adhesion-based functions required for cell spreading, migration and invasion.

INTRODUCTION

Integrin-mediated cell adhesion and signalling control numerous cellular processes, which are crucial for development, postnatal homeostasis and pathology. Integrin signalling is a multistep process that is initiated with integrin activation and ligand binding, followed by integrin clustering and the progressive assembly of signalling platforms consisting of adaptor, signalling/catalytic and cytoskeletal proteins. The first integrin-induced signalling platforms are small and unstable nascent adhesions (NAs), which eventually mature into large focal adhesions (FAs) that are connected to filamentous (f-) Actin.

Integrin signalling induces both short- and long-term effects. The short-term effects consist of cytoskeletal rearrangements that allow cells to adopt their characteristic shape and initiate migration, and are caused by the activation of Rho family GTPases and actin-binding proteins (Danen et al., 2002). Long-term effects of integrin signalling result from changes in gene expression, which regulate cell proliferation and differentiation. Integrin-dependent regulation of gene expression is primarily thought to arise from cross talk with growth factor receptors (GFR) that increase the activity of mitogen activating protein (MAP) kinase pathways. A recent study, however, reported that β1-class integrins can change gene programs of mesenchymal stem cells involved in lineage commitment to bone, fat or cartilage by activating Rho GTPase signalling cascades, which result in the nuclear localization of the transcriptional co-activators Yes-associated protein (YAP) and transcriptional co-activator with PDZ-binding motif (TAZ) (Tang et al., 2013). In addition to the control of YAP/TAZ, Rho family GTPases can also control gene transcription by releasing the association of the transcriptional co-activator Megakaryocyte Acute Leukemia protein (MAL; also known as MRTF-A or MKL1) from monomeric or globular (g-) Actin. Once g-Actin is assembled into Actin networks, free MAL translocates into the

nucleus, where it associates with and activates the transcription factor Serum Response Factor (SRF), which regulates the expression of cytoskeletal proteins including Actin and Focal Adhesion proteins. Thus it is possible that integrin-mediated activation of Rho GTPases regulates cytoskeletal dynamics but also adhesion through effector proteins and the control of MAL`s nucleo-cytoplasmic shuttling in order to initiate target gene transcription.

To test this hypothesis we investigated whether and which integrins regulate MAL/SRF-mediated gene expression. To achieve this goal, we used recently engineered cell lines that express Fibronectin (FN)-binding integrins of the αV- (αVβ3, αVβ5) and/or β1-class (α5β1) that allowed us to assign stress fibre formation to αV-class integrins and myosin II activation and lamellipodia formation to α5β1 integrin (Schiller et al., 2013). We report that αV- and β1-class integrins synergize to regulate expression of MAL/SRF target genes. One new MAL/SRF target is the ubiquitn-like modifier Interferon-specific gene 15 (ISG15), which becomes covalently attached to specific lysine residues of numerous known MAL/SRF target gene products including Vinculin, Talin and Eplin. ISG15 modifications are known and thought to negatively impact ubiquitination by a) inhibition of ubiquititin-specific E2 enzymes (Malakhova and Zhang, 2008; Okumura et al., 2008; Zou et al., 2005) and b) possible occupation of lysine residues also used by Ubiquitin through ISGylation . Thus it is possible that ISG15-linked proteins could be protected from proteasomal targeting (Liu et al., 2003). Our findings identify a new synergistic activity of fibronectin-binding integrins that controls cell invasion by regulating transcription and subsequent ISGylation.

RESULTS

FN bound α5β1 and αV-class integrins control f-Actin and nuclear MAL levels

We generated immortalized fibroblast cell lines lacking the expression of all integrins (pan-knockouts, pKO) and re-expression of β1 and/or αV integrin cDNAs produced cells expressing αV- (pKO-αV), β1- (pKO-β1) or αV- and β1-class integrins (pKO-αV,β1) ((Schiller et al., 2013) Fig.S1A). When the three cell lines were seeded on FN-coated, circular micropatterns separated by non-adhesive polyethylene glycol, pKO-αV cells expressing the FN-binding αVβ3 and αVβ5 integrins preferentially formed large focal adhesions (FAs) that were shown with labelled phalloidin to be connected by thick radial stress fibres. In contrast, pKO-β1 cells expressing the FN-binding α5β1 integrin preferentially formed small, nascent adhesions (NAs), thin stress fibres and a dense subcortical actin network, and pKO-αV,β1 cells developed both large FAs and small NAs with thick and thin stress fibres and a dense subcortical actin meshwork (Fig.1A, B; Fig.S1A). To visualize non-polymerized Actin in the cytoplasm of the three cell lines, we stained the cells with fluorescently labelled DNaseI (Gabbiani et al., 1984; Heacock and Bamburg, 1983; Hitchcock, 1980). Surprisingly, we observed that also the cytoplasmic g-Actin pool was highest in pKO-αV, intermediate in pKO-β1 and lowest in pKO-αV,β1 cells (Fig.1A, 1C). This finding was further confirmed by separating the cells into soluble (S, validated with GAPDH), nuclear (N) and cytoskeletal (C, validated with Vimentin) fractions and determining their β-Actin contents (Fig.1D). The experiment demonstrated that Actin contents in the soluble (representing g-Actin), cytoskeletal (representing f-Actin) and nuclear fraction as well as the calculated g-/f-Actin ratios were significantly higher in pKO-αV cells compared to pKO-β1 and pKO-αV,β1 cells (Fig.1D-F). The increased Actin contents in all fractions of pKO-αV cells indicated that the total Actin levels are higher in pKO-αV cells compared to pKO-β1 and pKO-αV,β1 cells, which was indeed confirmed by western blotting and immunostaining of cells with anti-β-Actin antibodies (Fig.S1B). To precisely determine the g-Actin levels in cytoplasm and nucleus, we performed precipitation assays with soluble and nuclear fractions using DNaseI coupled to beads and found significantly higher g-Actin contents in the cytoplasm and nucleus of pKO-αV compared to pKO-β1 and pKO-αV,β1 cells (Fig.1G, H). FACS analysis excluded differences in nuclear size in our cell lines as cause for the different actin contents (Fig.S1C).

Next we consulted our published whole cell proteome and phospho-proteome of pKO-αV, pKO-β1 and pKO-αV,β1 cells (Schiller et al., 2013) to evaluate whether a differential expression and activity of Actin sequestering, polymerizing and depolymerizing proteins either further aggravates or compensates for the different amounts of free g-Actin. Our analysis revealed significantly increased levels of Thymosin β4 (Tβ4) and phosphoSer3-Cofilin in pKO-β1 cells (Fig. S1D-F) indicating that g-Actin is significantly more

sequestered and f-Actin significantly less severed in pKO-β1 and pKO-αV,β1 cells compared to pKO-αV cells.

The pool of g-Actin regulates nuclear translocation and activity of the transcriptional transactivator MAL, whose binding to the transcription factor SRF induces the expression of genes encoding "immediate-early", cytoskeletal and focal adhesion proteins. Therefore, the different free g-Actin levels in pKO-αV, pKO-β1 and pKO-αV,β1 cells suggested that their nuclear MAL levels should also be different. To test this hypothesis, we seeded the three cell lines on FN and immunostained them with specific rabbit polyclonal anti-MAL antibodies. The results revealed lowest nuclear MAL levels in pKO-αV, intermediate in pKO-β1 and highest in pKO-αV,β1 cells (Fig.1I, S1G). Importantly, treatment with Jasplankinolide, which diminishes free g-Actin by stabilizing Actin filaments, increased nuclear MAL in the three cell lines (Fig.1I, S1G). Conversely, treatment with Latrunculin A, which increases free g-Actin by disassembling f-Actin, decreased nuclear MAL in the three cell lines (Fig.1I, S1G). Altogether these results show that FN-binding integrin classes differentially regulate cellular g-/f-Actin content, which significantly influences nuclear levels of MAL.

αV- and β1-class integrins cooperate to control SRF/MAL activity

To test functional consequences of the different nuclear MAL contents in the three cell lines, we first measured SRF/MAL activity with SRF luciferase reporter assays. Whereas pKO-αV cells showed low SRF reporter activity, pKO-β1 cells displayed 4-fold higher and pKO-αV,β1 cells ~10 fold higher SRF reporter activities. Importantly, Jasplankinolide treatment increased SRF activities to a similar extent in all three cell lines, while Latrunculin A (which had to be short due to cell lethality) showed as light opposite effect (Fig.2A). Treatment with serum (to induce nuclear translocation of MAL) or Leptomycine B (to inhibit nuclear export of MAL) increased SRF reporter activities in pKO-β1 and pKO-αV,β1 cells to a much higher extent as compared to pKO-αV cells (Fig.S2A, S2B). Expression of a dominant-negative MAL reduced SRF reporter activity to basal levels in the three cell lines (Fig.S2C), while overexpression of a g-Actin binding-deficient MAL (ΔN MAL, lacking the N-terminal G-actin binding motif) and a constitutive active mDia increased SRF/MAL induced luciferase activities to similar extents in the three cells (Fig.2B).

To exclude that cell spreading defects (Connelly et al., 2010) caused the reduced nuclear MAL levels and SRF/MAL reporter activities in pKO-αV cells, we seeded the three cell lines on FN-coated circular micropatterns with 28μm and 40μm diameters, respectively, and performed SRF reporter assays and immunostainings. The results of these experiments revealed that pKO-αV cells displayed similar SRF reporter activities and nuclear MAL levels on small and large FN-coated circular micropatterns, while

pKO-β1 and pKO-αV,β1 cells increased SRF activities and nuclear MAL levels on 40µm sized micropatterns compared to 28µm sized micropatterns (Fig.2C-E) indicating that the reduced cell spreading of pKO-αV cells is not responsible for the reduced MAL/SRF activity.

Next we performed experiments aimed at testing whether changes in the expression levels and/or activities of FN-binding integrin classes affect SRF reporter activity. First, Mn^{2+} treatment, which increases integrin activities, significantly elevated SRF reporter activity in all three cell lines, most prominently in pKO-β1 cells, intermediate in pKO-αV,β1 and lowest in pKO-αV cells (Fig.2F). Second, overexpression of αV- or β1-class integrins revealed that elevation of αV in pKO-αV did not change SRF activity, whereas elevation of β1 in pKO-β1 cells induced a small, significant increase of SRF activity and elevation of β1 in pKO-αV and αV in pKO-β1 cells induced a more prominent increase of SRF activity (Fig.2G). Similarly, overexpression of either αV or β1 in pKO-αV,β1 cells also significantly increased SRF/MAL activity. Third, pKO-αV,β1 cells were seeded on FN (bound by αV- and β1-class integrins), Vitronectin (VN) and Gelatin (both ligands bound by αV-class integrins only), treated with either anti-α5β1 blocking antibodies or the αV-class specific small molecule inhibitor cilengitide and immunostained for MAL and assayed for SRF reporter activity (Fig.2H, 2I). The experiments showed that inhibition of α5β1 or αVβ3 Integrins on FN adherent pKO-αV,β1 cells significantly reduced nuclear MAL levels and SRF activities and hence phenocopied the pKO-αV cells indicating efficient activation of SRF requires the cooperation of both FN-binding integrin classes. Similarly, when pKO-αV,β1 cells were seeded on VN and Gelatin, respectively, they showed low nuclear MAL activity, which was not further decreased with the inhibition of α5β1 integrin. As expected, treatment of VN- or Gelatin-seeded pKO-αV,β1 cells with cilengitide blocked adhesion (Fig.2H). Finally, loss of the integrin activator proteins in FN-adherent fibroblasts double deficient for either Kindlin-1 and -2 or Talin-1 and -2 abolished SRF reporter activities (Fig.S2D). Altogether these results show that FN-binding integrin classes cooperate to activate SRF/MAL.

αV- and β1-class integrins induce transcription of SRF/MAL target genes

The high nuclear MAL content and SRF activity in pKO-αV,β1 cells suggest that MAL/SRF-induced gene transcription is controlled, at least in part, by integrins. To test this hypothesis, we compared published MAL/SRF transcriptomes (Balza and Misra, 2006; Cooper et al., 2007; Descot et al., 2009; Philippar et al., 2004; Selvaraj and Prywes, 2004; Sun et al., 2006; Zhang et al., 2005) with the whole cell proteome of pKO-αV, pKO-β1 and pKO-αV,β1 cells (Schiller et al., 2013) and found a large number of MAL/SRF target genes including SRF and FA proteins such as Filamins, Vinculin, Talin, Eplin and integrins enriched in pKO-β1 and pKO-αV,β1 cells (Table 1). The increased levels of SRF, Talin, Vinculin and Eplin (Lima1) mRNA

and protein in pKO-β1 and pKO-αV,β1 cells were confirmed by qRT-PCR and western blotting (Fig.3A, 3B).

We also noted that ISG15 mRNA, dramatically down-regulated in SRF-deficient ES cells (Philippar et al., 2004), was significantly elevated in pKO-αV,β1, intermediate in pKO-β1 cells and low in pKO-αV cells (Fig.3A; Table 1). Western blotting confirmed high ISG15 levels in pKO-αV,β1, intermediate levels in pKO-β1 and low levels in pKO-αV cells but no secretion of ISG15 (Fig.3C, S3F). Similar results were obtained with immunostainings, which revealed ISG15 co-localisation with f-Actin fibres and the Actin cortex beneath membrane protrusions (Fig.3D) and with Paxillin in FAs of unroofed cells (Fig.3E). ISG15 is an ubiquitin-like modifier, whose expression is induced by type I (α and β) interferons (Farrell et al., 1979; Haas et al., 1987). ELISA and qRT-PCR excluded endogenous interferon α and β expression in pKO-αV,β1 cells as cause for the high ISG15 levels. Importantly, however, poly I:C treatment, which triggers endogenous interferon α and β expression, induced a strong ISG15 expression (Fig.S3A-E). To directly show that ISG15 and the FA protein Talin are new SRF/MAL target genes, we performed SRF and MAL chromatin-immunoprecipitation (CHIP) assays. SRF CHIPseq experiments performed in murine HL-1 cells (http://deepbase.sysu.edu.cn/index.php) identified potential SRF consensus binding sites (CArG box), which allowed designing primers to PCR amply the immunoprecipitaed DNA fragments (Fig.3F). The *vinculin* gene, as a known MAL/SRF target, and the *gapdh* gene not regulated by MAL/SRF were used as controls (Vartiainen et al., 2007) (Fig.3G, 3H). Immunoprecipitations of chromatin using either MAL or SRF antibodies resulted in a positive CHIP. In contrast, neither precipitation control rabbit IgG nor the *gapdh* gene resulted in a positive signal (Fig.3G, 3H).

ISG15 is an ubiquitin-like modifier, which might compete with Ubiquitin at specific lysine residues and hence stabilize target proteins, modify the Ubiquitin E2 enzyme Ubc13 and Nedd4 leading to its inhibition, and alter the function of proteins by inducing or preventing the recruitment of binding partners (Jeon et al., 2009; Malakhova and Zhang, 2008; Takeuchi et al., 2005; Zou et al., 2005). Since protein levels of Talin and Eplin are higher in pKO-αV,β1 cells than predicted from their mRNA levels (Fig. 3A, 3B), we hypothesized that they might be modified with ISG15 and protected from degradation. To test this hypothesis we precipitated ISGylated proteins in pKO-αV,β1 cells with an ISG15-specific antibody and subsequently analysed them by mass spectrometry (Table S1). This analysis revealed a large number of focal adhesion and cytoskeletal proteins including Talin and Vinculin. These findings indicate that αV-class and α5β1 integrin-mediated SRF/MAL activation triggers the expression of SRF/MAL targets that include cytoskeletal proteins, integrins, focal adhesion proteins and ISG15, which modifies SRF/MAL targets to stabilize them and/or change their activity.

αV- and β1-class integrin induced SRF/MAL activity and ISG15 levels to promote cell invasion

MAL/SRF and ISG15 promote tumour cell invasion and are up-regulated in cancer (Desai et al., 2012; Kressner et al., 2013). To test whether the invasive properties of MAL and ISG15 are associated and triggered by β1 integrin-mediated adhesion we analysed integrin, nuclear MAL and ISG15 levels of the non-invasive MCF-7 and invasive MDA-MB-231 breast cancer cell lines. FACS analysis revealed significantly higher α5 and β1 levels and higher Integrin β1 activity (by probing 9EG7 antibody) on MDA-MB-231 cells compared to MCF-7 cells (Fig.4A). The levels of αV integrin were significantly elevated in MCF-7 cells compared to MDA-MB-231 cells (Fig.4A). To test whether the high β1 integrin levels and activity are associated with high nuclear MAL activity in MDA-MB-231 cells we immunostained for f-Actin and MAL, and investigated MAL/SRF activities. We observed that MCF7 cells formed tight cell-cell contacts with f-Actin accumulating at these sites and contained MAL in the cytoplasm and nucleus. In contrast, MDA-MB-231 were not adhering to each other, contained numerous stress fibres and almost the entire pool of MAL protein in the nucleus (Fig.4B, 4C). In line with high nuclear MAL levels, MDA-MB-231 cells also displayed significantly higher SRF/MAL reporter activity (Fig.4D) expressed significantly higher levels of SRF/MAL target gene transcript levels (Fig.4E). The high levels of ISG15 resulted in an elevated ISGylation of target proteins in MDA-MB-231 compared to MCF-7 cells (Fig.4F).

The invasive properties of MDA-MB-231 cells depend on the expression of MAL (Hu et al., 2011; Medjkane et al., 2009). To test whether ISG15 is required for SRF/MAL-induced cell invasion, we depleted ISG15 or overexpressed the de-ISGylase UBP43 in MCF-7 and MDA-MB-231 cells and performed invasion assays with a basement membrane model (Fig.4G, H). While MCF-7 cells were unable to invade through the basement membrane model, MDA-MB-231 cells efficiently moved through the membrane. siRNA-mediated depletion of ISG15 or overexpression of the de-ISGylase UBP43 almost completely prevented the invasion of MDA-MB-231 cells (Fig.4G, H).

Next we tested whether high β1 integrin and ISG15 levels are prognostic markers for breast cancer patients. To this end, we consulted microarray data of breast cancer samples and correlated αV, β1 integrins and ISG15 transcript levels with patient survival. The analyses revealed that patients with high expression of αV, β1 integrin or ISG15 displayed a significant increase in the hazardous ratio (HR) and p-value compared to patients with low levels of either transcript (Fig.5A, 5B). Interestingly, patients with high levels of αV, β1 integrin and ISG15 transcripts in their cancer specimen show a significantly reduced survival rate compared to patients with low ISG15 levels (Fig.5C). To corroborate these *in silico* findings, we performed MAL and β1 integrin immunostainings of human breast cancer samples classified according to the Bloom-Richardson scale and modified by Elston and Ellis (1991) as grade 1 (G1), grade 2

(G2), and grade 3 (G3). Hereby the grading system involves a semi-quantitative evaluation of three morphological features a) the percentage of tubule formation, b) the degree of nuclear pleomorphism and c) an accurate mitotic count using a defined field area. By the usage of a numerical scoring system, the overall grade is derived from a summation of individual scores for the three grades (Elston and Ellis, 1991). (Fig.5D, 5E). Importantly to note, these patient biopsies also include normal healthy tissue next to pathologic malformations. In line with our findings, the overall expression of β1 integrin and nuclear MAL levels increased concomitantly from G1 to G2 and to G3 stage (Fig.5D, 5E, S5). Altogether our data show that integrin-mediated MAL/SRF/ISG15 signaling is elevated in cancer cell invasion *in vitro* and *in vivo.*

DISCUSSION

Tumour metastasis is initiated with the detachment of an individual tumour cell from a tumour cell aggregate followed by invasion into the surrounding tissue, entry into the circulation and finally settlement in a distant organ. The process of tumour cell invasion is critically dependent on the selection of tumour cells that are able to survive without tumour stroma, on the release of proteases that degrade and remodel the tumour- and tissue-derived ECM, and on cell adhesion molecules such as integrins (Hood and Cheresh, 2002). Integrins constitute the core components of the invasive machinery of tumour cells. They regulate the activity of small GTPases, Actin binding, bundling and modifying proteins to allow for cytoskeletal dynamics, membrane protrusions and invadopodia formation (Bishop and Hall, 2000; Hall, 2012; Hoshino et al., 2013; Murphy and Courtneidge, 2011). Since tumour cells express different types of integrins, it is unclear whether, and if yes, how they co-operate to achieve maximal efficiency in tissue invasion. The task of the present study was to define the integrin subfamily and the signalling pathways involved in tumour cell invasion.

We have recently engineered a fibroblast-like cell line that allows expressing the FN-binding integrin αVβ3 and/or α5β1. These cell lines were used to demonstrate that αVβ3 and α5β1 integrins control actomyosin-based cell contractility in a cooperative manner. In the present study we also observed that cells expressing αVβ3 and α5β1 integrins (pKO-αV,β1 cells) most pronouncedly decrease their g-Actin pool, which results in the nuclear translocation of the g-Actin binding transcriptional transactivator MAL (also referred as MRTF-A). The consequences of the nuclear accumulation of MAL include binding to the transcription factor SRF and the transcription of MAL/SRF target genes, which comprise known genes such as Actin, Vinculin, Filamin, etc, as well as novel genes such as Talin, EPLIN and ISG15, which all contain functional CArG boxes that bind SRF and are required for responding to the active MAL/SRF complex.

Our findings show that ISG15 is particularly highly elevated when αVβ3 and α5β1 bind FN. ISG15 is a ubiquitin like modifier protein and thought to be induced exquisitely by type I interferons (Farrell et al., 1979; Haas et al., 1987). ISG15 is highly expressed in all tumours investigated so far (www.oncomine.org). Since the tumour stroma is infiltrated by immune cells it is believed that they are the source of interferon α/β production and hence the trigger for the high expression of ISG15 in cancer cells (van der Veen and Ploegh, 2012). While immune cell-derived interferon α/β strongly promotes expression of ISG15 in tumours it is unknown why ISG15 remains upregulated in tumour cells isolated

and cultured *ex vivo* in the absence of immune cells and interferon α/β (Han et al., 2002; Hermeking et al., 1997; Lock et al., 2002). Based on our findings we propose that αVβ3/α5β1-induced nuclear translocation of MAL and activation of SRF are responsible for the high ISG15 transcription *ex vivo*.

ISG15 is conjugated to proteins (ISGylation) in a multistep process that requires E1, E2 and E3 enzymes comparable to the protein-ubiquitination pathway (Haas et al., 1987; Lenschow et al., 2005; Loeb and Haas, 1992; Morales and Lenschow, 2013; Okumura et al., 2008; Yuan and Krug, 2001). Furthermore, a protease called Ubp43 removes ISG15 resulting in deISGylation of proteins (Malakhov et al., 2002). Protein ISG15lyation can alter protein function. Rac1 and MAPK, for example, dissociate from ISG15-modified Filamin-B. This dissociation can terminate JNK signalling and inhibit apoptosis (Jeon et al., 2009). It has also been shown that ISG15 modification can stabilize proteins either by ISGylation and inhibition of ubiquititn-specific E2 enzymes (Desai et al., 2006; Malakhova and Zhang, 2008; Okumura et al., 2008) or by competing with free ubiquitin for lysine residues on target proteins (Liu et al., 2003). Finally, ISGylation was shown to inhibit protein translation by either increasing the cap structure-binding activity of the ISGylated translational suppressor 4EHP (Okumura et al., 2007) or by down-regulating eIF2α through ISGylation of dsRNA-dependent protein kinase (PKR) (Okumura et al., 2013).

The expression of ISG15 is high in tumour cells *in vivo* and *ex vivo* indicating that ISG15 modification represents a tumour promoting and oncogenic function in primary tumours where interferon α/β levels are high as well as during and after invasion when interferon levels decrease. Hence, it is conceivable that αVβ3/α5β1 signalling kicks in to compensate low interferon levels and to sustain high ISG15 expression. Our mass-spectrometry analysis of ISG15 modified protein (ISGylome) in pKO-αV,β1 cells revealed that numerous proteins including integrins, FA proteins (Talin, Vinculin, EPLIN, etc.) and Actin become ISGylated upon FN binding. We therefore, propose that αVβ3/α5β1 integrin-mediated signalling has two major consequences for tumour cell invasion; αVβ3/α5β1 integrins activate GTPases leading to polymerization of f-Actin networks and stress fibers, which are essential for membrane protrusions, cell contractility and adhesion reinforcement. In addition, the consumption of g-Actin for the f-Actin network formation results in liberation and nuclear translocation of MAL, binding to SRF and transcription of cytoskeletal, FA proteins and ISG15. ISG15 modifies integrins, FA proteins and Actin to increase their stability and/or improve their function (Fig. 6). This novel feed forward loop operates in fibroblasts as well as in invading cancer cells. The highly metastatic breast cancer cell line MDA-MB-231 expressed significantly more α5β1, contained higher levels of nuclear MAL and ISG15 modified proteins, and performed significantly better in invasion assays than the non-metastatic MCF7 cell line. Most

importantly, transcriptome analyses of breast cancer samples from large cohorts of patients revealed a statistically highly significant association between patient survival and high β1 integrin, MAL and ISG15 levels. These findings indicate that the selection of tumour cells for high integrin levels in a tumour aggregate renders them independent of decreasing interferon and growth factor levels. This independence is facilitated with an increased strength of integrin signalling, which has the principal task in a metastasizing tumour cells to establish and maintain an efficient invasive machinery that compensates essential cues from the tumour stroma and eventually allows a long and harshly journey to distant and extraneous organ to succeed.

EXPERIMENTAL PROCEDURES

Isolation, immortalization, viral reconstitution and transfection of cell lines.

Mouse pKO fibroblasts and reconstituted pKO-αV, pKO- β1 and pKO-αV,β1 cell lines were generated from fibroblasts (floxed parental) derived from the kidney of 21-day-old male mice carrying floxed αV and β1 alleles (αV flox/flox, β1flox/flox), and constitutive β2 and β7 null alleles (β2−/−, β7−/−). Individual kidney fibroblast clones were immortalized by retroviral delivery of the SV40 large T. The immortalized floxed fibroblast clones were then retrovirally transduced with mouse αV and/or β1 integrin cDNAs and the endogenous floxed β1 and αV integrin loci were simultaneously deleted by adenoviral transduction of the Cre recombinase. Reconstituted cell lines were FACS sorted to obtain cell populations with comparable integrin surface levels to the parental cell clones(Schiller et al., 2013) or to have high or low integrin expression levels. Fibroblasts homozygous for floxed kindlin-1 and -2 or talin-1 or -2 genes were isolated from kidneys of 21-day-old double-floxed mice (whose generation will be described elsewhere), immortalized as described above and cloned. To obtain Kindlin-1 and -2 double-null or Talin-1 and -2 double-null cells, the floxed kindlin alleles were removed by adenoviral Cre transduction. The breast cancer cell lines MDA-MB-231 and MCF-7 were purchased from ATCC (http://www.lgcstandards-atcc.org/Products/Cells_and_Microorganisms/Cell_Lines.aspx?geo_country=de).

Patient samples/biopsies

For histological and immunostaining analysis, staged human breast cancer samples were kindly provided by Prof. Ferdinand Hofstädter, Institute of Pathology, 93053 Regensburg, Germany.

Immunostainings and surface coating

For immunofluorescence microscopy, cells were seeded on micropatterns or coated glass surfaces (Coating: 5 µg/ml Fibronectin (Calbiochem) or 1% Gelatin (Sigma) or 1% Collagen (Advanced BioMatrix) or 10 µg/ml Laminin (Roche) or 10 µg/ml Vitronectin (STEMCELL technologies) in PBS or 0.01% Poly-L-lysine (Sigma)) in DMEM (GIBCO by Life Technologies) containing 10 % FCS at 37 °C, 5% CO_2. For micropatterns the cell culture medium contained 0.5% FCS. After indicated time points the medium was soaked off, and cells were fixed with 3% PFA in PBS for 10 min at room temperature, washed with PBS, blocked with 1% BSA in PBS for 1 h at room temperature and then incubated with antibodies in a solution of 0.1% Triton X-100, 3% BSA in PBS. The fluorescent images were collected with a laser scanning confocal microscope (Leica SP5). For visualization g- and f-Actin structures, we followed a protocol published earlier (Small et al., 1999). H&E staining was performed according to standard procedures.

Antibodies

All antibodies are listed in Supplementary Information Table S2.

Crosslinking

Enrichment for focal-adhesion-associated proteins was achieved by shortly fixing the ventral cell cortex using DSP crosslinker (DTSP; Dithiobis[succinimidyl propionate]), followed by removal of non-crosslinked proteins and big organelles by stringent cell lysis and hydrodynamic sheer flow washing.

Cell fractionation

For cell fractionation a kit (ProteoExtract® Cytoskeleton Enrichment and Isolation Kit purchased from Millipore) was used according to the manufacturer´s instructions or a centrifugation-based method. For the centrifugation-based method to isolate the nuclei, cells were washed with PBS and harvest in a buffer containing 250 mM Sucrose, 10 mM HEPES and 1.5 mM EDTA. With the help of a syringe and a 26Ga needle (Terumo) cells were opened further. After centrifugation the pellet (nuclei fraction) was washed 5 times with a buffer containing 20 mM Tris, 0.1 mM EDTA and 2 mM $MgCl_2$. The pellet was resuspended in FACS buffer or staining solution for immunostaining.

G-Actin-DNaseI pulldown

DNaseI (Sigma-Aldrich) was covalently linked to CNBr-activated Sepharose beads (Sigma-Aldrich) at a concentration of 1 mg/ml according to the manufacturer´s protocol. BSA-Sepharose beads, which served as control, were prepared in the same way. For g-Actin pulldown 15µg protein lysate in RIPA buffer was incubated with 35µl of DNaseI- or BSA-coupled Sepharose beads in a volume of 300 µl over night at 4°C in an end-over-end-mixer. Next day, the beads were washed five times with cold wash buffer (1% NP-40, 0.1 % SDS, 1mM DTT, 1mM PMSF in PBS). Beads were dried with a syringe and needle and SDS-sample buffer was added for subsequent western blot analysis.

Constructs and transfections

Constitutive active MAL (ΔNMAL), dominant negative MAL (DN MAL: ΔN1B1 and ΔNΔC), SRF:MAL reporter constructs were provided by Prof. Guido Posern, Institute of Physiological Chemistry, 06114 Halle, Germany. Constitutive active myc-mDia1 construct (myc-mDia1 FH1FH2) expression construct was amplified from an existing plasmid with forward primer 5'-gcc aag aat gaa atg gct tc-3' and reverse 5'-tgc

aga gct tct aga aga ct and the PCR product was cloned into the pCRII-TOPO vector and sequenced. The integrin αV-mCherry and integrin β1-mCherry were provided by Ralph Böttcher. The knockdown constructs for stable knockdown of murine ISG15 were purchased from Origene and the UBP43 overexpression construct was purchased from Addgene. All transfections were carried out with Lipofectamine 2000 (Invitrogen through Life Technologies) according to the manufacturer's instructions.

SRF/MAL reporter assay

Cells were plated on FN coated 12-well plates (6.0 x 105 cells per well) before transient transfection with 0.5 µg of MAL/SRF reporter (p3DA.luc) reporter (Sotiropoulos et al., 1999), indicated expression plasmid and 25 ng thymidine kinase-driven renilla (Promega) for controlling transfection efficiency. The total amount of transfected plasmid DNA was kept constant at 1.5 µg per well by using pEGFP-C1 expression vector (Clontech). After 24h luciferase activity was analyzed with a Dual Luciferase reporter assay system (Promega). Jasplankinolide (100 nM, #420107-50UG from Merck Millipore) and Latrunculin A (500 nM, L5163 from Sigma) treatment was performed 3h prior to reporter read-out.

Micropatterning

Micropatterns were generated on PEG-coated glass coverslips with deep-ultraviolet lithography(Azioune et al., 2010). Glass coverslips were incubated in a 1 mM solution of a linear PEG, CH3–(O–CH2–CH2)43–NH–CO–NH–CH2–CH2–CH2–Si(OEt)3 in dry toluene for 20 h at 80 °C under a nitrogen atmosphere. The substrates were removed, rinsed intensively with ethyl acetate, methanol and water, and dried with nitrogen. A pegylated glass coverslip and a chromium-coated quartz photomask (ML&C, Jena) were immobilized with vacuum onto a mask holder, which was immediately exposed to deep ultraviolet light using a low-pressure mercury lamp (NIQ 60/35 XL longlife lamp, quartz tube, 60 W from Heraeus Noblelight) at 5 cm distance for 7 min. The patterned substrates were subsequently incubated overnight with 100 µl of fibronectin (20 µg ml−1 in PBS) at 4 °C and washed once with PBS.

FACS analysis

For FACS analysis s suspension of fibroblasts was incubated for 1 h with primary antibodies on ice and then washed twice with FACS-PBS (3 mM EDTA, 2% FCS in PBS). Cell viability was assessed by propidium iodide staining. FACS analysis was carried out using a FACSCalibur Cytometer (BD Biosciences) and cell sorting with an AriaFACSII high-speed sorter (BD Biosciences), both equipped with FACS DiVa software

(BD Biosciences). Purity of sorted cells was determined by post sort FACS analysis and typically exceeded 95%. Data analysis was conducted using the FlowJo program (Version 9.4.10).

Real-time PCR

Total RNA from cells was extracted with RNeasy Mini extraction kit (Qiagen) following manufacturer's instructions. cDNA was prepared with a iScript cDNA Synthesis Kit (Biorad). Real Time PCR was performed with an iCycler (Biorad). Each sample was measured in triplicates and values were normalized to *gapdh.* PCR primers are listed in Supplementary Information Table S1.

Mass spectrometry

The mass spectrometry was performed and analyzed as previously described (Schiller et al., 2013). For the investigation of ISG15 target proteins, a Flag-murineISG15 construct was used for overexpression followed by a FLAG pulldown by using ANTI-FLAG® M2 Affinity Gel according to manufacturer´s instructions (Sigma, product #A2220), SDS PAGE gel electrophoresis and subsequent treatment for mass spectrometry analysis.

Interferon ELISA

Cells were plated on FN-coated tissue culture dishes for three days and the cells` supernatant was analyzed. To induce interferon production cells were transfected with 100 µg/ml Poly(I:C). ELISA for interferon α and interferon β secretion was performed with the VeriKine™ Mouse IFN-α and Mouse IFN-β ELISA kit (PBL Interferon Source, product #42120 and #42400) according to manufacturer´s instructions.

Invasion assay

Invasion assay was purchased (Merck Millipore's QCM™ Boyden chamber, 8 µm pore size) and performed according to manufacturer´s instructions 24 hours post-transfection with either shScr control, shISG15 or UBP43 constructs.

CHIP

For each immunoprecipitation, pKO-αV,β1 cells were used. Cross-linking, nuclei preparation and nuclease digestion of chromatin was performed according to manufacturer`s advice (SimpleCHIP Enzymatic Chromatin IP Kit (Magnetic Beads, #9003, Cell Signaling Technology). Then, 500 ml of

chromatin was incubated overnight at 4°C with 1 to 50 dilution of anti-SRF (#5147; Cell Signaling Technology) or 30 µl home-made anti-MAL rabbit serum (#79). After washing of the Immunoprecipitated chromatin, the DNA– protein complexes were eluted with supplied CHIP elution buffer. Crosslinks were reversed overnight at 65°C, and DNA purified via columns also provided in the kit. Quantification was done by quantitative real-time PCR and is shown as the percentage of input chromatin. Gene-specific primers for amplification of immunoprecipitated DNA are listed in supplementary material Table S3. Primers for *Gapdh* and *Srf* were published previously (Vartiainen et al., 2007).

RNA interference

Cells were infected with retroviral 29mer shISG15 expression constructs purchased from Origene (#TG502956). The pGFP-V-RS plasmid vector was created with an integrated turboGFP element to readily verify transfection efficiency and with a puromycine selection cassette to select for cells carrying integrations.

Kaplan Meier analysis of gene expression microarray

To analyze the prognostic value of integrin αV, integrin β1 and ISG15 gene the Kaplan-Meier plotter was used (http://kmplot.com/analysis/). The patient samples were split into two groups according to various quantile expressions of the proposed biomarker (low and high expression). The two patient cohorts were compared by a Kaplan-Meier survival plot, and the hazard ratio with 95% confidence intervals and logrank P value were calculated.

ACKNOWLEDGEMENTS

We thank the ERC, DFG and the Max Planck Society for financial support and Dr. Julien Polleux (our group) for material and excellent discussions. M.-R. H. was a fellow of the Boehringer Ingelheim Fonds.

AUTHOR CONTRIBUTIONS

RF and MRH designed the experiments and wrote the paper; MRH, ER, MJ, MW performed experiments; MRH, ER, MJ, MW, AY analyzed data; GP, FH, and BH provided important reagents and/or analytical tools;

All authors read and approved the manuscript.

REFERENCES

Andersen, J. B., Aaboe, M., Borden, E. C., Goloubeva, O. G., Hassel, B. A., and Orntoft, T. F. (2006). Stage-associated overexpression of the ubiquitin-like protein, ISG15, in bladder cancer. British journal of cancer *94*, 1465-1471.

Azioune, A., Carpi, N., Tseng, Q., Thery, M., and Piel, M. (2010). Protein micropatterns: A direct printing protocol using deep UVs. Methods in cell biology *97*, 133-146.

Balza, R. O., Jr., and Misra, R. P. (2006). Role of the serum response factor in regulating contractile apparatus gene expression and sarcomeric integrity in cardiomyocytes. The Journal of biological chemistry *281*, 6498-6510.

Bektas, N., Noetzel, E., Veeck, J., Press, M. F., Kristiansen, G., Naami, A., Hartmann, A., Dimmler, A., Beckmann, M. W., Knuchel, R.*, et al.* (2008). The ubiquitin-like molecule interferon-stimulated gene 15 (ISG15) is a potential prognostic marker in human breast cancer. Breast cancer research : BCR *10*, R58.

Brandt, D. T., Baarlink, C., Kitzing, T. M., Kremmer, E., Ivaska, J., Nollau, P., and Grosse, R. (2009). SCAI acts as a suppressor of cancer cell invasion through the transcriptional control of beta1-integrin. Nat Cell Biol *11*, 557-568.

Brooks, P. C., Clark, R. A., and Cheresh, D. A. (1994). Requirement of vascular integrin alpha v beta 3 for angiogenesis. Science *264*, 569-571.

Connelly, J. T., Gautrot, J. E., Trappmann, B., Tan, D. W., Donati, G., Huck, W. T., and Watt, F. M. (2010). Actin and serum response factor transduce physical cues from the microenvironment to regulate epidermal stem cell fate decisions. Nat Cell Biol *12*, 711-718.

Cooper, S. J., Trinklein, N. D., Nguyen, L., and Myers, R. M. (2007). Serum response factor binding sites differ in three human cell types. Genome research *17*, 136-144.

Danen, E. H., Sonneveld, P., Brakebusch, C., Fassler, R., and Sonnenberg, A. (2002). The fibronectin-binding integrins alpha5beta1 and alphavbeta3 differentially modulate RhoA-GTP loading, organization of cell matrix adhesions, and fibronectin fibrillogenesis. Journal of Cell Biology *159*, 1071-1086.

Desai, S. D., Haas, A. L., Wood, L. M., Tsai, Y. C., Pestka, S., Rubin, E. H., Saleem, A., Nur, E. K. A., and Liu, L. F. (2006). Elevated expression of ISG15 in tumor cells interferes with the ubiquitin/26S proteasome pathway. Cancer research *66*, 921-928.

Desai, S. D., Reed, R. E., Burks, J., Wood, L. M., Pullikuth, A. K., Haas, A. L., Liu, L. F., Breslin, J. W., Meiners, S., and Sankar, S. (2012). ISG15 disrupts cytoskeletal architecture and promotes motility in human breast cancer cells. Experimental biology and medicine *237*, 38-49.

Desai, S. D., Wood, L. M., Tsai, Y. C., Hsieh, T. S., Marks, J. R., Scott, G. L., Giovanella, B. C., and Liu, L. F. (2008). ISG15 as a novel tumor biomarker for drug sensitivity. Molecular cancer therapeutics *7*, 1430-1439.

Descot, A., Hoffmann, R., Shaposhnikov, D., Reschke, M., Ullrich, A., and Posern, G. (2009). Negative regulation of the EGFR-MAPK cascade by actin-MAL-mediated Mig6/Errfi-1 induction. Molecular cell *35*, 291-304.

Eduardo-Correia, B., Martinez-Romero, C., Garcia-Sastre, A., and Guerra, S. (2014). ISG15 is counteracted by vaccinia virus E3 protein and controls the proinflammatory response against viral infection. Journal of virology *88*, 2312-2318.

Elston, C. W., and Ellis, I. O. (1991). Pathological prognostic factors in breast cancer. I. The value of histological grade in breast cancer: experience from a large study with long-term follow-up. Histopathology *19*, 403-410.

Farrell, P. J., Broeze, R. J., and Lengyel, P. (1979). Accumulation of an mRNA and protein in interferon-treated Ehrlich ascites tumour cells. Nature *279*, 523-525.

Frisch, S. M., Vuori, K., Ruoslahti, E., and Chan-Hui, P. Y. (1996). Control of adhesion-dependent cell survival by focal adhesion kinase. The Journal of cell biology *134*, 793-799.
Gabbiani, G., Gabbiani, F., Heimark, R. L., and Schwartz, S. M. (1984). Organization of actin cytoskeleton during early endothelial regeneration in vitro. Journal of cell science *66*, 39-50.
Haas, A. L., Ahrens, P., Bright, P. M., and Ankel, H. (1987). Interferon induces a 15-kilodalton protein exhibiting marked homology to ubiquitin. The Journal of biological chemistry *262*, 11315-11323.
Han, S. Y., Kim, S. H., and Heasley, L. E. (2002). Differential gene regulation by specific gain-of-function JNK1 proteins expressed in Swiss 3T3 fibroblasts. The Journal of biological chemistry *277*, 47167-47174.
Heacock, C. S., and Bamburg, J. R. (1983). The quantitation of G- and F-actin in cultured cells. Analytical biochemistry *135*, 22-36.
Hermeking, H., Lengauer, C., Polyak, K., He, T. C., Zhang, L., Thiagalingam, S., Kinzler, K. W., and Vogelstein, B. (1997). 14-3-3 sigma is a p53-regulated inhibitor of G2/M progression. Molecular cell *1*, 3-11.
Hitchcock, S. E. (1980). Actin deoxyroboncuclease I interaction. Depolymerization and nucleotide exchange. The Journal of biological chemistry *255*, 5668-5673.
Hood, J. D., and Cheresh, D. A. (2002). Role of integrins in cell invasion and migration. Nature reviews Cancer *2*, 91-100.
Hu, Q., Guo, C., Li, Y., Aronow, B. J., and Zhang, J. (2011). LMO7 mediates cell-specific activation of the Rho-myocardin-related transcription factor-serum response factor pathway and plays an important role in breast cancer cell migration. Mol Cell Biol *31*, 3223-3240.
Jeon, Y. J., Choi, J. S., Lee, J. Y., Yu, K. R., Kim, S. M., Ka, S. H., Oh, K. H., Kim, K. I., Zhang, D. E., Bang, O. S., and Chung, C. H. (2009). ISG15 modification of filamin B negatively regulates the type I interferon-induced JNK signalling pathway. EMBO Rep *10*, 374-380.
Kressner, C., Nollau, P., Grosse, R., and Brandt, D. T. (2013). Functional interaction of SCAI with the SWI/SNF complex for transcription and tumor cell invasion. PloS one *8*, e69947.
Lenschow, D. J., Giannakopoulos, N. V., Gunn, L. J., Johnston, C., O'Guin, A. K., Schmidt, R. E., Levine, B., and Virgin, H. W. t. (2005). Identification of interferon-stimulated gene 15 as an antiviral molecule during Sindbis virus infection in vivo. Journal of virology *79*, 13974-13983.
Liu, M., Li, X. L., and Hassel, B. A. (2003). Proteasomes modulate conjugation to the ubiquitin-like protein, ISG15. The Journal of biological chemistry *278*, 1594-1602.
Lock, C., Hermans, G., Pedotti, R., Brendolan, A., Schadt, E., Garren, H., Langer-Gould, A., Strober, S., Cannella, B., Allard, J*., et al.* (2002). Gene-microarray analysis of multiple sclerosis lesions yields new targets validated in autoimmune encephalomyelitis. Nature medicine *8*, 500-508.
Loeb, K. R., and Haas, A. L. (1992). The interferon-inducible 15-kDa ubiquitin homolog conjugates to intracellular proteins. The Journal of biological chemistry *267*, 7806-7813.
Luo, X. G., Zhang, C. L., Zhao, W. W., Liu, Z. P., Liu, L., Mu, A., Guo, S., Wang, N., Zhou, H., and Zhang, T. C. (2014). Histone methyltransferase SMYD3 promotes MRTF-A-mediated transactivation of MYL9 and migration of MCF-7 breast cancer cells. Cancer letters *344*, 129-137.
Ma, Z., Morris, S. W., Valentine, V., Li, M., Herbrick, J. A., Cui, X., Bouman, D., Li, Y., Mehta, P. K., Nizetic, D*., et al.* (2001). Fusion of two novel genes, RBM15 and MKL1, in the t(1;22)(p13;q13) of acute megakaryoblastic leukemia. Nature genetics *28*, 220-221.
Malakhova, O. A., and Zhang, D. E. (2008). ISG15 inhibits Nedd4 ubiquitin E3 activity and enhances the innate antiviral response. The Journal of biological chemistry *283*, 8783-8787.
Matter, M. L., and Ruoslahti, E. (2001). A signaling pathway from the alpha5beta1 and alpha(v)beta3 integrins that elevates bcl-2 transcription. The Journal of biological chemistry *276*, 27757-27763.
Medjkane, S., Perez-Sanchez, C., Gaggioli, C., Sahai, E., and Treisman, R. (2009). Myocardin-related transcription factors and SRF are required for cytoskeletal dynamics and experimental metastasis. Nat Cell Biol *11*, 257-268.

Mercher, T., Coniat, M. B., Monni, R., Mauchauffe, M., Nguyen Khac, F., Gressin, L., Mugneret, F., Leblanc, T., Dastugue, N., Berger, R., and Bernard, O. A. (2001). Involvement of a human gene related to the Drosophila spen gene in the recurrent t(1;22) translocation of acute megakaryocytic leukemia. Proceedings of the National Academy of Sciences of the United States of America *98*, 5776-5779.
Mizejewski, G. J. (1999). Role of integrins in cancer: survey of expression patterns. Proceedings of the Society for Experimental Biology and Medicine *222*, 124-138.
Morales, D. J., and Lenschow, D. J. (2013). The Antiviral Activities of ISG15. Journal of molecular biology *425*, 4995-5008.
Okumura, A., Pitha, P. M., and Harty, R. N. (2008). ISG15 inhibits Ebola VP40 VLP budding in an L-domain-dependent manner by blocking Nedd4 ligase activity. Proceedings of the National Academy of Sciences of the United States of America *105*, 3974-3979.
Okumura, F., Okumura, A. J., Uematsu, K., Hatakeyama, S., Zhang, D. E., and Kamura, T. (2013). Activation of double-stranded RNA-activated protein kinase (PKR) by interferon-stimulated gene 15 (ISG15) modification down-regulates protein translation. The Journal of biological chemistry *288*, 2839-2847.
Okumura, F., Zou, W., and Zhang, D. E. (2007). ISG15 modification of the eIF4E cognate 4EHP enhances cap structure-binding activity of 4EHP. Genes Dev *21*, 255-260.
Philippar, U., Schratt, G., Dieterich, C., Muller, J. M., Galgoczy, P., Engel, F. B., Keating, M. T., Gertler, F., Schule, R., Vingron, M., and Nordheim, A. (2004). The SRF target gene Fhl2 antagonizes RhoA/MAL-dependent activation of SRF. Molecular cell *16*, 867-880.
Raff, M. C. (1992). Social controls on cell survival and cell death. Nature *356*, 397-400.
Schiller, H. B., Hermann, M. R., Polleux, J., Vignaud, T., Zanivan, S., Friedel, C. C., Sun, Z., Raducanu, A., Gottschalk, K. E., Thery, M*., et al.* (2013). beta1- and alphav-class integrins cooperate to regulate myosin II during rigidity sensing of fibronectin-based microenvironments. Nat Cell Biol *15*, 625-636.
Selvaraj, A., and Prywes, R. (2004). Expression profiling of serum inducible genes identifies a subset of SRF target genes that are MKL dependent. BMC molecular biology *5*, 13.
Small, J., Rottner, K., Hahne, P., and Anderson, K. I. (1999). Visualising the actin cytoskeleton. Microscopy research and technique *47*, 3-17.
Sotiropoulos, A., Gineitis, D., Copeland, J., and Treisman, R. (1999). Signal-regulated activation of serum response factor is mediated by changes in actin dynamics. Cell *98*, 159-169.
Stupack, D. G., Puente, X. S., Boutsaboualoy, S., Storgard, C. M., and Cheresh, D. A. (2001). Apoptosis of adherent cells by recruitment of caspase-8 to unligated integrins. The Journal of cell biology *155*, 459-470.
Sun, Q., Chen, G., Streb, J. W., Long, X., Yang, Y., Stoeckert, C. J., Jr., and Miano, J. M. (2006). Defining the mammalian CArGome. Genome research *16*, 197-207.
Takeuchi, T., Iwahara, S., Saeki, Y., Sasajima, H., and Yokosawa, H. (2005). Link between the ubiquitin conjugation system and the ISG15 conjugation system: ISG15 conjugation to the UbcH6 ubiquitin E2 enzyme. Journal of biochemistry *138*, 711-719.
Tang, Y., Rowe, R. G., Botvinick, E. L., Kurup, A., Putnam, A. J., Seiki, M., Weaver, V. M., Keller, E. T., Goldstein, S., Dai, J*., et al.* (2013). MT1-MMP-dependent control of skeletal stem cell commitment via a beta1-integrin/YAP/TAZ signaling axis. Dev Cell *25*, 402-416.
van der Veen, A. G., and Ploegh, H. L. (2012). Ubiquitin-like proteins. Annual review of biochemistry *81*, 323-357.
Vartiainen, M. K., Guettler, S., Larijani, B., and Treisman, R. (2007). Nuclear actin regulates dynamic subcellular localization and activity of the SRF cofactor MAL. Science *316*, 1749-1752.
Yuan, W., and Krug, R. M. (2001). Influenza B virus NS1 protein inhibits conjugation of the interferon (IFN)-induced ubiquitin-like ISG15 protein. The EMBO journal *20*, 362-371.

Zhang, C., Luo, X., Liu, L., Guo, S., Zhao, W., Mu, A., Liu, Z., Wang, N., Zhou, H., and Zhang, T. (2013). Myocardin-related transcription factor A is up-regulated by 17beta-estradiol and promotes migration of MCF-7 breast cancer cells via transactivation of MYL9 and CYR61. Acta biochimica et biophysica Sinica *45*, 921-927.

Zhang, S. X., Garcia-Gras, E., Wycuff, D. R., Marriot, S. J., Kadeer, N., Yu, W., Olson, E. N., Garry, D. J., Parmacek, M. S., and Schwartz, R. J. (2005). Identification of direct serum-response factor gene targets during Me2SO-induced P19 cardiac cell differentiation. The Journal of biological chemistry *280*, 19115-19126.

Zou, W., Papov, V., Malakhova, O., Kim, K. I., Dao, C., Li, J., and Zhang, D. E. (2005). ISG15 modification of ubiquitin E2 Ubc13 disrupts its ability to form thioester bond with ubiquitin. Biochemical and biophysical research communications *336*, 61-68.

FIGURE LEGENDS

Figure 1. FN bound α5β1 and αV-class integrins control f-Actin and nuclear MAL levels. (**A**) Superimposed picture (confocal stack) of indicated cell types immunostained for f-Actin (Phalloidin), g-Actin (DNaseI) and DAPI plated on FN-coated glass surfaces. The intensity map shows the cytoplasmic distribution of g-Actin. Scale bar, 20 µm. (**B**, **C**) Quantification of cytoplasmic g-Actin by DNaseI (B) and f-Actin fibres by Phalloidin (C) relative fluorescence intensities (n>20; 3 independent experiments). (**D**) Cell fractionation into soluble (S), nuclear (N) and cytoskeletal (C) components followed by western blot analysis with a β-Actin antibody. Antibodies against Vimentin and GAPDH confirm efficiency of subcellular protein fractionation (representative western blot of four independent experiments is shown). (**E, F**) Ratio of g-Actin versus GAPDH (E) and g-Actin versus f-Actin (F) of the indicated cell types is shown (n=4; 4 independent experiments). (**G**) Western blot analysis by Profilin and β-Actin antibody of g-Actin pulldown experiment with DNAseI- or BSA-coupled Sepharose beads (representative western blot of three independent experiments in technical duplicates is shown). (**H**) DNaseI-bound g-Actin in nuclear (N) and soluble (S) cell fraction was analysed (n=3; 3 independent experiments). (**I**) Immunostaining of indicated cell types plated on FN-coated glass coverslips and treated with DMSO (control), 100 nM Jasplankinolide (Jasp) and 500 nM Latrunculin A (LatA), respectively. The merged images display an overlay of Paxilin, MAL, f-Actin and nuclear staining (DAPI). Scale bar, 10 µm. All p-values were calculated using a paired Students-*t*-test.

Figure 2. αV-class integrins cooperate with α5β1 to induce SRF/MAL activity. (**A**) SRF-driven luciferase reporter activity in cells plated on FN and treated with DMSO, 100 nM Jasplankinolide (Jasp) or 500 nM Latrunculin A (LatA) (3 independent experiments). (**B**) SRF-driven luciferase reporter activity in cells plated on FN transfected with EGFP, a constitutive active (ca) MAL (ΔN-MAL) or a ca mDia construct (4 independent experiments). (**C**) SRF-driven luciferase reporter activity in cells plated on circular FN-coated micropatterns with either 40 µm or 28 µm diameter (3 independent experiments). (**D**) Z-stacks of immunostained cells seeded on circular FN-coated micropatterns with indicated diameters. The cartoon on the left illustrates the position of the indicated stack. The merged picture displays an overlay of MAL (yellow), f-Actin (white) and nuclear staining (DAPI). Scale bar, 10 µm. (**E**) Quantification of nuclear fluorescence intensity for MAL from superimposed images shown in (D) (n=5). (**F, G**) SRF-driven luciferase reporter activity in indicated cells treated with Mn^{++} (n=5) (F) or transfected with the αV or β1

Integrin (G) (n=4). (**H**) Immunostaining of pKO-αV,β1 cells plated on Fibronectin (FN), Vitronectin (VN) and Gelatin and untreated or treated with anti-α5β1 blocking antibodies or Cilengitide for MAL (red), f-Actin (white) and nucleus (DAPI; green). The inserts show MAL in the different settings. Scale bar, 25 µm. (**I**) SRF/MAL luciferase reporter activity (n=3) in pKO-αV,β1 cells plated on FN and untreated (n=15) or treated with anti-α5β1 blocking antibodies (n=22) or Cilengitide (n=27). All error bars represent ±SEM. All p-values were calculated using a paired Students-*t*-test. pKO-αV (green); pKO-β1 (orange); pKO-αV,β1 (blue).

Figure 3. αV- and β1-class integrins induce transcription of SRF/MAL target genes.

(**A**) Quantitative realtime-PCR of the SRF/MAL target genes *srf, talin, flnb, vcl, lima1* but also *mrtf-a* and *isg15*. mRNA levels are shown relative to GAPDH transcript levels (n>3; minimum of 3 independent RNA isolations, double blind). (**B**) Western blot analysis of SRF, Talin, Filamin B (FLN B), Vinculin (VCL), Lima1 but also MAL (or MRTF-A). GAPDH was used to control protein loading. (**C**) Densitometric analysis of free ISG15 protein in the indicated cell lines (5 independent experiments). (**D**) Immunostaining for Paxillin (Pxn), ISG15, f-Actin and DAPI. Arrowheads indicate co-localization of f-Actin and ISG15. Scale bar, 10 µm. (**E**) Immunostaining of ISG15, Paxillin, f-Actin and nucleus (DAPI) in FAs of cross-linked and unroofed indicated cells. The merged images display an overlay of ISG15, Paxillin, f-Actin and DAPI. Scale bar, 10 µm. (**F**) Scheme to illustrate location of CArG boxes (SRF binding sites; Blue boxes) in *isg15, vcl* as control and *tln-1* gene along Exons (Black boxes;). (**G, H**) Chromatin immunopreciptiation was performed with MAL, SRF or rabbit IgG antibody as control. *Isg15, vcl, tln* and *gapdh* as control CArG boxes were amplified by conventional PCR and visualized by agarose gel electrophoresis (G). Real-time PCR was performed from three independent chromatin preparations and IPs. Shown is the relative quantitation of *isg15, vcl* and *tln* relative to input chromatin (H). All error bars represent ±SEM. All p-values were calculated using a paired Students-*t*-test. pKO-αV (green); pKO-β1 (orange); pKO-αV,β1 (blue).

Figure 4. αV- and β1-class Integrin induced SRF/MAL activity and ISG15 levels to promote 3D cell invasion. (**A**) FACS analysis of integrin α5, αV and β1 surface levels and β1 activity by 9EG7 staining MCF-7 and MB231. (**B, C**) Immunostaining of non-invasive MCF-7 and highly invasive MB231 breast cancer cell lines seeded on FN (B). A representative example for threshold used for nuclear MAL quantification(C) is shown (In two independent experiment a minimum of 129 cells per cell line were analysed). The merged images display an overlay of MAL, f-Actin and nuclear staining (DAPI). Scale bar, 10 µm. (**D**) SRF/MAL luciferase reporter assay of MCF-7 and MDA-MB-231 cells (n=3; three independent experiments). (**E**) Quantitative real-time PCR was performed for *itgaV* and SRF/MAL targets *itgb1, isg15*,

srf, and lima1 but also for *mrtf-a*. Shown is the quantitation relative to *gapdh* (n=3, from 3 independent isolations, double blind). (**F**) Western blot of MDA-MB-231 and MCF-7 with ISG15 specific antibody. GAPDH was used to control loading. (**G-H**) FN-coated transwell cell invasion assay with MDA-MB-231 and MCF-7 cells upon ISG15 knockdown, UBP43 overexpression or scrambled shRNA control (n=3; 3 independent experiments). Immunostaining of transmigrated cell by Phalloidin and DAPI (G). Quantification of transmigrated cells compared to scrambled control (H). Scale bar, 100 µm. All error bars represent ±SEM. All p-values were calculated using a paired Students-*t*-test. ■ pKO-αV (green); ■ pKO-β1 (orange); and ■ pKO-αV,β1 (blue); □ MCF-7 (white); ■ MB231 (black);

Figure 5. αV- and β1-class integrin induced ISGylation of SRF/MAL targets results in bad breast cancer patient prognosis. (**A, B**) Kaplan Meier analysis indicates that breast cancer patients with high integrin β1 (A), or high ISG15 levels (B) die earlier. (**C**) Kaplan Meier analysis indicate bad patient outcome at high compared to low ISG15 transcript amounts by constant high α5 and β1 Integrin levels. (**D**) H/E staining of indicated breast cancer samples. Approximate area used for immunostaining (IF) is indicated. (**E**) Immunostaining of indicated patient samples for MAL, integrin β1 and f-Actin. The merged images display an overlay of MAL, integrin β1 and f-Actin and nuclear staining (DAPI). Scale bar, 50 µm.

Figure 6. Model of how α5β1/αV-class integrins synergistically induce MAL/SRF, leading to multi-layered protein ISGylation and enhanced 3D migration and invasion of tumour cells. Both, αV-class integrin induced RhoA/mDia and β1-class integrin induced Rac/WAVE/Arp2/3 activities are combined in FN-adherent pKO-αV,β1 cells leading to low g-Actin levels, the release and nuclear translocation of MAL, binding to SRF and transcription of target genes such as ISG15 and FA proteins. Production of ISG15 and its coupling machinery results in multi-layered protein ISGylation and subsequent stabilization of FA- and cytoskeletal-related proteins. Advanced cell migration properties leads to improved 3D migration and invasion of tumour cells.

TABLE

Table 1. Qualitative Comparison of SRF/MAL target genes to the proteome data of pKO-αV, pKO-β1 and pKO-αV,β1 cells published in Schiller and Hermann et al., NCB, 2013. Data mining and comparison of seven different SRF/MAL target gene screening approaches were manually filtered for association with FA and actin functions and co-localization. A qualitative comparison with the pKO-cell proteome

was performed. Data sources were cited by numbers: (**1**) Balza R. O. et al., JBC, 2006; (**2**) Philippar et al., MolCell, 2004; (**3**) Selvaraj A. et al., BMC, 2004; (**4**) Sun Q. et al., Genome Res, 2006; (**5**) Zhang S. X. et al., JBC, 2005; (**6**) Descot A. et al., MolCell, 2009; and (**7**) Cooper S. J. et al., Genome Res, 2007; ■ enrichment in pKO-αV cells (green); ■ enrichment in pKO-β1 cells (orange); and ■ enrichment in pKO-αV,β1 cells (blue); ■ not found in pKO-cell proteome list; □ not enriched in the indicated cell type.

SUPPLEMENTARY INFORMATION

Figure S1. Different total Actin levels and distribution in pKO-αV, pKO-β1 and pKO-αV,β1 cells. (**A**) Immunostaining of indicated cell types for Paxillin and f-Actin plated for 90 minutes on circular FN-coated micropatterns. The merged images display an overlay of Paxillin, f-Actin and nuclear (DAPI) staining. Scale bar, 25 µm. (**B**) Cell lysates were immunoblotted for total Actin. GAPDH was used as a loading control. Densitometric quantification of western blots (n=3) is depicted as fold changes below the corresponding blot with +/- SEM values. (**C**) FACS analysis of indicated cell types by propidium iodide staining to measure nuclear size. (**D**) Box plot of all actin modifying proteins (Schiller et al., 2013) in indicated cell lines classified into their effect on g-Actin pool: Neutral (black), decrease (blue), increase (yellow). Protein abundance is presented by Log2 ratios. Thymosin beta 4 (Tmsb4), Cofilin-1 (Cfl-1) and Advillin (Advil) were highlighted. (**E**) Log2 ratio of Tmsb4 expression in indicated cell lines (n=3; 3 independent experiments). (**F**) Western blot of Cofilin and phospho-Cofilin (Ser3) (representative western blot of 4 independent experiments is shown). (**G**) Microscopy of indicated cells upon Latrunculin A (LatA) or Jasplankinolide (Jasp) treatment. DMSO was used as control. Dashed lines highlight lamellipodia and long protrusions caused by Jasp treatment. Scale bar, 20µm.

Figure S2. αV-class integrins cooperate with α5β1 to induce SRF/MAL activity. (**A-C**) Reporter activity measurements of a SRF-driven firefly normalized to a thymidine kinase-driven renilla luciferase of cells plated on FN-coated culture dishes. Cells were starved and serum boosted with 40% FCS (A) and in (B) treated with Methanol (MeOH) as a control and Leptomycin B (LeptoB) to inhibit the nuclear export of MAL or (C) transfected with EGFP only or a dominant negative MAL (DN MAL) construct. (**D**) Reporter activity measurements of a SRF-driven firefly normalized to a thymidine kinase-driven renilla luciferase of Kindlin-1 and -2 or Talin-1 and -2 wild type (WT) and knockout cells (KO) seeded on FN. All error bars represent SEM and p-values were calculated using a paired Students-*t*-test. ■ pKO-αV (green); ■ pKO-β1 (orange); ■ pKO-αV,β1 (blue);

Figure S3. Type I interferon response independent but SRF/MAL dependent ISG15 transcription in pKO-αV, pKO-β1 and pKO-αV,β1 cells. (**A-C**) Quantitative real-time PCR of Interferon α (IFNα; A), Interferon β (IFNβ; B) and ISG15 upon 100µg/ml poly I:C stimulation (C) (n=3; 3 independent isolations). (**D, E**) ELISA-based quantification of IFNα (D) or IFNβ (E) levels in supernatants of indicated cells treated with Poly I:C. Error bars represent ±SEM. p-values were calculated using a paired Students-*t*-test. (**F**) Western blot of free ISG15 in total cell lysate or supernatant of 72h cultured indicated cells. GAPDH was used to control protein loading. FN was used as a secreted protein control. Densitometric quantification

of western blots (n>3; >3 independent experiments) is depicted as fold changes below the corresponding blot with +/- SEM values.

Figure S5. αV- and β1-class integrin induced ISGylation of SRF/MAL targets results in bad breast cancer patient prognosis. Quantification of nuclear MAL in grade (G) 1 to G3 breast cancer sections (G1: n=10, G2: n=12, G3: n=20).

SUPPLEMENTARY TABLES

Table S1. ISG15 pull-down mass spectrometry analysis

Table S2. List of primer sequences

Table S3. List of antibodies

Hermann et al., Fig.1

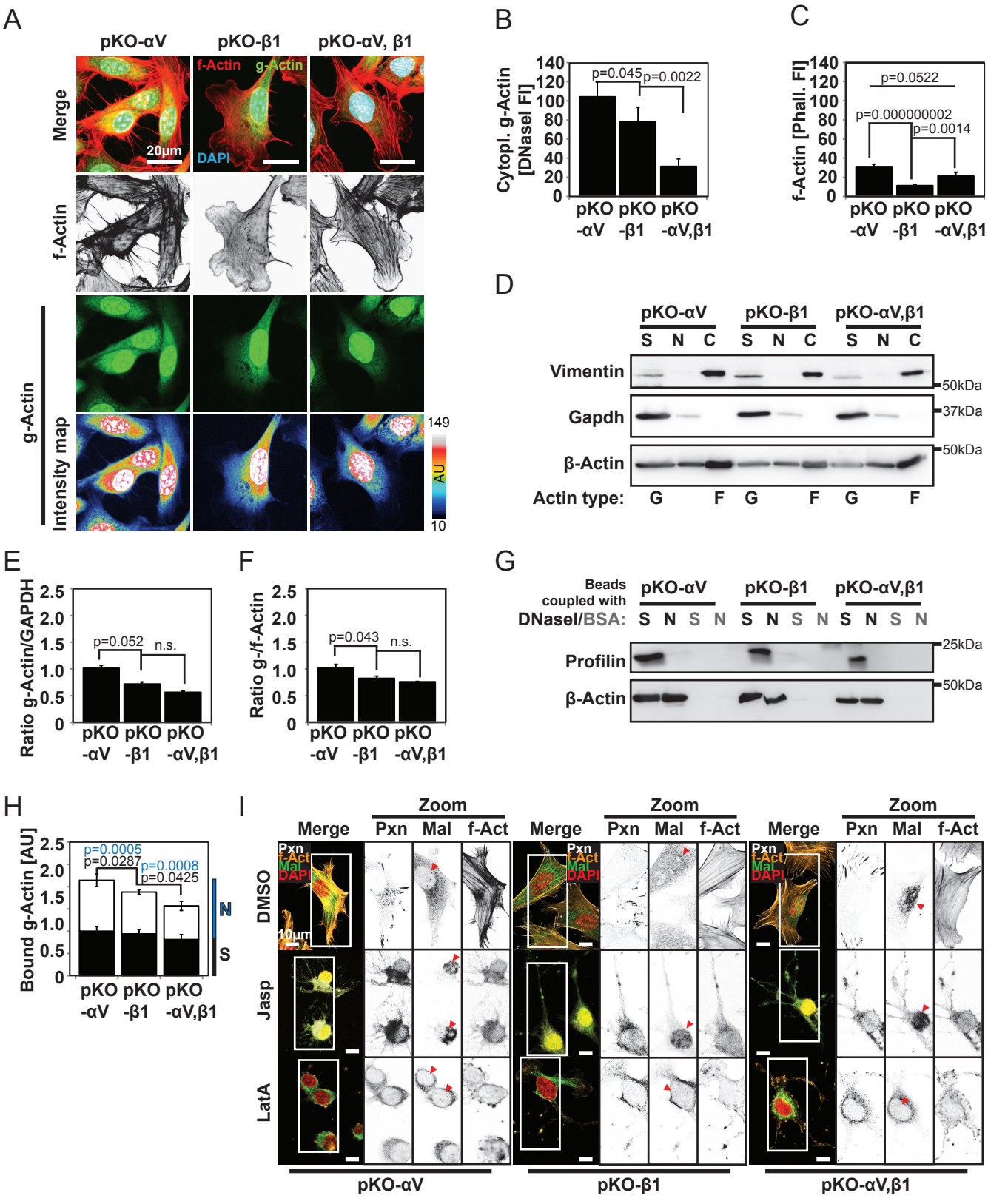

Hermann et al., Fig.2

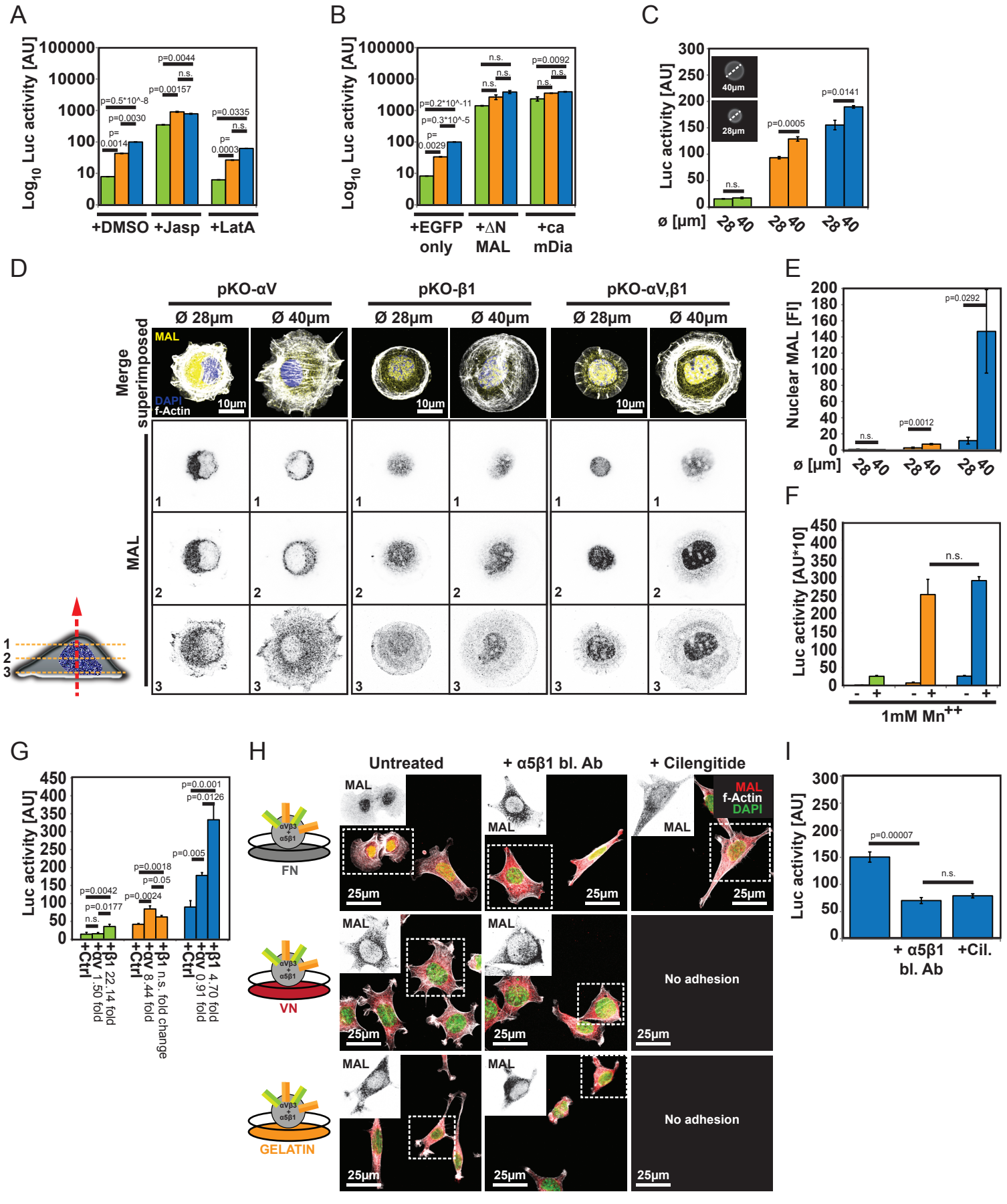

Hermann et al., Fig.3

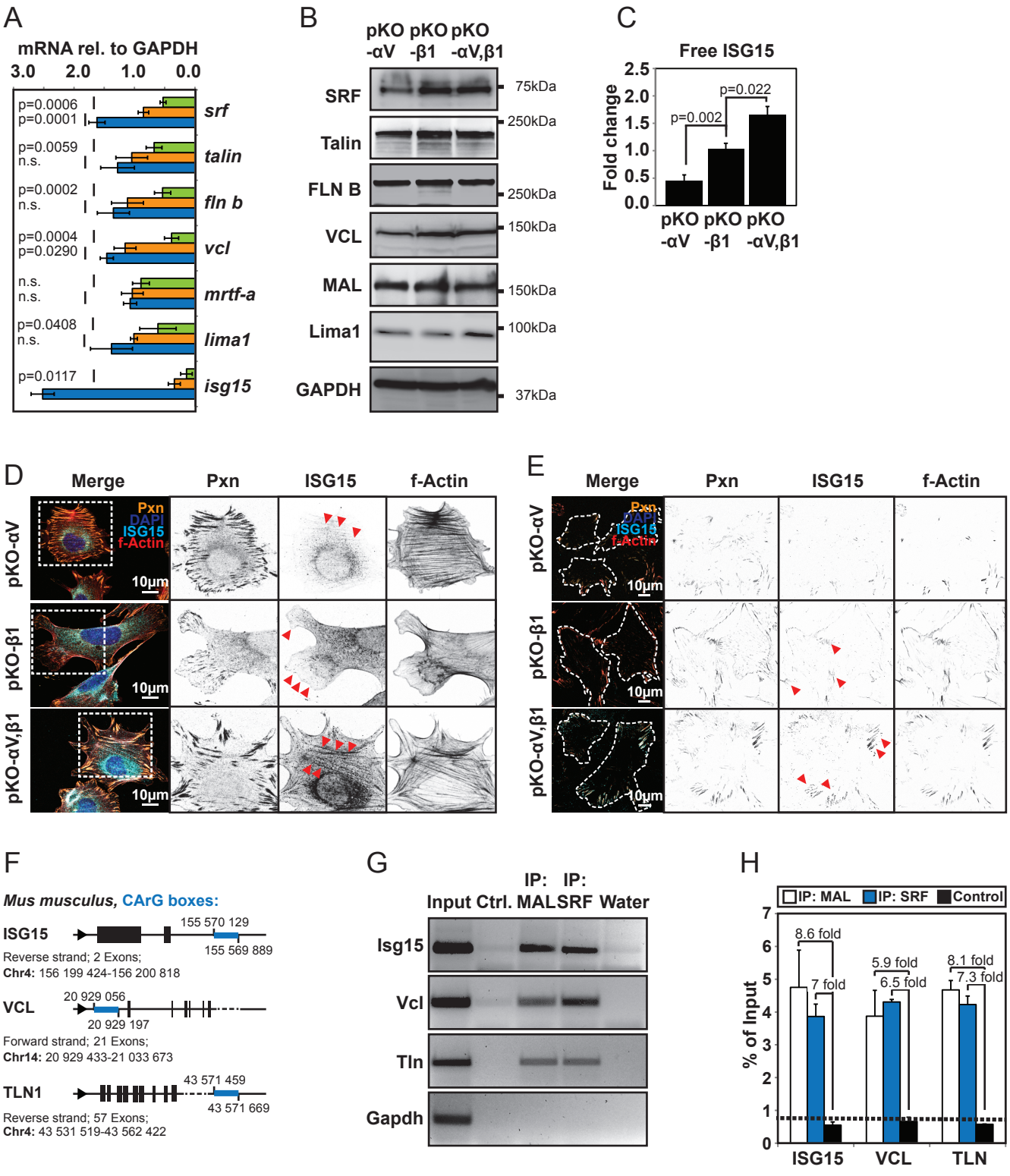

Hermann et al., Fig.4

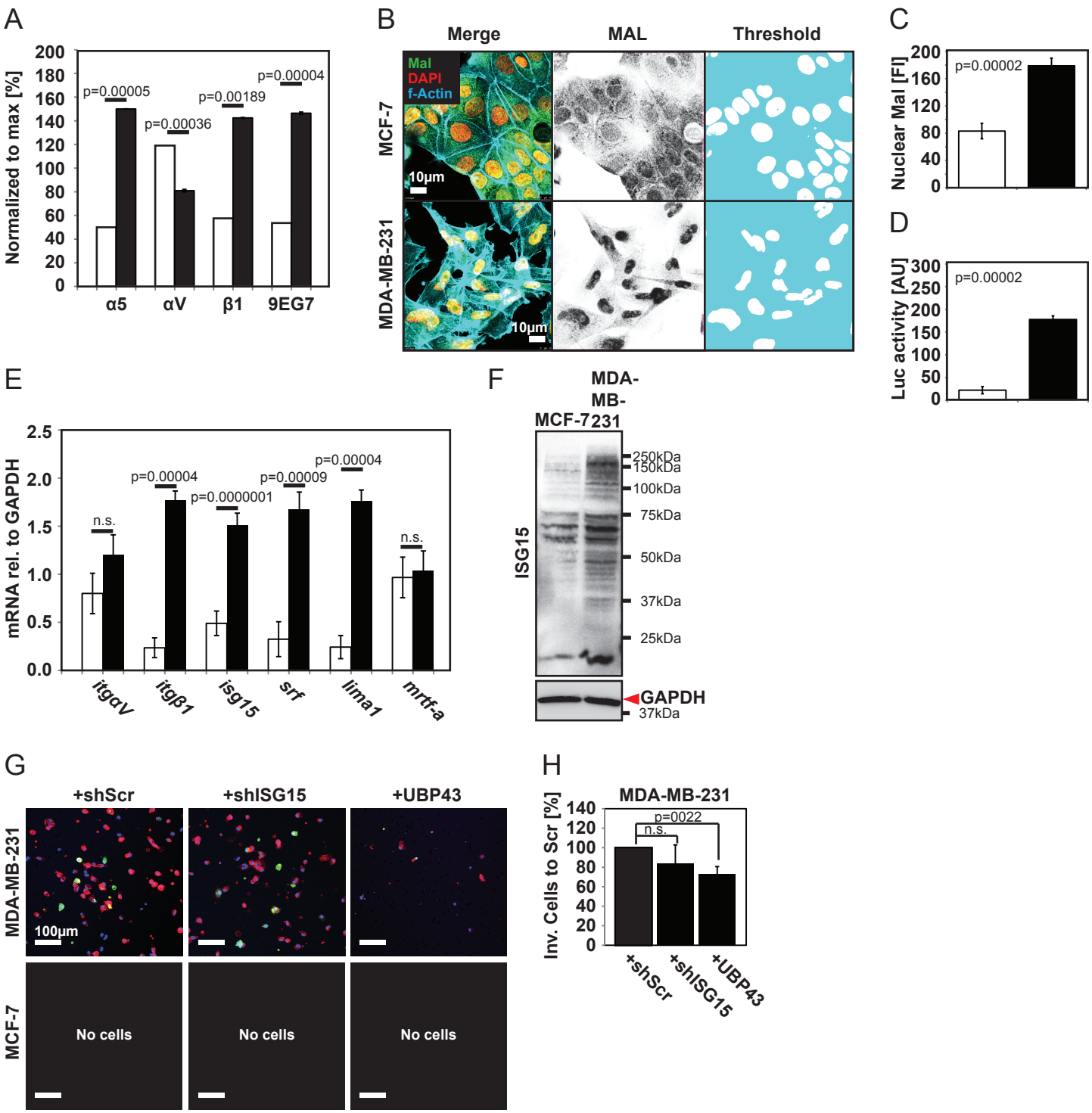

Hermann et al., Fig.5

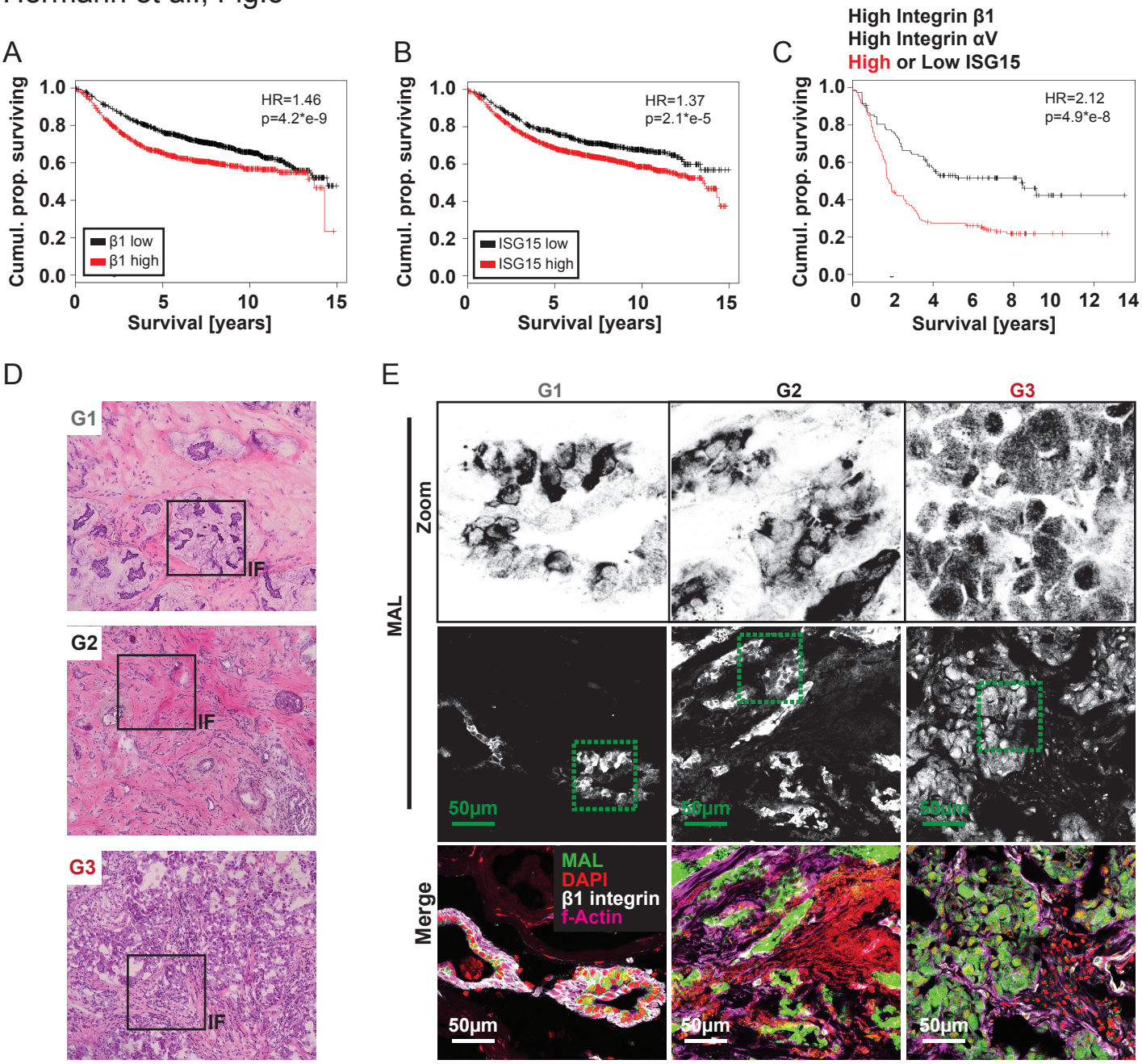

Hermann et al., Fig.6

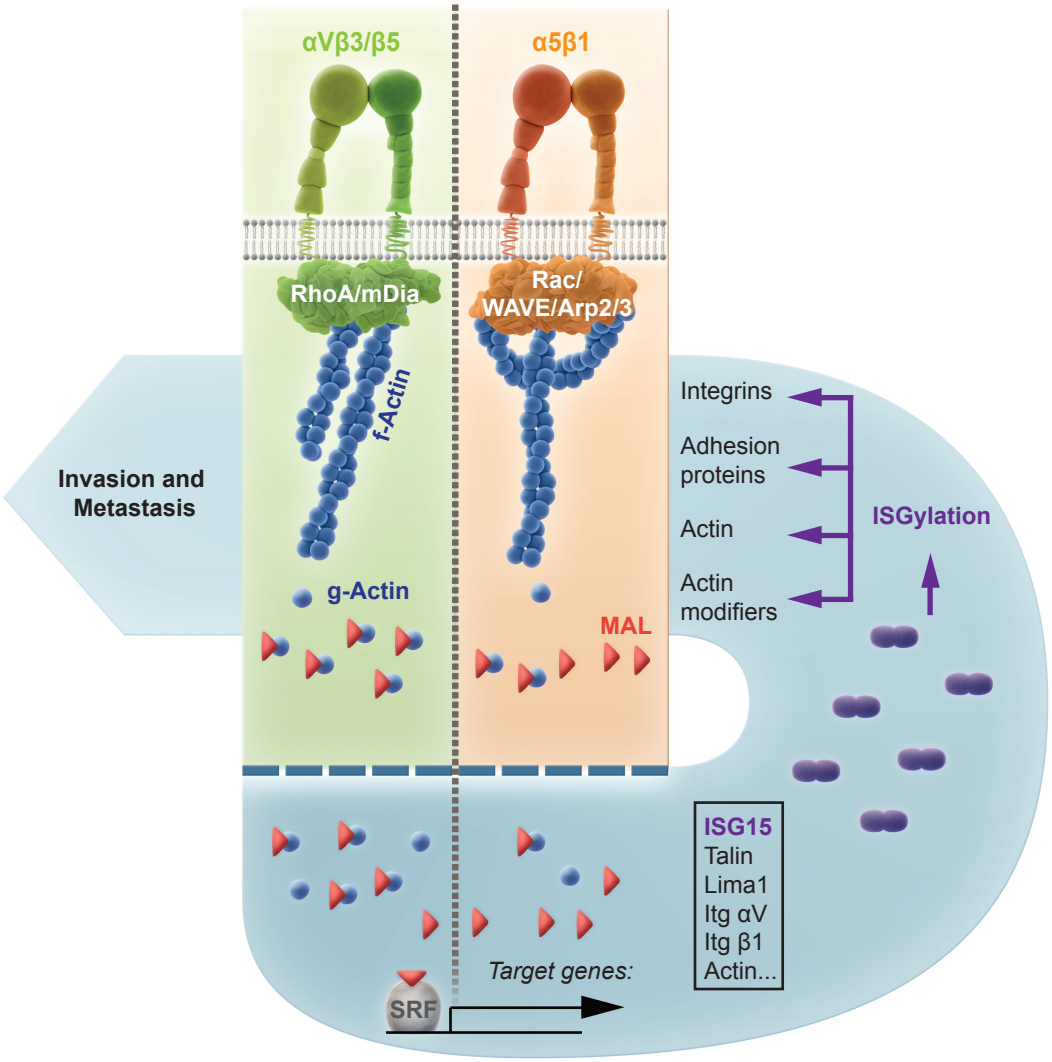

Hermann et al., Fig.S1

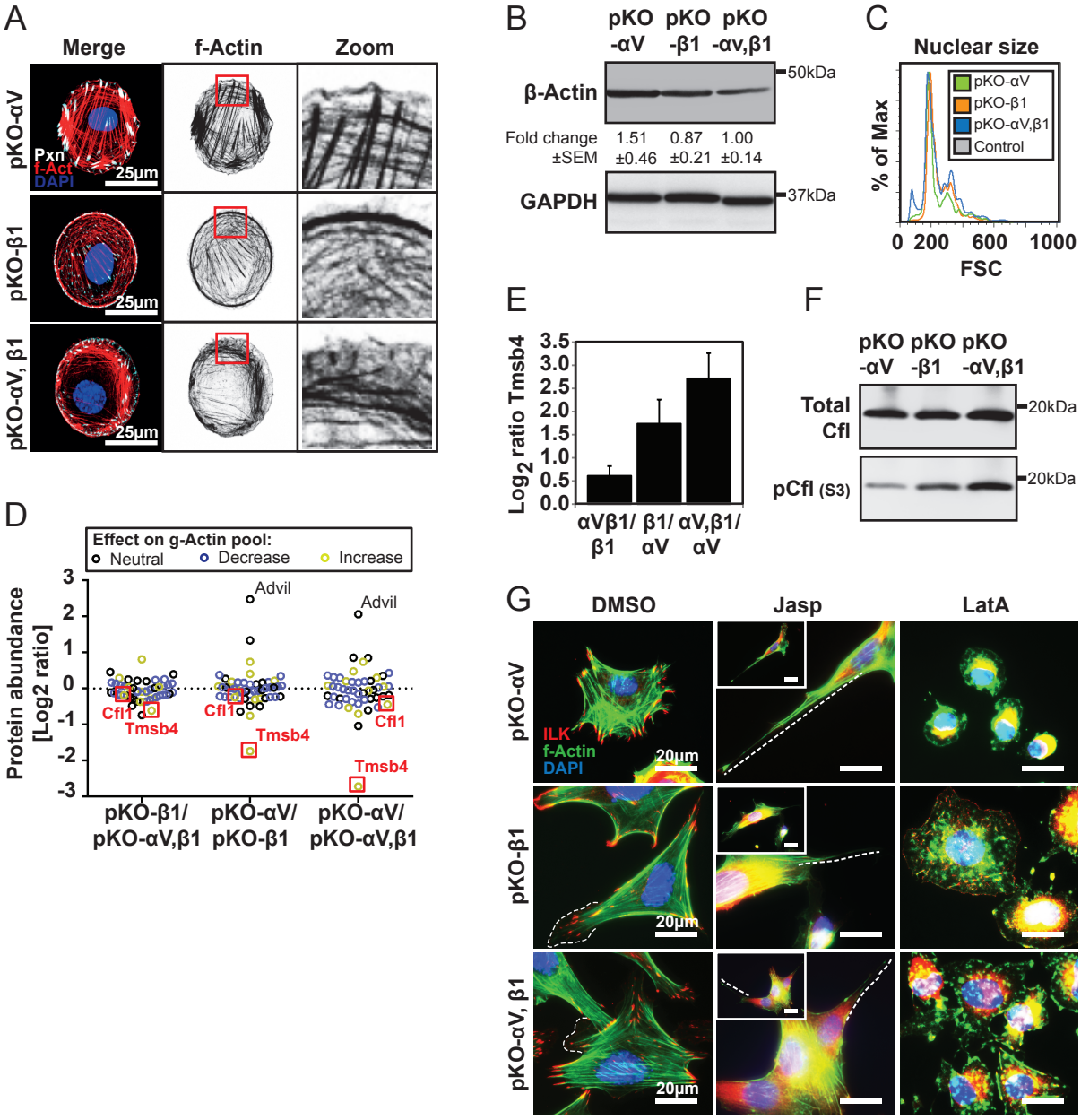

Hermann et al., Fig.S2

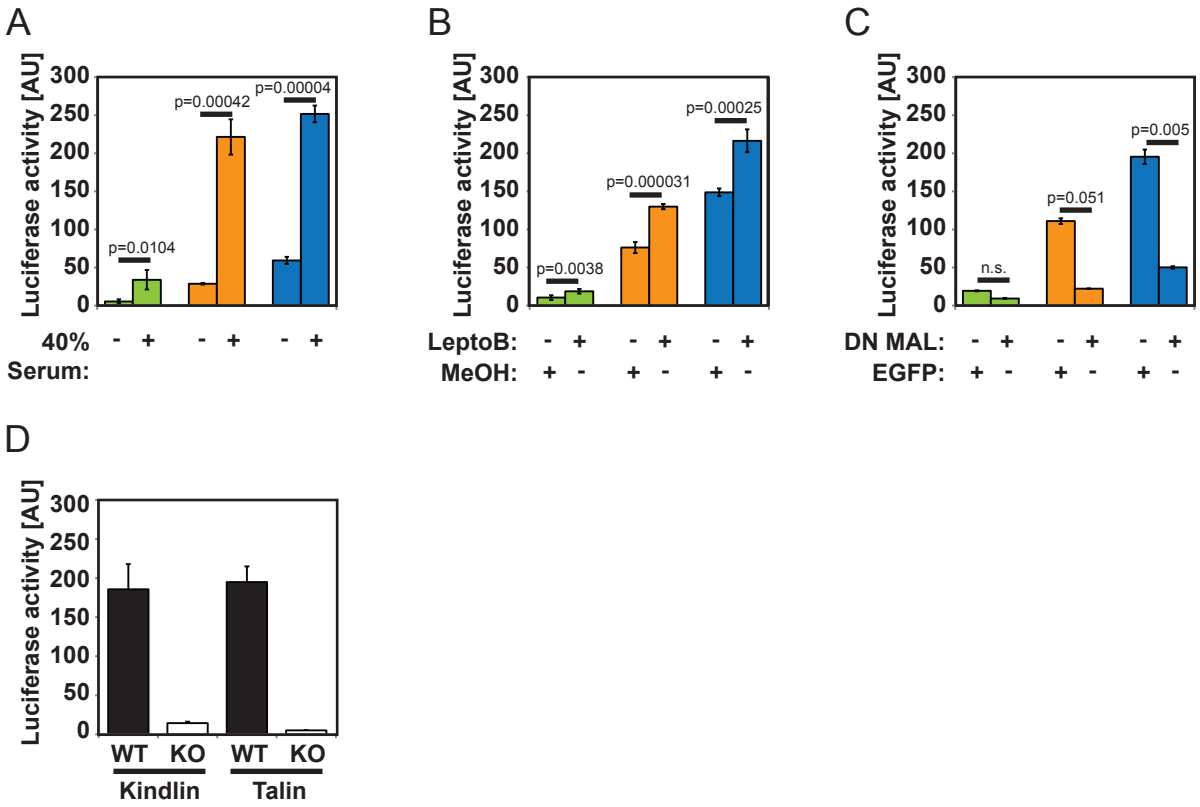

Hermann et al., Fig.S3

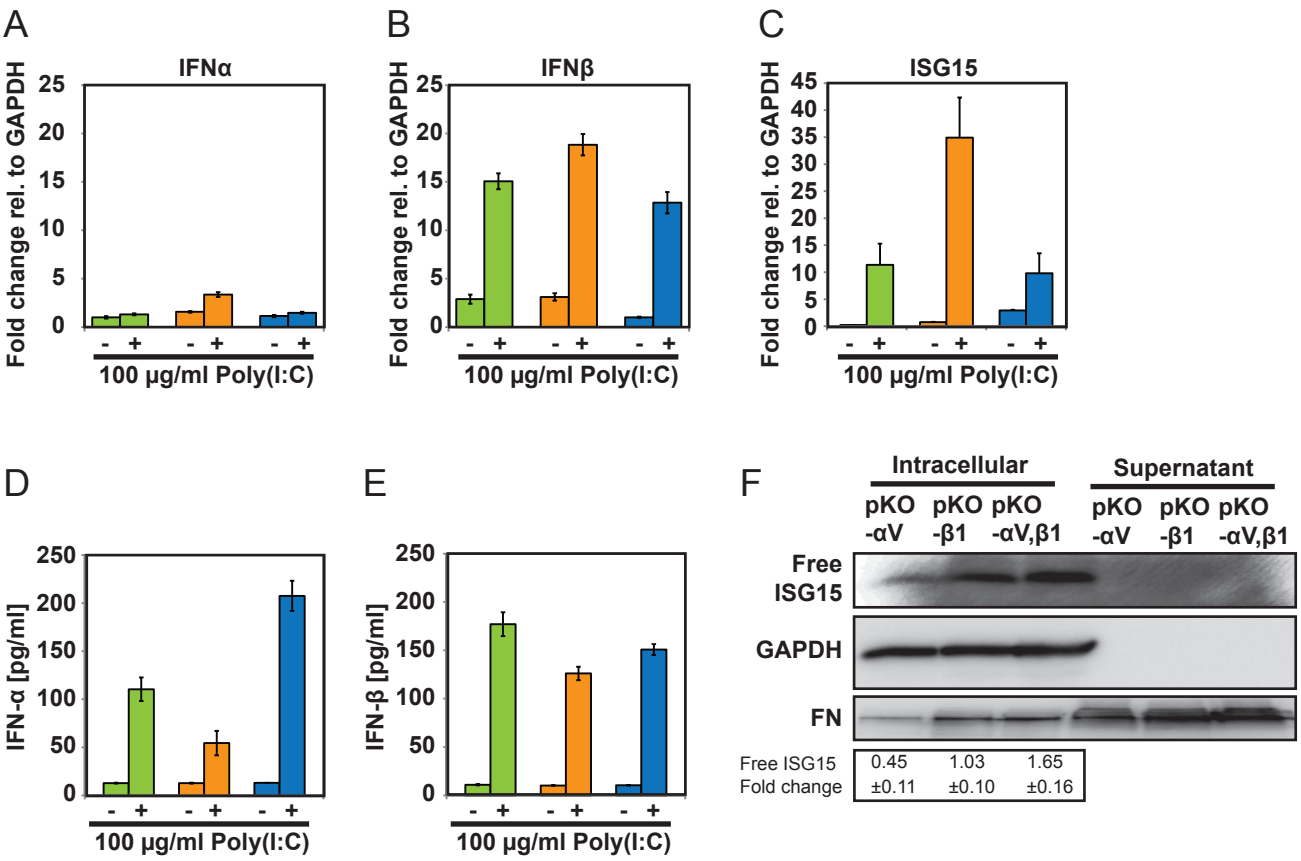

Hermann et al., Fig.S5

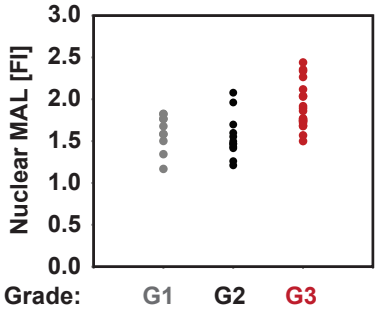

Hermann et al., Table 1

SRF target genes			Proteome		
Gene Name	**Annotation**	**Source**	**Enriched**		
ACTA1	Skeletal alpha actin	1,2,6			
ACTA2	Smooth muscle alpha actin	1,2,6			
ACTC	Alpha-cardiac actin	2			
ACTC1	Actin, alpha cardiac muscle 1	1,5,6			
ACTG	Actin, cytoplasmic 2	2			
ACTN1	Alpha-actinin-1	4			
CAPZA3	F-actin-capping protein subunit alpha-3	4			
CFL1	Cofilin, non-muscle isoform	4			
CFL2	Cofilin2, muscle	1,4			
DSTN	Destrin, Actin-depolymerizing factor, ADF	4,6,7			
ENAH, MENA	Protein enabled homolog	1			
EPLIN	LIM domain and actin-binding protein 1	6			
FBLN5	Fibulin-5	4			
FHL1	Four and a half LIM domains protein 1	4,6			
FHL2	Four and a half LIM domains protein 2	2,4			
FLNA	Filamin A	4			
FLNC	Filamin C	4			
FNBP1	Formin-binding protein 1	1			
IQGAP	Ras GTPase-activating-like protein IQGAP1				
ISG15	Interferon-induced 15kDa protein	2			
ITGA1	Integrin alpha 1	7			
ITGA5	Integrin alpha5	4,6			
ITGA9	Integrin alpha 9	1,5			
ITGB1	Integrin beta 1	1			
ITGB1BP2	Integrin beta 1 binding protein 2 (melusin)	1,4,7			
LPP	LIM domain-containing preferred translocation partner in lipoma	2,6			
MAP3K14	Mitogen-activated protein kinase kinase kinase 14	5,6			
MAP3K4	Mitogen-activated protein kinase kinase kinase 4	5			
MAPK10	Mitogen-activated protein kinase 10, JNK3	5			
MYH11	Myosin heavy chain, smooth muscle isoform, SMMHC	7			
MYH6	Myosin heavy chain, cardiac muscle alpha isoform, MyHC-alpha	1			
MYH7	Myosin heavy chain, cardiac muscle beta isoform, MyHC-beta	1			
MYH9	Non-muscle myosin heavy chain A, NMMHC-A, NMMHC-lia	6,7			
MYL3	Myosin light chain 1, slow-twitch muscle B/ventricular isoform, MLC1SB	1,5			
MYL4	Myosin light chain 1, atrial/fetal isoform, MLC1A	1			
MYL9	Myosin light chain 9, smooth muscle	1,5			
PDLIM5	Enh, Enigma homolog	4			
PDLIM7	Enigma	1,6			
PFN1	Profilin-1	4			
SRF	Serum response factor	1,3			
SVIL	Supervillin	1,7			
TLN	Talin	4			
TRIP6	Zyxin-related protein 1	4			
VCL	Vinculin	2,3,6,7			
VIL1	Villin-1	6			
ZYX	Zyxin	3			
			pKO-αV	**pKO-β1**	**pKO-αV,β1**